risks

Risks

Feature Papers 2020

Edited by

Mogens Steffensen

Printed Edition of the Special Issue Published in *Risks*

www.mdpi.com/journal/risks

MDPI

Risks: Feature Papers 2020

Risks: Feature Papers 2020

Editor

Mogens Steffensen

MDPI • Basel • Beijing • Wuhan • Barcelona • Belgrade • Manchester • Tokyo • Cluj • Tianjin

Editor
Mogens Steffensen
University of Copenhagen
Denmark

Editorial Office
MDPI
St. Alban-Anlage 66
4052 Basel, Switzerland

This is a reprint of articles from the Special Issue published online in the open access journal *Risks* (ISSN 2227-9091) (available at: https://www.mdpi.com/journal/risks/special_issues/Risks_Feature_Papers).

For citation purposes, cite each article independently as indicated on the article page online and as indicated below:

LastName, A.A.; LastName, B.B.; LastName, C.C. Article Title. *Journal Name* **Year**, *Volume Number*, Page Range.

ISBN 978-3-0365-0712-5 (Hbk)
ISBN 978-3-0365-0713-2 (PDF)

Contents

About the Editor

Mogens Steffensen is professor of Life Insurance Mathematics at the University of Copenhagen. He earned his Ph.D. degree from the same university in 2001. After visiting positions in Germany, England, and the USA, he became a professor in 2008. He has contributed to the development of market-based valuation methods in insurance. His research also covers various decision-making problems within insurance and finance, and, recently, he is mainly interested in integrating insurance and pension decisions into classical consumption–investment problems. He has written 45 articles and 2 monographs in the areas of actuarial science and mathematical finance. He participates actively in industrial discussions about accounting, solvency, and risk management, and he has taken part in several research projects together with partners in the Danish pension industry. He is member of the Solvency and Accounting Committee under the Danish Actuarial Association. He is member of the board of directors and the audit committee of PFA Pension, the largest Danish commercial pension fund and the 10th largest pension fund in Europe.

Preface to "Risks: Feature Papers 2020"

The advancements and applications of risk modeling, and the impact on individual, institutional, and national decision-making is the broad scope of *Risks*. Actuarial mathematics and mathematical finance is at the core of this area, where institutional is in reference to insurance and financial institutions. But around this core we find, more generally, actuarial science and financial economics. Actuarial science can be thought of as combining economic and other social scientific elements with actuarial mathematics, expanding the insurance domain beyond its formalizations. Further away from the core, but still within the scope of acturial mathematics and mathematical finance, we find other branches that either draw on the advances in risk modeling, or relate to the insurance and financial decision-making with new insights and ideas but not necessarily advancements in risk modeling itself.

This book contains eight articles that explore advancements that are being developed across the diverse range that this area touches upon, all encompassed within the description of the scope above. Advancements of probabilistic models beyond the standard, and their impact on pricing and hedging, is at the core of mathematical finance. Such studies are, currently, rarely found in finance journals but frequently, and most appropriately, found in *Risks*. Much of financial research over the past decade has evolved into taking more standard models and drawing new insights from the financial data, and such research is certainly also welcome in *Risks*. Real estate and agricultural economics is also about effectively pricing assets, the financial contracts written on those prices, and the understanding of the dynamics of observed prices. The methods of machine learning, their predictive power, and the statistical assumptions and methods behind them, are tools that will inevitably find their place in the market. Modeling pandemic risk is, for obvious reasons, topical in health science, but its applications in health and life insurance are similarly of keen interest at the moment. Finally, understanding the behavior of health insurance policy holders is a core aspect of actuarial science. We hope you enjoy this collection of feature articles and find it insightful!

Mogens Steffensen
Editor

risks

MDPI

Article

Modelling Volatile Time Series with V-Transforms and Copulas

Alexander J. McNeil

The York Management School, University of York, Freboys Lane, York YO10 5GD, UK; alexander.mcneil@york.ac.uk

Received: 29 November 2020; Accepted: 29 December 2020; Published: 5 January 2021

Abstract: An approach to the modelling of volatile time series using a class of uniformity-preserving transforms for uniform random variables is proposed. V-transforms describe the relationship between quantiles of the stationary distribution of the time series and quantiles of the distribution of a predictable volatility proxy variable. They can be represented as copulas and permit the formulation and estimation of models that combine arbitrary marginal distributions with copula processes for the dynamics of the volatility proxy. The idea is illustrated using a Gaussian ARMA copula process and the resulting model is shown to replicate many of the stylized facts of financial return series and to facilitate the calculation of marginal and conditional characteristics of the model including quantile measures of risk. Estimation is carried out by adapting the exact maximum likelihood approach to the estimation of ARMA processes, and the model is shown to be competitive with standard GARCH in an empirical application to Bitcoin return data.

Keywords: time series; volatility; probability-integral transform; ARMA model; copula

1. Introduction

In this paper, we show that a class of uniformity-preserving transformations for uniform random variables can facilitate the application of copula modelling to time series exhibiting the serial dependence characteristics that are typical of volatile financial return data. Our main aims are twofold: to establish the fundamental properties of v-transforms and show that they are a natural fit to the volatility modelling problem; to develop a class of processes using the implied copula process of a Gaussian ARMA model that can serve as an archetype for copula models using v-transforms. Although the existing literature on volatility modelling in econometrics is vast, the models we propose have some attractive features. In particular, as copula-based models, they allow the separation of marginal and serial dependence behaviour in the construction and estimation of models.

A distinction is commonly made between genuine stochastic volatility models, as investigated by Taylor (1994) and Andersen (1994), and GARCH-type models as developed in a long series of papers by Engle (1982), Bollerslev (1986), Ding et al. (1993), Glosten et al. (1993) and Bollerslev et al. (1994), among others. In the former an unobservable process describes the volatility at any time point while in the latter volatility is modelled as a function of observable information describing the past behaviour of the process; see also the review articles by Shephard (1996) and Andersen and Benzoni (2009). The generalized autoregressive score (GAS) models of Creal et al. (2013) generalize the observation-driven approach of GARCH models by using the score function of the conditional density to model time variation in key parameters of the time series model. The models of this paper have more in common with the observation-driven approach of GARCH and GAS but have some important differences.

In GARCH-type models, the marginal distribution of a stationary process is inextricably linked to the dynamics of the process as well as the conditional or innovation distribution; in most cases, it has no simple closed form. For example, the standard GARCH mechanism serves to create

power-law behaviour in the marginal distribution, even when the innovations come from a lighter-tailed distribution such as Gaussian (Mikosch and Stărică 2000). While such models work well for many return series, they may not be sufficiently flexible to describe all possible combinations of marginal and serial dependence behaviour encountered in applications. In the empirical example of this paper, which relates to log-returns on the Bitcoin price series, the data appear to favour a marginal distribution with sub-exponential tails that are lighter than power tails and this cannot be well captured by standard GARCH models. Moreover, in contrast to much of the GARCH literature, the models we propose make no assumptions about the existence of second-order moments and could also be applied to very heavy-tailed situations where variance-based methods fail.

Let $X_1, \ldots, X_n$ be a time series of financial returns sampled at (say) daily frequency and assume that these are modelled by a strictly stationary stochastic process (X_t) with marginal distribution function (cdf) F_X. To match the stylized facts of financial return data described, for example, by Campbell et al. (1997) and Cont (2001), it is generally agreed that (X_t) should have limited serial correlation, but the squared or absolute processes $\left(X_t^2\right)$ and $(|X_t|)$ should have significant and persistent positive serial correlation to describe the effects of volatility clustering.

In this paper, we refer to transformed series like $(|X_t|)$, in which volatility is revealed through serial correlation, as *volatility proxy series*. More generally, a volatility proxy series $(T(X_t))$ is obtained by applying a transformation $T : R \mapsto R$ which (i) depends on a change point μ_T that may be zero, (ii) is increasing in $X_t - \mu_T$ for $X_t \geq \mu_T$ and (iii) is increasing in $\mu_T - X_t$ for $X_t \leq \mu_T$.

Our approach in this paper is to model the probability-integral transform (PIT) series (V_t) of a volatility proxy series. This is defined by $V_t = F_{T(X)}(T(X_t))$ for all t, where $F_{T(X)}$ denotes the cdf of $T(X_t)$. If (U_t) is the PIT series of the original process (X_t), defined by $U_t = F_X(X_t)$ for all t, then a *v-transform* is a function describing the relationship between the terms of (V_t) and the terms of (U_t). Equivalently, a v-transform describes the relationship between quantiles of the distribution of X_t and the distribution of the volatility proxy $T(X_t)$. Alternatively, it characterizes the dependence structure or copula of the pair of variables $(X_t, T(X_t))$. In this paper, we show how to derive flexible, parametric families of v-transforms for practical modelling purposes.

To gain insight into the typical form of a v-transform, let $x_1, \ldots, x_n$ represent the realized data values and let $u_1, \ldots, u_n$ and $v_1, \ldots, v_n$ be the samples obtained by applying the transformations $v_t = F_n^{(|X|)}(|x_t|)$ and $u_t = F_n^{(X)}(x_t)$, where $F_n^{(X)}(x) = \frac{1}{n+1}\sum_{t=1}^{n} I_{\{x_t \leq x\}}$ and $F_n^{(|X|)}(x) = \frac{1}{n+1}\sum_{t=1}^{n} I_{\{|x_t| \leq x\}}$ denote scaled versions of the empirical distribution functions of the x_t and $|x_t|$ samples, respectively. The graph of (u_t, v_t) gives an empirical estimate of the v-transform for the random variables $(X_t, |X_t|)$. In the left-hand plot of Figure 1 we show the relationship for a sample of $n = 1043$ daily log-returns of the Bitcoin price series for the years 2016–2019. Note how the empirical v-transform takes the form of a slightly asymmetric 'V'.

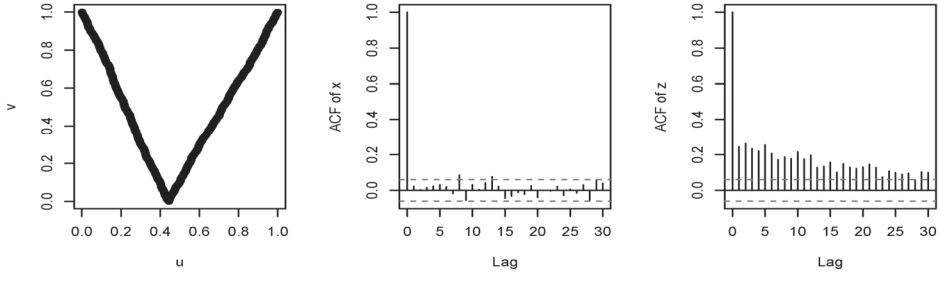

Figure 1. Scatterplot of v_t against u_t (left), sample acf of raw data x_t (centre) and sample acf of $z_t = \Phi^{-1}(v_t)$ (right). The transformed data are defined by $v_t = F_n^{(|X|)}(|x_t|)$ and $u_t = F_n^{(X)}(x_t)$ where $F_n^{(X)}$ and $F_n^{(|X|)}$ denote versions of the empirical distribution function of the x_t and $|x_t|$ values, respectively. The sample size is $n = 1043$ and the data are daily log-returns of the Bitcoin price for the years 2016–2019.

The right-hand plot of Figure 1 shows the sample autocorrelation function (acf) of the data given by $z_t = \Phi^{-1}(v_t)$ where Φ is the standard normal cdf. This reveals a persistent pattern of positive serial correlation which can be modelled by the implied ARMA copula. This pattern is not evident in the acf of the raw x_t data in the centre plot.

To construct a volatility model for (X_t) using v-transforms, we need to specify a process for (V_t). In principle, any model for a series of serially dependent uniform variables can be applied to (V_t). In this paper, we illustrate concepts using the Gaussian copula model implied by the standard ARMA dependence structure. This model is particularly tractable and allows us to derive model properties and fit models to data relatively easily.

There is a large literature on copula models for time series; see, for example, the review papers by Patton (2012) and Fan and Patton (2014). While the main focus of this literature has been on cross-sectional dependencies between series, there is a growing literature on models of serial dependence. First-order Markov copula models have been investigated by Chen and Fan (2006), Chen et al. (2009) and Domma et al. (2009) while higher-order Markov copula models using D-vines are applied by Smith et al. (2010). These models are based on the pair-copula apporoach developed in Joe (1996), Bedford and Cooke (2001, 2002) and Aas et al. (2009). However, the standard bivariate copulas that enter these models are not generally effective at describing the typical serial dependencies created by stochastic volatility, as observed by Loaiza-Maya et al. (2018).

The paper is structured as follows. In Section 2, we provide motivation for the paper by constructing a symmetric model using the simplest example of a v-transform. The general theory of v-transforms is developed in Section 3 and is used to construct the class of VT-ARMA processes and analyse their properties in Section 4. Section 5 treats estimation and statistical inference for VT-ARMA processes and provides an example of their application to the Bitcoin return data; Section 6 presents the conclusions. Proofs may be found in the Appendix A.

2. A Motivating Model

Given a probability space $(\Omega, \mathcal{F}, P)$, we construct a symmetric, strictly stationary process $(X_t)_{t\in N\setminus\{0\}}$ such that, under the even transformation $T(x) = |x|$, the serial dependence in the volatility proxy series $(T(X_t))$ is of ARMA type. We assume that the marginal cdf F_X of (X_t) is absolutely continuous and the density f_X satisfies $f_X(x) = f_X(-x)$ for all $x > 0$. Since F_X and $F_{|X|}$ are both continuous, the properties of the probability-integral (PIT) transform imply that the series (U_t) and (V_t) given by $U_t = F_X(X_t)$ and $V_t = F_{|X|}(|X_t|)$ both have standard uniform marginal distributions. Henceforth, we refer to (V_t) as the *volatility PIT process* and (U_t) as the *series PIT process*.

Any other volatility proxy series that can be obtained by a continuous and strictly increasing transformation of the terms of $(|X_t|)$, such as $\left(X_t^2\right)$, yields exactly the same volatility PIT process. For example, if $\widetilde{V}_t = F_{X^2}\left(X_t^2\right)$, then it follows from the fact that $F_{X^2}(x) = F_{|X|}\left(\sqrt[+]{x}\right)$ for $x \geq 0$ that $\widetilde{V}_t = F_{X^2}\left(X_t^2\right) = F_{|X|}(|X_t|) = V_t$. In this sense, we can think of classes of equivalent volatility proxies, such as $(|X_t|)$, $\left(X_t^2\right)$, $(\exp|X_t|)$ and $(\ln(1+|X_t|))$. In fact, (V_t) is itself an equivalent volatility proxy to $(|X_t|)$ since $F_{|X|}$ is a continuous and strictly increasing transformation.

The symmetry of f_X implies that $F_{|X|}(x) = 2F_X(x) - 1 = 1 - 2F_X(-x)$ for $x \geq 0$. Hence, we find that

$$V_t = F_{|X|}(|X_t|) = \begin{cases} F_{|X|}(-X_t) & = 1 - 2F_X(X_t) = 1 - 2U_t, \quad \text{if} X_t < 0 \\ F_{|X|}(X_t) & = 2F_X(X_t) - 1 = 2U_t - 1, \quad \text{if} X_t \geq 0 \end{cases}$$

which implies that the relationship between the volatility PIT process (V_t) and the series PIT process (U_t) is given by

$$V_t = \mathcal{V}(U_t) = |2U_t - 1| \tag{1}$$

where $\mathcal{V}(u) = |2u - 1|$ is a perfectly symmetric v-shaped function that maps values of U_t close to 0 or 1 to values of V_t close to 1, and values close to 0.5 to values close to 0. $\mathcal{V}$ is the canonical example

of a v-transform. It is related to the so-called tent-map transformation $\mathcal{T}(u) = 2\min(u, 1-u)$ by $\mathcal{V}(u) = 1 - \mathcal{T}(u)$.

Given (V_t), let the process (Z_t) be defined by setting $Z_t = \Phi^{-1}(V_t)$ so that we have the following chain of transformations:

$$X_t \overset{F_X}{\rightarrow} \quad U_t \overset{\mathcal{V}}{\rightarrow} \quad V_t \overset{\Phi^{-1}}{\rightarrow} \quad Z_t. \tag{2}$$

We refer to (Z_t) as a *normalized volatility proxy series*. Our aim is to construct a process (X_t) such that, under the chain of transformations in (2), we obtain a Gaussian ARMA process (Z_t) with mean zero and variance one. We do this by working back through the chain.

The transformation $\mathcal{V}$ is not an injection and, for any $V_t > 0$, there are two possible inverse values, $\frac{1}{2}(1 - V_t)$ and $\frac{1}{2}(1 + V_t)$. However, by randomly choosing between these values, we can 'stochastically invert' $\mathcal{V}$ to construct a random variable U_t such that $\mathcal{V}(U_t) = V_t$, This is summarized in Lemma 1, which is a special case of a more general result in Proposition 4.

Lemma 1. *Let V be a standard uniform variable. If $V = 0$, set $U = \frac{1}{2}$. Otherwise, let $U = \frac{1}{2}(1 - V)$ with probability 0.5 and $U = \frac{1}{2}(1 + V)$ with probability 0.5. Then, U is uniformly distributed and $\mathcal{V}(U) = V$.*

This simple result suggests Algorithm 1 for constructing a process (X_t) with symmetric marginal density f_X such that the corresponding normalized volatility proxy process (Z_t) under the absolute value transformation (or continuous and strictly increasing functions thereof) is an ARMA process. We describe the resulting model as a VT-ARMA process.

It is important to state that the use of the Gaussian process (Z_t) as the fundamental building block of the VT-ARMA process in Algorithm 1 has no effect on the marginal distribution of (X_t), which is F_X as specified in the final step of the algorithm. The process (Z_t) is exploited *only for its serial dependence structure*, which is described by a family of finite-dimensional Gaussian copulas; this dependence structure is applied to the volatility proxy process.

Algorithm 1:

1. Generate (Z_t) as a causal and invertible Gaussian ARMA process of order (p, q) with mean zero and variance one.
2. Form the volatility PIT process (V_t) where $V_t = \Phi(Z_t)$ for all t.
3. Generate a process of iid Bernoulli variables (Y_t) such that $P(Y_t = 1) = 0.5$.
4. Form the PIT process (U_t) using the transformation $U_t = 0.5(1 - V_t)^{I_{\{Y_t=0\}}}(1 + V_t)^{I_{\{Y_t=1\}}}$.
5. Form the process (X_t) by setting $X_t = F_X^{-1}(U_t)$.

Figure 2 shows a symmetric VT-ARMA(1,1) process with ARMA parameters $\alpha_1 = 0.95$ and $\beta_1 = -0.85$; such a model often works well for financial return data. Some intuition for this observation can be gained from the fact that the popular GARCH(1,1) model is known to have the structure of an ARMA(1,1) model for the squared data process; see, for example, McNeil et al. (2015) (Section 4.2) for more details.

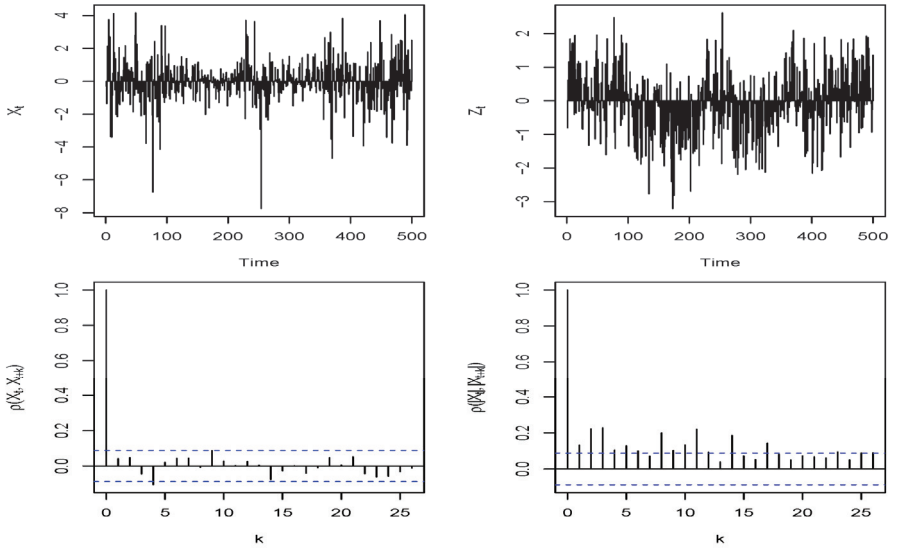

Figure 2. Realizations of length $n = 500$ of (X_t) and (Z_t) for a VT-ARMA(1,1) process with a marginal Student t distribution with $\nu = 3$ degrees of freedom and ARMA parameters $\alpha = 0.95$ and $\beta = -0.85$. ACF plots for (X_t) and $(|X_t|)$ are also shown.

3. V-Transforms

To generalize the class of v-transforms, we admit two forms of asymmetry in the construction described in Section 2: we allow the density f_X to be skewed; we introduce an asymmetric volatility proxy.

Definition 1 (Volatility proxy transformation and profile)**.** *Let T_1 and T_2 be strictly increasing, continuous and differentiable functions on $R^+ = [0, \infty)$ such that $T_1(0) = T_2(0)$. Let $\mu_T \in R$. Any transformation $T : R \to R$ of the form*

$$T(x) = \begin{cases} T_1(\mu_T - x) & x \leq \mu_T \\ T_2(x - \mu_T) & x > \mu_T \end{cases} \tag{3}$$

is a volatility proxy transformation. The parameter μ_T is the change point of T and the associated function $g_T : R^+ \to R^+$, $g_T(x) = T_2^{-1} \circ T_1(x)$ is the profile function of T.

By introducing μ_T, we allow for the possibility that the natural change point may not be identical to zero. By introducing different functions T_1 and T_2 for returns on either side of the change point, we allow the possibility that one or other may contribute more to the volatility proxy. This has a similar economic motivation to the *leverage* effects in GARCH models (Ding et al. 1993); falls in equity prices increase a firm's leverage and increase the volatility of the share price.

Clearly, the profile function of a volatility proxy transformation is a strictly increasing, continuous and differentiable function on R^+ such that $g_T(x) = 0$. In conjunction with μ_T, the profile contains all the information about T that is relevant for constructing v-transforms. In the case of a volatility proxy transformation that is symmetric about μ_T, the profile satisfies $g_T(x) = x$.

The following result shows how v-transforms $V = \mathcal{V}(U)$ can be obtained by considering different continuous distributions F_X and different volatility proxy transformations T of type (3).

Proposition 1. *Let X be a random variable with absolutely continuous and strictly increasing cdf F_X on R and let T be a volatility proxy transformation. Let $U = F_X(X)$ and $V = F_{T(X)}(T(X))$. Then, $V = \mathcal{V}(U)$ where*

$$\mathcal{V}(u) = \begin{cases} F_X\Big(\mu_T + g_T\Big(\mu_T - F_X^{-1}(u)\Big)\Big) - u, & u \le F_X(\mu_T) \\ u - F_X\Big(\mu_T - g_T^{-1}\Big(F_X^{-1}(u) - \mu_T\Big)\Big), & u > F_X(\mu_T)\,. \end{cases} \tag{4}$$

The result implies that any two volatility proxy transformations T and $\widetilde{T}$ which have the same change point μ_T and profile function g_T belong to an equivalence class with respect to the resulting v-transform. This generalizes the idea that $T(x)=|x|$ and $T(x) = x^2$ give the same v-transform in the symmetric case of Section 2. Note also that the volatility proxy transformations $T^{(V)}$ and $T^{(Z)}$ defined by

$$\begin{array}{rcl} T^{(V)}(x) & = & F_{T(X)}(T(x)) = \mathcal{V}(F_X(x)) \\ T^{(Z)}(x) & = & \Phi^{-1}\Big(T^{(V)}(x)\Big) = \Phi^{-1}(\mathcal{V}(F_X(x))) \end{array} \tag{5}$$

are in the same equivalence class as T since they share the same change point and profile function.

Definition 2 (v-transform and fulcrum)**.** *Any transformation $\mathcal{V}$ that can be obtained from Equation (4) by choosing an absolutely continuous and strictly increasing cdf F_X on R and a volatility proxy transformation T is a v-transform. The value $\delta = F_X(\mu_T)$ is the fulcrum of the v-transform.*

3.1. A Flexible Parametric Family

In this section, we derive a family of v-transforms using construction (4) by taking a tractable asymmetric model for F_X using the construction proposed by Fernández and Steel (1998) and by setting $\mu_T = 0$ and $g_T(x) = kx^\xi$ for $k > 0$ and $\xi > 0$. This profile function contains the identity profile $g_T(x) = x$ (corresponding to the symmetric volatility proxy transformation) as a special case, but allows cases where negative or positive returns contribute more to the volatility proxy. The choices we make may at first sight seem rather arbitrary, but the resulting family can in fact assume many of the shapes that are permissible for v-transforms, as we will argue.

Let f_0 be a density that is symmetric about the origin and let $\gamma > 0$ be a scalar parameter. Fernandez and Steel suggested the model

$$f_X(x;\gamma) = \begin{cases} \frac{2\gamma}{1+\gamma^2}\, f_0(\gamma x) & x \le 0 \\ \frac{2\gamma}{1+\gamma^2}\, f_0\Big(\frac{x}{\gamma}\Big) & x > 0\,. \end{cases} \tag{6}$$

This model is often used to obtain skewed normal and skewed Student distributions for use as innovation distributions in econometric models. A model with $\gamma > 1$ is skewed to the right while a model with $\gamma < 1$ is skewed to the left, as might be expected for asset returns. We consider the particular case of a Laplace or double exponential distribution $f_0(x) = 0.5\exp(-|x|)$ which leads to particularly tractable expressions.

Proposition 2. *Let $F_X(x;\gamma)$ be the cdf of the density (6) when $f_0(x) = 0.5\exp(-|x|)$. Set $\mu_T = 0$ and let $g_T(x) = kx^\xi$ for $k, \xi > 0$. The v-transform (4) is given by*

$$\mathcal{V}_{\delta,\kappa,\xi}(u) = \begin{cases} 1 - u - (1-\delta)\exp\Big(-\kappa\Big(-\ln\Big(\frac{u}{\delta}\Big)\Big)^\xi\Big) & u \le \delta, \\ u - \delta\exp\Big(-\kappa^{-1/\xi}\Big(-\ln\Big(\frac{1-u}{1-\delta}\Big)\Big)^{1/\xi}\Big) & u > \delta, \end{cases} \tag{7}$$

where $\delta = F_X(0) = \Big(1+\gamma^2\Big)^{-1} \in (0,1)$ and $\kappa = k/\gamma^{\xi+1} > 0$.

It is remarkable that (7) is a uniformity-preserving transformation. If we set $\xi = 1$ and $\kappa = 1$, we get

$$\mathcal{V}_\delta(u) = \begin{cases} (\delta - u)/\delta & u \le \delta, \\ (u - \delta)/(1 - \delta) & u > \delta \end{cases} \tag{8}$$

which obviously includes the symmetric model $\mathcal{V}_{0.5}(u) = |2u - 1|$. The v-transform $\mathcal{V}_\delta(u)$ in (8) is a very convenient special case, and we refer to it as the *linear* v-transform.

In Figure 3, we show the v-transform $\mathcal{V}_{\delta,\kappa,\xi}$ when $\delta = 0.55$, $\kappa = 1.4$ and $\xi = 0.65$. We will use this particular v-transform to illustrate further properties of v-transforms and find a characterization.

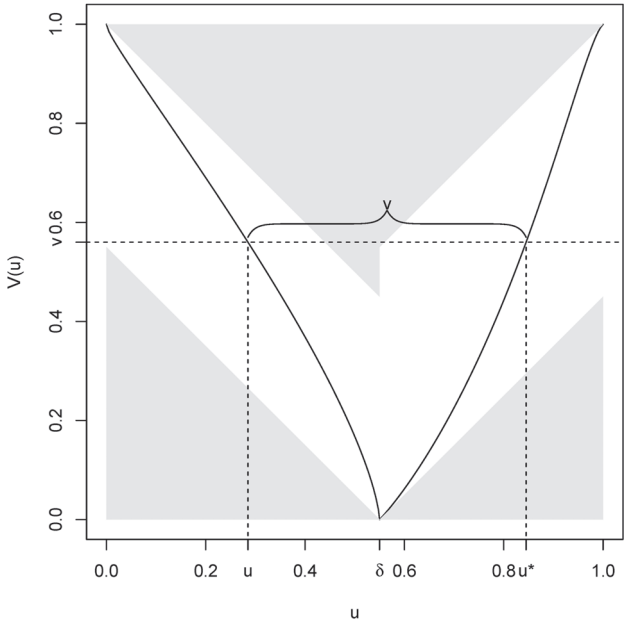

Figure 3. An asymmetric v-transform from the family defined in (7). For any v-transform, if $v = \mathcal{V}(u)$ and u^* is the dual of u, then the points $(u, 0)$, (u, v), $(u^*, 0)$ and (u^*, v) form the vertices of a square. For the given fulcrum δ, a v-transform can never enter the gray shaded area of the plot.

3.2. Characterizing v-Transforms

It is easily verified that any v-transform obtained from (4) consists of two arms or branches, described by continuous and strictly monotonic functions; the left arm is decreasing and the right arm increasing. See Figure 3 for an illustration. At the fulcrum δ, we have $\mathcal{V}(\delta) = 0$. Every point $u \in [0, 1] \backslash \{\delta\}$ has a *dual point* u^* on the opposite side of the fulcrum such that $\mathcal{V}(u^*) = \mathcal{V}(u)$. Dual points can be interpreted as the quantile probability levels of the distribution of X that give rise to the same level of volatility.

We collect these properties together in the following lemma and add one further important property that we refer to as the *square property* of a v-transform; this property places constraints on the shape that v-transforms can take and is illustrated in Figure 3.

Lemma 2. *A v-transform is a mapping* $\mathcal{V} : [0, 1] \to [0, 1]$ *with the following properties:*

1. $\mathcal{V}(0) = \mathcal{V}(1) = 1$;
2. *There exists a point* δ *known as the fulcrum such that* $0 < \delta < 1$ *and* $\mathcal{V}(\delta) = 0$;
3. $\mathcal{V}$ *is continuous;*

4. *$\mathcal{V}$ is strictly decreasing on $[0,\delta]$ and strictly increasing on $[\delta,1]$;*
5. *Every point $u \in [0,1]\backslash\{\delta\}$ has a dual point u^* on the opposite side of the fulcrum satisfying $\mathcal{V}(u) = \mathcal{V}(u^*)$ and $|u^* - u| = \mathcal{V}(u)$ (square property).*

It is instructive to see why the square property must hold. Consider Figure 3 and fix a point $u \in [0,1]\backslash\{\delta\}$ with $\mathcal{V}(u) = v$. Let $U \sim U(0,1)$ and let $V = \mathcal{V}(U)$. The events $\{V \le v\}$ and $\{\min(u,u^*) \le U \le \max(u,u^*)\}$ are the same and hence the uniformity of V under a v-transform implies that

$$v = P(V \le v) = P(\min(u,u^*) \le U \le \max(u,u^*)) = |u^* - u|. \tag{9}$$

The properties in Lemma 2 could be taken as the basis of an alternative definition of a v-transform. In view of (9), it is clear that any mapping $\mathcal{V}$ that has these properties is a uniformity-preserving transformation. We can characterize the mappings $\mathcal{V}$ that have these properties as follows.

Theorem 1. *A mapping $\mathcal{V} : [0,1] \to [0,1]$ has the properties listed in Lemma 2 if and only if it takes the form*

$$\mathcal{V}(u) = \begin{cases} (1-u) - (1-\delta)\Psi\left(\frac{u}{\delta}\right) & u \le \delta, \\ u - \delta\Psi^{-1}\left(\frac{1-u}{1-\delta}\right) & u > \delta, \end{cases} \tag{10}$$

where Ψ is a continuous and strictly increasing distribution function on $[0,1]$.

Our arguments so far show that every v-transform must have the form (10). It remains to verify that every uniformity-preserving transformation of the form (10) can be obtained from construction (4), and this is the purpose of the final result of this section. This allows us to view Definition 2, Lemma 2, and the characterization (10) as three equivalent approaches to the definition of v-transforms.

Proposition 3. *Let $\mathcal{V}$ be a uniformity-preserving transformation of the form (10) and F_X a continuous distribution function. Then, $\mathcal{V}$ can be obtained from construction (4) using any volatility proxy transformation with change point $\mu_T = F_X^{-1}(\delta)$ and profile*

$$g_T(x) = F_X^{-1}(F_X(\mu_T - x) + \mathcal{V}(F_X(\mu_T - x))) - \mu_T, x \ge 0. \tag{11}$$

Henceforth, we can view (10) as the general equation of a v-transform. Distribution functions Ψ on $[0,1]$ can be thought of as *generators* of v-transforms. Comparing (10) with (7), we see that our parametric family $\mathcal{V}_{\delta,\kappa,\xi}$ is generated by $\Psi(x) = \exp(-\kappa(-(\ln x)^{\xi}))$. This is a 2-parameter distribution whose density can assume many different shapes on the unit interval including increasing, decreasing, unimodal, and bathtub-shaped forms. In this respect, it is quite similar to the beta distribution which would yield an alternative family of v-transforms. The uniform distribution function $\Psi(x) = x$ gives the family of linear v-transforms $\mathcal{V}_\delta$.

In applications, we construct models starting from the building blocks of a tractable v-transform $\mathcal{V}$ such as (7) and a distribution F_X; from these, we can always infer an implied profile function g_T using (11). The alternative approach of starting from g_T and F_X and constructing $\mathcal{V}$ via (4) is also possible but can lead to v-transforms that are cumbersome and computationally expensive to evaluate if F_X and its inverse do not have simple closed forms.

3.3. V-Transforms and Copulas

If two uniform random variables are linked by the v-transform $V = \mathcal{V}(U)$, then the joint distribution function of (U,V) is a special kind of copula. In this section, we derive the form of the copula, which facilitates the construction of stochastic processes using v-transforms.

To state the main result, we use the notation $\mathcal{V}^{-1}$ and $\mathcal{V}'$ for the the inverse function and the gradient function of a v-transform $\mathcal{V}$. Although there is no unique inverse $\mathcal{V}^{-1}(v)$ (except when $v = 0$), the fact that the two branches of a v-transform mutually determine each other allows us to define $\mathcal{V}^{-1}(v)$ to be the inverse of the left branch of the v-transform given by $\mathcal{V}^{-1} : [0,1] \to [0,\delta]$, $\mathcal{V}^{-1}(v) = \inf\{u : \mathcal{V}(u) = v\}$. The gradient $\mathcal{V}'(u)$ is defined for all points $u \in [0,1]\backslash\{\delta\}$, and we adopt the convention that $\mathcal{V}'(\delta)$ is the left derivative as $u \to \delta$.

Theorem 2. *Let V and U be random variables related by the v-transform $V = \mathcal{V}(U)$.*

1. *The joint distribution function of (U, V) is given by the copula*

$$C(u,v) = (U \le u, V \le v) = \begin{cases} 0 & u < \mathcal{V}^{-1}(v) \\ u - \mathcal{V}^{-1}(v) & \mathcal{V}^{-1}(v) \le u < \mathcal{V}^{-1}(v) + v \\ v & u \ge \mathcal{V}^{-1}(v) + v\,. \end{cases} \tag{12}$$

2. *Conditional on $V = v$, the distribution of U is given by*

$$U = \begin{cases} \mathcal{V}^{-1}(v) & with probability \Delta(v) if v \neq 0 \\ \mathcal{V}^{-1}(v) + v & with probability 1 - \Delta(v) \text{if} v \neq 0 \\ \delta & if v = 0 \end{cases} \tag{13}$$

where

$$\Delta(v) = -\frac{1}{\mathcal{V}'(\mathcal{V}^{-1}(v))}\,. \tag{14}$$

3. $E(\Delta(V)) = \delta$.

Remark 1. *In the case of the symmetric v-transform $\mathcal{V}(u) = |1 - 2u|$, the copula in (12) takes the form $C(u,v) = \max\left(\min\left(u + \frac{v}{2} - \frac{1}{2}, v\right), 0\right)$. We note that this copula is related to a special case of the tent map copula family $C_\theta^{\mathcal{T}}$ in Rémillard (2013) by $C(u,v) = u - C_1^{\mathcal{T}}(u, 1-v)$.*

For the linear v-transform family, the conditional probability $\Delta(v)$ in (14) satisfies $\Delta(v) = \delta$. This implies that the value of V contains no information about whether U is likely to be below or above the fulcrum; the probability is always the same regardless of V. In general, this is not the case and the value of V does contain information about whether U is large or small.

Part (2) of Theorem 2 is the key to stochastically inverting a v-transform in the general case. Based on this result, we define the concept of stochastic inversion of a v-transform. We refer to the function Δ as the *conditional down probability* of $\mathcal{V}$.

Definition 3 (Stochastic inversion function of a v-transform)**.** *Let $\mathcal{V}$ be a v-transform with conditional down probability Δ. The two-place function $\boldsymbol{\mathcal{V}}^{-1} : [0,1] \times [0,1] \to [0,1]$ defined by*

$$\boldsymbol{\mathcal{V}}^{-1}(v,w) = \begin{cases} \mathcal{V}^{-1}(v) & if w \le \Delta(v) \\ v + \mathcal{V}^{-1}(v) & if w > \Delta(v). \end{cases} \tag{15}$$

is the stochastic inversion function of $\mathcal{V}$.

The following proposition, which generalizes Lemma 1, allows us to construct general asymmetric processes that generalize the process of Algorithm 1.

Proposition 4. *Let V and W be iid $U(0,1)$ variables and let $\mathcal{V}$ be a v-transform with stochastic inversion function $\boldsymbol{\mathcal{V}}$. If $U = \boldsymbol{\mathcal{V}}^{-1}(V, W)$, then $\mathcal{V}(U) = V$ and $U \sim U(0,1)$.*

In Section 4, we apply v-transforms and their stochastic inverses to the terms of time series models. To understand the effect this has on the serial dependencies between random variables, we need to consider multivariate componentwise v-transforms of random vectors with uniform marginal distributions and these can also be represented in terms of copulas. We now give a result which forms the basis for the analysis of serial dependence properties. The first part of the result shows the relationship between copula densities under componentwise v-transforms. The second part shows the relationship under the componentwise stochastic inversion of a v-transform; in this case, we assume that the stochastic inversion of each term takes place independently given $\boldsymbol{V}$ so that all serial dependence comes from $\boldsymbol{V}$.

Theorem 3. *Let $\mathcal{V}$ be a v-transform and let $\boldsymbol{U} = (U_1, \dots, U_d)'$ and $\boldsymbol{V} = (V_1, \dots, V_d)'$ be vectors of uniform random variables with copula densities $c_{\boldsymbol{U}}$ and $c_{\boldsymbol{V}}$, respectively.*

1. *If $\boldsymbol{V} = (\mathcal{V}(U_1), \dots, \mathcal{V}(U_d))'$, then*

$$c_{\boldsymbol{V}}(v_1, \dots, v_d) = \sum_{j_1=1}^{2} \cdots \sum_{j_d=1}^{2} c_{\boldsymbol{U}}\big(u_{1j_1}, \dots, u_{dj_d}\big) \prod_{i=1}^{d} \Delta(v_i)^{I_{\{j_i=1\}}} (1 - \Delta(v_i))^{I_{\{j_i=2\}}} \tag{16}$$

   where $u_{i1} = \mathcal{V}^{-1}(v_i)$ and $u_{i2} = \mathcal{V}^{-1}(v_i) + v_i$ for all $i \in \{1, \dots, d\}$.

2. *If $\boldsymbol{U} = \big(\boldsymbol{\mathcal{V}}^{-1}(V_1, W_1), \dots, \boldsymbol{\mathcal{V}}^{-1}(V_d, W_d)\big)'$ where $W_1, \dots, W_d$ are iid uniform random variables that are also independent of $V_1, \dots, V_d$, then*

$$c_{\boldsymbol{U}}(u_1, \dots, u_d) = c_{\boldsymbol{V}}(\mathcal{V}(u_1), \dots, \mathcal{V}(u_d)). \tag{17}$$

4. VT-ARMA Copula Models

In this section, we study some properties of the class of time series models obtained by the following algorithm, which generalizes Algorithm 1. The models obtained are described as VT-ARMA processes since they are stationary time series constructed using the fundamental building blocks of a v-transform $\mathcal{V}$ and an ARMA process.

We can add any marginal behaviour in the final step, and this allows for an infinitely rich choice. We can, for instance, even impose an infinite-variance or an infinite-mean distribution, such as the Cauchy distribution, and still obtain a strictly stationary process for (X_t). We make the following definitions.

Definition 4 (VT-ARMA and VT-ARMA copula process)**.** *Any stochastic process (X_t) that can be generated using Algorithm 2 by choosing an underlying ARMA process with mean zero and variance one, a v-transform $\mathcal{V}$, and a continuous distribution function F_X is a VT-ARMA process. The process (U_t) obtained at the penultimate step of the algorithm is a VT-ARMA copula process.*

Figure 4 gives an example of a simulated process using Algorithm 2 and the v-transform $\mathcal{V}_{\delta,\kappa,\xi}$ in (7) with $\kappa = 0.9$ and MA parameter $\xi = 1.1$. The marginal distribution is a heavy-tailed skewed Student distribution of type (6) with degrees-of-freedom $\nu = 3$ and skewness $\gamma = 0.8$, which gives rise to more large negative returns than large positive returns. The underlying time series model is an ARMA(1,1) model with AR parameter $\alpha = 0.95$ and MA parameter $\beta = -0.85$. See the caption of the figure for full details of parameters.

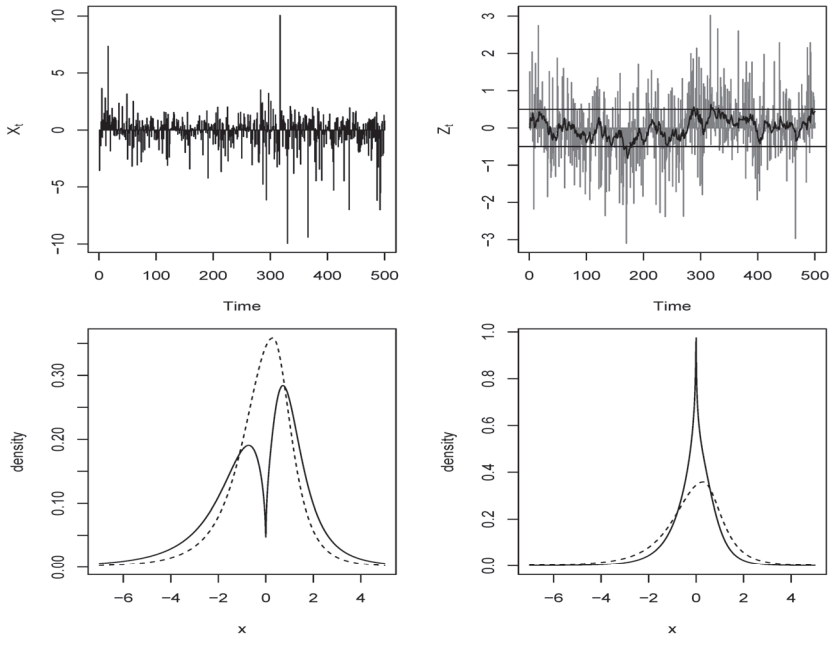

Figure 4. Top left: realization of length $n = 500$ of (X_t) for a process with a marginal skewed Student distribution (parameters: $\nu = 3$, $\gamma = 0.8$, $\mu = 0.3$, $\sigma = 1$) a v-transform of the form (7) (parameters: $\delta = 0.50$, $\kappa = 0.9$, $\xi = 1.1$) and an underlying ARMA process ($\alpha = 0.95$, $\beta = -0.85$, $\sigma_\epsilon = 0.95$). Top right: the underlying ARMA process (Z_t) in gray with the conditional mean (μ_t) superimposed in black; horizontal lines at $\mu_t = 0.5$ (a high value) and $\mu_t = -0.5$ (a low value). The corresponding conditional densities are shown in the bottom figures with the marginal density as a dashed line.

Algorithm 2:

1. Generate (Z_t) as a causal and invertible Gaussian ARMA process of order (p, q) with mean zero and variance one.
2. Form the volatility PIT process (V_t) where $V_t = \Phi(Z_t)$ for all t.
3. Generate iid $U(0, 1)$ random variables (W_t).
4. Form the series PIT process (U_t) by taking the stochastic inverses $U_t = \boldsymbol{\mathcal{V}}^{-1}(V_t, W_t)$.
5. Form the process (X_t) by setting $X_t = F_X^{-1}(U_t)$ for some continuous cdf F_X.

In the remainder of this section, we concentrate on the properties of VT-ARMA copula processes (U_t) from which related properties of VT-ARMA processes (X_t) may be easily inferred.

4.1. Stationary Distribution

The VT-ARMA copula process (U_t) of Definition 4 is a strictly stationary process since the joint distribution of $\left(U_{t_1}, \ldots, U_{t_k}\right)$ for any set of indices $t_1 < \cdots < t_k$ is invariant under time shifts. This property follows easily from the strict stationarity of the underlying ARMA process (Z_t) according to the following result, which uses Theorem 3.

Proposition 5. *Let (U_t) follow a VT-ARMA copula process with v-transform $\boldsymbol{\mathcal{V}}$ and an underlying ARMA(p,q) structure with autocorrelation function $\rho(k)$. The random vector $\left(U_{t_1}, \ldots, U_{t_k}\right)$ for $k \in N$ has joint density*

$c^{Ga}_{P(t_1,\dots,t_k)}(\mathcal{V}(u_1),\dots,\mathcal{V}(u_k))$, *where* $c^{Ga}_{P(t_1,\dots,t_k)}$ *denotes the density of the Gaussian copula* $C^{Ga}_{P(t_1,\dots,t_k)}$ *and* $P(t_1,\cdots,t_k)$ *is a correlation matrix with* (i,j) *element given by* $\rho\big(|t_j - t_i|\big)$.

An expression for the joint density facilitates the calculation of a number of dependence measures for the bivariate marginal distribution of (U_t, U_{t+k}). In the bivariate case, the correlation matrix of the underlying Gaussian copula $C^{\text{Ga}}_{P(t,t+k)}$ contains a single off-diagonal value $\rho(k)$ and we simply write $C^{\text{Ga}}_{\rho(k)}$. The Pearson correlation of (U_t, U_{t+k}) is given by

$$\rho(U_t, U_{t+k}) = 12 \int_0^1 \int_0^1 u_1 u_2 c^{\text{Ga}}_{\rho(k)}(\mathcal{V}(u_1), \mathcal{V}(u_2)) \mathrm{d}u_1 \mathrm{d}u_2 - 3 \,. \tag{18}$$

This value is also the value of the Spearman rank correlation $\rho_S(X_t, X_{t+k})$ for a VT-ARMA process (X_t) with copula process (U_t) (since the Spearman's rank correlation of a pair of continuous random variables is the Pearson correlation of their copula). The calculation of (18) typically requires numerical integration. However, in the special case of the linear v-transform $\mathcal{V}_\delta$ in (8), we can get a simpler expression as shown in the following result.

Proposition 6. *Let* (U_t) *be a VT-ARMA copula process satisfying the assumptions of Proposition 5 with linear v-transform* $\mathcal{V}_\delta$. *Let* (Z_t) *denote the underlying Gaussian ARMA process. Then,*

$$\rho(U_t, U_{t+k}) \quad = \quad (2\delta - 1)^2 \rho_S(Z_t, Z_{t+k}) = \frac{6(2\delta-1)^2 \arcsin\left(\frac{\rho(k)}{2}\right)}{\pi} \,. \tag{19}$$

For the symmetric v-transform $\mathcal{V}_{0.5}$, Equation (19) obviously yields a correlation of zero so that, in this case, the VT-ARMA copula process (U_t) is a white noise with an autocorrelation function that is zero, except at lag zero. However, even a very asymmetric model with $\delta = 0.4$ or $\delta = 0.6$ gives $\rho(U_t, U_{t+k}) = 0.04\rho_S(Z_t, Z_{t+k})$ so that serial correlations tend to be very weak.

When we add a marginal distribution, the resulting process (X_t) has a different auto-correlation function to (U_t), but the same rank autocorrelation function. The symmetric model of Section 2 is a white noise process. General asymmetric processes (X_t) are not perfect white noise processes but have only very weak serial correlation.

4.2. Conditional Distribution

To derive the conditional distribution of a VT-ARMA copula process, we use the vector notation $\boldsymbol{U}_t = (U_1, \dots, U_t)'$ and $\boldsymbol{Z}_t = (Z_1, \dots, Z_t)'$ to denote the history of processes up to time point t and $\boldsymbol{u}_t$ and $\boldsymbol{z}_t$ for realizations. These vectors are related by the componentwise transformation $\boldsymbol{Z}_t = \Phi^{-1}(\mathcal{V}(\boldsymbol{U}_t))$. We assume that all processes have a time index set given by $t \in \{1, 2, \dots\}$.

Proposition 7. *For* $t > 1$, *the conditional density* $f_{U_t|\boldsymbol{U}_{t-1}}(u \mid \boldsymbol{u}_{t-1})$ *is given by*

$$f_{U_t|\boldsymbol{U}_{t-1}}(u \mid \boldsymbol{u}_{t-1}) = \frac{\phi\left(\frac{\Phi^{-1}(\mathcal{V}(u)) - \mu_t}{\sigma_\epsilon}\right)}{\sigma_\epsilon \phi(\Phi^{-1}(\mathcal{V}(u)))} \tag{20}$$

where $\mu_t = E\big(Z_t \mid \boldsymbol{Z}_{t-1} = \Phi^{-1}(\mathcal{V}(\boldsymbol{u}_{t-1}))\big)$ *and* σ_ϵ *is the standard deviation of the innovation process for the ARMA model followed by* (Z_t).

When (Z_t) is iid white noise $\mu_t = 0$, $\sigma_\epsilon = 1$ and (20) reduce to the uniform density $f_{U_t|\boldsymbol{U}_{t-1}}(u \mid \boldsymbol{u}_{t-1}) = 1$ as expected. In the case of the first-order Markov AR(1) model $Z_t = \alpha_1 Z_{t-1} + \epsilon_t$, the conditional mean of Z_t is $\mu_t = \alpha_1 \Phi^{-1}(\mathcal{V}(u_{t-1}))$ and $\sigma_\epsilon^2 = 1 - \alpha_1^2$. The conditional density (20)

can be easily shown to simplify to $f_{U_t|U_{t-1}}(u \mid u_{t-1}) = c^{\mathrm{Ga}}_{\alpha_1}(\mathcal{V}(u), \mathcal{V}(u_{t-1}))$ where $c^{\mathrm{Ga}}_{\alpha_1}(\mathcal{V}(u_1), \mathcal{V}(u_2))$ denotes the copula density derived in Proposition 5. In this special case, the VT-ARMA model falls within the class of first-order Markov copula models considered by Chen and Fan (2006), although the copula is new.

If we add a marginal distribution F_X to the VT-ARMA copula model to obtain a model for (X_t) and use similar notational conventions as above, the resulting VT-ARMA model has conditional density

$$f_{X_t|\boldsymbol{X}_{t-1}}(x \mid \boldsymbol{x}_{t-1}) = f_X(x) f_{U_t|\boldsymbol{U}_{t-1}}(F_X(x) \mid F_X(\boldsymbol{x}_{t-1})) \tag{21}$$

with $f_{U_t|\boldsymbol{U}_{t-1}}$ as in (20). An interesting property of the VT-ARMA process is that the conditional density (21) can have a pronounced bimodality for values of μ_t in excess of zero that is in high volatility situations where the conditional mean of Z_t is higher than the marginal mean value of zero; in low volatility situations, the conditional density appears more concentrated around zero. This phenomenon is illustrated in Figure 4. The bimodality in high volatility situations makes sense: in such cases, it is likely that the next return will be large in absolute value and relatively less likely that it will be close to zero.

The conditional distribution function of (X_t) is $F_{X_t|\boldsymbol{X}_{t-1}}(x \mid \boldsymbol{x}_{t-1}) = F_{U_t|\boldsymbol{U}_{t-1}}(F_X(x) \mid F_X(\boldsymbol{x}_{t-1}))$ and hence the ψ-quantile $x_{\psi,t}$ of $F_{X_t|\boldsymbol{X}_{t-1}}$ can be obtained by solving

$$\psi = F_{U_t|\boldsymbol{U}_{t-1}}\big(F_X\big(x_{\psi,t}\big) \mid F_X(\boldsymbol{x}_{t-1})\big). \tag{22}$$

For $\psi < 0.5$, the negative of this value is often referred to as the conditional $(1-\psi)$-VaR (value-at-risk) at time t in financial applications.

5. Statistical Inference

In the copula approach to dependence modelling, the copula is the object of central interest and marginal distributions are often of secondary importance. A number of different approaches to estimation are found in the literature. As before, let $x_1, \ldots, x_n$ represent realizations of variables $X_1, \ldots, X_n$ from the time series process (X_t).

The semi-parametric approach developed by Genest et al. (1995) is very widely used in copula inference and has been applied by Chen and Fan (2006) to first-order Markov copula models in the time series context. In this approach, the marginal distribution F_X is first estimated non-parametrically using the scaled empirical distribution function $F_n^{(X)}$ (see definition in Section 1) and the data are transformed onto the $(0,1)$ scale. This has the effect of creating pseudo-copula data $u_t = \mathrm{rank}(x_t)/(n+1)$ where $\mathrm{rank}(x_t)$ denotes the rank of x_t within the sample. The copula is fitted to the pseudo-copula data by maximum likelihood (ML).

As an alternative, the inference-functions-for-margins (IFM) approach of Joe (2015) could be applied. This is also a two-step method although in this case a parametric model $\hat{F}_X$ is estimated under an iid assumption in the first step and the copula is fitted to the data $u_t = \hat{F}_X(x_t)$ in the second step.

The approach we adopt for our empirical example is to first use the semi-parametric approach to determine a reasonable copula process, then to estimate marginal parameters under an iid assumption, and finally to estimate all parameters jointly using the parameter estimates from the previous steps as starting values.

We concentrate on the mechanics of deriving maximum likelihood estimates (MLEs). The problem of establishing the asymptotic properties of the MLEs in our setting is a difficult one. It is similar to, but appears to be more technically challenging than, the problem of showing consistency and efficiency of MLEs for a Box-Cox-transformed Gaussian ARMA process, as discussed in Terasaka and Hosoya (2007). We are also working with a componentwise transformed ARMA process, although, in our case, the transformation $(X_t) \to (Z_t)$ is via the nonlinear, non-increasing volatility proxy transformation

$T^{(Z)}(x)$ in (5), which is not differentiable at the change point μ_T. We have, however, run extensive simulations which suggests good behaviour of the MLEs in large samples.

5.1. Maximum Likelihood Estimation of the VT-ARMA Copula Process

We first consider the estimation of the VT-ARMA copula process for a sample of data $u_1, \ldots, u_n$. Let $\boldsymbol{\theta}^{(V)}$ and $\boldsymbol{\theta}^{(A)}$ denote the parameters of the v-transform and ARMA model, respectively. It follows from Theorem 3 (part 2) and Proposition 5 that the log-likelihood for the sample $u_1, \ldots, u_n$ is simply the log density of the Gaussian copula under componentwise inverse v-transformation. This is given by

$$\begin{aligned} L\big(\boldsymbol{\theta}^{(V)}, \boldsymbol{\theta}^{(A)} \mid u_1, \ldots, u_n\big) = L^*\Big(\boldsymbol{\theta}^{(A)} \mid \Phi^{-1}\big(\mathcal{V}_{\boldsymbol{\theta}^{(V)}}(u_1)\big), \ldots, \Phi^{-1}\big(\mathcal{V}_{\boldsymbol{\theta}^{(V)}}(u_n)\big)\Big) \\ - \sum_{t=1}^{n} \ln \phi\Big(\Phi^{-1}\big(\mathcal{V}_{\boldsymbol{\theta}^{(V)}}(u_t)\big)\Big) \end{aligned} \tag{23}$$

where the first term L^* is the log-likelihood for an ARMA model with a standard N(0,1) marginal distribution. Both terms in the log-likelihood (23) are relatively straightforward to evaluate.

The evaluation of the ARMA likelihood $L^*(\boldsymbol{\theta}^{(A)} \mid z_1, \ldots, z_n)$ for parameters $\boldsymbol{\theta}^{(A)}$ and data $z_1, \ldots, z_n$ can be accomplished using the Kalman filter. However, it is important to note that the assumption that the data $z_1, \ldots, z_n$ are standard normal requires a bespoke implementation of the Kalman filter, since standard software always treats the error variance σ_ϵ^2 as a free parameter in the ARMA model. In our case, we need to constrain σ_ϵ^2 to be a function of the ARMA parameters so that $\mathrm{var}(Z_t) = 1$. For example, in the case of an ARMA(1,1) model with AR parameter α_1 and MA parameter β_1, this means that $\sigma_\epsilon^2 = \sigma_\epsilon^2(\alpha_1, \beta_1) = \big(1 - \alpha_1^2\big)/\big(1 + 2\alpha_1\beta_1 + \beta_1^2\big)$. The constraint on σ_ϵ^2 must be incorporated into the state-space representation of the ARMA model.

Model validation tests for the VT-ARMA copula can be based on residuals

$$r_t = z_t - \hat{\mu}_t, z_t = \Phi^{-1}(\mathcal{V}_{\hat{\boldsymbol{\theta}}^{(V)}}(u_t)) \tag{24}$$

where z_t denotes the implied realization of the normalized volatility proxy variable and where an estimate $\hat{\mu}_t$ of the conditional mean $\mu_t = E(Z_t \mid \boldsymbol{Z}_{t-1} = \boldsymbol{z}_t)$ may be obtained as an output of the Kalman filter. The residuals should behave like an iid sample from a normal distribution.

Using the estimated model, it is also possible to implement a likelihood-ratio (LR) test for the presence of stochastic volatility in the data. Under the null hypothesis that $\boldsymbol{\theta}^{(A)} = \mathbf{0}$, the log-likelihood (23) is identically equal to zero. Thus, the size of the maximized log-likelihood $L(\hat{\boldsymbol{\theta}}^{(V)}, \hat{\boldsymbol{\theta}}^{(A)}; u_1, \ldots, u_n)$ provides a measure of the evidence for the presence of stochastic volatility.

5.2. Adding a Marginal Model

If F_X and f_X denote the cdf and density of the marginal model and the parameters are denoted $\boldsymbol{\theta}^{(M)}$, then the full log-likelihood for the data $x_1, \ldots, x_n$ is simply

$$\begin{aligned} L^{\text{full}}(\boldsymbol{\theta} \mid x_1, \ldots, x_n) &= \sum_{t=1}^{n} \ln f_X\big(x_t\,;\, \boldsymbol{\theta}^{(M)}\big) \\ &\quad + L\Big(\boldsymbol{\theta}^{(V)}, \boldsymbol{\theta}^{(A)} \mid F_X\big(x_1\,;\, \boldsymbol{\theta}^{(M)}\big), \ldots, F_X\big(x_n\,;\, \boldsymbol{\theta}^{(M)}\big)\Big) \end{aligned} \tag{25}$$

where the first term is the log-likelihood for a sample of iid data from the marginal distribution F_X and the second term is (23).

When a marginal model is added, we can recover the implied form of the volatility proxy transformation using Proposition 3. If $\hat{\delta}$ is the estimated fulcrum parameter of the v-transform, then the estimated change point is $\hat{\mu}_T = F_X^{-1}(\hat{\delta}; \hat{\boldsymbol{\theta}}^{(M)})$ and the implied profile function is

$$\hat{g}_T(x) \quad = \quad \hat{F}_X^{-1}\Big(\hat{F}_X(\hat{\mu}_T - x) - \mathcal{V}_{\hat{\boldsymbol{\theta}}^{(V)}}\big(\hat{F}_X(\hat{\mu}_T - x)\big)\Big) - \hat{\mu}_T. \tag{26}$$

Note that is is possible to force the change point to be zero in a joint estimation of marginal model and copula by imposing the constraint $F_X(0; \boldsymbol{\theta}^{(M)}) = \delta$ on the fulcrum and marginal parameters during the optimization. However, in our experience, superior fits are obtained when these parameters are unconstrained.

5.3. Example

We analyse $n = 1043$ daily log-returns for the Bitcoin price series for the period 2016–2019; values are multiplied by 100. We first apply the semi-parametric approach of Genest et al. (1995) using the log-likelihood (23) which yields the results in Table 1. Different models are referred to by VT(n)-ARMA(p, q), where (p, q) refers to the ARMA model and n indexes the v-transform: 1 is the linear v-transform $\mathcal{V}_\delta$ in (8); 3 is the three-parameter transform $\mathcal{V}_{\delta,\kappa,\xi}$ in (7); 2 is the two-parameter v-transform given by $\mathcal{V}_{\delta,\kappa} := \mathcal{V}_{\delta,\kappa,1}$. In unreported analyses, we also tried the three-parameter family based on the beta distribution, but this had negligible effect on the results.

Table 1. Analysis of daily Bitcoin return data 2016–2019. Parameter estimates, standard errors (below estimates) and information about the fit: SW denotes Shapiro–Wilks p-value; L is the maximized value of the log-likelihood and AIC is the Akaike information criterion.

Model	α_1	β_1	δ	κ	ξ	SW	L	AIC
VT(1)-ARMA(1,0)	0.283		0.460			0.515	37.59	−71.17
	0.026		0.001					
VT(1)-ARMA(1,1)	0.962	−0.840	0.416			0.197	92.91	−179.81
	0.012	0.028	0.004					
VT(2)-ARMA(1,1)	0.965	−0.847	0.463	0.920		0.385	94.73	−181.45
	0.011	0.026	0.001	0.131				
VT(3)-ARMA(1,1)	0.962	−0.839	0.463	0.881	0.995	0.407	94.82	−179.64
	0.012	0.028	0.001	0.123	0.154			

The column marked L gives the value of the maximized log-likelihood. All values are large and positive showing strong evidence of stochastic volatility in all cases. The model VT(1)-ARMA(1,0) is a first-order Markov model with linear v-transform. The fit of this model is noticeably poorer than the others suggesting that Markov models are insufficient to capture the persistence of stochastic volatility in the data. The column marked SW contains the p-value for a Shapiro–Wilks test of normality applied to the residuals from the VT-ARMA copula model; the result is non-significant in all cases.

According to the AIC values, the VT(2)-ARMA(1,1) is the best model. We experimented with higher order ARMA processes, but this did not lead to further significant improvements. Figure 5 provides a visual of the fit of this model. The pictures in the panels show the QQplot of the residuals against normal, acf plots of the residuals and squared residuals and the estimated conditional mean process $(\hat{\mu}_t)$, which can be taken as an indicator of high and low volatility periods. The residuals and absolute residuals show very little evidence of serial correlation and the QQplot is relatively linear, suggesting that the ARMA filter has been successful in explaining much of the serial dependence structure of the normalized volatility proxy process.

We now add various marginal distributions to the VT(2)-ARMA(1,1) copula model and estimate all parameters of the model jointly. We have experimented with a number of location-scale families including Student-t, Laplace (double exponential), and a double-Weibull family which generalizes the Laplace distribution and is constructed by taking back-to-back Weibull distributions. Estimation results are presented for these three distributions in Table 2. All three marginal distributions are symmetric around their location parameters μ, and no improvement is obtained by adding skewness using the construction of Fernández and Steel (1998) described in Section 3.1; in fact, the Bitcoin returns in this time period show a remarkable degree of symmetry. In the table, the shape and scale parameters of the distributions are denoted η and σ, respectively; in the case of Student, an infinite-variance distribution

with degree-of-freedom parameter $\eta = 1.94$ is fitted, but this model is inferior to the models with Laplace and double-Weibull margins; the latter is the favoured model on the basis of AIC values.

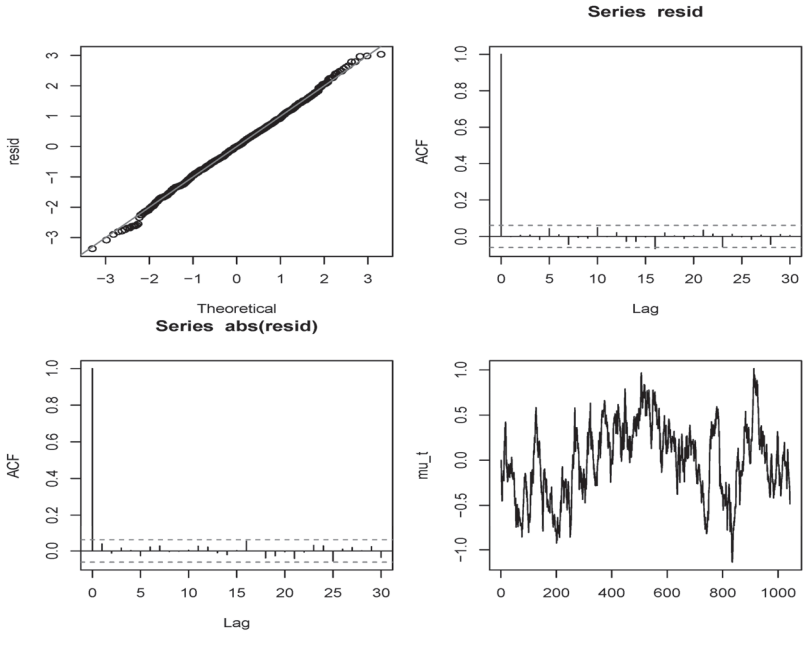

Figure 5. Plots for a VT(2)-ARMA(1,1) model fitted to the Bitcoin return data: QQplot of the residuals against normal (**upper left**); acf of the residuals (**upper right**); acf of the absolute residuals (**lower left**); estimated conditional mean process (μ_t) (**lower right**).

Table 2. VT(2)-ARMA(1,1) model with three different margins: Student-t, Laplace, double Weibull. Parameter estimates, standard errors (alongside estimates) and information about the fit: SW denotes Shapiro–Wilks *p*-value; *L* is the maximized value of the log-likelihood and AIC is the Akaike information criterion.

	Student		**Laplace**		**dWeibull**	
α_1	0.954	0.012	0.953	0.012	0.965	0.021
β_1	−0.842	0.026	−0.847	0.025	−0.847	0.035
δ	0.478	0.001	0.480	0.002	0.463	0.000
κ	0.790	0.118	0.811	0.129	0.939	0.138
η	1.941	0.005			0.844	0.022
μ	0.319	0.002	0.315	0.002	0.192	0.001
σ	2.427	0.003	3.194	0.004	2.803	0.214
SW	0.585		0.551		0.376	
L	−2801.696		−2791.999		−2779.950	
AIC	5617.392		5595.999		5573.899	

Figure 6 shows some aspects of the joint fit for the fully parametric VT(2)-ARMA(1,1) model with double-Weibull margin. A QQplot of the data against the fitted marginal distribution confirms that the double-Weibull is a good marginal model for these data. Although this distribution is sub-exponential (heavier-tailed than exponential), its tails do not follow a power law and it is in the maximum domain of attraction of the Gumbel distribution (see, for example, McNeil et al. 2015, Chapter 5).

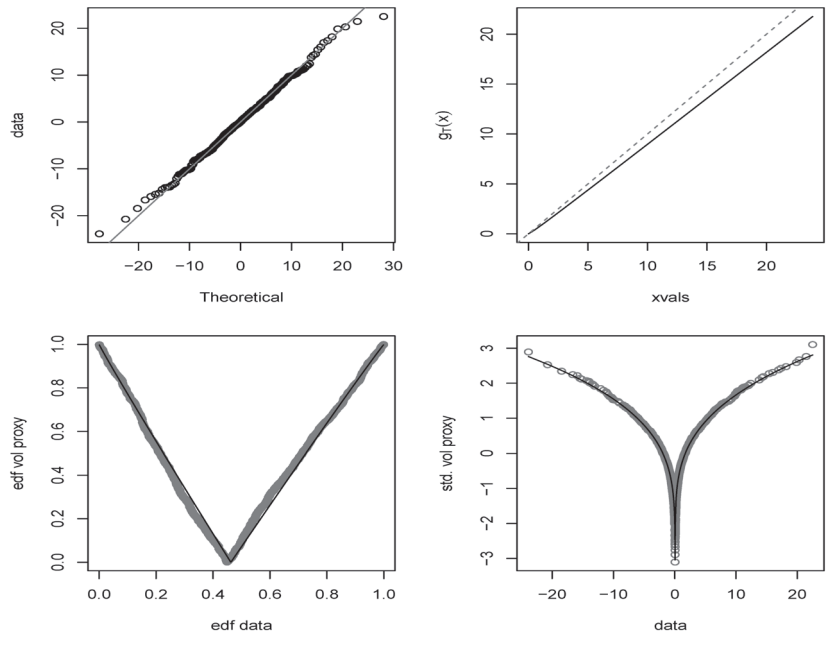

Figure 6. Plots for a VT(2)-ARMA(1,1) model combined with a double Weibull marginal distribution fitted to the Bitcoin return data: QQplot of the data against fitted double Weibull model (**upper left**); estimated volatility proxy profile function g_T (**upper right**); estimated v-transform (**lower left**); implied relationship between data and volatility proxy variable (**lower right**).

Using (26), the implied volatility proxy profile function $\hat{g}_T$ can be constructed and is found to lie just below the line $y = x$ as shown in the upper-right panel. The change point is estimated to be $\hat{\mu}_T = 0.06$. We can also estimate an implied volatility proxy transformation in the equivalence class defined by $\hat{g}_T$ and $\hat{\mu}_T$. We estimate the transformation $T = T^{(Z)}$ in (5) by taking $\hat{T}(x) = \Phi^{-1}(\mathcal{V}_{\hat{\boldsymbol{\theta}}^{(V)}}(F_X(x; \hat{\boldsymbol{\theta}}^{(M)})))$. In the lower-left panel of Figure 6, we show the empirical v-transform formed from the data $(x_t, \hat{T}(x_t))$ together with the fitted parametric v-transform $\mathcal{V}_{\hat{\boldsymbol{\theta}}^{(V)}}$. We recall from Section 1 that the empirical v-transform is the plot (u_t, v_t) where $u_t = F_n^{(X)}(x_t)$ and $v_t = F_n^{(\hat{T}(X))}(\hat{T}(x_t))$. The empirical v-transform and the fitted parametric v-transform show a good degree of correspondence. The lower-right panel of Figure 6 shows the volatility proxy transformation $\hat{T}(x)$ as a function of x superimposed on the points $\left(x_t, \Phi^{-1}(v_t)\right)$. Using the curve, we can compare the effects of, for example, a log-return ($\times$ 100) of -10 and a log-return of 10. For the fitted model, these are 1.55 and 1.66 showing that the up movement is associated with slightly higher volatility.

As a comparison to the VT-ARMA model, we fit standard GARCH(1,1) models using Student-t and generalized error distributions for the innovations; these are standard choices available in the popular `rugarch` package in R. The generalized error distribution (GED) contains normal and Laplace as special cases as well as a model that has a similar tail behaviour to Weibull; note, however, that, by the theory of Mikosch and Stărică (2000), the tails of the marginal distribution of the GARCH decay according to a power law in both cases. The results in Table 3 show that the VT(2)-ARMA(1,1) models with Laplace and double-Weibull marginal distributions outperform both GARCH models in terms of AIC values.

Figure 7 shows the in-sample 95% conditional value-at-risk (VaR) estimate based on the VT(2)-ARMA(1,1) model which has been calculated using (22). For comparison, a dashed line shows the corresponding estimate for the GARCH(1,1) model with GED innovations.

Table 3. Comparison of three VT(2)-ARMA(1,1) models with different marginal distributions with two GARCH(1,1) models with different innovation distributions.

	Parameters	AIC
VT-ARMA (Student)	7	5617.39
VT-ARMA (Laplace)	6	5596.00
VT-ARMA (dWeibull)	7	5573.90
GARCH (Student)	5	5629.02
GARCH (GED)	5	5611.53

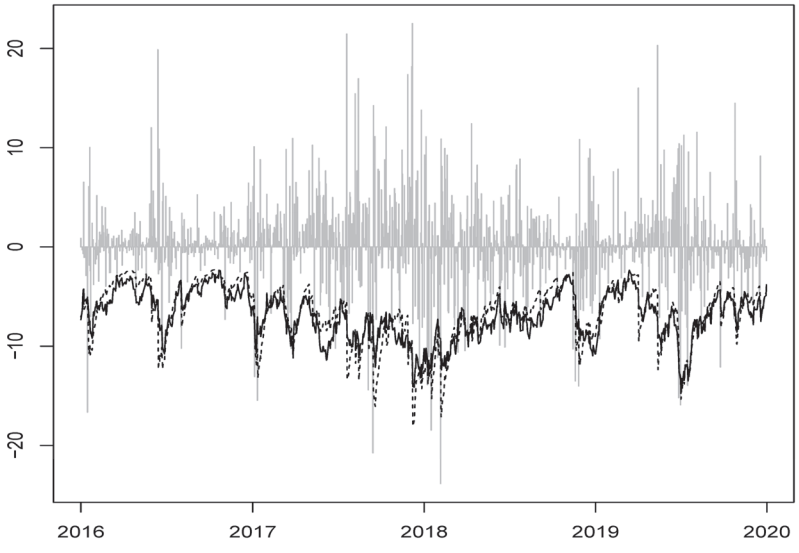

Figure 7. Plot of estimated 95% value-at-risk (VaR) for Bitcoin return data superimposed on log returns. Solid line shows VaR estimated using the VT(2)-ARMA(1,1) model combined with a double-Weibull marginal distribution; the dashed line shows VaR estimated using a GARCH(1,1) model with GED innovation distribution.

Finally, we carry out an out-of-sample comparison of conditional VaR estimates using the same two models. In this analysis, the models are estimated daily throughout the 2016–2019 period using a 1000-day moving data window and one-step-ahead VaR forecasts are calculated. The VT-ARMA model gives 47 exceptions of the 95% VaR and 11 exceptions of the 99% VaR, compared with expected numbers of 52 and 10 for a 1043 day sample, while the GARCH model leads to 57 and 12 exceptions; both models pass binomial tests for these exception counts. In a follow-up paper (Bladt and McNeil 2020), we conduct more extensive out-of-sample backtests for models using v-transforms and copula processes and show that they rival and often outperform forecast models from the extended GARCH family.

6. Conclusions

This paper has proposed a new approach to volatile financial time series in which v-transforms are used to describe the relationship between quantiles of the return distribution and quantiles of the distribution of a predictable volatility proxy variable. We have characterized v-transforms

mathematically and shown that the stochastic inverse of a v-transform may be used to construct stationary models for return series where arbitrary marginal distributions may be coupled with dynamic copula models for the serial dependence in the volatility proxy.

The construction was illustrated using the serial dependence model implied by a Gaussian ARMA process. The resulting class of VT-ARMA processes is able to capture the important features of financial return series including near-zero serial correlation (white noise behaviour) and volatility clustering. Moreover, the models are relatively straightforward to estimate building on the classical maximum-likelihood estimation of an ARMA model using the Kalman filter. This can be accomplished in the stepwise manner that is typical in copula modelling or through joint modelling of the marginal and copula process. The resulting models yield insights into the way that volatility responds to returns of different magnitude and sign and can give estimates of unconditional and conditional quantiles (VaR) for practical risk measurement purposes.

There are many possible uses for VT-ARMA copula processes. Because we have complete control over the marginal distribution, they are very natural candidates for the innovation distribution in other time series models. For example, they could be applied to the innovations of an ARMA model to obtain ARMA models with VT-ARMA errors; this might be particularly appropriate for longer interval returns, such as weekly or monthly returns, where some serial dependence is likely to be present in the raw return data.

Clearly, we could use other copula processes for the volatility PIT process (V_t). The VT-ARMA copula process has some limitations: the radial symmetry of the underlying Gaussian copula means that the serial dependence between large values of the volatility proxy must mirror the serial dependence between small values; moreover, this copula does not admit tail dependence in either tail and it seems plausible that very large values of the volatility proxy might have a tendency to occur in succession.

To extend the class of models based on v-transforms, we can look for models for the volatility PIT process (V_t) with higher dimensional marginal distributions given by asymmetric copulas with upper tail dependence. First-order Markov copula models as developed in Chen and Fan (2006) can give asymmetry and tail dependence, but they cannot model the dependencies at longer lags that we find in empirical data. D-vine copula models can model higher-order Markov dependencies and Bladt and McNeil (2020) show that this is a promising alternative specification for the volatility PIT process.

Funding: This research received no external funding.

Data Availability Statement: The analyses were carried out using R 4.0.2 (R Core Team, 2020) and the `tscopula` package (Alexander J. McNeil and Martin Bladt, 2020) available at https://github.com/ajmcneil/tscopula. The full reproducible code and the data are available at https://github.com/ajmcneil/vtarma.

Acknowledgments: The author is grateful for valuable input from a number of researchers including Hansjoerg Albrecher, Martin Bladt, Valérie Chavez-Demoulin, Alexandra Dias, Christian Genest, Michael Gordy, Yen Hsiao Lok, Johanna Nešlehová, Andrew Patton, and Ruodu Wang. Particular thanks are due to Martin Bladt for providing the Bitcoin data and advice on the data analysis. The paper was completed while the author was a guest at the Forschungsinstitut für Mathematik (FIM) at ETH Zurich.

Conflicts of Interest: The author declares no conflict of interest.

Appendix A. Proofs

Appendix A.1. Proof of Proposition 1

We observe that, for $x \geq 0$,

$$F_{T(X)}(x) = P\big(\mu_T - T_1^{-1}(x) \leq X_t \leq \mu_T + T_2^{-1}(x)\big) = F_X\big(\mu_T + T_2^{-1}(x)\big) - F_X\big(\mu_T - T_1^{-1}(x)\big).$$

$\{X_t \le \mu_T\} \Leftrightarrow \{U \le F_X(\mu_T)\}$ and in this case

$$V = F_{T(X)}(T(X_t)) = F_{T(X)}(T_1(\mu_T - X_t)) = F_X\Big(\mu_T + T_2^{-1}(T_1(\mu_T - X_t))\Big) - F_X(X_t)$$
$$= F_X\Big(\mu_T + g_T\Big(\mu_T - F_X^{-1}(U)\Big)\Big) - U.$$

$\{X_t > \mu_T\} \Leftrightarrow \{U > F_X(\mu_T)\}$ and in this case

$$V = F_{T(X)}(T(X_t)) = F_{T(X)}(T_2(X_t - \mu_T)) = F_X(X_t) - F_X\Big(\mu_T - T_1^{-1}(T_2(X_t - \mu_T))\Big)$$
$$= U - F_X\Big(\mu_T - g_T^{-1}\Big(F_X^{-1}(U) - \mu_T\Big)\Big).$$

Appendix A.2. Proof of Proposition 2

The cumulative distribution function $F_0(x)$ of the double exponential distribution is equal to $0.5e^x$ for $x \le 0$ and $1 - 0.5e^{-x}$ if $x > 0$. It is straightforward to verify that

$$F_X(x;\gamma) = \begin{cases} \delta e^{\gamma x} & x \le 0 \\ 1 - (1-\delta)e^{-\frac{x}{\gamma}} & x > 0 \end{cases} \text{ and} F_X^{-1}(u;\gamma) = \begin{cases} \frac{1}{\gamma}\ln\Big(\frac{u}{\delta}\Big) & u \le \delta \\ -\gamma\ln\Big(\frac{1-u}{1-\delta}\Big) & u > \delta\,. \end{cases}$$

When $g_T(x) = kx^\xi$, we obtain for $u \le \delta$ that

$$\mathcal{V}_{\delta,\kappa,\xi}(u) = F_X\left(\frac{k}{\gamma^\xi}\left(\ln\Big(\frac{\delta}{u}\Big)^\xi\right);\gamma\right) - u = 1 - u - (1-\delta)\exp\left(-\frac{k}{\gamma^{\xi+1}}\Big(-\ln\Big(\frac{u}{\delta}\Big)\Big)^\xi\right).$$

For $u > \delta$, we make a similar calculation.

Appendix A.3. Proof of Theorem 1

It is easy to check that Equation (10) fulfills the list of properties in Lemma 2. We concentrate on showing that a function that has these properties must be of the form (10). It helps to consider the picture of a v-transform in Figure 3. Consider the lines $v = 1 - u$ and $v = \delta - u$ for $u \in [0, \delta]$. The areas above the former and below the latter are shaded gray.

The left branch of the v-transform must start at $(0, 1)$, end at $(\delta, 0)$, and lie strictly between these lines in $(0, \delta)$. Suppose, on the contrary, that $v = \mathcal{V}(u) \le \delta - u$ for $u \in (0, \delta)$. This would imply that the dual point u^* given by $u^* = u + v$ satisfies $u^* \le \delta$ which contradicts the requirement that u^* must be on the opposite side of the fulcrum. Similarly, if $v = \mathcal{V}(u) \ge 1 - u$ for $u \in (0, \delta)$, then $u^* \ge 1$ and this is also not possible; if $u^* = 1$, then $u = 0$, which is a contradiction.

Thus, the curve that links $(0, 1)$ and $(\delta, 0)$ must take the form

$$\mathcal{V}(u) = (\delta - u)\Psi\Big(\frac{u}{\delta}\Big) + (1-u)\Big(1 - \Psi\Big(\frac{u}{\delta}\Big)\Big) = (1-u) - (1-\delta)\Psi\Big(\frac{u}{\delta}\Big)$$

where $\Psi(0) = 0$, $\Psi(1) = 1$ and $0 < \Psi(x) < 1$ for $x \in (0, 1)$. Clearly, Ψ must be continuous to satisfy the conditions of the v-transform. It must also be strictly increasing. If it were not, then the derivative would satisfy $\mathcal{V}'(u) \ge -1$, which is not possible: if at any point $u \in (0, \delta)$, we have $\mathcal{V}'(u) = -1$, then the opposite branch of the v-transform would have to jump vertically at the dual point u^*, contradicting continuity; if $\mathcal{V}'(u) > -1$, then $\mathcal{V}$ would have to be a decreasing function at u^*, which is also a contradiction.

Thus, Ψ fulfills the conditions of a continuous, strictly increasing distribution function on $[0, 1]$, and we have established the necessary form for the left branch equation. To find the value of the right branch equation at $u > \delta$, we invoke the square property. Since $\mathcal{V}(u) = \mathcal{V}(u^*) = \mathcal{V}(u - \mathcal{V}(u))$, we need to solve the equation $x = \mathcal{V}(u - x)$ for $x \in [0, 1]$ using the formula for the left branch equation of $\mathcal{V}$. Thus, we solve $x = 1 - u + x - (1-\delta)\Psi\Big(\frac{u-x}{\delta}\Big)$ for x, and this yields the right branch equation as asserted.

Appendix A.4. Proof of Proposition 3

Let $g_T(x)$ be as given in (11) and let $u(x) = F_X(\mu_T - x)$. For $x \in R^+$, $u(x)$ is a continuous, strictly decreasing function of x starting at $u(0) = \delta$ and decreasing to 0. Since Ψ is a cumulative distribution function, it follows that

$$u^*(x) = u(x) + \mathcal{V}(u(x)) = 1 - (1-\delta)\Psi\left(\frac{u(x)}{\delta}\right)$$

is a continuous, strictly increasing function starting at $u^*(0) = \delta$ and increasing to 1. Hence, $g_T(x) = F_X^{-1}(u^*(x)) - \mu_T$ is continuous and strictly increasing on R^+ with $g_T(0) = 0$ as required of the profile function of a volatility proxy transformation. It remains to check that, if we insert (11) in (4), we recover $\mathcal{V}(u)$, which is straightforward.

Appendix A.5. Proof of Theorem 2

1. For any $0 \le v \le 1$, the event $\{U \le u, V \le v\}$ has zero probability for $u < \mathcal{V}^{-1}(v)$. For $u \ge \mathcal{V}^{-1}(v)$, we have
$$\{U \le u, V \le v\} = \left\{\mathcal{V}^{-1}(v) \le U \le \min\left(u, \mathcal{V}^{-1}(v) + v\right)\right\}$$
and hence $P(U \le u, V \le v) = \min\left(u, \mathcal{V}^{-1}(v) + v\right) - \mathcal{V}^{-1}(v)$ and (12) follows.
2. We can write $P(U \le u, V \le v) = C(u, v)$, where C is the copula given by (12). It follows from the basic properties of a copula that
$$P(U \le u, V = v) = \frac{\mathrm{d}}{\mathrm{d}v}C(u,v) = \begin{cases} 0 & u < \mathcal{V}^{-1}(v) \\ -\frac{\mathrm{d}}{\mathrm{d}v}\mathcal{V}^{-1}(v) & \mathcal{V}^{-1}(v) \le u < \mathcal{V}^{-1}(v) + v \\ 1 & u \ge \mathcal{V}^{-1}(v) + v \end{cases}$$
This is the distribution function of a binomial distribution, and it must be the case that $\Delta(v) = -\frac{\mathrm{d}}{\mathrm{d}v}\mathcal{V}^{-1}(v)$. Equation (14) follows by differentiating the inverse.
3. Finally, $E(\Delta(V)) = \delta$ is easily verified by making the substitution $x = \mathcal{V}^{-1}(v)$ in the integral $E(\Delta(V)) = -\int_0^1 \frac{1}{\mathcal{V}'(\mathcal{V}^{-1}(v))}\mathrm{d}v$.

Appendix A.6. Proof of Proposition 4

It is obviously true that $\mathcal{V}\left(\boldsymbol{\mathcal{V}}^{-1}(v, W)\right) = v$ for any W. Hence, $\mathcal{V}(U) = \mathcal{V}\left(\boldsymbol{\mathcal{V}}^{-1}(V, W)\right) = V$. The uniformity of U follows from the fact that

$$P\left(\boldsymbol{\mathcal{V}}^{-1}(V,W) = \mathcal{V}^{-1}(v) \mid V = v\right) = P(W \le \Delta(v) \mid V = v) = P(W \le \Delta(v)) = \Delta(v)\,.$$

Hence, the pair of random variables (U, V) has the conditional distribution (13) and is distributed according to the copula C in (12).

Appendix A.7. Proof of Theorem 3

1. Since the event $\{V_i \le v_i\}$ is equal to the event $\left\{\mathcal{V}^{-1}(v_i) \le U_i \le \mathcal{V}^{-1}(v_i) + v_i\right\}$, we first compute the probability of a box $[a_1, b_1] \times \cdots \times [a_d, b_d]$ where $a_i = \mathcal{V}^{-1}(v_i) \le \mathcal{V}^{-1}(v_i) + v_i = b_i$. The standard formula for such probabilities implies that the copulas $C_{\boldsymbol{V}}$ and $C_{\boldsymbol{U}}$ are related by
$$C_{\boldsymbol{V}}(v_1, \ldots, v_d) = \sum_{j_1=1}^{2} \cdots \sum_{j_d=1}^{2} (-1)^{j_1+\cdots+j_d} C_{\boldsymbol{U}}\left(u_{1j_1}, \ldots, u_{dj_d}\right);$$

see, for example, McNeil et al. (2015), p. 221. Thus, the copula densities are related by

$$c_{\boldsymbol{V}}(v_1,\ldots,v_d) = \sum_{j_1=1}^{2}\cdots\sum_{j_d=1}^{2} c_{\boldsymbol{U}}\big(u_{1j_1},\ldots,u_{dj_d}\big)\prod_{i=1}^{d}\frac{\mathrm{d}}{\mathrm{d}v_i}(-1)^{j_i}u_{ij_i},$$

and the result follows if we use (14) to calculate that

$$\frac{\mathrm{d}}{\mathrm{d}v_i}(-1)^j u_{ij} = \begin{cases} \frac{\mathrm{d}}{\mathrm{d}v_i}\big(-\mathcal{V}^{-1}(v_i)\big) = \Delta(v_i) & \text{if} j=1,\\ \frac{\mathrm{d}}{\mathrm{d}v_i}\big(v_i+\mathcal{V}^{-1}(v_i)\big) = 1-\Delta(v_i) & \text{if} j=2. \end{cases}$$

2. For the point $(u_1,\ldots,u_d)\in[0,1]^d$, we consider the set of events $A_i(u_i)$ defined by

$$A_i(u_i) = \begin{cases} \{U_i \le u_i\} & \text{if} u_i \le \delta\\ \{U_i > u_i\} & \text{if} u_i > \delta \end{cases}$$

The probability $P(A_1(u_1),\ldots,A_d(u_d))$ is the probability of an orthant defined by the point $(u_1,\ldots,u_d)$ and the copula density at this point is given by

$$c_{\boldsymbol{U}}(u_1,\ldots,u_d) = (-1)^{\sum_{i=1}^{d} I_{\{u_i>\delta\}}}\frac{\mathrm{d}^d}{\mathrm{d}u_1\cdots\mathrm{d}u_d}P\left(\bigcap_{i=1}^{d}A_i(u_i)\right).$$

The event $A_i(u_i)$ can be written

$$A_i(u_i) = \begin{cases} \{V_i \ge \mathcal{V}(u_i), W_i \le \Delta(V_i)\} & \text{if} u_i \le \delta\\ \{V_i > \mathcal{V}(u_i), W_i > \Delta(V_i)\} & \text{if} u_i > \delta \end{cases}$$

and hence we can use Theorem 2 to write

$$P\left(\bigcap_{i=1}^{d}A_i(u_i)\right) = \int_{\mathcal{V}(u_1)}^{1}\cdots\int_{\mathcal{V}(u_d)}^{1} c_{\boldsymbol{V}}(v_1,\ldots,v_d)\prod_{i=1}^{d}\Delta(v_i)^{I_{\{u_i\le\delta\}}}(1-\Delta(v_i))^{I_{\{u_i>\delta\}}}\mathrm{d}v_1\cdots\mathrm{d}v_d\,.$$

The derivative is given by

$$\frac{\mathrm{d}^d}{\mathrm{d}u_1\cdots\mathrm{d}u_d}P\left(\bigcap_{i=1}^{d}A_i(u_i)\right) = (-1)^d c_{\boldsymbol{V}}(\mathcal{V}(u_1),\ldots,\mathcal{V}(u_d))\prod_{i=1}^{d}p(u_i)^{I_{\{u_i\le\delta\}}}(1-p(u_i))^{I_{\{u_i>\delta\}}}\mathcal{V}'(u_i)$$

where $p(u_i)=\Delta(\mathcal{V}(u_i))$ and hence we obtain

$$c_{\boldsymbol{U}}(u_1,\ldots,u_d) = c_{\boldsymbol{V}}(\mathcal{V}(u_1),\ldots,\mathcal{V}(u_d))\prod_{i=1}^{d}(-p(u_i))^{I_{\{u_i\le\delta\}}}(1-p(u_i))^{I_{\{u_i>\delta\}}}\mathcal{V}'(u_i).$$

It remains to verify that each of the terms in the product is identically equal to 1. For $u_i\le\delta$, this follows easily from (14) since $-p(u_i) = -\Delta(\mathcal{V}(u_i)) = 1/\mathcal{V}'(u_i)$. For $u_i>\delta$, we need an expression for the derivative of the right branch equation. Since $\mathcal{V}(u_i)=\mathcal{V}(u_i-\mathcal{V}(u_i))$, we obtain

$$\mathcal{V}'(u_i) = \mathcal{V}'(u_i-\mathcal{V}(u_i))(1-\mathcal{V}'(u_i)) = \mathcal{V}'\big(u_i^*\big)(1-\mathcal{V}'(u_i)) \Longrightarrow \mathcal{V}'(u_i) = \frac{\mathcal{V}'\big(u_i^*\big)}{1+\mathcal{V}'\big(u_i^*\big)}$$

implying that

$$1-p(u_i)=1-\Delta(\mathcal{V}(u_i))=1-\Delta\Big(\mathcal{V}\Big(u_i^*\Big)\Big)=1+\frac{1}{\mathcal{V}'\Big(u_i^*\Big)}=\frac{1+\mathcal{V}'\Big(u_i^*\Big)}{\mathcal{V}'\Big(u_i^*\Big)}=\frac{1}{\mathcal{V}'(u_i)}\,.$$

Appendix A.8. Proof of Proposition 5

Let $V_t=\mathcal{V}(U_t)$ and $Z_t=\Phi^{-1}(V_t)$ as usual. The process (Z_t) is an ARMA process with acf $\rho(k)$ and hence $\big(Z_{t_1},\dots,Z_{t_k}\big)$ are jointly standard normally distributed with correlation matrix $P(t_1,\dots,t_k)$. This implies that the joint distribution function of $\big(V_{t_1},\dots,V_{t_k}\big)$ is the Gaussian copula with density $c^{\mathrm{Ga}}_{P(t_1,\dots,t_k)}$ and hence by Part 2 of Theorem 3 the joint distribution function of $\big(U_{t_1},\dots,U_{t_k}\big)$ is the copula with density $c^{\mathrm{Ga}}_{P(t_1,\dots,t_k)}(\mathcal{V}(u_1),\dots,\mathcal{V}(u_k))$.

Appendix A.9. Proof of Proposition 6

We split the integral in (18) into four parts. First, observe that, by making the substitutions $v_1=\mathcal{V}(u_1)=1-u_1/\delta$ and $v_2=\mathcal{V}(u_2)=1-u_2/\delta$ on $[0,\delta]\times[0,\delta]$, we get

$$\begin{aligned}\int_0^\delta\int_0^\delta u_1u_2c^{\mathrm{Ga}}_{\rho(k)}(\mathcal{V}(u_1),\mathcal{V}(u_2))\mathrm{d}u_1\mathrm{d}u_2&=\delta^4\int_0^1\int_0^1(1-v_1)(1-v_2)c^{\mathrm{Ga}}_{\rho(k)}(v_1,v_2)\mathrm{d}v_1\mathrm{d}v_2\\&=\delta^4E((1-V_t)(1-V_{t+k}))\\&=\delta^4(1-E(V_t)-E(V_{t+k})+E(V_tV_{t+k}))=\delta^4E(V_tV_{t+k})\end{aligned}$$

where (V_t,V_{t+k}) has joint distribution given by the Gaussian copula $C^{\mathrm{Ga}}_{\rho(k)}$. Similarly, by making the substitutions $v_1=\mathcal{V}(u_1)=1-u_1/\delta$ and $v_2=\mathcal{V}(u_2)=(u_2-\delta)/(1-\delta)$ on $[0,\delta]\times[\delta,1]$, we get

$$\begin{aligned}&\int_0^\delta\int_\delta^1u_1u_2c^{\mathrm{Ga}}_{\rho(k)}(\mathcal{V}(u_1),\mathcal{V}(u_2))\mathrm{d}u_1\mathrm{d}u_2\\&=\int_0^1\int_0^1\delta^2(1-\delta)(1-v_1)(\delta+(1-\delta)v_2)c^{\mathrm{Ga}}_{\rho(k)}(v_1,v_2)\mathrm{d}v_1\mathrm{d}v_2\\&=\delta^3(1-\delta)E(1-V_t)+\delta^2(1-\delta)^2E((1-V_t)V_{t+k})=\tfrac{\delta^2(1-\delta)}{2}-\delta^2(1-\delta)^2E(V_tV_{t+k})\end{aligned}$$

and the same value is obtained on the quadrant $[\delta,1]\times[0,\delta]$. Finally, making the substitutions $v_1=\mathcal{V}(u_1)=(u_1-\delta)/(1-\delta)$ and $v_2=\mathcal{V}(u_2)=(u_2-\delta)/(1-\delta)$ on $[\delta,1]\times[\delta,1]$, we get

$$\begin{aligned}&\int_\delta^1\int_\delta^1u_1u_2c^{\mathrm{Ga}}_{\rho(k)}(\mathcal{V}(u_1),\mathcal{V}(u_2))\mathrm{d}u_1\mathrm{d}u_2\\&=\int_0^1\int_0^1(1-\delta)^2(\delta+(1-\delta)v_1)(\delta+(1-\delta)v_2)c^{\mathrm{Ga}}_{\rho(k)}(v_1,v_2)\mathrm{d}v_1\mathrm{d}v_2\\&=\int_0^1\int_0^1(1-\delta)^2\Big(\delta^2+\delta(1-\delta)v_1+\delta(1-\delta)v_2+(1-\delta)^2v_1v_2\Big)c^{\mathrm{Ga}}_{\rho(k)}(v_1,v_2)\mathrm{d}v_1\mathrm{d}v_2\\&=\delta^2(1-\delta)^2+\delta(1-\delta)^3E(V_t)+\delta(1-\delta)^3E(V_{t+k})+(1-\delta)^4E(V_tV_{t+k})\\&=\delta(1-\delta)^2+(1-\delta)^4E(V_tV_{t+k})\end{aligned}$$

Collecting all of these terms together yields

$$\int_0^1\int_0^1u_1u_2c^{\mathrm{Ga}}_{\rho(k)}(\mathcal{V}(u_1),\mathcal{V}(u_2))\mathrm{d}u_1\mathrm{d}u_2=\delta(1-\delta)+(2\delta-1)^2E(V_tV_{t+k})$$

and, since $\rho_S(Z_t, Z_{t+k}) = 12E(V_t V_{t+k}) - 3$, it follows that

$$\begin{aligned}\rho(U_t, U_{t+k}) = 12E(U_t U_{t+k}) - 3 &= 12\int_0^1\int_0^1 u_1 u_2 c^{\mathrm{Ga}}_{\rho(k)}(\mathcal{V}(u_1), \mathcal{V}(u_2))\mathrm{d}u_1\mathrm{d}u_2 - 3\\ &= 12\delta(1-\delta) + 12(2\delta-1)^2 E(V_t V_{t+k}) - 3\\ &= 12\delta(1-\delta) + (2\delta-1)^2(\rho_S(Z_t, Z_{t+k}) + 3) - 3\\ &= (2\delta-1)^2\rho_S(Z_t, Z_{t+k})\,.\end{aligned}$$

The value of Spearman's rho $\rho_S(Z_t, Z_{t+k})$ for the bivariate Gaussian distribution is well known; see, for example, McNeil et al. (2015).

Appendix A.10. Proof of Proposition 7

The conditional density satisfies

$$f_{U_t|\boldsymbol{U}_{t-1}}(u \mid \boldsymbol{u}_{t-1}) = \frac{c_{\boldsymbol{U}_t}(u_1,\ldots,u_{t-1},u)}{c_{\boldsymbol{U}_{t-1}}(u_1,\ldots,u_{t-1})} = \frac{c^{\mathrm{Ga}}_{P(1,\ldots,t)}(\mathcal{V}(u_1),\ldots,\mathcal{V}(u_{t-1}),\mathcal{V}(u))}{c^{\mathrm{Ga}}_{P(1,\ldots,t-1)}(\mathcal{V}(u_1),\ldots,\mathcal{V}(u_{t-1}))}\,.$$

The Gaussian copula density is given in general by

$$c^{\mathrm{Ga}}_P(v_1,\ldots,v_d) = \frac{f_{\boldsymbol{Z}}\big(\Phi^{-1}(v_1),\ldots,\Phi^{-1}(v_d)\big)}{\prod_{i=1}^d \phi(\Phi^{-1}(v_i))}$$

where $\boldsymbol{Z}$ is a multivariate Gaussian vector with standard normal margins and correlation matrix P. Hence, it follows that we can write

$$\begin{aligned}f_{U_t|\boldsymbol{U}_{t-1}}(u \mid \boldsymbol{u}_{t-1}) &= \frac{f_{\boldsymbol{Z}_t}\big(\Phi^{-1}(\mathcal{V}(u_1)),\ldots,\Phi^{-1}(\mathcal{V}(u_{t-1})),\Phi^{-1}(\mathcal{V}(u))\big)}{f_{\boldsymbol{Z}_{t-1}}(\Phi^{-1}(\mathcal{V}(u_1)),\ldots,\Phi^{-1}(\mathcal{V}(u_{t-1})))\phi(\Phi^{-1}(\mathcal{V}(u)))}\\ &= \frac{f_{Z_t|\boldsymbol{Z}_{t-1}}\big(\Phi^{-1}(\mathcal{V}(u))|\Phi^{-1}(\mathcal{V}(\boldsymbol{u}_{t-1}))\big)}{\phi(\Phi^{-1}(\mathcal{V}(u)))}\end{aligned}$$

where $f_{Z_t|\boldsymbol{Z}_{t-1}}$ is the conditional density of the ARMA process, from which (20) follows easily.

References

Aas, Kjersti, Claudia Czado, Arnoldo Frigessi, and Henrik Bakken. 2009. Pair-copula constructions of multiple dependence. *Insurance: Mathematics and Economics* 44: 182–98. [CrossRef]

Andersen, Torben G. 1994. Stochastic autoregressive volatility: A framework for volatility modeling. *Mathematical Finance* 4: 75–102.

Andersen, Torben G., and Luca Benzoni. 2009. Stochastic Volatility. In *Complex Systems in Finance and Econometrics*. Edited by Robert A. Meyers. New York: Springer.

Bedford, Tim, and Roger M. Cooke. 2001. Probability density decomposition for conditionally independent random variables modeled by vines. *Annals of Mathematics and Artificial Intelligence* 32: 245–68. [CrossRef]

Bedford, Tim, and Roger M. Cooke. 2002. Vines—A new graphical model for dependent random variables. *Annals of Statistics* 30: 1031–68. [CrossRef]

Bladt, Martin, and Alexander J. McNeil. 2020. Time series copula models using d-vines and v-transforms: An alternative to GARCH modelling. *arXiv* arXiv:2006.11088.

Bollerslev, Tim. 1986. Generalized autoregressive conditional heteroskedasticity. *Journal of Econometrics* 31: 307–27. [CrossRef]

Bollerslev, Tim, Robert F. Engle, and Daniel B. Nelson. 1994. ARCH models. In *Handbook of Econometrics*. Edited by Robert F. Engle and Daniel L. McFadden. Amsterdam: North-Holland, vol. 4, pp. 2959–3038.

Campbell, John Y., Anrew W. Lo, and A. Craig MacKinlay. 1997. *The Econometrics of Financial Markets*. Princeton: Princeton University Press.

Chen, Xiaohong, and Yanqin Fan. 2006. Estimation of copula-based semiparametric time series models. *Journal of Econometrics* 130: 307–35. [CrossRef]

Chen, Xiaohong, Wei Biao Wu, and Yanping Yi. 2009. Efficient estimation of copula-based semiparametric Markov models. *Annals of Statistics* 37: 4214–53. [CrossRef]

Cont, Rama. 2001. Empirical properties of asset returns: stylized facts and statistical issues. *Quantitative Finance* 1: 223–36. [CrossRef]

Creal, Drew, Siem Jan Koopman, and André Lucas. 2013. Generalized autoregressive score models with applications. *Journal of Applied Econometrics* 28: 777–95. [CrossRef]

Ding, Zhuanxin, Clive W. Granger, and Robert F. Engle. 1993. A long memory property of stock market returns and a new model. *Journal of Empirical Finance* 1: 83–106. [CrossRef]

Domma, Filippo, Sabrina Giordano, and Pier Francesco Perri. 2009. Statistical modeling of temporal dependence in financial data via a copula function. *Communications if Statistics: Simulation and Computation* 38: 703–28. [CrossRef]

Engle, Robert F. 1982. Autoregressive conditional heteroskedasticity with estimates of the variance of United Kingdom inflation. *Journal of the Econometric Society* 50: 987–1008. [CrossRef]

Fan, Yanqin, and Andrew J. Patton. 2014. Copulas in econometrics. *Annual Review of Economics* 6: 179–200. [CrossRef]

Fernández, Carmen, and Mark F. J. Steel. 1998. On Bayesian modeling of fat tails and skewness. *Journal of the American Statistical Association* 93: 359–71.

Genest, Christian, Kilani Ghoudi, and Louis-Paul Rivest. 1995. A semi-parametric estimation procedure of dependence parameters in multivariate families of distributions. *Biometrika* 82: 543–52. [CrossRef]

Glosten, Lawrence R., Ravi Jagannathan, and David E. Runkle. 1993. On the relation between the expected value and the volatility of the nominal excess return on stocks. *The Journal of Finance* 48: 1779–801. [CrossRef]

Joe, Harry. 1996. Families of m-variate distributions with given margins and $m(m-1)/2$ bivariate dependence parameters. In *Distributions with Fixed Marginals and Related Topics*. Edited by Ludger Rüschendorf, Berthold Schweizer and Michael D. Taylor. Lecture Notes–Monograph Series; Hayward: Institute of Mathematical Statistics, vol. 28, pp. 120–41.

Joe, Harry. 2015. *Dependence Modeling with Copulas*. Boca Raton: CRC Press.

Loaiza-Maya, Rubén, Michael S. Smith, and Worapree Maneesoonthorn. 2018. Time series copulas for heteroskedastic data. *Journal of Applied Econometrics* 33: 332–54. [CrossRef]

McNeil, Alexander J., Rüdiger Frey, and Paul Embrechts. 2015. *Quantitative Risk Management: Concepts, Techniques and Tools*, 2nd ed. Princeton: Princeton University Press.

Mikosch, Thomas, and Catalin Stărică. 2000. Limit theory for the sample autocorrelations and extremes of a GARCH(1,1) process. *The Annals of Statistics* 28: 1427–51.

Patton, Andew J. 2012. A review of copula models for economic time series. *Journal of Multivariate Analysis* 110: 4–18. [CrossRef]

Rémillard, Bruno. 2013. *Statistical Methods for Financial Engineering*. London: Chapman & Hall.

Shephard, Neil. 1996. Shephard, Neil 1996. Statistical aspects of ARCH and stochastic volatility. In *Time Series Models in Econometrics, Finance and Other Fields*. Edited by David R. Cox, David V. Hinkley and Ole E. Barndorff-Nielsen. London: Chapman & Hall, pp. 1–55.

Smith, Michael S., Aleksey Min, Carlos Almeida, and Claudia Czado. 2010. Modeling Longitudinal Data Using a Pair-Copula Decomposition of Serial Dependence. *Journal of the American Statistical Association* 105: 1467–79. [CrossRef]

Taylor, Stephen J. 1994. Modeling stochastic volatility: A review and comparative study. *Mathematical Finance* 4: 183–204. [CrossRef]

Terasaka, Takahiro, and Yuzo Hosoya. 2007. A modified Box-Cox transformation in the multivariate ARMA model. *Journal of the Japan Statistical Society* 37: 1–28. [CrossRef]

risks

MDPI

Article

Pricing, Risk and Volatility in Subordinated Market Models

Jean-Philippe Aguilar [1,*], Justin Lars Kirkby [2] and Jan Korbel [3,4,5,6]

[1] Covéa Finance, Quantitative Research Team, 8-12 rue Boissy d'Anglas, FR75008 Paris, France
[2] School of Industrial and Systems Engineering, Georgia Institute of Technology, Atlanta, GA 30318, USA; jkirkby3@gatech.edu
[3] Section for the Science of Complex Systems, Center for Medical Statistics, Informatics, and Intelligent Systems (CeMSIIS), Medical University of Vienna, Spitalgasse 23, 1090 Vienna, Austria; jan.korbel@meduniwien.ac.at
[4] Complexity Science Hub Vienna, Josefstädterstrasse 39, 1080 Vienna, Austria
[5] Faculty of Nuclear Sciences and Physical Engineering, Czech Technical University, 11519 Prague, Czech Republic
[6] The Czech Academy of Sciences, Institute of Information Theory and Automation, Pod Vodárenskou Věží 4, 182 00 Prague 8, Czech Republic
* Correspondence: jean-philippe.aguilar@covea-finance.fr

Received: 26 October 2020; Accepted: 13 November 2020; Published: 17 November 2020

Abstract: We consider several market models, where time is subordinated to a stochastic process. These models are based on various time changes in the Lévy processes driving asset returns, or on fractional extensions of the diffusion equation; they were introduced to capture complex phenomena such as volatility clustering or long memory. After recalling recent results on option pricing in subordinated market models, we establish several analytical formulas for market sensitivities and portfolio performance in this class of models, and discuss some useful approximations when options are not far from the money. We also provide some tools for volatility modelling and delta hedging, as well as comparisons with numerical Fourier techniques.

Keywords: Lévy process; subordination; option pricing; risk sensitivity; stochastic volatility; Greeks; time-change

1. Introduction

In this opening section, we provide a general introduction to the class of subordinated market models; we also present the key points investigated in the paper, as well as the work's overall structure.

1.1. Time Subordination in Financial Modelling

Among the most striking patterns that are observable in financial time series are the phenomena of regime switching, clustering, and long memory or autocorrelation (see e.g., Cont (2007) and references therein). Such stylized facts have been evidenced for several decades, Mandelbrot famously remarking in Mandelbrot (1963) that large price changes tend to cluster together ("*large changes tend to be followed by large changes, of either sign, and small changes tend to be followed by small changes*"), thus creating periods of market turbulence (high volatility) alternating with periods of relative calm (low volatility). These empirical observations can be described, among other approaches, by agent based models focusing on economic interpretation, such as Lux and Marchesi (2000); Niu and Wang (2013), by tools from statistical

mechanics and econophysics (Krawiecki et al. 2002), or by the introduction of multifractals (Calvet and Fischer 2008).

Another prominent approach to describe this subtle volatility behavior consists of introducing a time change in the stochastic process driving the market prices. Besides stochastic volatility, time changed market models also capture several stylized facts, like non-Normality of returns (the presence of jumps, asymmetry) and negative correlation between the returns and their volatility (see a complete overview in Carr and Wu (2004)). They are motivated by the observation that market participants do not operate uniformly through a trading period, but, on the contrary, the volume, and frequency of transactions greatly vary over time. Following the terminology of Geman (2009), the time process is called the stochastic clock, or business time, while the stochastic process for the underlying market (a Brownian motion, or a more general Lévy process) is said to evolve in operational time.

Historically, the first introduction of a time change in a diffusion process goes back to Bochner (1949); it was first applied to financial modeling in Clark (1973) in the context of the cotton futures market and for a continuous-time change. During the late 1990s and early 2000s, the approach was extended to discontinuous time changes, with the introduction of subordinators (i.e., non-negative Lévy processes, see the theoretical details in Bertoin (1999)). In other words, the business time now admits increasing staircase-like realizations, describing peak periods of activity (following, for instance, earning announcements, central bank reports, or major political events) alternating with less busy periods. Perhaps the best-known subordinators are the Gamma process, like in the Variance Gamma (VG) model by Madan et al. (1998), and the inverse Gaussian process, like in the Normal inverse Gaussian (NIG) model by Barndorff-Nielsen (1997). Let us also mention that subordination has been successfully applied in many other fields of applied science. For instance, Gamma subordination has been employed for modeling the deterioration of production equipment in order to optimize their maintenance (see de Jonge et al. (2017) and references therein), and inverse Gaussian subordination was originally introduced in Barndorff-Nielsen (1977) to model the influence of wind on dunes and beach sands.

Recently, a new type of time subordination, based on fractional calculus, has emerged. Indeed, Lévy processes are closely related to fractional calculus because, for many of them (including stable and tempered stable processes), their probability densities satisfy a space fractional diffusion equation (see details and applications to option pricing in Cartea and del-Castillo-Negrete (2007) and in Luchko et al. (2019)). By also allowing the time derivative to be fractional, as, e.g., in Jizba et al. (2018); Kleinert and Korbel (2016); Korbel and Luchko (2016); Tarasov (2019); Tomovski et al. (2020), it provides a new type of subordinated models: while the order of the space fractional derivative controls the heavy tail behavior of the distribution of returns, the order of the time fractional derivative acts as a temporal subordination parameter whose purpose is to capture time-related phenomena, such as temporal risk redistribution. This model, which we shall refer to as the fractional diffusion (FD) model, is an alternative to time-change models, or to subordinated random walks (Gorenflo et al. 2006).

Regarding the practical implementation and valuation of financial derivatives within subordinated market models, the literature is dominated by numerical techniques. In time changed models notably, tools from Fourier transform (Lewis 2001) or Fast Fourier transform (Carr and Madan 1999), and their many refinements, such as the COS method by Fang and Osterlee (2008) or the PROJ method by Kirkby (2015). These methods are popular, notably because such models' characteristic functions are known in relatively simple closed-forms. Similarly, Cui et al. (2019) provides a numerical pricing framework for a general time changed Markov processes, and Li and Linetsky (2014) employs eigenfunction expansion techniques. However, recently, closed-form pricing formulas have been derived, for the VG model in Aguilar (2020a) and for the NIG model in Aguilar (2020b). The technique has also been employed in the FD model, for vanilla payoffs in Aguilar et al. (2018) and for more exotic options in Aguilar (2020c).

In this paper, we extend these pricing tools to the calculation of risk sensitivities and to profit-and-loss (P&L) explanation, and we provide comparisons between time changed models (such as the NIG and the VG models) and the FD model. Like for the pricing case, risk sensitivities in the context of time changed market models (and of Lévy market models in general) are traditionally evaluated by means of numerical methods based on Fourier inversion (Eberlein et al. 2010; Takahashi and Yamazaki 2008); in the present paper, we will therefore show that they can be expressed in a tractable way, under the form of fast convergent series whose terms explicitly depend on the model parameters. This will allow for us to construct and compare the performance of option based portfolios, and discuss, both quantitatively and qualitatively, the impact on the parameters on risks and P&L. Related topics, such as volatility modeling, will also be discussed.

1.2. Contributions of the Paper

Our purpose in the present work is to investigate and provide details on the following key points:

(a) demonstrate that the recent pricing formulas for the VG, NIG and FD models are precise and fast converging, and can be successfully used for other applications (e.g., calculations of volatility curve);
(b) provides efficient closed-form formulas for first and second-order risk sensitivities (Delta, Gamma) and compare them with numerical techniques; and,
(c) deduce from these formulas several practical features regarding delta-hedging policies and portfolio performance.

1.3. Structure of the Paper

The paper is organized as follows: in Section 2 we recall some fundamental concepts on Lévy processes and option pricing and, in Section 3, we introduce the class of subordinated market models and their main implications in financial modeling.Subsequently, in Section 4, we mention the various closed pricing formulas that have been obtained for this class of models. Approximating these formulas when options are not far from the money, we establish formulas for computing the market volatility in this configuration, thus generalizing the usual Black-Scholes implied volatility. In Section 5 (resp. Section 6), we derive the expressions for the first (resp. second) order market sensitivities, and for the P&L of a delta-hedged portfolio; the impact of the subordination parameter is discussed, and a comparison with numerical techniques is provided. Last, Section 7 is dedicated to concluding remarks.

2. Exponential Lévy Processes

Let us start by recalling some fundamentals on Lévy processes (see full details in Sato (1999) and in Cont and Tankov (2004) for their applications to financial modeling) and, following the classical setup of Schoutens (2003), how they are implemented for the purpose of option pricing.

2.1. Basics of Lévy Processes

Let $(\Omega, \mathcal{F}, \{\mathcal{F}_t\}_{t\geq 0}, \mathbb{P})$ be a probability space that is equipped with its natural filtration. Recall that a Lévy process $\{X_t\}_{t\geq 0}$ is a stochastically continuous process satisfying $X_0 = 0$ ($\mathbb{P}$-almost surely), and whose increments are independent and stationary. This implies that the characteristic function $\Psi(u,t) := \mathbb{E}^{\mathbb{P}}\left[e^{iuX_t}\right]$ of a Lévy process has a semi-group structure and it admits an infinitesimal generator $\psi(u)$, called Lévy symbol or characteristic exponent, which satisfies

$$\Psi(u,t) \;=\; e^{t\psi(u)}, \qquad \psi(u) \;:=\; \log \Psi(u,1). \tag{1}$$

The characteristic exponent is entirely determined by the triplet $(a, b, \Pi(\mathrm{d}x))$, which corresponds to Lévy–Khintchine representation

$$\psi(u) \;=\; a\,iu \;-\; \frac{1}{2}b^2u^2 \;+\; \int_{-\infty}^{+\infty}\left(e^{iux} - 1 - iux\mathbb{1}_{\{|x|<1\}}\right)\Pi(\mathrm{d}x), \tag{2}$$

where a is the drift and is b the Brownian (or diffusion) component. The measure $\Pi(\mathrm{d}x)$, assumed to be concentrated on $\mathbb{R}\backslash\{0\}$ and satisfy

$$\int_{-\infty}^{+\infty}\min(1, x^2)\,\Pi(\mathrm{d}x) \;<\; \infty, \tag{3}$$

is called the Lévy measure of the process, and determines its tail behavior and the distribution of jumps. When $\Pi(\mathbb{R}) < \infty$, one speaks of a process with finite activity (or intensity); this is the case for jump-diffusion processes, like in the Kou Model (Kou 2002) or the Merton model (Merton 1976), where only a finite number of jumps can occur on each time interval. When $\Pi(\mathbb{R}) = \infty$, one speaks of a process with infinite activity (or intensity); this class is far richer, because an infinite number of jumps can occur on any finite time interval and, as a consequence, no Brownian component b is even needed to generate a very complex dynamics. A prominent model with infinite activity is the Variance Gamma process, introduced in Madan et al. (1998). When $\Pi(\mathbb{R}_-) = 0$ (i.e., the process has only positive jumps), one speaks of a subordinator.

An important class of Lévy measures, which will be of particular interest to us in this paper, corresponds to the so-called class of tempered stable processes:

$$\Pi(\mathrm{d}x) \;:=\; \left[\frac{c_+e^{-\lambda_+x}}{x^{1+\alpha_+}}\mathbb{1}_{\{x>0\}} \;+\; \frac{c_-e^{-\lambda_-|x|}}{|x|^{1+\alpha_-}}\mathbb{1}_{\{x<0\}}\right]\mathrm{d}x. \tag{4}$$

This class contains several sub-classes, such as the tempered stable subordinators ($c_- = 0$) or the stable processes ($\lambda_+ = \lambda_- = 0$). When $c_+ = c_- := C$, $\alpha_+ = \alpha_- := Y$, $\lambda_- := G$ and $\lambda_+ := M$, one speaks of a CGMY process (introduced in Carr et al. (2002)). By requiring the further restriction that $Y = 0$, we obtain the Variance Gamma process of Madan et al. (1998); the symmetric case $G = M$ was considered earlier in Madan and Seneta (1990). We also note that the CGMY (and VG) models are members of the KoBoL family, see Boyarchenko and Levendorskiĭ (2000).

2.2. Exponential Lévy Motions

Let $T > 0$ and $S : t \in [0, T] \to S_t$ be the market price of some financial asset, seen as the realization of a time dependent random variable $\{S_t\}_{t\in[0,T]}$ on the canonical space $\Omega = \mathbb{R}_+$. We assume that there exists a risk-neutral measure $\mathbb{Q}$ under which the instantaneous variations of S_t can be written down as:

$$\frac{\mathrm{d}S_t}{S_t} \;=\; (r - q)\,\mathrm{d}t \;+\; \mathrm{d}X_t \tag{5}$$

where $r \in \mathbb{R}$ is the risk-free interest rate and $q \geq 0$ is the dividend yield (both being assumed to be deterministic and continuously compounded), and where $\{X_t\}_{t\in[0,T]}$ is a Lévy process. Under the dynamics (5), the terminal market price is given by

$$S_T \;=\; S_te^{(r-q+\omega)\tau+X_\tau}, \tag{6}$$

where $\tau := T - t$ is the time horizon and ω is the martingale adjustment (also called convexity adjustment, or compensator), which is determined by the martingale condition

$$\mathbb{E}^{\mathbb{Q}}\left[S_T \,|\, \mathcal{F}_t\right] \;=\; e^{(r-q)\tau} S_t. \tag{7}$$

Given the form of the exponential process (6), the condition (7) is equivalent to:

$$\omega \;=\; -\psi(-i) \;=\; -\log \mathbb{E}^{\mathbb{P}}\left[e^{X_1}\right]. \tag{8}$$

2.3. Option Pricing

Given a path-independent payoff function $\mathcal{P}$, i.e., a positive function depending only on the terminal value S_T of the market price and on some strike parameters $K_1, \ldots, K_N > 0$, then the value at time t of a contingent claim delivering a payoff $\mathcal{P}$ at its maturity is equal to the following risk-neutral expectation:

$$\mathcal{C} \;=\; \mathbb{E}^{\mathbb{Q}}\left[e^{-r\tau}\mathcal{P}(S_T, K_1, \ldots, K_n) \,|\, \mathcal{F}_t\right]. \tag{9}$$

If the Lévy process $\{X_t\}_{t\in[0,T]}$ admits a density $f(x,t)$, then the conditional expectation (9) can be achieved by integrating all possible realizations for the payoff over the Lévy density, thus resulting in:

$$\mathcal{C} \;=\; e^{-r\tau} \int_{-\infty}^{+\infty} \mathcal{P}(S_t\, e^{(r-q+\omega)\tau + x}, K_1, \ldots, K_n)\, f(x,\tau)\, \mathrm{d}x. \tag{10}$$

3. Subordinated Models

In this section, we introduce the class of subordinated market models, which is, models for which time is driven by a particular subordinator. We also provide a review of their main financial applications.

3.1. Exponential VG Model

3.1.1. Model Characteristics

In the exponential VG model by (Madan et al. 1998), one chooses the Lévy process in (5) to be a VG process; this process is defined by

$$X_t^{(VG)} \;:=\; \theta G_t \;+\; \sigma W_{G_t} \tag{11}$$

where W_t is the standard Wiener process, and $\gamma(t,1,\nu)$ is a Gamma process (i.e., a process whose increments $\gamma(t+h,1,\nu) - \gamma(t,1,\nu)$ follow a Gamma distribution with mean $1 \times h$ and variance $\nu \times h$). It follows from definition (11) that the VG process is actually distributed according to a so-called Normal variance–mean mixture (see Barndorff-Nielsen et al. (1982)), where the mixing distribution is the Gamma distribution; this distribution materializes the business time, and it is a particular case of a tempered stable subordinator, as it admits the following Lévy measure (see Sato (1999) for instance):

$$\Pi_G(\mathrm{d}x) \;=\; \frac{1}{\nu}\,\frac{e^{-\frac{1}{\nu}x}}{x}\,\mathbb{1}_{\{x>0\}}\,\mathrm{d}x. \tag{12}$$

It follows from (12) that $\Pi_G(\mathbb{R}) = \infty$, which means that the Gamma process has infinite activity; note also that the Gamma measure (12) is concentrated around 0, which means that most jumps in the business time are small, and become bigger in the high ν regime. The VG process is actually a

tempered stable process itself (and, more precisely, a CGMY process), its Lévy measure admitting the following representation:

$$\Pi_{VG}(\mathrm{d}x) = \frac{e^{\frac{\theta x}{\sigma^2}}}{\nu|x|} e^{-\frac{\sqrt{\frac{\theta^2}{\sigma^2}+\frac{2}{\nu}}}{\sigma}|x|}\,\mathrm{d}x. \tag{13}$$

Note that (13) is symmetric around the origin when $\theta = 0$ (i.e., positive and negative jumps in asset prices occur with the same probability). The density function of the VG process is obtained by integrating the normal density conditionally to the Gamma time-change, and it reads:

$$f_{VG}(x,t) = \frac{2e^{\theta\frac{x}{\sigma^2}}}{\nu^{\frac{t}{\nu}}\sqrt{2\pi}\sigma\Gamma(\frac{t}{\nu})}\left(\frac{x^2}{\frac{2\sigma^2}{\nu}+\theta^2}\right)^{\frac{t}{2\nu}-\frac{1}{4}} K_{\frac{t}{\nu}-\frac{1}{2}}\left(\frac{1}{\sigma^2}\sqrt{\frac{2\sigma^2}{\nu}+\theta^2}|x|\right) \tag{14}$$

where $K_a(X)$ denotes the modified Bessel function of the second kind, sometimes also called MacDonald function (see definition and properties in Abramowitz and Stegun (1972)). The Lévy symbol is known in the exact form:

$$\psi_{VG}(u) = -\frac{1}{\nu}\log\left(1 - i\theta\nu u + \frac{\sigma^2\nu}{2}u^2\right), \tag{15}$$

allowing for a simple representation for the VG martingale adjustment:

$$\omega_{VG} = -\psi_{VG}(-i) = \frac{1}{\nu}\log\left(1 - \theta\nu - \frac{\sigma^2\nu}{2}\right). \tag{16}$$

Remark 1. *Note that, when $\theta = 0$ and $\nu \to \infty$, then $\omega_{VG} \to -\frac{\sigma^2}{2}$, which is the usual Gaussian adjustment, and, in this limit, the exponential VG model degenerates into the Black–Scholes model (Black and Scholes 1973). The limiting regime, $VG(\sigma,\nu,0) \xrightarrow{\nu\to 0} BS(\sigma)$, is illustrated in Figure 1 for decreasing ν. In particular, ν directly controls the excess kurtosis for the VG model.*

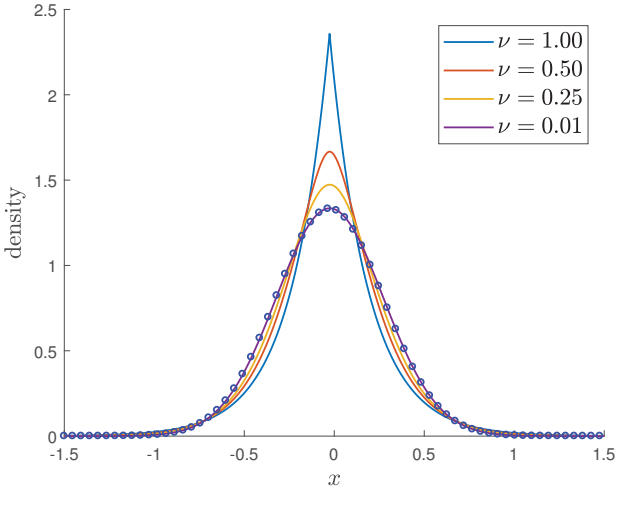

Figure 1. Black–Scholes (circles) as the limit of $\mathrm{VG}(\sigma,\nu,0) \xrightarrow{\nu\to 0} \mathrm{BS}(\sigma)$.

3.1.2. Financial Applications

As already noted, the presence of the subordination parameter ν is particularly attractive for modeling time-induced phenomena, as it allows for a non-uniform passage of time. When ν is small, realizations of the Gamma subordinator are quasi-linear, which corresponds to a situation where the business time is the same as the operational time. On the contrary, for bigger values of ν, realizations of the Gamma process are highly discontinuous and staircase-like (because the process is non decreasing), capturing the alternation of intense and quieter trading periods.

The exponential VG model has been successfully tested on real market data and shown to perform better than Black–Scholes or Jump-Diffusion models in multiple situations, e.g., for European-style options on the HSI index in Lam et al. (2002) or for currency options in Madan and Dual (2005). Several extensions of the model have been subsequently developed, such as the generalization of the subordination to a bivariate or multivariate Brownian motion (Luciano and Schoutens 2006; Semeraro 2008) (with an application to basket options calibration in Linders and Stassen (2015)). Other recent extensions include the possibility of negative jumps in the linear drift rate of the price process in Ivanov (2018). Last, let us also mention that the exponential VG model has also found its way to applications in other fields of quantitative finance, such as credit risk in Fiorani et al. (2007).

3.2. Exponential NIG Model

3.2.1. Model Characteristics

In the exponential NIG model (see Barndorff-Nielsen (1997)), one chooses the Lévy process in (5) to be the NIG process, defined by

$$X_t^{(NIG)} \;=\; \beta\delta^2\, I_t \;+\; \delta W_{I_t} \tag{17}$$

where $\{I_t\}_{t\in[0,T]}$ follows an Inverse Gamma distribution of shape $\delta\sqrt{\alpha^2-\beta^2}$ and mean rate 1. $\alpha > 0$ is a tail or steepness parameter controlling the kurtosis of the NIG distribution; the large α regime gives birth to light tails, while small α corresponds to heavier tails. $\beta \in (-\alpha, \alpha-1)$ is the skewness parameter: $\beta < 0$ (resp. $\beta > 0$) implies that the distribution is skewed to the left (resp. the right), and $\beta = 0$ that the distribution is symmetric. $\delta > 0$ is the scale parameter and it plays an analogous role to the variance term σ^2 in the Normal distribution. Let us mention that a location parameter $\mu \in \mathbb{R}$ can also be incorporated, but it has no impact on option prices (see e.g., Aguilar (2020b)), and, therefore, we will assume that it is equal to 0. Let us also note that, again, we are in the presence of a tempered stable subordination, as the Lévy measure of the Inverse Gamma process $\{I_t\}_{t\in[0,T]}$ satisfies

$$\Pi_{IG}(\mathrm{d}x) \;=\; \frac{e^{-\frac{\delta^2(\alpha^2-\beta^2)}{2}x}}{x^{\frac{3}{2}}}\,\mathbb{1}_{\{x>0\}}\,\mathrm{d}x, \tag{18}$$

while the Lévy measure of the NIG process itself is given by

$$\Pi_{NIG}(\mathrm{d}x) \;:=\; \frac{\alpha\delta}{\pi}\,e^{\beta x}\,\frac{K_1(\alpha|x|)}{|x|}\,\mathrm{d}x. \tag{19}$$

It follows from definition (17) that, like in the VG case, the NIG process is also distributed according to a Normal variance-mean mixture, where the mixing distribution is now the IG distribution; this mixture is a particular case of the more general class of hyperbolic processes (see discussion and applications to finance in Eberlein and Keller (1995)), the mixing distributions in that case being the Generalized Inverse

Gaussian (GIG) distribution. The probability density function for the NIG process is obtained by an integration of the Normal density over the IG distribution and it reads

$$f_{NIG}(x,t) := \frac{\alpha\delta t}{\pi} e^{\delta t\sqrt{\alpha^2-\beta^2}+\beta(x-\mu t)} \frac{K_1\left(\alpha\sqrt{(\delta t)^2+(x-\mu t)^2}\right)}{\sqrt{(\delta t)^2+(x-\mu t)^2}}, \tag{20}$$

and its Lévy symbol is given by

$$\psi_{NIG}(u) = -\delta\left(\sqrt{\alpha^2-(\beta+iu)^2}-\sqrt{\alpha^2-\beta^2}\right). \tag{21}$$

It follows that the NIG convexity adjustment reads

$$\omega_{NIG} = -\psi_{NIG}(-i) = \delta\left(\sqrt{\alpha^2-(\beta+1)^2}-\sqrt{\alpha^2-\beta^2}\right). \tag{22}$$

Remark 2. *When $\alpha\to\infty$ (large steepness regime), then $\omega_{NIG}\to-\frac{\sigma^2}{2}(1+2\beta)$ where $\sigma^2:=\frac{\delta}{\alpha}$; when, furthermore, $\beta=0$ (symmetric process) then one recovers the usual Gaussian adjustment $-\frac{\sigma^2}{2}$ and the exponential NIG model degenerates into the Black–Scholes model.*

3.2.2. Financial Applications

The exponential NIG model has been proved to provide a distinguished fitting to financial data many times. Let us mention, among others, initial tests for daily returns on Danish and German markets in Rydberg (1997) and, subsequently, on the FTSE All-share index (also known as "Actuaries index") in Venter and de Jongh (2002). More recently, the impact of high-frequency trading has also been taken into account, and calibrations have been performed on intraday returns, e.g., in Figueroa-López et al. (2012) for different sampling frequencies. Like in the VG case, multivariate extensions have also been considered (see Luciano and Semeraro (2010) and references therein), and applications to credit risk have also been provided (Luciano 2009).

In Figure 2, we display the log-return density for a VG and NIG example, each being recovered from their characteristic functions while using the method of Kirkby (2015). While both models exhibit heavy-tails, the VG model is characterized by a pronounced cusp, especially for shorter maturities. This near singular behavior presents challenges for Fourier pricing methods, and techniques, such as spectral filtering, have been proposed as a remedy Cui et al. (2017); Phelan et al. (2019); Ruijter et al. (2015). In contrast, the closed form pricing formulas presented here exhibit smooth exponential convergence without special handling, as demonstrated in Section 4.

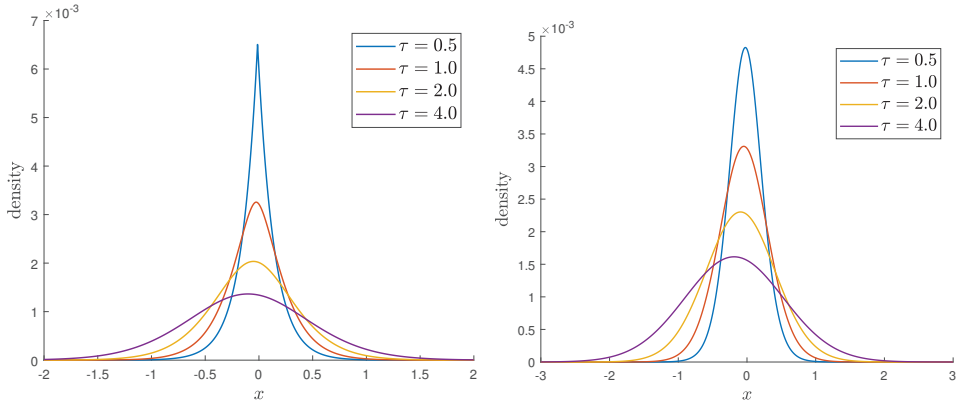

Figure 2. Log-return densities for several maturities τ, for the VG$(0.3, 0.5, 0)$ model (**Left**) and the NIG$(9.0,\ 0,\ 1.2)$ model (**Right**).

3.3. Fractional Diffusion Model

The FD model by Kleinert and Korbel (2016); Korbel and Luchko (2016) aims at generalizing the Lévy stable model by introducing a time-fractional derivative in the equation governing the probability densities, whose order will be interpreted as a subordination parameter. Before introducing the model and its characteristics, we briefly recall some basics of stable distributions and their link with fractional calculus.

3.3.1. Lévy-Stable Processes and Fractional Derivatives

Taking $\lambda_+ = \lambda_- = 0$ and $\alpha_+ = \alpha_- := \alpha \in (0,2)$ in (4) yields the Lévy measure of the stable (or α-stable) process $\{X_t^{(stable)}\}_{t\in[0,T]}$:

$$\Pi_{stable}(x) = \frac{c_-}{|x|^{1+\alpha}}\mathbb{1}_{\{x<0\}} + \frac{c_+}{x^{1+\alpha}}\mathbb{1}_{\{x>0\}}. \tag{23}$$

It is known that, when using Feller's parametrization,

$$\begin{cases} \sigma^\alpha := -(c_+ + c_-)\Gamma(-\alpha)\cos\dfrac{\pi\alpha}{2} \\ \beta := \dfrac{c_+ - c_-}{c_+ + c_-} \end{cases} \tag{24}$$

then the Lévy symbol of the stable process can be written as

$$\psi_{stable}(u) = \sigma^\alpha |u|^\alpha \left(1 - i\beta\tan\frac{\alpha\pi}{2}\mathrm{sgn}u\right) + iau \tag{25}$$

where the drift term a equals the expectation $\mathbb{E}^{\mathbb{Q}}[X_t^{(stable)}]$ as soon as $\alpha \in (1,2)$, that is, for the class of stable Paretian distributions. This class is the one with the greatest financial meaning and historical importance, with initial calibrations going back to Mandelbrot (1963) with $\alpha \simeq 1.7$ for cotton prices; see a comprehensive overview of these distributions in Zolotarev (1986), and of their financial applications in Mittnik and Rachev (2000). However, we may note that, due to the polynomial decay of (23) on the positive axis, the moment generating function and moments of all order do not exist unless $c_+ = 0$, or,

equivalently, in terms of the parametrization (24), $\beta = -1$. This condition, which is known as the maximal negative asymmetry (or skewness) hypothesis, is the key assumption in the Finite Moment Log Stable (FMLS) model by Carr and Wu (2003); it follows from (25) that the FMLS martingale adjustment is

$$\omega_{FMLS} = \frac{\left(\frac{\sigma}{\sqrt{2}}\right)^{\alpha}}{\cos\frac{\pi\alpha}{2}} = \frac{1}{\pi}\Gamma\left(\frac{1-\alpha}{2}\right)\Gamma\left(\frac{1+\alpha}{2}\right)\left(\frac{\sigma}{\sqrt{2}}\right)^{\alpha} \tag{26}$$

where we have introduced the $\sqrt{2}$ normalization, so as to recover the Gaussian adjustment when $\alpha = 2$, and where the second equality is a consequence of the reflection formula for the Gamma function; in the limiting case $\alpha = 2$, the stable distribution degenerates into the Normal one, and, therefore, the FMLS model recovers the Black–Scholes model.

Another consequence of the characteristic exponent (25) with $\beta = -1$ is that the FMLS probability density $f_{FMLS}(x,t)$ satisfies the space fractional diffusion equation

$$\frac{\partial f_{FMLS}}{\partial t} + \omega_\alpha \, \mathcal{D}_x^\alpha f_{FMLS}(x,t) = 0, \quad x \in \mathbb{R}, \quad t \in [0,T], \tag{27}$$

where $\mathcal{D}_x^\alpha :=^{\alpha-2} \mathcal{D}_x^\alpha$ is a particular case of the Riesz–Feller derivative defined (via its Fourier transform) by

$$\widehat{{}^{\theta}\mathcal{D}_x^\alpha f}(u) = |k|^\alpha e^{i(\mathrm{sign}u)\theta\pi/2}\hat{f}(u), \quad |\theta| \le \min\{\alpha, \alpha-2\}. \tag{28}$$

Remark 3. *When $\theta = 0$, the Riesz–Feller derivative is simply called Riesz derivative (as the operator inverse to the Riesz potential, see all details and definitions e.g., in the classical monograph Samko et al. (1993)); the choice $\theta = \alpha - 2$ in Equation (27) is the fractional calculus analogue to the maximal negative asymmetry hypothesis $\beta = -1$. When $\alpha = 2$ then the Riesz-Feller derivative degenerates into the usual second derivative; in that case, (27) becomes the usual heat equation, whose fundamental solution (the heat kernel) is the probability density of the Wiener process.*

3.3.2. Model Characteristics

The FD model generalizes the FMLS model, by allowing the time derivative in the Equation (27) for the probability density to be fractional as well:

$$\left({}^{*}\mathcal{D}_t^\gamma + \omega_{FD}\,\mathcal{D}_x^\alpha\right) f_{FD}(x,t) = 0, \quad x \in \mathbb{R}, \quad t \in [0,T], \tag{29}$$

where $\alpha \in (1,2]$, $\gamma \in (0,\alpha]$ and ${}^{*}\mathcal{D}_\gamma^t$ denotes the Caputo fractional derivative (see the definitions and properties in Li et al. (2011) for instance); when $\gamma = 1$, it coincides with the usual first-order derivative.

The fundamental solution to (29) has been determined in Mainardi et al. (2001) and admits the following Mellin–Barnes representation

$$f_{FD}(x,t) = \frac{1}{\alpha x}\int_{c-i\infty}^{c+i\infty}\left(G_+^*(s)\mathbb{1}_{\{x>0\}} + G_-^*(s)\mathbb{1}_{\{x<0\}}\right)\left(\frac{|x|}{(-\mu_{\alpha,\gamma}t^\gamma)^{\frac{1}{\alpha}}}\right)^s \frac{\mathrm{d}s}{2i\pi}, \tag{30}$$

where we have defined

$$G_+^*(s) := \frac{\Gamma(1-s)}{\Gamma(1-\gamma\frac{s}{\alpha})}, \quad G_-^*(s) := \frac{\Gamma\left(\frac{s}{\alpha}\right)\Gamma\left(1-\frac{s}{\alpha}\right)\Gamma(1-s)}{\Gamma\left(1-\frac{\gamma}{\alpha}s\right)\Gamma\left(\frac{\alpha-1}{\alpha}s\right)\Gamma\left(1-\frac{\alpha-1}{\alpha}s\right)}. \tag{31}$$

By analogy with (10), the price of a contingent claim $\mathcal{C}$ delivering a path independent payoff $\mathcal{P}$ at its maturity is defined to be

$$\mathcal{C} \;=\; e^{-r\tau} \int_{-\infty}^{+\infty} \mathcal{P}(S_t\, e^{(r-q+\omega_{FD})\tau + x}, K_1, \ldots, K_n)\, f_{FD}(x,\tau)\, \mathrm{d}x \tag{32}$$

and the martingale adjustment is defined in terms of the cumulant generating function by

$$\omega_{FD} \;=\; -\log \int_{-\infty}^{+\infty} e^x f_{FD}(x,1)\, \mathrm{d}x. \tag{33}$$

It has been shown in Aguilar et al. (2018) that ω_{FD} can be conveniently expressed in the form of a series

$$\omega_{FD} \;=\; -\log \sum_{n=0}^{\infty} \frac{(-1)^n}{n!} \frac{\Gamma(1+\alpha n)}{\Gamma(1+\gamma\alpha n)}\, \omega_{FMLS}^n \tag{34}$$

where ω_{FMLS} is the FMLS martingale adjustment that is defined in (26), and under the condition that $\gamma \in (1-\frac{1}{\alpha}\,,\, \alpha)$; using a first-order Taylor expansion for $\log(1+u)$ and the expression (26), we obtain the useful approximation:

$$\omega_{FD} \;=\; \frac{1}{\pi} \frac{\Gamma(1+\alpha)\Gamma\left(\frac{1-\alpha}{2}\right)\Gamma\left(\frac{1+\alpha}{2}\right)}{\Gamma(1+\gamma\alpha)} \left(\frac{\sigma}{\sqrt{2}}\right)^{\alpha} + O\left(\sigma^{2\alpha}\right). \tag{35}$$

Remark 4. *When $\alpha = 2$, we are left with*

$$\omega_{FD} \;=\; -\frac{\sigma^2}{\Gamma(1+2\gamma)} + O\left(\sigma^4\right) \tag{36}$$

which coincides with the Black–Scholes adjustment $-\frac{\sigma^2}{2}$ when $\gamma = 1$; we call the situation $\alpha = 2$ and $\gamma \in (0,2]$ the "subordinated Black-Scholes" (sub-BS) model. This is a slight abuse of terminology, because we are not directly in the presence of a subordinating process (i.e., a non decreasing Lévy process) like in the VG and the NIG cases; subordination is achieved here via the introduction of a fractional time derivative whose order γ acts as a supplementary degree of freedom in the time dynamics. When $\gamma = 1$, then the sub-BS model recovers the Black–Scholes model, like the VG model with $\nu \to 0$ and the NIG model with $\alpha \to \infty$; we summarize the situation in Table 1.

Table 1. Some subordinated market models, and their limiting cases. Time changed models (exponential VG and NIG), FD, and sub-BS models recover the Black–Scholes (BS) model for specific values of their subordination parameters.

Subordinated Model	**Limiting Regimes**
$\mathrm{VG}(\sigma,\nu,\theta)$	$\mathrm{VG}(\sigma,\nu,0) \xrightarrow{\nu\to 0} \mathrm{BS}(\sigma)$
$\mathrm{NIG}(\alpha,\beta,\delta)$	$\mathrm{NIG}(\alpha,0,\delta) \xrightarrow{\alpha\to\infty} \mathrm{BS}(\sqrt{\delta/\alpha})$
$\mathrm{FD}(\sigma,\alpha,\gamma)$	$\mathrm{FD}(\sigma,\alpha,\gamma) \xrightarrow{\gamma\to 1} \mathrm{FMLS}(\sigma,\alpha) \xrightarrow{\alpha\to 2} \mathrm{BS}(\sigma)$
$\text{sub-BS}(\sigma,\gamma) := \mathrm{FD}(\sigma,2,\gamma)$	$\text{sub-BS}(\sigma,\gamma) \xrightarrow{\gamma\to 1} \mathrm{BS}(\sigma)$

3.3.3. Financial Applications

The purpose of the FD model is to allow more flexibility in the risk redistribution of returns. When the tail index α departs from 2, the model shifts the returns towards more significant losses due to the presence of the left fat tail. Similarly, when the order of the fractional derivative γ is different from 1, the risk is shifted either towards shorter ($\gamma < 1$) or longer ($\gamma > 1$) maturities: for instance, when $\gamma < 1$, the prices of short term options increase while the prices of long term options slightly decrease (see details, e.g., in Korbel and Luchko (2016)). This behavior is particularly relevant in periods of stressed market conditions: for instance, it has been observed during the 2020 market turmoils (consecutive to the COVID19 pandemics) that short-term implied volatility on the Euro Stoxx 50 index had increased sharply while remaining more stable for long-term options. Several calibrations have been made, notably on market data from turbulent times; in particular, in Kleinert and Korbel (2016), the FD model has been calibrated on data from S&P 500 options traded during November 2008. Such calibrations have shown that α could be quite different from 2: typically, $\alpha \simeq 1.6$–1.7, that turns out to be quite remote from the log-normal hypothesis ($\alpha = 2$), but relatively close to the initial Mandelbrot estimate for the stable law on cotton futures market (Mandelbrot 1963). Moreover, it has been noted that both fractional parameters α and γ appeared to vary simultaneously and in the same direction, leaving the diffusion scaling exponent γ/α relatively stable.

4. Pricing and Volatility Modelling

In this section, we first recall the pricing formulas that were obtained in recent works for the VG, NIG, and FD models, in the case of a European option C delivering a payoff equal to $[S_T - K]^+$ at maturity. Then, we discuss some volatility properties when asset prices are not far from the money. In all of the following, we will denote the forward strike price and the log-forward moneyness by

$$F := Ke^{-r\tau}, \qquad k := \log\frac{S_t}{K} + (r-q)\tau. \tag{37}$$

We will also use the notations

$$k_{VG} := k + \omega_{VG}\tau, \quad k_{NIG} := k + \omega_{NIG}\tau, \quad k_{FD} := k + \omega_{FD}\tau \tag{38}$$

and, in the specific case of the VG model, we will denote

$$\tau_\nu := \frac{\tau}{\nu} - \frac{1}{2} \qquad \sigma_\nu := \sigma\sqrt{\frac{\nu}{2}}. \tag{39}$$

We will assume that the underlying VG (resp. NIG) processes are symmetric, which is, $\theta = 0$ (resp. $\beta = 0$); this is to simplify the notations, but also because symmetric time-changed models extend the Black–Scholes setup (see Table 1). Therefore, we will be better able to compare the results with usual formulas known in the Black-Scholes model. We will also assume that $\tau_\nu \notin \mathbb{Q}$; note that this condition is not restrictive, due to the density of $\mathbb{Q}$ in $\mathbb{R}$: if $\tau_\nu \in \mathbb{Q}$, it is easy to make τ_ν irrational by adding an arbitrary small perturbation, for instance, $\tau_\nu \to \tau_\nu + e/10^{10}$). Last, whenever the exponential NIG model is concerned, we will always assume that

$$\frac{|k_{NIG}|}{\delta\tau} < 1 \tag{40}$$

to ensure the convergence of the series. Please note that this condition is automatically satisfied when options are not far from the money because, in this case, k_{NIG} is small. When S_t is far from K, condition (40) necessitates a restriction on options maturities in order to be satisfied; for a typical set of parameters,

maturities shorter than two or three months should be excluded, which remains a reasonable limitation (see details in Aguilar (2020b)).

For convenience, we summarize the pricing formulas for a European call option.

Formula 1 (European call: pricing formulas)**.**
(i) The value at time t of a European call option in the exponential VG model is:

- *(OTM price) If* $k_{VG} < 0$,

$$C^{-}_{VG}(k_{VG},\sigma_\nu) = \frac{F}{2\Gamma(\frac{\tau}{\nu})}\sum_{\substack{n_1=0\\ n_2=1}}^{\infty}\frac{(-1)^{n_1}}{n_1!}\left[\frac{\Gamma(\frac{-n_1+n_2+1}{2}+\tau_\nu)}{\Gamma(\frac{-n_1+n_2}{2}+1)}\left(\frac{-k_{VG}}{\sigma_\nu}\right)^{n_1}\sigma_\nu^{n_2} + 2\,\frac{\Gamma(-2n_1-n_2-1-2\tau_\nu)}{\Gamma(-n_1+\frac{1}{2}-\tau_\nu)}\left(\frac{-k_{VG}}{\sigma_\nu}\right)^{2n_1+1+2\tau_\nu}(-k_{VG})^{n_2}\right]. \quad (41)$$

- *(ITM price) If* $k_{VG} > 0$,

$$C^{+}_{VG}(k_{VG},\sigma_\nu) = S_t e^{-q\tau} - F - C^{-}_{VG}(k_{VG},-\sigma_\nu). \quad (42)$$

- *(ATM price) If* $k_{VG} = 0$,

$$C^{-}_{VG}(k_{VG},\sigma_\nu) = C^{+}_{VG}(k_{VG},\sigma_\nu) = \frac{F}{2\Gamma(\frac{\tau}{\nu})}\sum_{n=1}^{\infty}\frac{\Gamma(\frac{n+1}{2}+\tau_\nu)}{\Gamma(\frac{n}{2}+1)}\sigma_\nu^{n}. \quad (43)$$

(ii) The value at time t of a European call option in the exponential NIG model is:

$$C_{NIG} = \frac{F\alpha e^{\alpha\delta\tau}}{\sqrt{\pi}}\sum_{\substack{n_1=0\\ n_2=1}}^{\infty}\frac{k_{NIG}^{n_1}}{n_1!\Gamma(1+\frac{-n_1+n_2}{2})}K_{\frac{n_1-n_2+1}{2}}(\alpha\delta\tau)\left(\frac{\delta\tau}{2\alpha}\right)^{\frac{-n_1+n_2+1}{2}}. \quad (44)$$

(iii) The value at time t of a European call option in the FD model is:

$$C_{FD} = \frac{F}{\alpha}\sum_{\substack{n_1=0\\ n_2=1}}^{\infty}\frac{k_{FD}^{n_1}}{n_1!\Gamma(1+\gamma\frac{-n_1+n_2}{\alpha})}(-\omega_{FD}\tau^{\gamma})^{\frac{-n_1+n_2}{\alpha}}. \quad (45)$$

Proof. (i) is proved in Aguilar (2020a), (ii) is proved in Aguilar (2020b) and (iii) in Aguilar et al. (2018). □

The pricing formulas in Formula (1) converge exponentially fast to the true prices, as exhibited in Figure 3 for the VG model (Left). The reference prices are obtained with $N = 50$ terms, and they are verified by the method of Kirkby (2015). Recalling Remark 1, $\mathrm{VG}(\sigma,\nu,0) \xrightarrow{\nu\to 0} \mathrm{BS}(\sigma)$, and fewer terms are required to accurately price the option as $\nu \to 0$. A nearly identical convergence profile is observed for NIG (Right), displayed for several values of α. Recalling that $\mathrm{NIG}(\alpha,0,\delta) \xrightarrow{\alpha\to\infty} \mathrm{BS}(\sqrt{\delta/\alpha})$ (see Table 1), we again see that fewer terms are required in order to accurately price under NIG for larger α.

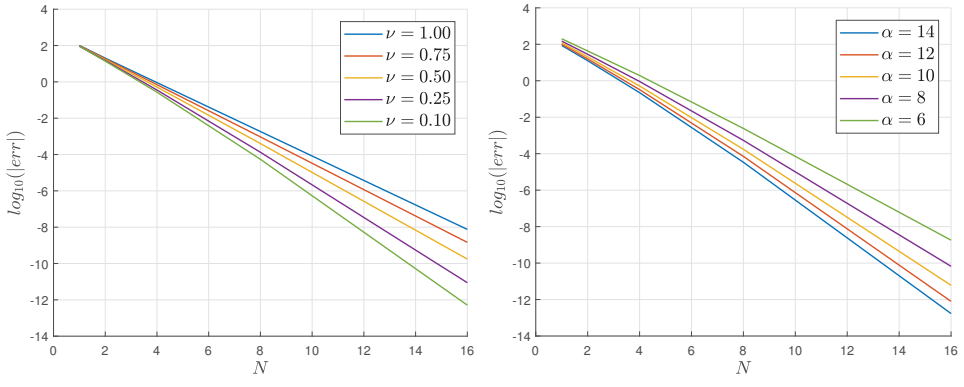

Figure 3. Exponential convergence of pricing Formula (1) for a call option: $\tau = 1, S_t = K = 4000, r = 0.01, q = 0$. **(Left)** VG$(\sigma, \nu, 0)$ with $\sigma = 0.3$. **(Right)** NIG$(\alpha, 0, \delta)$ with $\delta = 1.2$. Here $N = n_1 = n_2$ is the number of terms in the truncated series.

4.1. At-the-Money Forward Approximations

Let us assume that options are at-the-money forward (ATMF), that is, $S_t = F$ (or, equivalently, $k = 0$). If we approximate the European call price in the exponential VG model by the first term of the series (41), which is, the term for $n_1 = 0$, $n_2 = 1$, we obtain (recall that $\Gamma(3/2) = \sqrt{\pi}/2$):

$$C_{VG}^{-} = \frac{S_t}{\sqrt{2\pi}} \frac{\Gamma(\frac{1}{2} + \frac{\tau}{\nu})}{\Gamma(\frac{\tau}{\nu})} \sigma\sqrt{\nu}. \tag{46}$$

Using the Stirling approximation for the Gamma function, we know that

$$\frac{\Gamma\left(\frac{1}{2} + \frac{\tau}{\nu}\right)}{\Gamma\left(\frac{\tau}{\nu}\right)} \underset{\nu \to 0}{\sim} \sqrt{\frac{\tau}{\nu}}, \tag{47}$$

and, therefore, in the low variance regime, we recover the well-known approximation for the ATMF Black–Scholes price

$$C_{BS} \simeq \frac{S_t}{\sqrt{2\pi}} \sigma \sqrt{\tau}. \tag{48}$$

The approximation (48) is often known to market practitioners under the form $C \simeq 0.4 S\sigma\sqrt{\tau}$, because $1/\sqrt{2\pi} = 0.399\ldots$, and it was first derived in Brenner and Subrahmanyam (1994).

In a similar way, the ATMF price in the exponential NIG model can be approximated by the first term of the series (44), resulting in

$$C_{NIG} = \frac{S_t \delta \tau e^{\alpha\delta\tau}}{\pi} K_0(\alpha\delta\tau). \tag{49}$$

Using the large argument behavior of the Bessel function (see Abramowitz and Stegun (1972))

$$K_0(\alpha\delta\tau) \underset{\alpha \to \infty}{\sim} \sqrt{\frac{\pi}{2\alpha\delta\tau}} e^{-\alpha\delta\tau}, \tag{50}$$

it is immediate to see that (49) also recovers the approximation (48) in the large steepness regime, with $\sigma^2 := \delta/\alpha$. Likewise, in the FD model, the ATMF price is approximated by the first term of the series (45), resulting in

$$C_{FD} \;=\; \frac{S_t}{\alpha}\frac{1}{\Gamma(1+\frac{\gamma}{\alpha})}(-\omega_{FD}\tau^{\gamma})^{\frac{1}{\alpha}}. \tag{51}$$

Taking $\alpha = 2$ and using (36), the ATMF price in the sub-BS model becomes

$$C_{sub-BS} \;=\; \frac{S_t}{2}\frac{1}{\Gamma(1+\frac{\gamma}{2})\sqrt{\Gamma(1+2\gamma)}}\sigma\tau^{\frac{\gamma}{2}} \tag{52}$$

which recovers (48) when $\gamma \to 1$.

4.2. Implied Volatility

One key benefit of the subordinated models is their ability to capture the heavy-tails that were observed in financial markets. For the VG model, ν directly controls the tail-heaviness, as illustrated in Figure 4. In particular, large values of ν lead to steep implied volatility smiles. The ATMF prices that are obtained in Section 4.1 are helpful to approximate the implied volatility σ_I of the subordinated models, when S_t is close to F. Denoting by C_t the market price of an ATMF European call option at time t and inverting (46), we immediately see that the VG implied volatility is

$$\sigma_{VG} \;=\; \sqrt{\frac{2\pi}{\nu}}\frac{\Gamma(\frac{\tau}{\nu})}{\Gamma(\frac{1}{2}+\frac{\tau}{\nu})}\frac{C_t}{S_t}, \tag{53}$$

and, similarly, inverting Equation (52), the sub-BS implied volatility is

$$\sigma_{sub-BS} \;=\; \frac{2\sqrt{\Gamma(1+2\gamma)}\Gamma(1+\frac{\gamma}{2})}{\tau^{\frac{\gamma}{2}}}\frac{C_t}{S_t}. \tag{54}$$

As expected, VG and sub-BS both implied volatilities recover the BS implied volatility in their limiting regimes ($\nu \to 0$ and $\gamma \to 1$):

$$\sigma_{BS} \;=\; \sqrt{\frac{2\pi}{\tau}}\frac{C_t}{S_t}. \tag{55}$$

In the NIG case, things are a bit more complicated, because one has to solve

$$\frac{S_t\delta\tau e^{\alpha\delta\tau}}{\pi}K_0(\alpha\delta\tau) \;=\; C_t \tag{56}$$

for which there is no exact solution in an analytical form. Nevertheless, an analytical approximation can be determined by using Hankel's expression for the Bessel function (see Andrews (1992) or any monograph on special functions), which goes, as follows: define, for $\rho \in \mathbb{R}$,

$$\begin{cases} a_0(\rho) \;=\; 1 \\ a_k(\rho) \;=\; \dfrac{(4\rho^2-1^2)(4\rho^2-3^2)\ldots(4\rho^2-(2k-1)^2)}{k!8^k}, \quad k \geq 1, \end{cases} \tag{57}$$

then, for large z and fixed ρ, we have:

$$K_\rho(z) \underset{z\to\infty}{=} \sqrt{\frac{\pi}{2z}}\, e^{-z} \sum_{k=0}^{\infty} \frac{a_k(\rho)}{z^k}. \tag{58}$$

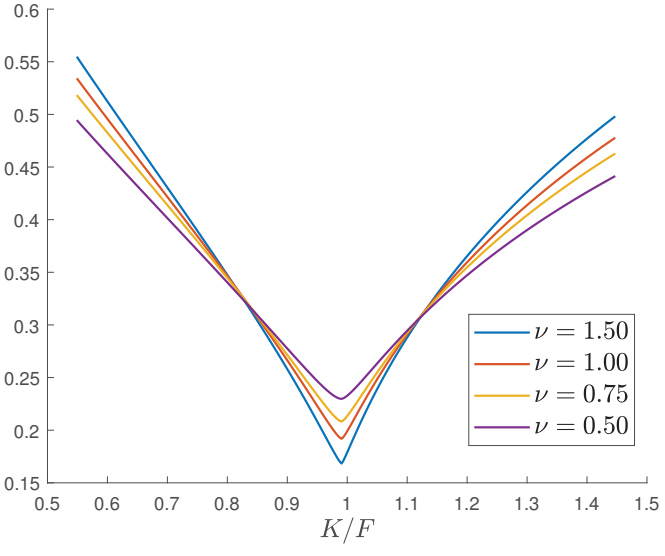

Figure 4. Implied volatility smiles of $\mathrm{VG}(\sigma, \nu, 0)$ obtained by Formula (1). Params: $\sigma = 0.3$, $\tau = 0.2$, $r = 1\%, q = 0\%$, $S_t = 4000$. The moneyness is determined by $F := S_t \exp((r-q)\tau)$.

In particular, when $4\rho^2 - 1 = 0$, i.e., when $\rho = \frac{1}{2}$, all the $a_k(\rho)$ are null in definition (57) when $k \geq 1$, and we are left with:

$$K_{\frac{1}{2}}(z) = \sqrt{\frac{\pi}{2z}}\, e^{-z} \tag{59}$$

for all z. Using (58) up to $k = 1$ for $z = \alpha\delta\tau$ and inserting into (56), we are left with the quadratic equation

$$X^2 - \alpha\sqrt{2\pi}\frac{C_t}{S_t}X - \frac{1}{8} = 0 \quad (X := \sqrt{\alpha\delta\tau}), \tag{60}$$

whose positive solution reads

$$X = \frac{1}{2}\left(\alpha\sqrt{2\pi}\frac{C_t}{S_t} + \sqrt{2\pi\alpha^2\frac{C_t^2}{S_t^2} + \frac{1}{2}}\right). \tag{61}$$

Taylor expanding for large α and turning back to the δ variable, we obtain

$$\delta = \frac{2\pi\alpha}{\tau}\frac{C_t^2}{S_t^2} + \frac{1}{4\alpha\tau} + O\left(\frac{1}{\alpha^3}\right) \tag{62}$$

which, at first order, recovers (55) for $\sigma^2 := \delta/\alpha$. We summarize these results in Table 2.

Table 2. Volatility modelling for ATMF options in various subordinated models, and their limiting cases.

ATMF Implied Volatility (European Options)	
Exponential VG	$\sigma_{VG} = \sqrt{\frac{2\pi}{\nu}} \frac{\Gamma(\frac{\tau}{\nu})}{\Gamma(\frac{1}{2}+\frac{\tau}{\nu})} \frac{C_t}{S_t}$ Low variance regime ($\nu \to 0$): $\sigma_{VG} \to \sqrt{\frac{2\pi}{\tau}} \frac{C_t}{S_t}$
Exponential NIG	Solve $\frac{S_t \delta \tau e^{\alpha\delta\tau}}{\pi} K_0(\alpha\delta\tau) = C_t$ Large steepness regime ($\alpha \to \infty$): $\delta = \frac{2\pi\alpha}{\tau} \frac{C_t^2}{S_t^2} + \frac{1}{4\alpha\tau} + O\left(\frac{1}{\alpha^2}\right)$ At order α^0: $\sigma_{NIG} := \sqrt{\frac{\delta}{\alpha}} = \sqrt{\frac{2\pi}{\tau}} \frac{C_t}{S_t}$
sub-BS	$\sigma_{FD} = \frac{2\sqrt{\Gamma(1+2\gamma)}\Gamma(1+\frac{\gamma}{2})}{\tau^{\frac{\gamma}{2}}} \frac{C_t}{S_t}$ Non-fractional regime ($\gamma \to 1$): $\sigma_{FD} \to \sqrt{\frac{2\pi}{\tau}} \frac{C_t}{S_t}$

5. First-Order Sensitivities

The sensitivity of a contingent claim $\mathcal{C}$ to the underlying asset, often denoted Delta or Δ, is defined by $\Delta := \partial\mathcal{C}/\partial S_t$; by deriving Formula (1) with respect to S_t and re-arranging the terms, we obtain the following expressions for European options in subordinated market models:

Formula 2 (European call: Delta)**.**
(i) The Delta at time t of a European call option in the exponential VG model is:

- *(OTM sensitivity) If* $k_{VG} < 0$,

$$\Delta^{-}_{VG}(k_{VG},\sigma_\nu) = \frac{F}{2S_t\Gamma(\frac{\tau}{\nu})} \sum_{\substack{n_1=0 \\ n_2=1}}^{\infty} \frac{(-1)^{n_1}}{n_1!} \left[-\frac{n_1\Gamma(\frac{-n_1+n_2+1}{2}+\tau_\nu)}{\Gamma(\frac{-n_1+n_2}{2}+1)} \left(\frac{-k_{VG}}{\sigma_\nu}\right)^{n_1-1} \sigma_\nu^{n_2-1} + 2\frac{\Gamma(-2n_1-n_2-2\tau_\nu)}{\Gamma(-n_1+\frac{1}{2}-\tau_\nu)} \left(\frac{-k_{VG}}{\sigma_\nu}\right)^{2n_1+1+2\tau_\nu} (-k_{VG})^{n_2-1} \right]. \quad (63)$$

- *(ITM sensitivity) If* $k_{VG} > 0$,

$$\Delta^{+}_{VG}(k_{VG},\sigma_\nu) = e^{-q\tau} - \Delta^{-}_{VG}(k_{VG},-\sigma_\nu). \quad (64)$$

- *(ATM sensitivity) If* $k_{VG} = 0$,

$$\Delta^{-}_{VG}(k_{VG},\sigma_\nu) = \Delta^{+}_{VG}(k_{VG},\sigma_\nu) = \frac{F}{2S_t\Gamma(\frac{\tau}{\nu})} \sum_{n=1}^{\infty} \frac{\Gamma(\frac{n}{2}+\tau_\nu)}{\Gamma(\frac{n+1}{2})} \sigma_\nu^{n-1}. \quad (65)$$

(ii) The Delta at time t of a European call option in the exponential NIG model is:

$$\Delta_{NIG} = \frac{F\alpha e^{\alpha\delta\tau}}{S_t\sqrt{\pi}} \sum_{\substack{n_1=0 \\ n_2=1}}^{\infty} \frac{k_{NIG}^{n_1}}{n_1!\Gamma(\frac{-n_1+n_2+1}{2})} K_{\frac{n_1-n_2}{2}+1}(\alpha\delta\tau) \left(\frac{\delta\tau}{2\alpha}\right)^{\frac{-n_1+n_2}{2}}. \quad (66)$$

(iii) The Delta at time t of a European call option in the FD model is:

$$\Delta_{FD} = \frac{F}{\alpha S_t} \sum_{\substack{n_1=0 \\ n_2=0}}^{\infty} \frac{k_{FD}^{n_1}}{n_1! \Gamma(1+\gamma\frac{-n_1+n_2}{\alpha})} \left(-\omega_{FD}\tau^{\gamma}\right)^{\frac{-n_1+n_2}{\alpha}}. \tag{67}$$

For illustration, in Figure 5 we compare the Delta of VG$(\sigma, \nu, 0)$ while using Formula (2) with that of BS(σ). Similarly, we compare the Dollar Gamma using Formula (3). Figure 6 provides a comparison for NIG$(\alpha, 0, \delta)$. For both models, we can see the substantial impact of the heavy-tailed assumption and its implications for hedging. In the next section, we discuss delta hedging in more detail, and provide some simplified approximations for the ATMF case.

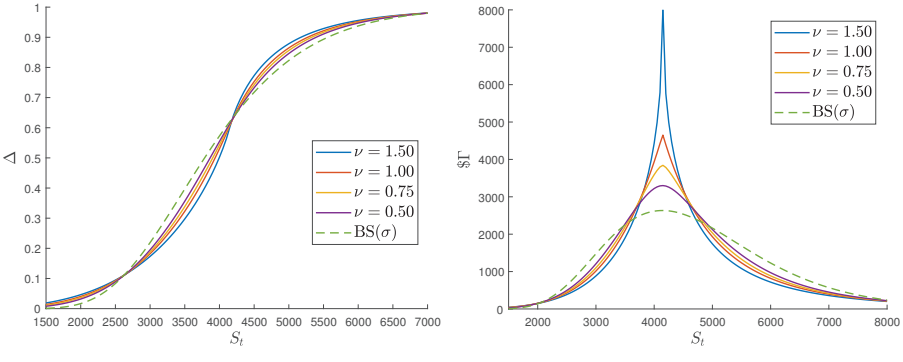

Figure 5. Delta (**Left**) and Dollar Gamma (**Right**) of a call option under VG$(\sigma, \nu, 0)$ using Formula (2) and Formula (3). Greeks of BS(σ) are provided for reference (dash lines). Params: $\sigma = 0.3$, $\tau = 1$, $r = 1\%, q = 0\%, K = 4000$.

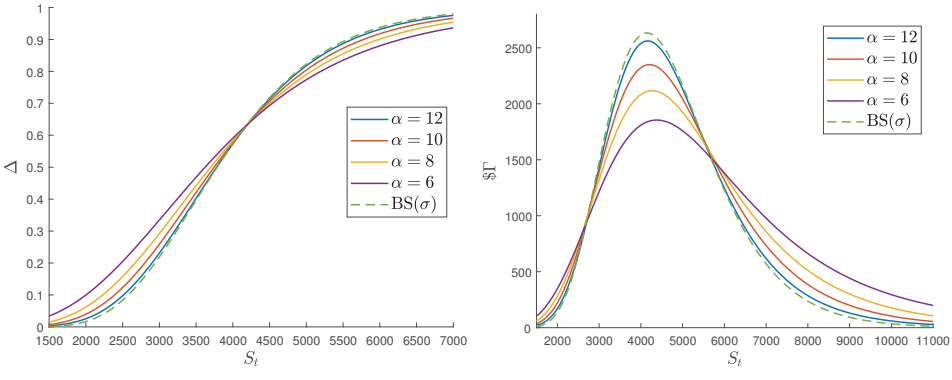

Figure 6. Delta (**Left**) and Dollar Gamma (**Right**) of a call option under NIG$(\alpha, 0, \delta)$ using Formulas (2) and (3). Greeks of BS$(\sigma = 0.3)$ are provided for reference (dash lines). Params: $\delta = 1.2$, $\tau = 1$, $r = 1\%$, $q = 0\%$, $K = 4000$.

5.1. Delta Hedging

The leading term for the Delta of the European option in the exponential VG case is given for $n_1 = n_2 = 1$ in (63) and it reads:

$$\Delta^{-}_{VG} \;=\; \frac{F}{2S_t\Gamma(\frac{\tau}{\nu})}\left[\Gamma\left(\frac{1}{2}+\tau_\nu\right) \;-\; 2\frac{\Gamma(-3-3\tau_\nu)}{\Gamma(-\frac{1}{2}-\tau_\nu)}\left(\frac{-k_{VG}}{\sigma_\nu}\right)^{-3+2\tau_\nu}\right]; \tag{68}$$

In the ATMF situation ($S_t = F$, i.e., $k = 0$), we can re-write the martingale adjustment and Taylor expand for small σ

$$k_{VG} \;=\; \omega_{VG}\tau \;=\; -\frac{\sigma^2}{2}\tau + O\left(\sigma^4\right) \tag{69}$$

and, recalling $\tau_\nu = \frac{\tau}{\nu} - \frac{1}{2}$, we obtain

$$\Delta^{-}_{VG} \;=\; \frac{1}{2} + O\left(\sigma^{4(\tau_\nu+1)}\right). \tag{70}$$

It is interesting to note that, in the ATMF situation, $\Delta^{-}_{VG} \simeq \frac{1}{2}$, which is, it suffices to be long one unit of the asset S and short two units of an European call written on this asset, to offset the impact of the variations of S on a portfolio; this fact is well-known in the usual Black–Scholes theory, and is therefore preserved in the exponential VG model. The same observation actually also holds for the exponential NIG model: indeed, the leading term in the series (66) (obtained for $n_1 = 0$, $n_2 = 1$) reads

$$\frac{F\alpha e^{\alpha\delta\tau}}{S_t\sqrt{\pi}}K_{\frac{1}{2}}(\alpha\delta\tau)\sqrt{\frac{\delta\tau}{2\alpha}} \;=\; \frac{F}{2S_t} \tag{71}$$

where we have used the particular value of the Bessel function of index $\frac{1}{2}$ (59) in order to simplify the expression; when $F = S_t$, we obtain $\Delta_{NIG} = \frac{1}{2}$, which, again, turns out to be similar to the usual Black–Scholes behavior. This effect is clearly illustrated in Figures 5 and 6. We can conclude that in both the exponential VG and NIG models, the presence of a time subordination does not modify the delta hedging policy, at least when options are not far from the money. In contrast, the option Gamma is significantly influenced by time subordination, and it is discussed further in Section 6.

In the FD model, things are a bit different; keeping only the leading term ($n_1 = n_2 = 0$) in (67) yields

$$\Delta_{FD} \;=\; \frac{F}{\alpha S_t} \;\overset{S_t\to F}{\longrightarrow}\; \frac{1}{\alpha} \tag{72}$$

which explicitly depends on the tail parameter α and resumes to $\frac{1}{2}$ in the sub-BS model, for any subordination parameter γ. Again, the subordination parameter plays no role in the delta-hedging policy of the portfolio, which is entirely governed by the tail parameter α; in other words, it suffices to be long one unit of the underlying asset S and short α European calls to offset the effect of the variations of S on the portfolio's value.

5.2. Comparisons with Numerical Techniques

In this subsection, we show that the series formulas for the first order sensitivity Δ provided by Formula (2) are a very efficient alternative to Fourier-based computations. Such calculations are typically based on a representation for the price of an European call in terms of Arrau–Debreu securities (see e.g., Lewis (2001))

$$\mathbb{E}^{\mathbb{Q}}\left[e^{-r\tau}(S_T-K)^+ \,|\, S_t\right] \;=\; S_t e^{-q\tau}\Pi_1 \;-\; Ke^{-r\tau}\Pi_2, \tag{73}$$

where $e^{-q\tau}\Pi_1$ is the option's Delta. This quantity is known to admit a convenient representation in the Fourier space:

$$\Delta \;=\; e^{-q\tau}\Pi_1 \;=\; \frac{1}{2} + \frac{1}{\pi}\int_0^\infty Re\left[\frac{e^{iuk}\Psi(u-i,\tau)}{iu}\right]\mathrm{d}u \tag{74}$$

where k is the log forward moneyness defined in (37), and the "risk-neutralized" characteristic function is defined by:

$$\Psi(u,t) \;:=\; e^{iu\omega t}\Psi(u,t) \;=\; e^{(iu\omega+\psi(u))t} \tag{75}$$

In the case of the exponential VG and NIG models, the integral in (74) can be easily carried out by inserting the expressions for the Lévy symbol $\psi(u)$ and the martingale adjustment ω, and by evaluating the integral by any classical recursive algorithm (such as a simple trapezoidal rule, for instance). In Table 3, we compare the results of such numerical evaluations, with several truncations of the series in Formula (2), and for various market configurations. We can observe that the convergence is extremely accurate and fast, notably in the ATM region: this is because, in that case, $k \simeq 0$, which tends to accelerate the overall convergence of the series.

Table 3. First order sensitivity (Delta) of European call options in the exponential VG and NIG models, obtained by truncations of Formula (2), and by a numerical evaluation of (74). Here, $N = n_1 = n_2$ is the number of terms in the truncated series. Parameters: $K = 4000$, $r = 1\%$, $q = 0\%$, $\tau = 1$.

Exponential VG Model [$\sigma = 0.2$, $\nu = 0.85$]					
	Formula (2)				**Lewis (74)**
	$N = 3$	$N = 5$	$N = 10$	$N = 15$	
Deep OTM ($S_t = 3000$)	2.1823	0.6347	0.0941	0.0940	0.0940
OTM ($S_t = 3500$)	0.4113	0.2567	0.2455	0.2455	0.2455
ATM ($S_t = 4040.90$)	0.5703	0.5718	0.5719	0.5719	0.5719
ITM ($S_t = 4500$)	0.7569	0.8113	0.8134	0.8134	0.8134
Deep ITM ($S_t = 5000$)	0.4729	0.8589	0.9206	0.9206	0.9206
Exponential NIG Model [$\alpha = 9$, $\delta = 1.2$]					
	Formula (2)				**Lewis (74)**
	$N = 3$	$N = 5$	$N = 10$	$N = 15$	
Deep OTM ($S_t = 3000$)	0.2921	0.2722	0.2747	0.2748	0.2748
OTM ($S_t = 3500$)	0.4289	0.4309	0.4311	0.4311	0.4311
ATM ($S_t = 4234.09$)	0.6336	0.6410	0.6412	0.6412	0.6412
ITM ($S_t = 4500$)	0.6936	0.7030	0.7033	0.7033	0.7033
Deep ITM ($S_t = 5000$)	0.7827	0.7966	0.7971	0.7971	0.7971

6. Second-Order Sensitivities and Portfolio Performance

6.1. Gamma, Dollar Gamma

The second order derivative of a contingent claim $\mathcal{C}$ with respect to S_t is often denoted by $\Gamma := \partial^2\mathcal{C}/\partial S_t^2$. It is closely related to the performance, or Profit and Loss (P&L) of a portfolio: if $t_2 > t_1$ are two trading days, then the P&L between t_1 and t_2 is

$$\mathrm{P\&L} \;=\; \Theta\,\Delta t \;+\; \text{market P\&L}\,, \qquad \Delta t := t_2 - t_1, \tag{76}$$

where Θ is the time sensitivity of the portfolio, and the market P&L is, at order 2:

$$\text{market P\&L} := \Delta(\Delta S_t) + \frac{1}{2}\Gamma(\Delta S_t)^2 \qquad \Delta S_t := S_{t_2} - S_{t_1}. \tag{77}$$

Assuming that the portfolio has been delta-hedged, then we are left with

$$\text{market P\&L} = \$\Gamma \left(\frac{\Delta S_t}{S_t}\right)^2 \tag{78}$$

where the Dollar Gamma has been defined by $\$\Gamma := \frac{1}{2}S_t^2\Gamma$; relation (78) is widely employed in financial engineering, because it allows for expressing the performance of the portfolio as a simple function of the realized variance of the underlying S. In the usual Black–Scholes theory, it is well known that the Dollar Gamma of the European call is

$$\$\Gamma_{BS} = \frac{S_t}{2\sigma\sqrt{2\pi\tau}}. \tag{79}$$

Remarkably, as shown by Formula (3), the Gamma of European options admits a simple form in subordinated market models: while the series expansion for the price or the first-order sensitivity is expressed in terms of a double sum, the Gamma can be expressed as a sum over a single index.

Formula 3 (European call: Gamma)**.**
(i) The Gamma at time t of a European call option in the exponential VG model is:

- *(OTM sensitivity) If* $k_{VG} < 0$,

$$\Gamma^-_{VG}(k_{VG},\sigma_\nu) = \frac{F}{2S_t^2\sigma_\nu\Gamma(\frac{\tau}{\nu})}\sum_{n=0}^{\infty}\frac{(-1)^n}{n!}\left[\frac{\Gamma(-\frac{n}{2}+\tau_\nu)}{\Gamma(\frac{-n+1}{2})}\left(\frac{-k_{VG}}{\sigma_\nu}\right)^n + 2\,\frac{\Gamma(-2n-2\tau_\nu)}{\Gamma(-n+\frac{1}{2}-\tau_\nu)}\left(\frac{-k_{VG}}{\sigma_\nu}\right)^{2n+2\tau_\nu}\right]. \tag{80}$$

- *(ITM sensitivity) If* $k_{VG} > 0$,

$$\Gamma^+_{VG}(k_{VG},\sigma_\nu) = -\Gamma^-_{VG}(k_{VG},-\sigma_\nu). \tag{81}$$

- *(ATM sensitivity) If* $k_{VG} = 0$,

$$\Gamma^-_{VG}(k_{VG},\sigma_\nu) = \Gamma^+_{VG}(k_{VG},\sigma_\nu) = \frac{F}{2\sqrt{\pi}S_t^2\sigma_\nu\Gamma(\frac{\tau}{\nu})}\frac{\Gamma(\tau_\nu-\frac{1}{2})}{\Gamma(\frac{\tau}{\nu})}. \tag{82}$$

(ii) The Gamma at time t of a European call option in the exponential NIG model is:

$$\Gamma_{NIG} = \frac{F\alpha e^{\alpha\delta\tau}}{S_t^2\sqrt{\pi}}\sum_{n=0}^{\infty}\frac{k_{NIG}^n}{n!\Gamma(\frac{-n+1}{2})}K_{\frac{n}{2}+1}(\alpha\delta\tau)\left(\frac{\delta\tau}{2\alpha}\right)^{-\frac{n}{2}}. \tag{83}$$

(iii) The Gamma at time t of a European call option in the FD model is:

$$\Gamma_{FD} = \frac{F}{\alpha S_t^2}\sum_{n=0}^{\infty}\frac{k_{FD}^n}{n!\Gamma(1-\frac{\gamma}{\alpha}(n+1))}\left(-\omega_{FD}\tau^\gamma\right)^{-\frac{n+1}{\alpha}}. \tag{84}$$

Proof. The formulas are all straightforward to obtain, by deriving the series in Formula (2) with respect to S_t and making an appropriate change of variables. For instance, in the NIG case, we have

$$\Gamma_{NIG} = \frac{F\alpha e^{\alpha\delta\tau}}{S_t^2\sqrt{\pi}}\left[-\sum_{\substack{n_1=0\\n_2=1}}^{\infty}\frac{k_{NIG}^{n_1}}{n_1!\Gamma(\frac{-n_1+n_2+1}{2})}K_{\frac{n_1-n_2}{2}+1}(\alpha\delta\tau)\left(\frac{\delta\tau}{2\alpha}\right)^{\frac{-n_1+n_2}{2}}\right.$$
$$\left.+\sum_{\substack{n_1=1\\n_2=1}}^{\infty}\frac{k_{NIG}^{n_1-1}}{(n_1-1)!\Gamma(\frac{-n_1+n_2+1}{2})}K_{\frac{n_1-n_2}{2}+1}(\alpha\delta\tau)\left(\frac{\delta\tau}{2\alpha}\right)^{\frac{-n_1+n_2}{2}}\right]. \quad (85)$$

Performing the change of variables $\tilde{n}_1 := n_1 + 1$, $\tilde{n}_2 \to n_2 + 1$ in the second sum shows that only the terms for $\tilde{n}_2 = 0$ survive; renaming $\tilde{n}_1 := n$ yields Formula (83). □

6.2. Properties and Particular Cases

Let us discuss some useful approximations and qualitative properties of Formula (3). First, in the VG case, the leading term ($n = 0$) in (80) is

$$\frac{F}{2S_t^2\sigma_\nu\Gamma(\frac{\tau}{\nu})}\left[\frac{\Gamma(\tau_\nu)}{\sqrt{\pi}}+2\frac{\Gamma(-2\tau_\nu)}{\Gamma(\frac{1}{2}-\tau_\nu)}\left(-\frac{k_{VG}}{\sigma_\nu}\right)^{2\tau_\nu}\right]. \quad (86)$$

Taylor expanding the VG martingale adjustment for small ν and assuming that we are not far from the money forward ($S_t \to F$), we have

$$k_{VG} \underset{\nu\to 0}{\sim} k - \frac{\sigma^2}{2}\tau \underset{S_t\to F}{\sim} -\frac{\sigma^2}{2}\tau, \quad (87)$$

therefore, the Gamma writes, at first order:

$$\Gamma_{VG}^{-} = \frac{1}{2\sqrt{\pi}S_t\sigma_\nu}\frac{\Gamma(\frac{\tau}{\nu}-\frac{1}{2})}{\Gamma(\frac{\tau}{\nu})} \quad (88)$$

and the Dollar Gamma immediately follows:

$$\$\Gamma_{VG}^{-} = \frac{S_t}{4\sqrt{\pi}\sigma_\nu}\frac{\Gamma(\frac{\tau}{\nu}-\frac{1}{2})}{\Gamma(\frac{\tau}{\nu})}. \quad (89)$$

While using the functional relation $\Gamma(z+1) = z\Gamma(z)$ and the Stirling approximation (47), we have:

$$\frac{\Gamma(\frac{\tau}{\nu}-\frac{1}{2})}{\Gamma(\frac{\tau}{\nu})} = \frac{1}{\frac{\tau}{\nu}-\frac{1}{2}}\frac{\Gamma(\frac{\tau}{\nu}+\frac{1}{2})}{\Gamma(\frac{\tau}{\nu})} \underset{\nu\to 0}{\sim} \sqrt{\frac{\nu}{\tau}} \quad (90)$$

and, therefore, we obtain the behavior of (89) in the low variance regime:

$$\$\Gamma_{VG}^{-} \overset{\nu\to 0}{\to} \frac{S_t}{2\sigma\sqrt{2\pi\tau}}, \quad (91)$$

thus recovering the Black–Scholes Dollar Gamma (79) in this limit. It is interesting to note that, contrary to the first order sensitivity Delta (70), which appeared to be independent of ν; this is no longer the case with

the second order sensitivity Gamma (89) that explicitly depends on the subordination parameter. In other words, while the subordination parameter does not modify the Delta Hedging policy of the portfolio (when not far from the money), it directly impacts its performance. This observation also holds in the exponential NIG model; indeed, the leading term in (83) for $S_t \to F$ reads

$$\Gamma_{NIG} = \frac{\alpha e^{\alpha\delta\tau}}{\pi S_t} K_1(\alpha\delta\tau) \tag{92}$$

and therefore the Dollar Gamma is

$$\$\Gamma_{NIG} = \frac{\alpha S_t e^{\alpha\delta\tau}}{2\pi} K_1(\alpha\delta\tau). \tag{93}$$

Using the asymptotic behavior for large argument (58) for the Bessel function, we know that

$$K_1(\alpha\delta\tau) \underset{\alpha\to\infty}{\sim} \sqrt{\frac{\pi}{2\alpha\delta\tau}} e^{-\alpha\delta\tau} \tag{94}$$

and, therefore

$$\$\Gamma_{NIG} \overset{\alpha\to\infty}{\longrightarrow} \frac{S_t}{2\sigma\sqrt{2\pi\tau}}, \qquad \sigma^2 := \frac{\delta}{\alpha}, \tag{95}$$

recovering the Black–Scholes Dollar Gamma (79). Last in the FD model, the leading term in the series (84) for $S_t \to F$ is

$$\Gamma_{FD} = \frac{1}{\alpha S_t} \frac{(-\omega_{FD}\tau^\gamma)^{-\frac{1}{\alpha}}}{\Gamma(1-\frac{\gamma}{\alpha})}, \tag{96}$$

and, in the sub-BS model ($\alpha = 2$), using the approximation (36) for the martingale adjustment,

$$\Gamma_{sub-BS} = \frac{1}{2S_t} \frac{\sqrt{\Gamma(1+2\gamma)}}{\Gamma(1-\frac{\gamma}{2})\sigma\tau^{\frac{\gamma}{2}}}. \tag{97}$$

Therefore, the Dollar Gamma in the sub-BS model is

$$\$\Gamma_{sub-BS} = \frac{S_t}{4} \frac{\sqrt{\Gamma(1+2\gamma)}}{\Gamma(1-\frac{\gamma}{2})\sigma\tau^{\frac{\gamma}{2}}}. \tag{98}$$

and, in the non fractional limit ($\gamma \to 1$), we have, again,

$$\$\Gamma_{sub-BS} \overset{\gamma\to 1}{\longrightarrow} \frac{S_t}{2\sigma\sqrt{2\pi\tau}}. \tag{99}$$

In Table 4, we summarize these observations, as well as the properties that are discussed for the first-order sensitivity in Section 5.

Table 4. First and second order market sensitivities (ATMF situation) for European call options in various subordinated models, and their limiting cases. Time subordination does not affect the Delta, but it directly impacts the Gamma of options.

	1st Order (Δ)	2nd Order (Γ)
Exponential VG	$\frac{1}{2}$	$\frac{1}{2\sqrt{\pi S_t \sigma_\nu}} \frac{\Gamma(\frac{\tau}{\nu}-\frac{1}{2})}{\Gamma(\frac{\tau}{\nu})}$ Low variance regime ($\nu \to 0$): $\frac{1}{S_t \sigma \sqrt{2\pi\tau}}$
Exponential NIG	$\frac{1}{2}$	$\frac{\alpha e^{\alpha\delta\tau}}{\pi S_t} K_1(\alpha\delta\tau)$ Large steepness regime ($\alpha \to \infty$): $\frac{1}{S_t \sigma \sqrt{2\pi\tau}}$, $\sigma^2 := \frac{\delta}{\alpha}$
FD	$\frac{1}{\alpha}$	$\frac{1}{\alpha S_t} \frac{(-\omega_{FD}\tau^\gamma)^{-\frac{1}{\alpha}}}{\Gamma(1-\frac{\gamma}{\alpha})}$
sub-BS	$\frac{1}{2}$	$\frac{1}{2S_t} \frac{\sqrt{\Gamma(1+2\gamma)}}{\Gamma(1-\frac{\gamma}{2})\sigma\tau^{\frac{\gamma}{2}}}$ Non fractional regime ($\gamma \to 1$): $\frac{1}{S_t \sigma \sqrt{2\pi\tau}}$

7. Concluding Remarks

In this article, we have provided a review of several subordinated market models and recalled their main properties. We have also recalled recent formulas while used for European option pricing in this context. Our main conclusions are the following:

(a) The pricing formulas are smooth and fast converging, and provide excellent agreement with efficient numerical techniques (such as the PROJ method). Moreover, these formulas can provide useful approximations for at-the-money options, and allow for the construction of volatility curves.

(b) We have derived several analytical formulas for risk sensitivities and shown that they also provide excellent agreement with standard numerical (Fourier) evaluations.

(c) Thanks to these formulas, we were able to show that the presence of a time subordination in the VG, NIG, and FD models has a minimal impact on the delta hedging policy of an at-the-money option, but, on the contrary, has a direct impact on the P&L of the delta hedged portfolio.

Future work should include extending the pricing and sensitivities formulas to path-dependent instruments or to options written on several assets. It would also be interesting to determine whether these analytical results could be extended if the risk-neutral hypothesis is replaced, for instance, by approaches based on optimal quadratic hedging or utility functions.

Author Contributions: J.-P.A. and J.L.K. performed conceptualization and calculations and prepared the original manuscript draft. J.-P.A., J.L.K. and J.K. reviewed and finalized the manuscript. All authors have read and agreed to the published version of the manuscript.

Funding: J. K. acknowledges support from Grant Agency of the Czech Republic, grant No. 19-16066S, and grant No. 20-17295S.

Conflicts of Interest: The authors declare no conflict of interest.

References

Abramowitz, Milton, and Irene Stegun. 1972. *Handbook of Mathematical Functions*. Mineola: Dover Publications.

Aguilar, Jean-Philippe. 2020a. Some pricing tools for the Variance Gamma model. *International Journal of Theoretical and Applied Finance* 23: 2050025.

Aguilar, Jean-Philippe. 2020b. Explicit option valuation in the exponential NIG model. *arXiv* arXiv:2006.04659.

Aguilar, Jean-Philippe. 2020c. Pricing Path-Independent Payoffs with Exotic Features in the Fractional Diffusion Model. *Fractal Fract* 4: 2.

Aguilar, Jean-Philippe, Cyril Coste, and Jan Korbel. 2018. Series representation of the pricing formula for the European option driven by space-time fractional diffusion. *Fractional Calculus and Applied Analysis* 21: 981–1004.

Andrews, Larry. 1992. *Special Functions of Mathematics for Engineers*. New York: McGraw & Hill.

Barndorff-Nielsen, Ole. 1977. Exponentially decreasing distributions for the logarithm of particle size. *Proceedings of the Royal Society of London* 353: 401–19.

Barndorff-Nielsen, Ole, John Kent, and Michael Sørensen. 1982. Normal Variance-Mean Mixtures and z Distributions. *International Statistical Review* 50: 145–59.

Barndorff-Nielsen, Ole. 1997. Normal inverse Gaussian distributions and stochastic volatility models. *Scandinavian Journal of Statistics* 24: 1–133.

Bertoin, Jean. 1999. Subordinators: Examples and Applications. In *Lectures on Probability Theory and Statistics. Lecture Notes in Mathematics*. Edited by Bernard Pierre. Berlin and Heidelberg: Springer, vol. 1717.

Black, Fischer, and Myron Scholes. 1973. The Pricing of Options and Corporate Liabilities. *The Journal of Political Economy* 81: 637–54.

Bochner, Salomon. 1949. Diffusion equation and stochastic processes. *Proceedings of the National Academy of Science of the United States of America* 35: 368–70.

Boyarchenko, Svetlana, and Sergei Levendorskiĭ. 2000. Option pricing for truncated Lévy Processes. *International Journal of Theoretical and Applied Finance* 3: 549–52.

Brenner, Menahem, and Marti G. Subrahmanyam. 1994. A simple approach to option valuation and hedging in the Black-Scholes Model. *Financial Analysts Journal* 50: 25–28.

Calvet, Laurent, and Adlai Fischer. 2008. *Multifractal Volatility: Theory, Forecasting and Pricing*. Burlington: Academic Press.

Carr, Peter, and Dilip Madan. 1999. Option valuation using the Fast Fourier Transform. *Journal of Computational Finance* 2: 61–73.

Carr, Peter, Hélyette Geman, Dilip Madan, and Marc Yor. 2002. The Fine Structure of Asset Returns: An Empirical Investigation. *Journal of Business* 75: 305–32.

Carr, Peter, and Liurn Wu. 2003. The Finite Moment Log Stable Process and Option Pricing. *The Journal of Finance* 58: 753–77.

Carr, Peter, and Liuren Wu. 2004. Time-changed Lévy processes and option pricing. *Journal of Financial Economics* 71: 113–41.

Cartea, Alavaro, and Diego del-Castillo-Negrete. 2007. Fractional diffusion models of option prices in markets with jumps. *Physica A* 374: 749–63.

Cont, Rama, and Peter Tankov. 2004. *Financial Modelling with Jump Processes*. New York: Chapman & Hall.

Cont, Rama. 2007. Volatility Clustering in Financial Markets: Empirical Facts and Agent-Based Models. In *Long Memory in Economics*. Edited by Teyssière Gilles and Kirman Alan. Berlin and Heidelberg: Springer.

Clark, Peter K. 1973. A subordinated stochastic process model with fixed variance for speculative prices. *Econometrica* 41: 135–55.

Cui, Zhenyu, Justin L. Kirkby, and Duy Nguyen. 2017. Equity-linked annuity pricing with cliquet-style guarantees in regime-switching and stochastic volatility models with jumps. *Insurance: Mathematics and Economics* 74: 46–62.

Cui, Zhenyu, Justin L. Kirkby, and Duy Nguyen. 2019. A general framework for time-changed Markov processes and applications. *European Journal of Operational Research* 273: 785–800.

de Jonge, Bram, Ruud Teunter, and Tiedo Tinga. 2017. The influence of practical factors on the benefits of condition-based maintenance over time-based maintenance. *Reliability Engineering & System Safety* 158: 21–30.

Eberlein, Ernst, and Ulrich Keller. 1995. Hyperbolic distributions in finance. *Bernoulli* 1: 281–99.

Eberlein, Ernst, Kathrin Glau, and Antonis Papapantoleon. 2010. Analysis of Fourier Transform Valuation Formulas and Applications. *Applied Mathematical Finance* 17: 211–40.

Fang, Fang, and Cornelis W. Oosterlee. 2008. A novel pricing method for European options based on Fourier cosine series expansions. *SIAM Journal on Scientific Computing* 31: 826–48.

Figueroa-López, José E., Steven R. Lancette, Kiseop Lee, and Yanhui Mi. 2012. Estimation of NIG and VG models for high frequency financial data. In *Handbook of Modeling High-Frequency Data in Finance*. Edited by Viens Frederi, Mariani Maria and Florescu Ionut. Hoboken: John Wiley & Sons.

Fiorani, Filippo, Elisa Luciano, and Patrizia Semeraro. 2007. Single and Joint Default in a Structural Model with Purely Discontinuous Assets. *Carlo Alberto Notebooks* Working Paper 41. Available online: https://EconPapers.repec.org/RePEc:cca:wpaper:41 (accessed on 8 November 2020).

Geman, Hélyette. 2009. Stochastic Clock and Financial Markets. *Handbook of Numerical Analysis* 15: 649–63.

Gorenflo, Rudolf, Francesco Mainardi, and Alessandro Vivoli. 2006. Discrete and Continuous Random Walk Models for Space-Time Fractional Diffusion. *Journal of Mathematical Sciences* 132: 614–28.

Ivanov, Roman. 2018. Option pricing in the variance-gamma model under the drift jump. *International Journal of Theoretical and Applied Finance* 21: 1–19.

Jizba, Petr, Jan Korbel, Hynek Lavička, Martin Prokš, Václav Svoboda, and Christian Beck. 2018. Transition between superstatistical regimes: Validity, breakdown and applications. *Physica A* 493: 29–46.

Kirkby, Justin L. 2015. Efficient Option Pricing by Frame Duality with the Fast Fourier Transform. *SIAM Journal on Financial Mathematics* 6: 713–47.

Kleinert, Hagen, and Jan Korbel. 2016. Option Pricing Beyond Black-Scholes Based on Double-Fractional Diffusion. *Physica A* 449: 200–14.

Korbel, Jan, and Yuri Luchko. 2016. Modeling of financial processes with a space-time fractional diffusion equation of varying order. *Fractional Calculus and Applied Analysis* 19: 1414–33.

Kou, Steven. 2002. A jump-diffusion model for option pricing. *Management Science* 48: 1086–101.

Krawiecki, Andrzej, Janusz A. Holyst, and Dirk Helbing. 2002. Volatility Clustering and Scaling for Financial Time Series due to Attractor Bubbling. *Physical Review Letters* 89: 158701.

Lam, Kin, Eric Chang, and Matthew C. Lee. 2002. An empirical test of the variance gamma option pricing model. *Pacific-Basin Finance Journal* 10: 267–85.

Lewis, Alan. 2001. A Simple Option Formula for General Jump-Diffusion and Other Exponential Lévy Processes. *SSRN*. SSRN 282110. Available online: https://ssrn.com/abstract=282110 (accessed on 8 November 2020).

Li, Changpin, Deliang Qian, and YangQuan Chen. 2011. On Riemann-Liouville and Caputo Derivatives. *Discrete Dynamics in Nature and Society* 2011: 562494.

Li, Lingfei, and Vadim Linetsky. 2014. Time-Changed Ornstein-Uhlenbeck processes and their applications in commodity derivative models. *Mathematical Finance* 24: 289–330.

Linders, Daniel, and Ben Stassen. 2015. The multivariate Variance Gamma model: Basket option pricing and calibration. *Quantitative Finance* 16: 555–72.

Luchko, Yuri, Jean-Philippe Aguilar, and Jan Korbel. 2019. Applications of the Fractional Diffusion Equation to Option Pricing and Risk Calculations. *Mathematics* 7: 796.

Luciano, Elisa, and Wim Schoutens. 2006. A multivariate jump-driven financial asset model. *Quantitative Finance* 6: 385–402.

Luciano, Elisa. 2009. Business Time and New Credit Risk Models. *Convegno Economia e Incertezza*. Available online: https://ideas.repec.org/p/icr/wpmath/16-2010.html#download (accessed on 1 October 2020).

Luciano, Elisa, and Patrizia Semeraro. 2010. Multivariate time changes for Lévy asset models: Characterization and calibration. *Journal of Computational and Applied Mathematics* 223: 1937–53.

Lux, Thomas, and Michele Marchesi. 2000. Volatility Clustering in Financial Markets: A MicroSimulation of Interacting Agents. *International Journal of Theoretical and Applied Finance* 3: 675–702.

Madan, Dilip, Peter Carr, and Eric Chang. 1998. The Variance Gamma Process and Option Pricing. *European Finance Review* 2: 79–105.

Madan, Dilip, and Eugene Seneta. 1990. The Variance Gamma (V.G.) Model for Share Market Returns. *The Journal of Business* 63: 511–24.

Madan, Dilip, and Elton A. Daal. 2005. An Empirical Examination of the Variance Gamma Model for Foreign Currency Options. *The Journal of Business* 78: 2121–52.

Mainardi, Francesco, Yuri Luchko, and Gianni Pagnini. 2001. The fundamental solution of the space-time fractional diffusion equation. *Fractional Calculus and Applied Analysis* 4: 153–92.

Mandelbrot, Benoit. 1963. The Variation of Certain Speculative Prices. *The Journal of Business* 36: 384–419.

Merton, Robert. 1976. Option pricing when underlying stock returns are discontinuous. *Journal of Financial Economics* 3: 125–44.

Mittnik, Svetlozar, and Stefan Rachev. 2000. *Stable Paretian Models in Finance*. Hoboken: John Wiley & Sons.

Niu, Hongli, and Jun Wang. 2013. Volatility clustering and long memory of financial time series and financial price model. *Digital Signal Processing* 23: 489–98.

Phelan, Carolyn E., Daniele Marazzina, Gianluca Fusai, and Guido Germano. 2019. Hilbert transform, spectral filters and option pricing. *Annals of Operations Research* 282: 273–98.

Ruijter, Marjon, Mark Versteegh, and Cornelis W. Oosterlee. 2015. On the application of spectral filters in a Fourier option pricing technique. *Journal of Computational Finance* 19: 76–106.

Rydberg, Tina Hviid. 1997. The Normal inverse Gaussian Lévy process: Simulation and approximation. *Communications in Statistics. Stochastic Models* 13: 887–910.

Samko, Stefan, Anatoly A. Kilbas, and Oleg Marichev. 1993. *Fractional Integrals and Derivatives, Theory and Applications*. Yverdon: Gordon and Breach Science Publishers.

Sato, Ken-iti. 1999. *Lévy Processes and Infinitely Divisible Distributions*. Cambridge: Cambridge University Press.

Schoutens, Wim. 2003. *Lévy Processes in Finance: Pricing Financial Derivatives*. Hoboken: Wiley & Sons.

Semeraro, Patrizia. 2008. A multivariate Variance Gamma model for financial applications. *International Journal of Theoretical and Applied Finance* 11: 1–18.

Takahashi, Akihiko, and Akira Yamazaki. 2008. Efficient static replication of European options under exponential Lévy models. *The Journal of Futures Markets* 29: 1–15.

Tarasov, Vasily E. 2019. On history of mathematical economics: Application of fractional calculus. *Mathematics* 7: 509.

Tomovski, Živorad, Johan L. A. Dubbeldam, and Jan Korbel. 2020. Applications of Hilfer-Prabhakar operator to option pricing financial model. *Fractional Calculus and Applied Analysis* 23: 996–1012.

Venter, Johannes, and Riaan de Jongh. 2002. Risk estimation using the Normal inverse Gaussian distribution. *The Journal of Risks* 2: 1–25.

Zolotarev, Vladimir. 1986. *One-dimensional Stable Distributions*. Providence: American Mathematical Soc.

risks

MDPI

Article

The Importance of Economic Variables on London Real Estate Market: A Random Forest Approach

Susanna Levantesi [1] and Gabriella Piscopo [2,*]

[1] Department of Statistics, Sapienza University of Rome, 00161 Rome, Italy; susanna.levantesi@uniroma1.it
[2] Department of Economics and Statistical Science, University of Naples Federico II, 80138 Naples, Italy
* Correspondence: gabriella.piscopo@unina.it

Received: 6 August 2020; Accepted: 12 October 2020; Published: 21 October 2020

Abstract: This paper follows the recent literature on real estate price prediction and proposes to take advantage of machine learning techniques to better explain which variables are more important in describing the real estate market evolution. We apply the random forest algorithm on London real estate data and analyze the local variables that influence the interaction between housing demand, supply and price. The variables choice is based on an urban point of view, where the main force driving the market is the interaction between local factors like population growth, net migration, new buildings and net supply.

Keywords: house price prediction; real estate; machine learning; random forest

JEL Classification: R31; G170

1. Introduction

Urban economy and real estate markets are two interconnected fields of research. They overlap in so far as the real estate price evolution is analyzed under an urban approach: it has been shown that less than 8% of the variation in price levels across cities can be accounted for by national effects Glaeser et al. (2014), while the remaining part is explained by local factors. In other words, national macroeconomic variables such as population growth, global migration, interest rates or national income, have really tiny power in explaining the real estate market, comparing with the macroeconomic variables accounted at a local level, such as the city population, the migration towards a particular city or the opportunities of jobs in a given urban area, that directly press on built environment and housing demand. On the other hand, the local real estate market influences the urban economy as long as it offers advantageous investment opportunities and facilities able to attract w orkers and economic activities: according to Arvanitidis (2014), the property market institution has a pivotal role through which local economic potential can be realized and served. In this sense, urban economy and real estate market influence each other.

Recently, some phenomena are affecting both urban economy and real estate market evolution. According to the United Nations (2019), the world's population is expected to grow by 5.9 billion by the end of the century, and about the 80% of which is expected to live in or move toward cities, due to economic and political motivations. Moreover, the population is aging and the proportion of elderly who remains to live in the city is increasing, thanks to alternative pension products based on the property value, like home equity plan and reverse mortgages Di Lorenzo et al. (2020a). In Europe, 25% of the population is already aged 60 years and the proportion who lives in city is growing: by 2050, two-thirds of the world population are expected to live in cities Lopez-Alcala (2016). A complete overview of the urban situation has to take into account data on migration: according to the International Organization of Migration, in 2015 in Europe there have been one million migrants, and many of them stay i n cities McKinsey (2016). As population grows and the urbanization goes on,

real estate markets have to face pressure on prices and affordability van Doorn et al. (2019), caused by the mismatch between demand and supply: inflows of people in cities are pressing and asking for new buildings. On the other hand, the increase of working population into metropolitan areas are bearing long-term opportunities for investors. In this context, understanding real estate market evolution is crucial for various real estate stakeholders such as house owners, investors, banks, insurances and other institutional investors like real estate funds. The housing demand is supported by both the need of a house to live in and the research of competitive yields. As highlighted by the emerging trend in Real Estate Europe survey Morrison et al. (2019), real estate has grown as a proportion of the balance sheets of many institutional investors because it has provided the yield and returns that other asset types have not. In particular, in the last decade we have experienced geopolitical uncertainty and decrease in the interest rate and this has reinforced the longing of secure and profitable long-term income. Moreover, many financial intermediaries offer financial and insurance products whose valuation is influenced by the expectation on the real estate market, like mortgages or reverse mortgages Di Lorenzo et al. (2020a). The link between real estate markets and financial market is evident from the recent world economic crisis. Moreover, real estate property represents a major part of the individual wealth Arvanitidis (2014), so it is clear that real estate pricing mechanism is an important driver of the economy.

In light of these considerations, the importance of a precise awareness of the inner workings in the real estate market and an accurate price prediction is evident. The academic literature on this topic is fervent. In order to describe the dynamics of the market and produce predictions, the features that influence the real estate price have to be identified. Gao et al. (2019) grouped these features into two categories: non-geographical factors, that concern the peculiarities of the house, such as the number of bedrooms or the floor space area; and geographical factors, such as the distance to the city center and to main services like the schools. Rahadi et al. (2015) divide the variables explanatory of the house price into three groups: physical conditions, concept and location Chica-Olmo (2007). Physical conditions are properties possessed by the house; the concept concerns internalized ideas of home like minimalist home or healthy and green environment (Ozdenerool et al. 2007; Miller et al. 2009; Coen et al. 2018). Another point of view is the macroeconomic perspective Grum and Govekar (2016), according to which many factors drive the behavior of the real estate market, such as interest rates, government regulation, economic growth, political instability and so on. However, Glaeser et al. (2014) presents an urban approach and show how most variation in housing price changes is local and not national. The empirical evidence confirms that the most important factors driving the value of a house are the size and the location: (Bourassa et al. 2010; Case et al. 2004; Gerek 2014 and Montero et al. 2018) show how different locations have a strong impact on their prices. Spatial location broadly aims to analyze the role of geography and location in economic phenomena, and a particular strand of research is devoted to the analysis of real estate market fluctuations as one of the economic phenomenon in a particular geographic area.

Once the explanatory variables have been chosen, the prediction model has to be identified. The hedonic pricing model has proposed extensively in the literature of house price prediction (Krol 2013; Selim et al. 2009; Del Giudice et al. 2017b). It is essentially used for analyzing the relationship between house price and house features through classical regression methods, assuming that the value of a house is the sum of all its attributes value Liang et al. (2015). Manjula et al. (2017) uses multivariate regression models. Some related works Greenstein et al. (2015) are concerned with trying to estimate the health of a real estate market using the housing index price. Alfiyatin et al. (2017) model house price combine regression analysis and particle swarm optimization. In the last few years, with the diffusion of the application of artificial intelligence in various fields and in the context of real estate Zurada et al. (2011), many authors have used machine learning algorit hms to gain a better fitting of the models. House price predictions have been produced through machine learning (Baldominos et al. 2018; Winson 2018) and deep learning methods, such as artificial neural networks (Nghiep et al. 2001; Selim et al. 2009; Yacim et al. 2016; Yacim et al. 2018; Di Lorenzo et al. 2020b), support vector machine (Gu et al. 2011; Wang et al. 2014) and adaptive boosting

Park and Bae (2015). Other contributions deepen the expert systems based on fuzzy logic (Sarip et al. 2016; Del Giudice et al. 2017a; Guan et al. 2008). Guan et al. (2014) propose adaptive neuro-fuzzy inference systems for real estate appraisal. Park and Bae (2015) analyze the problem of classification of an investment in worthy or not, performing different algorithms: decision trees, Naive Bayes and AdaBoost. Manganelli et al. (2007) study the sales of residential property in a city in the Campania region in Italy using linear programming to analyze the real estate da ta. Del Giudice et al. (2017b) predict house price through a Markov chain hybrid Monte Carlo method, and test neural networks, multiple regression analysis and penalized spline semiparametric method. Gao et al. (2019) describe a multi task learning approach to predict location centered house price.

This paper follows the recent developments of the literature on real estate and proposes to take advantage of the random forest algorithm to better explain which variables have more importance in describing the evolution of the house price following an urban approach. To this aim, we focus on a given city, and analyze the local variables that influences the interaction between housing demand and supply and the price. We perform random forest on real estate data of London, that already in the 1990s was attracting literature attention for the economy of its agglomeration Crampton and Evans (1992) and continues to stimulate the international debate for having experienced in the three last decades an extraordinary building boom National Geographic (2018). The novelty of our paper consists in deepening a machine learning (ML) technique for real estate price prediction under an urban approach. In order to achieve this goal, we insert in the algorithm the house price in London as output variable, and some local urban economic variables as input variables. The random forest provides useful support for understanding the relationships between information variables and the target variable and highlighting the importance of each factor. There is a lot of research articles that employ the random forest approach. For instance, it has been considered in early warning systems that signal a country's vulnerability to financial crises. Tanaka et al. (2016) proposed a novel random forests-based early warning system for predicting bank failures. Tanaka et al. (2019) developed a vulnerability analysis by building bankruptcy models for multiple industries using random forests to predict the probability of firm bankruptcy. Beutel et al. (2019) compared the predictive performance of different machine learning (including random forest) models applied to early warning for systemic banking crises.

In the research concerning real estate, several articles use different ML algorithms to calculate housing prices, such as (Antipov and Pokryshevskaya 2012; Čeh et al. 2018; Hong et al. 2020 and Pai and Wang 2020).

Moreover, we use different explanatory variables with respect to those previously listed. The variables choice is based on an urban point of view, where the main force driving the market is the interaction between local demand and supply, explained by factors like the population growth or the net migration for the demand side, and new buildings and net supply.

The paper is structured as follows. Section 2 describes the regression tree architecture, the random forest technique and the variable importance measure. In Section 3 we present the case study based on the London real estate market. Final remarks are provided in Section 4.

2. The Model

In this section we introduce machine learning techniques for regression problems. In Section 2.1 we briefly describe the regression tree architecture on which the random forest algorithm is based. In Section 2.2 we illustrate the functioning of the random forest and in Section 2.3 we present the variable importance measure used in the case study to catch the importance of each predictor in predicting the target variable.

Machine learning is generally used to perform classification or regression over large datasets. However, it is also proved useful in small datasets to identify hidden patterns that are difficult to detect through more traditional regression techniques such as Generalized Linear Models (GLMs) and Generalized Additive Models (GAMs).

Consider a generic regression problem to estimate the relationship between a target (or response) variable, Y, and a set of predictors (or features), $X_1, X_2, \ldots, X_p$:

$$Y = f(X_1, X_2, \ldots, X_p) + \epsilon \tag{1}$$

where ϵ is the error term. The quantity $E(Y - \hat{Y})^2$ represents the expected squared prediction error. It can rewritten as the sum of the reducible error $E[f(X_1, X_2, \ldots, X_p) - \hat{f}(X_1, X_2, \ldots, X_p)]^2$ and the irreducible error $Var(\epsilon)$. A machine learning technique aims at estimating f by minimizing the reducible error.

Among the machine learning algorithms, we refer to the random forest that falls into the category of the ensemble methods. It allows obtaining the error decrease by reducing the prediction variance, maintaining the bias, which is the difference between the model prediction and the real value of the target variable.

2.1. Regression Tree Architecture

The random forest algorithm is founded on the regression tree architecture. The regression trees enable attaining the best function approximation $\hat{f}(X_1, X_2, \ldots, X_p)$ through a procedure consisting in the following steps Loh (2011):

- The predictor space (i.e., the set of possible values for $X_1, X_2, \ldots, X_p$) is divided into J distinct and non-overlapping regions, $R_1, R_2, \ldots, R_J$.
- For each observation that falls into the region R_j, the algorithm provides the same prediction, which is the mean of the response values for the training observations in R_j.

As described in James et al. (2017), the fundamental concept is to split the predictors' space into rectangles, identifying the regions $R_1, \ldots, R_J$ that minimize the Residual Sum of Squares (RSS):

$$\sum_{j=1}^{J} \sum_{i \in R_j} (y_i - \hat{y}_{R_j})^2$$

Once building the regions $R_1, \ldots, R_J$, the response is predicted for a given test observation using the mean of the training observations in the region to which that test observation appertain.

The consideration of all the possible partitions of the feature is computationally infeasible, thus we use a top-down approach through a recursive binary partition Quinlan (1986): the algorithm starts at the top of the tree, where all values of the target variable stand in a single region, and then successively partitions the predictors' space. The best split is identified according to the entropy or the index of Gini that is a homogeneity measure for every node. The highest homogeneity (or purity) is achieved when only one class of the target variable is attending the node.

Breiman (2001) has listed the most interesting properties of regression tree-based methods. They belong to non-parametric methods able to catch tricky relations between inputs and outputs, without involving any a-priori assumption. They manage miscellaneous data by applying features selection so as to be robust to not significant or noisy variables. They are also robust to outliers or missing values and easy to be unfolded.

2.2. Random Forest

The random forest (RF) algorithm creates a collection of decision trees from a casually variant of the tree. Once one specific learning set is defined, the RF presents a random perturbation to the learning procedure and in this way a differentiation among the trees is produced. Successively the predictions of all these trees is derived through the impelementation of aggregation techniques. The first aggregation procedure was described by Breiman (1996); the authors proposed the well know bagging based on random bootstrap copies of the original data to assemble different trees. Later in 2001 the same authors

Breiman (2001) proposed the random forest as an extention of the procedure of the bagging such that it combines the bootstrap with randomization of the input variables to separate internal nodes t. This means that the algorithm does not identify the best split $s_t = s^*$ among all variables, but firstly creates a random subset of K variables for each node and among them determines the best split.

The RF estimator of the target variable $\hat{y}_{R_j}$ is a function of the regression tree estimator, $\hat{f}^{tree}(\mathbf{X}) = \sum_{j\in J} \hat{y}_{R_j} \mathbf{1}_{\{\mathbf{x}\in R_j\}}$, where $\mathbf{X} = (X_1, X_2, \ldots, X_p)$ is the vector of the predictors, $\mathbf{1}_{\{.\}}$ represents the indicator function and $(R_j)_{j\in J}$ are the regions of the predictors space obtained by minimizing RSS. It is identified by the average values of the variable belonging to the same region R_j. Therefore, denoting the number of bootstrap samples by B and the decision tree estimator developed on the sample $b \in B$ by $\hat{f}^{tree}(\mathbf{X}|b)$, the RF estimator is defined as follows:

$$\hat{f}^{RF}(\mathbf{x}) = \frac{1}{B}\sum_{b=1}^{B} \hat{f}^{tree}(\mathbf{X}|b) \tag{2}$$

The choice of the number of trees to include in the forest should be done carefully, in order to reach the highest percentage of explained variance and the lowest mean of squared residuals (MSR).

2.3. Variable Importance

ML algorithms are usually viewed as a black-box, as the large number of trees makes the understanding of the prediction rule hard. To get from the algorithm interpretable information on the contribution of different variables we follow the common approach consisting in the calculation of the variable importance measures.

Variable importance is determined according to the relative influence of each predictor, by measuring the number of times a predictor is selected for splitting during the tree building process, weighted by the squared error improvement to the model as a result of each split, and averaged over all trees.

According to the definition provided by Breiman (2001), the RF variable importance is a measure providing the importance of a variable in the RF prediction rule. These measures are often able to detect the interaction effects, i.e., when the predictor variables interact with each other, without any a priori specification Wright et al. (2016).

A weighted impurity measure has been proposed in Breiman (2001) for evaluating the importance of a variable X_m in predicting the target Y, for all nodes t averaged over all N_T trees in the forest. Among the variants of the variable importance measures, we refer to the Gini importance, obtained assigning the Gini index to the impurity $i(t)$ index. This measure is often called Mean Decrease Gini, here denoted by $IncNodePurity$:

$$IncNodePurity(X_m) = \frac{1}{N_T}\sum_{T}\sum_{t\in T: v(s_t)=X_m} p(t)\Delta i(s_t, t, t_l, t_r) \tag{3}$$

where $v(s_t)$ is the variable used in split s_t and $\Delta i(s_t, t, t_l, t_r)$ is the impurity decrease of a binary split s_t dividing node t into a left node t_l and a right node t_r:

$$\Delta i(s_t, t, t_l, t_r) = i(t) - \frac{N_{t_l}}{N_t}\cdot i(t_l) - \frac{N_{t_r}}{N_t}\cdot i(t_r) \tag{4}$$

where N is the sample size, $p(t) = \frac{N_t}{N}$ the proportion of samples reaching t, and $p(t_l) = \frac{N_{t_l}}{N}$ and $p(t_r) = \frac{N_{t_r}}{N}$ are the proportion of samples reaching the left node t_l and the right node t_r respectively.

The $IncNodePurity(X_m)$ defined in Equation (3) provides the importance of feature X_m, which takes into account the number of splits enclosing the variable. The study of the importance of the feature provides more insight into the learning mode of the algorithm.

3. Case Study

As highlighted in Section 1, in this research we look for the urban explanatory variables of the house price starting from the consideration that the main force driving the market is the interaction between demand and supply. For this reason, we select some local variables that influence the need of house and its the demand, like the population growth or the net migration, and other linked to supply, like new buildings and net supply.

3.1. Data Description

We consider data on survey "Housing in London 2018", collected by the Greater London Authority City Hall Survey (2018), that provides the average house price (AHP) and the following set of explanatory variables over the period 1997–2016 that are the input of our regression model:

- POP: historic London population
- OO: annual trend in household tenure owned outright
- OM: annual trend in household tenure owned with mortgage
- NB: new build homes
- NS: net housing supply
- NM: net migration (domestic and international)
- TJ: trend of jobs in London

The output variable is the average price across the whole of London. The data considered are purposely generic to highlight the generality of the approach used; it is evident that further ad hoc analyzes can be conducted for individual neighborhoods or areas to obtain more specific results. In this application we are not interested so much in explaining the real estate market of a specific area as in highlighting the results of the application of RF to real estate market. For the precise description of all predictors we refer to Survey (2018).

The Survey (2018) describes the urban situation of London: the London's population has reached a new peak in 2016, becoming estimated equal to 8.8 million. London's population boom has been driven by both net international migration and natural change due the annual surplus of births over deaths. Net international migration has risen from around 50,000 a year in 1996 to over 100,000 a year in 2016 and also has explained a part of the increase in natural change, because reducing the average age of London's population. Moreover net domestic migration has been less volatile than net international migration and has been negative throughout the last 20 years with a net outflow from London equal to 93,000 in 2016. In the same year, more homes than households have been recorded, in contrast to the first half of the 20th century, because the number of people for every home has risen, while falling across the rest of the country. We are attending the declining share of mortgagors for ho me ownership and the growth in people living in a shared private rented home. The number of homes built in London in 2017 is the highest since 1977, but in the same time the population is projected to be equal to 10.5 in 2035, so two thirds of Londoners say they would support new homes being built. Another aspect that detects the home demand is its composition, that is changing: the proportion of households that own their home with a mortgage fell from 38% in 2000 to 29% in 2011, while the proportion that rent privately rose from 15% to 25%. In particular, in 2017 22% of households in London owned their home outright, 29% had a mortgage, 27% rented privately and 21% were in social housing. Another factor that has influenced the urbanization of London has been its flourishing economy. Since 1997, both London's population and economy have grown consistently. In the last two decades, the number of jobs in London grew by 42%, while the population grew by 26%. However, this rap id economic and demographic growth was not matched by an increase in the housing stock: the new buildings have increased the number of homes by 16% over the same period. The constructions of new buildings are expected to further increase to satisfy the growing demand.

3.2. Regression Model and Main Statistics

In order to understand how this scenario influences the house price, the regression problem is then formulated as follows:

$$\text{AHP} \sim \text{YEAR} + \text{POP} + \text{OO} + \text{OM} + \text{NB} + \text{NS} + \text{NM} + \text{TJ} \tag{5}$$

Table 1 shows the summary statistics for the input variables in the data. In addition to mean (μ) and standard deviation (σ), we also show the coefficient of variation (CV), or relative standard deviation, that is a standardized measure of dispersion of frequency distribution. It shows the extent of variability in relation to the mean of the average house price ($cv = \frac{\sigma}{\mu}$).

Table 1. Summary statistics across years 1997–2016.

Variable	Summary Statistics		
POP	μ = 7,776,538.90	σ = 554,808	CV = 7.13%
OO	μ = 21.56	σ = 1.00	CV = 4.64%
OM	μ = 33.33	σ = 3.96	CV = 11.88%
NB	μ = 18,385.00	σ = 3695.46	CV = 20.10%
NS	μ = 27,314.00	σ = 7929.26	CV = 29.03%
NM	μ = 23,752.40	σ = 24,129.15	CV = 101.59%
TJ	μ = 4,857,200.00	σ = 424,621.52	CV = 8.74%
AHP	μ = 320,045.95	σ = 89,380.52	CV = 27.93%

In addition, we show in Figure 1 a graphical display of the correlation matrix. Positive correlations are depicted in blue and negative correlations in red color. The color intensity and the size of the circle are proportional to the correlation coefficients. We observe strong correlations between some of the features. The average house price (AHP) is positively strongly correlated with YEAR and then with the population (POP) and trend of jobs (TJ) while it is negatively correlated with the annual trend in household tenure—owned with mortgage (OM). Moreover, POP is in turn positively correlated with TJ and YEAR and negatively correlated with OM.

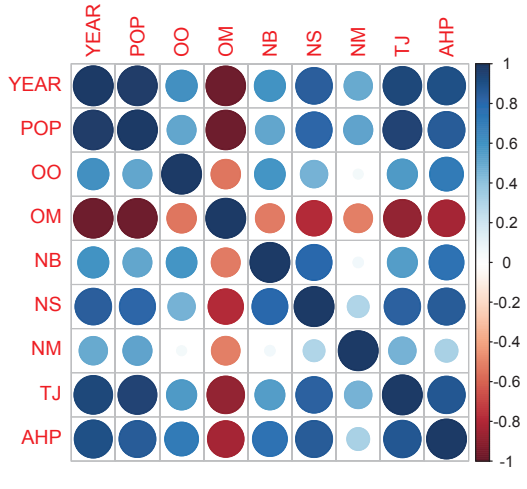

Figure 1. Correlation matrix.

3.3. RF Estimation of AHP

We solve Equation (5) through the random forest algorithm presented in Section 2. We denote $\widehat{\text{AHP}}$ the random forest estimator, obtained by applying the random forest algorithm implemented in the R package `randomForest` Liaw (2018) to the London average house prices.

A machine learning algorithm provides different outcomes when changing the seed and the number of trees. Therefore, we initially consider a set of 1000 random seeds for the pseudo-random generator used in the RF algorithm, as well as a set of reasonable number of trees ($\leq$50) and we choose the combination of seed/number of trees producing the lowest mean of squared residuals, MSR. This allows to obtain a high percentage of variance explained and avoid model's over-fitting. Therefore, the algorithm's parameters have been set as follows: number of trees (ntrees) equal to 21 and the number of input variables to be used in each node (mtry) equal to 3. The percentage of variance explained by the random forest algorithm, RSS, and the level of MSR resulting from the application of the RF algorithm to the dataset are given in Table 2.

Table 2. Residual Sum of Squares (RSS) and mean of squared residuals (MSR) by the random forest algorithm. Years 1997–2016.

Indicator	Value
RSS	94.01%
MSR	454,451,969

In order to find the best model explaining our data, we have to balance bias and variance. Models with high bias simplify the relationship between target variable and predictors, providing a high error on both training and test set. Meanwhile, models with high variance, focusing too much on the training set, lose the generalization capacity providing a very low error on the training set and very high error on the test set. Models trained on small datasets could result in high variance and high error on the test set, giving rise to overfitting. This can be avoided by reducing the maximum depth so improving the model's ability to disregard patterns that do not exist. To this purpose, we calculate the distribution of the mean minimal depth, illustrated in Figure 2. The mean value placed at the vertical bar indicates the mean minimal depth: the smaller its value, the more important the variable is. The rainbow gradient provides the minimum and maximum minimal depth for each predictor. The higher the width of red blocks, more frequently the variable is the root of a tree. As missing values appears when a feature is not used for tree splitting, the higher the width gray blocks, less frequently the variable is used for splitting trees.

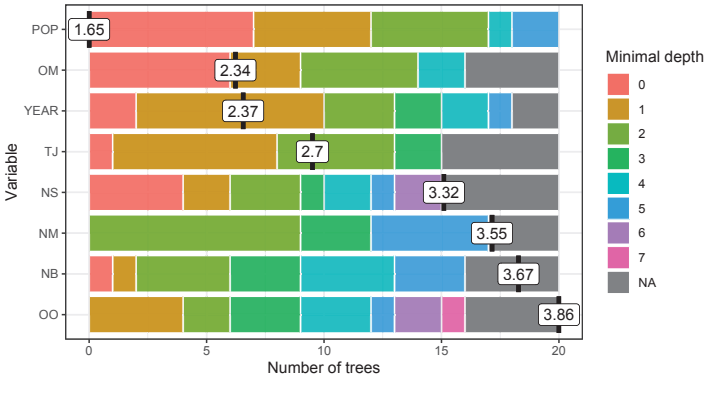

Figure 2. Distribution of minimal depth and its mean.

The values of the mean decrease Gini of features attributed by the algorithm, in descending order from top to bottom, are depicted in Figure 3. It allows to identify which predictor are the most important to understand the underlying process that is the average house price. Despite the decline in the proportion of households that own their home with a mortgage Survey (2018), the annual trend in household tenure owned with mortgage (OM) is the one of most explanatory variables of the house price between those selected. Quite the opposite, annual trend in household tenure owned outright (OO) is one of the less important variable, supporting by the data according to which the proportion of households owned their home outright is very low. We can note that RF algorithm selects POP as the most explicative variable, but since it is strongly positively correlated with YEAR the two variables have the same explicative power in the description of the output. Consequently, the algorithm includes just one of these latter variables among those having a greater importance. Instead, since POP and OM are negatively correlated, they offer different information in the prediction of AHP, so they are both selected as important.

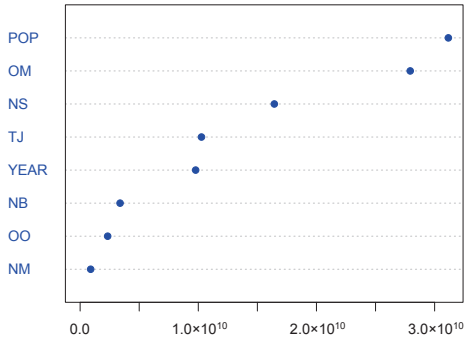

Figure 3. Mean decrease Gini values of features.

Figure 4 shows the marginal effect of the three most important predictors on the the target variable averaged over the joint values of the other predictors. These plots are called partial dependence plots. We show the effect of the population, annual trend in household tenure—owned with mortgage and net housing supply on the London average house price.

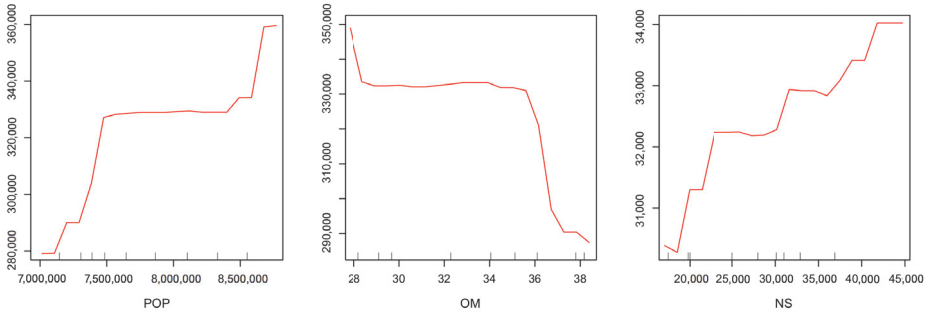

Figure 4. Single variable partial dependence plot. Predictors: POP, OM and NS.

All these variables clearly show non-linear pattern, further confirming the choice of the RF model. In fact, in case of linear pattern a simple linear (or logistic for binary target variables) regression model should be preferable to more complex ones. While, if the data shows non-linear and irregular pattern, like in our dataset, then random forest can be widely considered a very good choice, as we will demonstrate in the following.

3.4. Sensitivity to Predictor

As shown in the previous sub-section, the *IncNodePurity*, measuring the importance of the variables, provides the highest value of node purity for POP, which therefore represents the most important variable in the RF (Figure 3). In this sub-section we perform a predictors sensitivity analysis by progressively adding one predictor in modeling $\widehat{\text{AHP}}$, aiming at measuring the contribution of each predictor to refine the model accuracy. Then, we combine the selected predictors two by two. We consider the first three predictors in terms of importance. Table 3 shows the values of $\widehat{\text{AHP}}$ obtained by RF algorithm in a regression model based on one/two predictors. While, Figure 5 reports the residuals of these models. Looking at the panels with POP, NS, POP + NS and OM + NS predictors, the highest values of residuals correspond to years 1997 and 2003, when the London population data show two inflection points (Figure 6).

Table 3. RF estimation of $\widehat{\text{AHP}}$ according to different predictors.

YEAR	POP	OM	NS	POP + OM	POP + NS	OM + NS	Obs.
1997	183,781	177,594	220,706	177,349	199,614	202,211	149,616
1998	193,924	173,391	225,909	157,184	214,491	198,730	170,720
1999	211,542	212,472	208,978	198,043	202,130	229,106	179,888
2000	217,570	178,742	201,503	203,084	195,192	187,088	217,691
2001	236,617	205,580	199,442	237,029	228,907	208,593	243,062
2002	264,721	317,158	190,907	328,907	254,313	273,101	272,549
2003	271,452	301,789	215,949	275,967	261,350	262,067	322,936
2004	331,517	342,420	354,699	339,730	352,269	342,233	332,406
2005	348,727	334,189	346,321	331,844	341,708	332,266	342,173
2006	346,830	347,434	349,716	353,006	352,616	339,709	344,887
2007	343,530	351,773	377,760	354,995	377,016	368,037	369,225
2008	361,114	363,370	373,558	359,544	357,437	354,736	395,803
2009	364,396	365,626	350,713	355,699	349,910	353,876	335,008
2010	352,958	345,881	344,328	343,831	341,911	340,788	357,004
2011	351,097	346,328	340,926	348,378	339,996	354,018	349,730

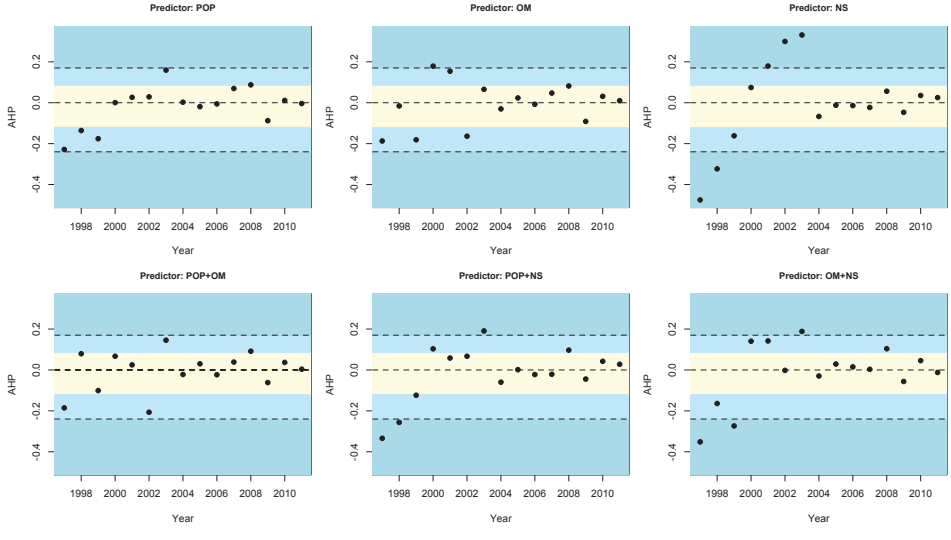

Figure 5. Residuals of the RF model based on different predictors.

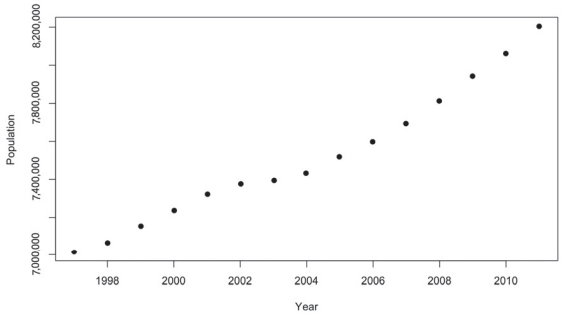

Figure 6. Historic London population. Years 1997–2011.

As shown in Table 4, the results of RF prediction confirm that *POP* is the most explicative feature with a percentage of explained variance (RSS) equal to 91.29%, followed by *OM* with 86.74%.

Table 4. RF estimation of $\widehat{\text{AHP}}$ according to different predictors: % of explained variance (RSS).

Predictor	RSS
POP	91.29%
OM	86.74%
NS	69.08%
POP + OM	87.53%
POP + NS	84.77%
OM + NS	82.41%

3.5. RF Predictive Performance and Comparison with GLM

To perform the prediction we partition the dataset into training set (1997–2011) and testing set (2012–2016). The data have been randomly partitioned, however there are a set of popular data splitting methods that could potentially work well with alternative data. Among them, cross-validation (CC)[1], bootstrapping, bootstrapped Latin partition, Kennard-Stone algorithm (KS) and sample set partitioning based on joint X-Y distances algorithm (SPXY) (see e.g., Xu and Goodacre (2018) for further details).

The ability of the RF algorithm to predict the average house price according to our sample is compared to the performance of a GLM.

In a GLM, the explanatory variables, $\mathbf{X} = (X_1, X_2, \ldots, X_p)$, are related to the response variable, Y, via a link function, $g()$. Denoting $\eta = g(E(Y))$ the linear predictor, the following equation describes how the mean of the response variable depends on the linear predictor:

$$\eta = \beta_0 + \beta_1 X_1 + ... + \beta_p X_p \tag{6}$$

where $\beta_1, \ldots, \beta_p$ are the regression coefficients that need to be estimated and β_0 is the intercept. We assume a Gaussian distribution for Y and an identity for the link function, so that: $\eta = E(Y)$. To assess the importance of variables, we measure the significance of the predictors by the Wald test with the null hypothesis: $H_0 : \beta = 0$. The GLM performance and the estimate of the regression coefficients are reported in Table 5, where $z = \frac{\hat{\beta}}{SE(\hat{\beta})}$ is the value of the Wald test, $Pr(> |z|)$ is the corresponding p-value, and $SE(\hat{\beta})$ is the standard error of the model.

[1] e.g., k-fold cross-validation where the original sample is randomly partitioned into k equal size subsamples, leave-p-out cross-validation (LpOCV) which considers p observations as the validation set and the remaining observations as the training set, or Leave-one-out cross-validation (LOOCV) that is a particular case of the previous method with $p = 1$)

Table 5. GLM results.

Coefficient	$\hat{\beta}$	$SE(\hat{\beta})$	z Value	$Pr(>\|z\|)$
(Intercept)	-1.004×10^8	3.099×10^7	-3.239	0.00789 **
YEAR	5.092×10^4	1.542×10^4	3.302	0.00705 **
POP	-2.961×10^{-1}	1.932×10^{-1}	-1.533	0.15363
OO	-1.094×10^4	1.240×10^4	-0.882	0.39640
OM	1.972×10^4	2.287×10^4	0.862	0.40706
NB	1.606	3.738	0.430	0.67569
NS	-8.192×10^{-1}	2.453	-0.334	0.74467
NM	-4.009×10^{-1}	3.267×10^{-1}	-1.227	0.24538
TJ	8.134×10^{-2}	1.138×10^{-1}	0.715	0.48958

Significance codes: $p < 0.1$, ** $p < 0.01$.

Apart from the intercept, the GLM assigns the greatest importance to the predictor YEAR. This result differs from that obtained through the RF algorithm, which ascribes greater importance to the variables population and household tenure owned with mortgage (POP and OM).

We measure the goodness of prediction through the root mean square error (RMSE) and mean absolute percent error (MAPE), respectively defined as:

$$RMSE = \frac{\sum_i (y_i - \hat{y}_i)^2}{n} \tag{7}$$

$$MAPE = \frac{100}{N} \sum_i \left| \frac{y_i - \hat{y}_i}{y_i} \right| \tag{8}$$

The resulting values of RMSE and MAPE are shown in Table 6 for RF and GLM: the improvement in the prediction obtained by applying RF with respect to the traditional GLM is strong, reducing the MAPE from 5.75% to 1.68%.

Table 6. RMSE and MAPE on predicted values, years 2012–2016.

Measure	RF	GLM
RMSE	8505	24,416
MAPE	1.68%	5.75%

Figure 7 illustrates the predicted average house prices obtained by the random forest algorithm compared to the values predicted by GLM. We can observe that GLM overestimates the AHP values in the period 2012–2014 and underestimates them in 2015–2016. The RF algorithm turns out to be more flexible, characterized by a better adaptive capacity.

In addition, we apply the Diebold–Mariano test (Diebold and Mariano 1995) for comparing the accuracy of forecast performance between RF and GLM. We define the forecast error e_{it} as:

$$e_{it} = \hat{y}_{it} - y_t \quad i = 1, 2 \tag{9}$$

where $\hat{y}_{it}$ and y_t are the predicted and actual values at time t, respectively. The loss associated with forecast i is assumed to be a function of the forecast error and is denoted by $g(e_{it})$. We assume $g(e_{it}) = e_{it}^2$. The two forecasts have equal accuracy if and only if the loss differential between the two forecasts, $d_t = g(e_{1t}) - g(e_{2t})$, has zero expectation for all t.

The DM test statistic is defined as follows:

$$DM = \frac{\bar{d}}{\sqrt{\frac{s}{N}}} \tag{10}$$

where $\bar{d}$ is the sample mean of the loss differential, s is the variance, and N the sample size. The null hypothesis of this test is that the models have the same forecast accuracy, i.e., $H_0 : E[d_t] = 0, \forall t$, while the alternative hypothesis is that $H_1 : E[d_t] \neq 0, \forall t$. If H_0 is true, then the DM statistic is asymptotically distributed as a normal standard normal distribution with 0 mean and standard deviation equal to 1.

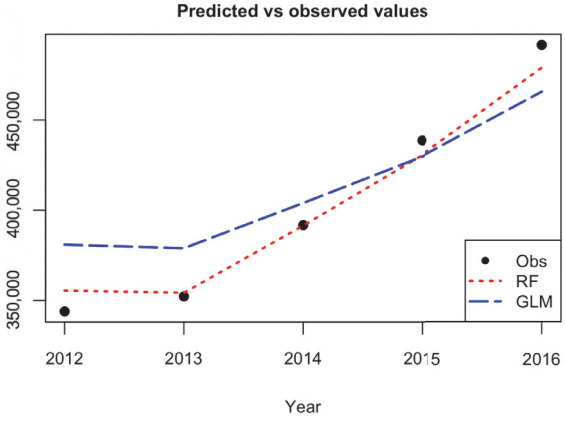

Figure 7. AHP: predicted (RF, GLM) versus observed values (Obs), years 2012–2016.

According to the DM test, since $DM = -2.416$ with p-value = 0.0365, the null hypothesis is rejected at the 5% level of significance, indicating that the observed differences between RF and GLM are significant and the forecasting accuracy of RF is better than that of GLM.

At the end of this section we briefly focus on a problem often ignored by the literature: the endogeneity of predictors that produces bias in the forecast results of regression algorithms. In our case, for instance, newly built homes may certainly affect home prices, but also the opposite could be true as well. The endogeneity could generate bias in the regression models and impacts on statistical significance of the coefficients. In the ordinary least square regression the bootstrapping method is used to reduce the bias of the coefficients. However, nonlinear methods in machine learning cannot provide coefficients of each feature, and thus it is not possible to bias correct the nonlinear regression. Recently, to overcome this problem Ghosal (2018) develop the one-step boost random forest for bias correction.

4. Conclusions

In this paper we have implemented a machine learning algorithm, RF, to predict houses price with an application to UK real estate data. In particular, we have analyzed the average house price of the center of London, taking in consideration urban explicative variables of the demand and supply of the houses. The point of view offered is different and complementary with respect to the literature on the field, which considers features attaining the buildings like size and location, and is based on an urban perspective to explain the evolution of the local real estate market. This is the main reason our data set has been selected. Despite the dataset size being small, the numerical results show a better prediction improvement by RF with respect to the traditional regression approach based on GLM. The use of RF in small datasets is common among data scientists as the bootstrapping, on which RF is based, allows the algorithm to perform well anyway. RF is relatively easy to build and does not require expensive hyperparameters tuning. Besides, to avoid overfitting that generally affects the models trained on small datasets, we control both the number of trees and the maximum depth. This improves the model's ability to do not see patterns that do not exist. As regard to the importance of variables, the algorithm selects the local population as the most predictive variable. This result confirms that the

demand size is the main driver of the real estate market. The space for further works is twofold: on one hand the model presented is flexible and can be easily extended to combine variables related to supply and demand with others attaining to the physical features of the house, on the other hand, different machine learning algorithms, like that deals with the problem of the endogeneity of predictors and the bias of results, can be implemented and compared. The research conducted can be reproduced for the analysis of other real estate dataset. A more accurate forecast of the evolution of real estate market prices must exploit not only variables relating to local characteristics of the market, but also combine them with different information sources such as macroeconomic ones. The improvements achieved can show practical feedback for the whole society. As population and urbanization grow, the need for models able to catch the possible evolution of the real estate market concerns more stakeholders, from homeowners to real estate companies to insurance companies and so on. In modern society we are witnessing the growth of the elderly "cash poor house rich", those who own a home but have retirement incomes so low that they cannot ensure a decent survival and the necessary medical care. Faced with this phenomenon, the insurance market of Reverse Mortgage is developing considerably. In this context, the role that data play will be at the core of the forecasting of assets future value in terms of real-world evaluation and of the cost of insurance contracts related to house valuation.

Author Contributions: The authors have equally contributed to the paper. All authors have read and agreed to the published version of the manuscript.

Funding: This research received no external funding.

Conflicts of Interest: The authors declare no conflict of interest.

References

Alfiyatin, Adyan Nur, Ruth Ema Febrita, Hilman Taufiq, and Wayan Firdaus Mahmudy. 2017. Modeling House Price Prediction using Regression Analysis and Particle Swarm Optimization Case Study: Malang, East Java, Indonesia. *International Journal of Advanced Computer Science and Applications* 8. [CrossRef]

Antipov, Evgeny A., and Elena B. Pokryshevskaya. 2012. Mass appraisal of residential apartments: An application of Random forest for valuation and a CART-based approach for model diagnostics. *Expert Systems with Applications* 39: 1772–78. [CrossRef]

Arvanitidis, Pachalis A. 2014. *The Economics of Urban Property Markets: An Institutional Economics Analysis*. Series: Routledge Studies in the European Economy. London and New York: Routledge, Taylor & Francis Group. ISBN 9780415426824.

Baldominos, Alejandro, Ivan Blanco, Antonio José Moreno, Rubén Iturrarte, Oscar Bernardez, and Carlos Alfonso. 2018. Identifying Real Estate Opportunities Using Machine Learning. *Applied Science* 8. [CrossRef]

Beutel, Johannes, Sophia List, and Gregor von Schweinitz. 2019. Does machine learning help us predict banking crises? *Journal of Financial Stability* 45. [CrossRef]

Bourassa, Steven C., Eva Cantoni, and Martin Hoesli. 2010. Predicting house prices with spatial dependence: A comparison of alternative methods. *Journal of Real Estate Research* 32: 139–59.

Breiman, Leo. 1996. Bagging predictors. *Machine Learning* 24: 123–40. [CrossRef]

Breiman, Leo. 2001. Random forests. *Machine Learning* 45: 5–32. [CrossRef]

Case, Bradford, John Clapp, Robin Dubin, and Mauricio Rodriguez. 2004. Modeling spatial and temporal house price patterns: A comparison of four models. *The Journal of Real Estate Finance and Economics* 29: 167–91. [CrossRef]

Čeh, Marian, Milan Kilibarda, Anka Lisec, and Branislav Bajat. 2018. Estimating the Performance of Random Forest versus Multiple Regression for Predicting Prices of the Apartments. *ISPRS International Journal of Geo-Information* 7: 168. [CrossRef]

Chica-Olmo, Jorge. 2007. Prediction of Housing Location Price by a Multivariate Spatial Method. *Cokriging, Journal of Real Estate Research* 29: 91–114.

Coen, Alan, Patrick Lecomte, and Dorra Abdelmoula. 2018. The Financial Performance of Green Reits Revisited. *Journal of Real Estate Portfolio Management* 24: 95–105. [CrossRef]

Crampton, Graham, and Alan Evans. 1992. The economy of an agglomeration: The case of London. *Urban Studies* 29: 259–71. [CrossRef]

Del Giudice, Vincenzo, Pierfrancesco de Paola, and Giovanni Battista Cantisani. 2017a. Valuation of Real Estate Investments through Fuzzy Logic. *Buildings* 7: 26. [CrossRef]

Del Giudice, Vincenzo, Benedetto Manganelli, and Pierfrancesco de Paola. 2017b. Hedonic analysis of housing sales prices with semiparametric methods. *International Journal of Agricoltural and Environmental Information System* 8: 65–77. [CrossRef]

Diebold, Francis X., and Roberto S. Mariano. 1995. Comparing Predictive Accuracy. *Journal of Business and Economic Statistics* 13: 253–63.

Di Lorenzo, Emilia, Gabriella Piscopo, Marilena Sibillo, and Roberto Tizzano. 2020a. Reverse Mortgages: Risks and Opportunities. In *Demography of Population Health, Aging and Health Expenditures*. Edited by Christos Skiadas and Charilaos Skiadas. Springer Series on Demographic Methods and Population Analysis. Cham: Springer, pp. 435–42. ISBN 978-3-030-44695-6.

Di Lorenzo, Emilia, Gabriella Piscopo, Marilena Sibillo, and Roberto Tizzano. 2020b. Reverse mortgages through artificial intelligence: New opportunities for the actuaries. *Decision in Economics and Finance* doi:10.1007/s10203-020-00274-y. [CrossRef]

Gao, Guangliang, Zhifeng Bao, Jie Cao, A. K. Quin, and Timos Sellis. 2019. Location Centered House Price Prediction: A Multi-Task Learning Approach. *arXiv* arXiv:1901.01774.

Gerek, Ibrahim Halil. 2014. House selling price assessment using two different adaptive neuro fuzzy techniques. *Automation in Construction* 41: 33–39. [CrossRef]

Ghosal, Indrayudh, and Giles Hooker. 2018. Boosting random forests to reduce bias; One step boosted forest and its variance estimate. *arXiv* arXiv:1803.08000.

Glaeser, Edward L., Joseph Gyourko, Eduardo Morales, and Charles G. Nathanson. 2014. Housing dynamics: An urban approach. *Journal of Urban Economics* 81: 45–56. [CrossRef]

Greater London Authority, Housing in London. 2018. *The Evidence Base for the Mayor's Housing Strategy*. London: Greater London Authority, City Hall.

Greenstein, Shane M., Catherine E. Tucker, Lynn Wu, and Erik Brynjolfsson. 2015. The Future of Prediction: How Google Searches Foreshadow Housing Prices and Sales. In *Economic Analysis of the Digital Economy*. Chicago: The University of Chicago Press, pp. 89–118.

Grum, Bojan, and Darja Kobe Govekar. 2016. Influence of Macroeconomic Factors on Prices of Real Estate in Various Cultural Environments: Case of Slovenia, Greece, France, Poland and Norway. *Procedia Economics and Finance* 39: 597–604. [CrossRef]

Gu, Jirong, Mingcang Zhu, and Jiang Liuguangyan. 2011. Housing price forecasting based on genetic algorithm and support vector machine. *Expert Systems with Applications* 38: 3383–86. [CrossRef]

Guan, Jian, Jozef M. Zurada, and Alan S. Levitan. 2008. An Adaptive Neuro-Fuzzy Inference System Based Approach to Real Estate Property Assessment. *Journal of Real Estate Research* 30: 395–422.

Guan, Jian, Donghui Shi, Jozef M. Zurada, and Alan S. Levitan. 2014. Analyzing Massive Data Sets: An Adaptive Fuzzy Neural Approach for Prediction, with a Real Estate Illustration. *Journal of Organizational Computing and Electronic Commerce* 24: 94–112. [CrossRef]

Hong, Jengei, Heeyoul Choi, and Woo-sung Kim. 2020. A house price valuation based on the random forest approach: The mass appraisal of residential property in South Korea. *International Journal of Strategic Property Management* 24: 140–52. [CrossRef]

James, Gareth, Daniela Witten, Trevor Hastie, and Robert Tibshirani. 2017. *An Introduction to Statistical Learning: With Applications in R. Springer Texts in Statistics*. Cham: Springer Publishing Company, Incorporated. ISBN 10: 1461471370.

Krol, Anna. 2013. Application of hedonic methods in modelling real estate prices in Poland. In *Data Science, Learning by Latent Structures and Knowledge Discovery*. Berlin: Springer, pp. 501–11.

Liang, Jiang, Peter C. B. Phillips, and Jun Yu. 2015. A New Hedonic Regression for Real Estate Prices Applied to the Singapore Residential Market. *Journal of Banking and Finance* 61: 121–31.

Liaw, Andy. 2018. Package. *Randomforest*. Available online: https://cran.r-project.org/web/packages/randomForest/randomForest.pdf (accessed on 20 April 2020).

Loh, Wei-Yin. 2011. Classification and regression trees. *Wiley Interdisciplinary Reviews: Data Mining and Knowledge Discovery* 1. [CrossRef]

Lopez-Alcala, Mario. 2016. *The Crisis of Affordability in Real Estate*. London: MSCI. McKinsey Global Institute.

Manganelli, Benedetto, Pierfrancesco de Paola, and Vincenzo Del Giudice. 2016. Linear Programming in a Multi-Criteria Model for Real Estate Appraisal. Paper presented at the International Conference on Computational Science and Its Applications, Part I, Beijing, China, July 4–7.

Manjula, Raja, Shubham Jain, Sharad Srivastava, and Pranav Rajiv Kher. 2017. Real estate value prediction using multivariate regression models. In *IOP Conf. Ser.: Materials Science and Engineering*. Bristol: IOP Publishing.

McKinsey Global Institute. 2016. *People on the Move: Global Migration's Impact and Opportunity*. London: McKinsey Global Institute.

Miller, Norm G., Dave Pogue, Quiana D. Gough, and Susan M. Davis. 2009. Green Buildings and Productivity. *Journal of Sustainable Real Estate* 1: 65–89.

Montero, José Maria, Roman Minguez, and Gema Fernandez Avilés. 2018. Housing price prediction: Parametric versus semiparametric spatial hedonic models. *Journal of Geographical Systems* 20: 27–55. [CrossRef]

Morrison, Doug, Adam Branson, Mike Phillips, Jane Roberts, and Stuart Watson. 2019. *Emerging Trend in Real Estate. Creating an Impact*. Washington: PwC and Urban Land Institute.

National Geographic. 2018. How London became the centre of the world. *National Geographic*, October 27.

Nghiep, Nguyen, and Al Cripps. 2001. Predicting Housing Value: A Comparison of Multiple Regression Analysis and Artificial Neural Networks. *Journal of Real Estate Research* 22: 313–36.

Ozdenerol, Esra, Ying Huang, Farid Javadnejad, and Anzhelika Antipova. 2015. The Impact of Traffic Noise on Housing Values. *Journal of Real Estate Practice and Education* 18: 35–54. [CrossRef]

Pai, Ping-Feng, and Wen-Chang Wang. 2020. Using Machine Learning Models and Actual Transaction Data for Predicting Real Estate Prices. *Applied Sciences* 10: 5832. [CrossRef]

Park, Byeonghwa, and Jae Kwon Bae. 2015. Using machine learning algorithms for housing price prediction: The case of fairfax county, virginia housing data. *Expert Systems with Applications* 42: 2928–34. [CrossRef]

Quinlan, John Ross 1986. Induction of decision trees. *Machine Learning* 1: 81–106. [CrossRef]

Rahadi, Raden Aswin, Sudarso Wiryono, Deddy Koesrindartotoor, and Indra Budiman Syamwil. 2015. Factors influencing the price of housing in Indonesia. *International Journal of House Market Analysis* 8: 169–88. [CrossRef]

Sarip, Abdul Ghani, Muhammad Burhan Hafez, and Md Nasir Daud. 2016. Application of Fuzzy Regression Model for Real Estate Price Prediction. *The Malaysian Journal of Computer Science* 29: 15–27. [CrossRef]

Selim, Hasan. 2009. Determinants of house prices in turkey: Hedonic regression versus artificial neural network. *Expert Systems with Applications* 36: 2843–52. [CrossRef]

Tanaka, Katsuyuki, Takuo Higashide, Takuji Kinkyo, and Shigeyuki Hamori. 2019. Analyzing industry-level vulnerability by predicting financial bankruptcy. *Economic Inquiry* 57: 2017–34. [CrossRef]

Tanaka, Katsuyuki, Takuo Kinkyo, and Shigeyuki Hamori. 2016. Random Forests-based Early Warning System for Bank Failures. *Economics Letters* 148: 118–21. [CrossRef]

United Nations. 2019. *World Population Prospects: The 2017 Revision, Key Findings & Advance Tables*. Working Paper No. ESA/P/WP/248. New York: United Nations.

Van Doorn, Lisette, Amanprit Arnold, and Elizabeth Rapoport. 2019. In the Age of Cities: The Impact of Urbanisation on House Prices and Affordability. In *Hot Property*. Edited by Rob Nijskens, Melanie Lohuis, Paul Hilbers and Willem Heeringa. Cham: Springer.

Wang, Xibin, Junhao Wen, Yihao Zhang, and Yubiao Wang. 2014. Real estate price forecasting based on svm optimized by pso. *Optik-International Journal for Light and Electron Optics* 125: 1439–43. [CrossRef]

Winson Geideman, Kimberly. 2018. Sentiments and Semantics: A Review of the Content Analysis Literature in the Era of Big Data. *Journal of Real Estate Literature* 26: 1–12.

Wright, Marvin, Andreas Ziegler, and Inke König. 2016. Do little interactions get lost in dark random forests? *BMC Bioinformatics* 17: 145. [CrossRef]

Xu, Yun, and Roystone Goodacre. 2018. On Splitting Training and Validation Set: A Comparative Study of Cross-Validation, Bootstrap and Systematic Sampling for Estimating the Generalization Performance of Supervised Learning. *Journal of Analysis and Testing* 2: 249–62. [CrossRef] [PubMed]

Yacim, Joseph Awoamim, and Douw Boshoff. 2018. Impact of Artificial Neural Networks Training Algorithms on Accurate Prediction of Property Values. *Journal of Real Estate Research* 40: 375–418.

Yacim, Joseph Awoamim, Douw Boshoff, and Abdullah Khan. 2016. Hybridizing Cuckoo Search with Levenberg Marquardt Algorithms in Optimization and Training Of ANNs for Mass Appraisal of Properties. *Journal of Real Estate Literature* 24: 473–92.

Zurada, Jozef, Alan Levitan, and Jian Guan. 2011. A Comparison of Regression and Artificial Intelligence Methods in a Mass Appraisal Context. *Journal of Real Estate Research* 33: 349–87.

risks

MDPI

Article

Pricing with Variance Gamma Information

Lane P. Hughston [1,*] and Leandro Sánchez-Betancourt [2]

[1] Department of Computing, Goldsmiths University of London, New Cross, London SE14 6NW, UK
[2] Mathematical Institute, University of Oxford, Oxford OX2 6GG, UK; leandro.sanchezbetancourt@maths.ox.ac.uk
* Correspondence: L.Hughston@gold.ac.uk

Received: 11 September 2020; Accepted: 30 September 2020; Published: 10 October 2020

Abstract: In the information-based pricing framework of Brody, Hughston & Macrina, the market filtration $\{\mathcal{F}_t\}_{t\geq 0}$ is generated by an information process $\{\xi_t\}_{t\geq 0}$ defined in such a way that at some fixed time T an $\mathcal{F}_T$-measurable random variable X_T is "revealed". A cash flow H_T is taken to depend on the market factor X_T, and one considers the valuation of a financial asset that delivers H_T at time T. The value of the asset S_t at any time $t \in [0, T)$ is the discounted conditional expectation of H_T with respect to $\mathcal{F}_t$, where the expectation is under the risk neutral measure and the interest rate is constant. Then $S_{T^-} = H_T$, and $S_t = 0$ for $t \geq T$. In the general situation one has a countable number of cash flows, and each cash flow can depend on a vector of market factors, each associated with an information process. In the present work we introduce a new process, which we call the normalized variance-gamma bridge. We show that the normalized variance-gamma bridge and the associated gamma bridge are jointly Markovian. From these processes, together with the specification of a market factor X_T, we construct a so-called variance-gamma information process. The filtration is then taken to be generated by the information process together with the gamma bridge. We show that the resulting extended information process has the Markov property and hence can be used to develop pricing models for a variety of different financial assets, several examples of which are discussed in detail.

Keywords: information-based asset pricing; Lévy processes; gamma processes; variance gamma processes; Brownian bridges; gamma bridges; nonlinear filtering

1. Introduction

The theory of information-based asset pricing proposed by Brody et al. (2007, 2008a, 2008b) and Macrina (2006) is concerned with the determination of the price processes of financial assets from first principles. In particular, the market filtration is constructed explicitly, rather than simply assumed, as it is in traditional approaches. The simplest version of the model is as follows. We fix a probability space $(\Omega, \mathscr{F}, \mathbb{P})$. An asset delivers a single random cash flow H_T at some specified time $T > 0$, where time 0 denotes the present. The cash flow is a function of a random variable X_T, which we can think of as a "market factor" that is in some sense revealed at time T. In the general situation there will be many factors and many cash flows, but for the present we assume that there is a single factor $X_T : \Omega \to \mathbb{R}$ such that the sole cash flow at time T is given by $H_T = h(X_T)$ for some Borel function $h : \mathbb{R} \to \mathbb{R}^+$. For simplicity we assume that interest rates are constant and that $\mathbb{P}$ is the risk neutral measure. We require that H_T should be integrable. Under these assumptions, the value of the asset at time 0 is

$$S_0 = \mathrm{e}^{-rT}\,\mathbb{E}\left[h(X_T)\right], \tag{1}$$

where $\mathbb{E}$ denotes expectation under $\mathbb{P}$ and r is the short rate. Since the single "dividend" is paid at time T, the value of the asset at any time $t \geq 0$ is of the form

$$S_t = \mathrm{e}^{-r(T-t)} \mathbb{1}_{\{t<T\}} \mathbb{E}\left[h(X_T) \,\middle|\, \mathscr{F}_t\right], \tag{2}$$

where $\{\mathscr{F}_t\}_{t\geq 0}$ is the market filtration. The task now is to model the filtration, and this will be done explicitly.

In traditional financial modelling, the filtration is usually taken to be fixed in advance. For example, in the widely-applied Brownian-motion-driven model for financial markets, the filtration is generated by an n-dimensional Brownian motion. A detailed account of the Brownian framework can be found, for example, in Karatzas and Shreve (1998). In the information-based approach, however, we do not assume the filtration to be given *a priori*. Instead, the filtration is constructed in a way that specifically takes into account the structures of the information flows associated with the cash flows of the various assets under consideration.

In the case of a single asset generating a single cash flow, the idea is that the filtration should contain partial or "noisy" information about the market factor X_T, and hence the impending cash flow, in such a way that X_T is $\mathscr{F}_T$-measurable. This can be achieved by allowing $\{\mathscr{F}_t\}$ to be generated by a so-called information process $\{\xi_t\}_{t\geq 0}$ with the property that for each t such that $t \geq T$ the random variable ξ_t is $\sigma\{X_T\}$-measurable. Then by constructing specific examples of cádlàg processes having this property, we are able to formulate a variety of specific models. The resulting models are finely tuned to the structures of the assets that they represent, and therefore offer scope for a useful approach to financial risk management. In previous work on information-based asset pricing, where precise definitions can be found that expand upon the ideas summarized above, such models have been constructed using Brownian bridge information processes (Brody et al. (2007, 2008a, 2009, 2010, 2011), Filipović et al. (2012), Hughston and Macrina (2012), Macrina (2006), Mengütürk (2013), Rutkowski and Yu (2007)), gamma bridge information processes (Brody et al. (2008b)), Lévy random bridge information processes (Hoyle (2010), Hoyle et al. (2011, 2015, 2020), Mengütürk (2018)) and Markov bridge information processes (Macrina (2019)). In what follows we present a new model for the market filtration, based on the variance-gamma process. The idea is to create a two-parameter family of information processes associated with the random market factor X_T. One of the parameters is the information flow-rate σ. The other is an intrinsic parameter m associated with the variance gamma process. In the limit as m tends to infinity, the variance-gamma information process reduces to the type of Brownian bridge information process considered by Brody et al. (2007, 2008a) and Macrina (2006).

The plan of the paper is as follows. In Section 2 we recall properties of the gamma process, introducing the so-called scale parameter $\kappa > 0$ and shape parameter $m > 0$. A standard gamma subordinator is defined to be a gamma process with $\kappa = 1/m$. The mean at time t of a standard gamma subordinator is t. In Theorem 1 we prove that an increase in the shape parameter m results in a transfer of weight from the Lévy measure of any interval $[c, d]$ in the space of jump size to the Lévy measure of any interval $[a, b]$ such that $b - a = d - c$ and $c > a$. Thus, roughly speaking, an increase in m results in an increase in the rate at which small jumps occur relative to the rate at which large jumps occur. This result concerning the interpretation of the shape parameter for a standard gamma subordinator is new as far as we are aware.

In Section 3 we recall properties of the variance-gamma process and the gamma bridge, and in Definition 1 we introduce a new type of process, which we call a normalized variance-gamma bridge. This process plays an important role in the material that follows. In Lemmas 1 and 2 we work out various properties of the normalized variance-gamma bridge. Then in Theorem 2 we show that the normalized variance-gamma bridge and the associated gamma bridge are jointly Markov, a property that turns out to be crucial in our pricing theory. In Section 4, at Definition 2, we introduce the so-called

variance-gamma information process. The information process carries noisy information about the value of a market factor X_T that will be revealed to the market at time T, where the noise is represented by the normalized variance-gamma bridge. In Equation (58) we present a formula that relates the values of the information process at different times, and by use of that we establish in Theorem 3 that the information process and the associated gamma bridge are jointly Markov.

In Section 5, we consider a market where the filtration is generated by a variance gamma information process along with the associated gamma bridge. In Lemma 3 we work out a version of the Bayes formula in the form that we need for asset pricing in the present context. Then in Theorem 4 we present a general formula for the price process of a financial asset that at time T pays a single dividend given by a function $h(X_T)$ of the market factor. In particular, the *a priori* distribution of the market factor can be quite arbitrary, specified by a measure $F_{X_T}(\mathrm{d}x)$ on $\mathbb{R}$, the only requirement being that $h(X_T)$ should be integrable. In Section 6 we present a number of examples, based on various choices of the payoff function and the distribution for the market factor, the results being summarized in Propositions 1–4. We conclude with comments on calibration, derivatives, and how one determines the trajectory of the information process from market prices.

2. Gamma Subordinators

We begin with some remarks about the gamma process. Let us as usual write $\mathbb{R}^+$ for the non-negative real numbers. Let κ and m be strictly positive constants. A continuous random variable $G : \Omega \to \mathbb{R}^+$ on a probability space $(\Omega, \mathscr{F}, \mathbb{P})$ will be said to have a gamma distribution with scale parameter κ and shape parameter m if

$$\mathbb{P}\left[G \in \mathrm{d}x\right] = \mathbb{1}_{\{x>0\}} \frac{1}{\Gamma[m]} \kappa^{-m} x^{m-1} \mathrm{e}^{-x/\kappa} \mathrm{d}x\,, \tag{3}$$

where

$$\Gamma[a] = \int_0^\infty x^{a-1} \mathrm{e}^{-x} \mathrm{d}x \tag{4}$$

denotes the standard gamma function for $a > 0$, and we recall the relation $\Gamma[a+1] = a\Gamma[a]$. A calculation shows that $\mathbb{E}\left[G\right] = \kappa\, m$, and $\mathrm{Var}[G] = \kappa^2\, m$. There exists a two-parameter family of gamma processes of the form $\Gamma : \Omega \times \mathbb{R}^+ \to \mathbb{R}^+$ on $(\Omega, \mathscr{F}, \mathbb{P})$. By a gamma process with scale κ and shape m we mean a Lévy process $\{\Gamma_t\}_{t\geq 0}$ such that for each $t > 0$ the random variable Γ_t is gamma distributed with

$$\mathbb{P}\left[\Gamma_t \in \mathrm{d}x\right] = \mathbb{1}_{\{x>0\}} \frac{1}{\Gamma[m\,t]} \kappa^{-m\,t} x^{m\,t-1} \mathrm{e}^{-x/\kappa} \mathrm{d}x\,. \tag{5}$$

If we write $(a)_0 = 1$ and $(a)_k = a(a+1)(a+2)\cdots(a+k-1)$ for the so-called Pochhammer symbol, we find that $\mathbb{E}[\Gamma_t^n] = \kappa^n (mt)_n$. It follows that $\mathbb{E}[\Gamma_t] = \mu\, t$ and $\mathrm{Var}[\Gamma_t] = \nu^2\, t$, where $\mu = \kappa\, m$ and $\nu^2 = \kappa^2\, m$, or equivalently $m = \mu^2/\nu^2$, and $\kappa = \nu^2/\mu$.

The Lévy exponent for such a process is given for $\alpha < 1$ by

$$\psi_\Gamma(\alpha) = \frac{1}{t} \log \mathbb{E}\left[\exp(\alpha \Gamma_t)\right] = -m\, \log\left(1 - \kappa\alpha\right), \tag{6}$$

and for the corresponding Lévy measure we have

$$\nu_\Gamma(\mathrm{d}x) = \mathbb{1}_{\{x>0\}}\, m\, \frac{1}{x}\, \mathrm{e}^{-x/\kappa}\, \mathrm{d}x\,. \tag{7}$$

One can then check that the Lévy-Khinchine relation

$$\psi_\Gamma(\alpha) = \int_{\mathbb{R}} \left(\mathrm{e}^{\alpha x} - 1 - \mathbb{1}_{\{|x|<1\}}\, \alpha x \right) \nu_\Gamma(\mathrm{d}x) + p\alpha \tag{8}$$

holds for an appropriate choice of p (Kyprianou 2014, Lemma 1.7).

By a standard gamma subordinator we mean a gamma process $\{\gamma_t\}_{t\geq 0}$ for which $\kappa = 1/m$. This implies that $\mathbb{E}[\gamma_t] = t$ and $\mathrm{Var}[\gamma_t] = m^{-1}\, t$. The standard gamma subordinators thus constitute a one-parameter family of processes labelled by m. An interpretation of the parameter m is given by the following:

Theorem 1. *Let $\{\gamma_t\}_{t\geq 0}$ be a standard gamma subordinator with parameter m. Let $\nu_m[a,b]$ be the Lévy measure of the interval $[a,b]$ for $0 < a < b$. Then for any interval $[c,d]$ such that $c > a$ and $d - c = b - a$ the ratio*

$$R_m(a,b\,;c,d) = \frac{\nu_m[a,b]}{\nu_m[c,d]} \tag{9}$$

is strictly greater than one and strictly increasing as a function of m.

Proof. By the definition of a standard gamma subordinator we have

$$\nu_m[a,b] = \int_a^b m\, \frac{1}{x}\, \mathrm{e}^{-m\,x}\, \mathrm{d}x\,. \tag{10}$$

Let $\delta = c - a > 0$ and note that the integrand in the right hand side of (10) is a decreasing function of the variable of integration. This allows one to conclude that

$$\nu_m[a+\delta, b+\delta] = \int_{a+\delta}^{b+\delta} m\, \frac{1}{x}\, \mathrm{e}^{-m\,x}\, \mathrm{d}x < \int_a^b m\, \frac{1}{x}\, \mathrm{e}^{-m\,x}\, \mathrm{d}x\,, \tag{11}$$

from which it follows that $0 < \nu_m[c,d] < \nu_m[a,b]$ and hence $R_m(a,b\,;c,d) > 1$. To show that $R_m(a,b;c,d)$ is strictly increasing as a function of m we observe that

$$\nu_m[a,b] = m \int_a^\infty \frac{1}{x}\, \mathrm{e}^{-m\,x}\, \mathrm{d}x - m \int_b^\infty \frac{1}{x}\, \mathrm{e}^{-m\,x}\, \mathrm{d}x \;=\; m\, \left(E_1[m\,a] - E_1[m\,b] \right), \tag{12}$$

where the so-called exponential integral function $E_1(z)$ is defined for $z > 0$ by

$$E_1(z) = \int_z^\infty \frac{\mathrm{e}^{-x}}{x} \mathrm{d}x\,. \tag{13}$$

See Abramowitz and Stegun (1972), Section 5.1.1, for properties of the exponential integral. Next, we compute the derivative of $R_m(a,b\,;c,d)$, which gives

$$\frac{\partial}{\partial m} R_m(a,b\,;c,d) = \frac{1}{m\, \left(E_1[m\,c] - E_1[m\,d] \right)}\, \mathrm{e}^{-m\,a}\, \left(1 - \mathrm{e}^{-m\,\Delta} \right) \left(R_m(a,b\,;c,d) - \mathrm{e}^{m(c-a)} \right), \tag{14}$$

where

$$\Delta = d - c = b - a\,. \tag{15}$$

We note that

$$\frac{1}{m\, \left(E_1[m\,c] - E_1[m\,d] \right)}\, \mathrm{e}^{-m\,a}\, \left(1 - \mathrm{e}^{-m\,\Delta} \right) \;>\; 0\,, \tag{16}$$

which shows that the sign of the derivative in (14) is strictly positive if and only if

$$R_m(a,b\,;c,d) \;>\; \mathrm{e}^{m(c-a)}. \tag{17}$$

But clearly

$$\int_0^{\Delta m} \frac{\mathrm{e}^{-u}}{u + a\,m}\,\mathrm{d}u \;>\; \int_0^{\Delta m} \frac{\mathrm{e}^{-u}}{u + c\,m}\,\mathrm{d}u \tag{18}$$

for $c > a$, which after a change of integration variables and use of (15) implies

$$\mathrm{e}^{m\,a} \int_{a\,m}^{b\,m} \frac{\mathrm{e}^{-x}}{x}\,\mathrm{d}x \;>\; \mathrm{e}^{m\,c} \int_{c\,m}^{d\,m} \frac{\mathrm{e}^{-x}}{x}\,\mathrm{d}x, \tag{19}$$

which is equivalent to (17), and that completes the proof. □

We see therefore that the effect of an increase in the value of m is to transfer weight from the Lévy measure of any jump-size interval $[c, d] \subset \mathbb{R}^+$ to any possibly-overlapping smaller-jump-size interval $[a, b] \subset \mathbb{R}^+$ of the same length. The Lévy measure of such an interval is the rate of arrival of jumps for which the jump size lies in that interval.

3. Normalized Variance-Gamma Bridge

Let us fix a standard Brownian motion $\{W_t\}_{t\geq 0}$ on $(\Omega, \mathscr{F}, \mathbb{P})$ and an independent standard gamma subordinator $\{\gamma_t\}_{t\geq 0}$ with parameter m. By a standard variance-gamma process with parameter m we mean a time-changed Brownian motion $\{V_t\}_{t\geq 0}$ of the form

$$V_t = W_{\gamma_t}\,. \tag{20}$$

It is straightforward to check that $\{V_t\}$ is itself a Lévy process, with Lévy exponent

$$\psi_V(\alpha) = -m\,\log\left(1 - \frac{\alpha^2}{2\,m}\right). \tag{21}$$

Properties of the variance-gamma process, and financial models based on it, have been investigated extensively in Madan (1990), Madan and Milne (1991), Madan et al. (1998), Carr et al. (2002) and many other works.

The other object we require going forward is the gamma bridge (Brody et al. (2008b), Emery and Yor (2004), Yor (2007)). Let $\{\gamma_t\}$ be a standard gamma subordinator with parameter m. For fixed $T > 0$ the process $\{\gamma_{tT}\}_{t\geq 0}$ defined by

$$\gamma_{tT} = \frac{\gamma_t}{\gamma_T} \tag{22}$$

for $0 \leq t \leq T$ and $\gamma_{tT} = 1$ for $t > T$ will be called a standard gamma bridge, with parameter m, over the interval $[0, T]$. One can check that for $0 < t < T$ the random variable γ_{tT} has a beta distribution (Brody et al. 2008b, pp. 6–9). In particular, one finds that its density is given by

$$\mathbb{P}\left[\gamma_{tT} \in \mathrm{d}y\right] = \mathbb{1}_{\{0<y<1\}}\,\frac{y^{mt-1}(1-y)^{m(T-t)-1}}{B[mt, m(T-t)]}\,\mathrm{d}y\,, \tag{23}$$

where

$$B[a, b] = \frac{\Gamma[a]\,\Gamma[b]}{\Gamma[a+b]}\,. \tag{24}$$

It follows then by use of the integral formula

$$B[a, b] = \int_0^1 y^{a-1}(1-y)^{b-1}\mathrm{d}y \tag{25}$$

that for all $n \in \mathbb{N}$ we have

$$\mathbb{E}\left[\gamma_{tT}^{n}\right] = \frac{B[mt+n, m(T-t)]}{B[mt, m(T-t)]}, \tag{26}$$

and hence

$$\mathbb{E}\left[\gamma_{tT}^{n}\right] = \frac{(mt)_n}{(mT)_n}. \tag{27}$$

Accordingly, one has

$$\mathbb{E}[\gamma_{tT}] = t/T, \quad \mathbb{E}[\gamma_{tT}^2] = t(mt+1)/T(mT+1) \tag{28}$$

and therefore

$$\mathrm{Var}[\gamma_{tT}] = \frac{t(T-t)}{T^2(1+mT)}. \tag{29}$$

One observes, in particular, that the expectation of γ_{tT} does not depend on m, whereas the variance of γ_{tT} decreases as m increases.

Definition 1. *For fixed $T > 0$, the process $\{\Gamma_{tT}\}_{t\geq 0}$ defined by*

$$\Gamma_{tT} = {\gamma_T}^{-\frac{1}{2}} \left(W_{\gamma_t} - \gamma_{tT} W_{\gamma_T}\right) \tag{30}$$

for $0 \leq t \leq T$ and $\Gamma_{tT} = 0$ for $t > T$ will be called a normalized variance gamma bridge.

We proceed to work out various properties of this process. We observe that Γ_{tT} is conditionally Gaussian, from which it follows that $\mathbb{E}\left[\Gamma_{tT} \mid \gamma_t, \gamma_T\right] = 0$ and $\mathbb{E}\left[\Gamma_{tT}^2 \mid \gamma_t, \gamma_T\right] = \gamma_{tT}(1-\gamma_{tT})$. Therefore $\mathbb{E}[\Gamma_{tT}] = 0$ and $\mathbb{E}[\Gamma_{tT}^2] = \mathbb{E}[\gamma_{tT}] - \mathbb{E}[\gamma_{tT}^2]$; and thus by use of (28) we have

$$\mathrm{Var}\left[\Gamma_{tT}\right] = \frac{mt\,(T-t)}{T\,(1+mT)}. \tag{31}$$

Now, recall (Yor (2007), Emery and Yor (2004)) that the gamma process and the associated gamma bridge have the following fundamental independence property. Define

$$\mathscr{G}_t^* = \sigma\left\{\gamma_s/\gamma_t,\ s \in [0,t]\right\}, \quad \mathscr{G}_t^+ = \sigma\left\{\gamma_u,\ u \in [t,\infty)\right\}. \tag{32}$$

Then, for every $t \geq 0$ it holds that $\mathscr{G}_t^*$ and $\mathscr{G}_t^+$ are independent. In particular γ_{st} and γ_u are independent for $0 \leq s \leq t \leq u$ and $t > 0$. It also holds that γ_{st} and γ_{uv} are independent for $0 \leq s \leq t \leq u \leq v$ and $t > 0$. Furthermore, we have:

Lemma 1. *If $0 \leq s \leq t \leq u$ and $t > 0$ then Γ_{st} and γ_u are independent.*

Proof. We recall that if a random variable X is normally distributed with mean μ and variance ν^2 then

$$\mathbb{P}\left[X < x\right] = N\left(\frac{x-\mu}{\nu}\right), \tag{33}$$

where $N : \mathbb{R} \to (0,1)$ is defined by

$$N(x) = \frac{1}{\sqrt{2\pi}} \int_{-\infty}^{x} \exp\left(-\frac{1}{2}y^2\right) \mathrm{d}y. \tag{34}$$

Since Γ_{tT} is conditionally Gaussian, by use of the tower property we find that

$$\begin{aligned} F_{\Gamma_{st},\gamma_u}(x,y) &= \mathbb{E}\left[\mathbb{1}_{\{\Gamma_{st}\le x\}}\,\mathbb{1}_{\{\gamma_u\le y\}}\right] \\ &= \mathbb{E}\left[\mathbb{E}\left[\mathbb{1}_{\{\Gamma_{st}\le x\}}\,\mathbb{1}_{\{\gamma_u\le y\}}\,\middle|\,\gamma_s\,,\gamma_t\,,\gamma_u\right]\right] \\ &= \mathbb{E}\left[\mathbb{1}_{\{\gamma_u\le y\}}\,\mathbb{E}\left[\mathbb{1}_{\{\Gamma_{st}\le x\}}\,\middle|\,\gamma_s\,,\gamma_t\,,\gamma_u\right]\right] \\ &= \mathbb{E}\left[\mathbb{1}_{\{\gamma_u\le y\}}\,N\left(x\,(\gamma_{st}\;(1-\gamma_{st}))^{-\frac{1}{2}}\right)\right] \\ &= \mathbb{E}\left[\mathbb{1}_{\{\gamma_u\le y\}}\right]\mathbb{E}\left[N\left(x\,(\gamma_{st}\;(1-\gamma_{st}))^{-\frac{1}{2}}\right)\right], \end{aligned} \tag{35}$$

where the last line follows from the independence of γ_{st} and γ_u. □

By a straightforward extension of the argument we deduce that if $0 \le s \le t \le u \le v$ and $t > 0$ then Γ_{st} and γ_{uv} are independent. Further, we have:

Lemma 2. *If $0 \le s \le t \le u \le v$ and $t > 0$ then Γ_{st} and Γ_{uv} are independent.*

Proof. We recall that the Brownian bridge $\{\beta_{tT}\}_{0\le t\le T}$ defined by

$$\beta_{tT} = W_t - \frac{t}{T}\,W_T \tag{36}$$

for $0 \le t \le T$ and $\beta_{tT} = 0$ for $t > T$ is Gaussian with $\mathbb{E}[\beta_{tT}] = 0$, $\mathrm{Var}[\beta_{tT}] = t\,(T-t)/T$, and $\mathrm{Cov}[\beta_{sT},\,\beta_{tT}] = s(T-t)/T$ for $0 \le s \le t \le T$. Using the tower property we find that

$$\begin{aligned} F_{\Gamma_{st},\Gamma_{uv}}(x,y) &= \mathbb{E}\left[\mathbb{1}_{\{\Gamma_{st}\le x\}}\,\mathbb{1}_{\{\Gamma_{uv}\le y\}}\right] \\ &= \mathbb{E}\left[\mathbb{E}\left[\mathbb{1}_{\{\Gamma_{st}\le x\}}\,\mathbb{1}_{\{\Gamma_{uv}\le y\}}\,\middle|\,\gamma_s\,,\gamma_t\,,\gamma_u\,,\gamma_v\right]\right] \\ &= \mathbb{E}\left[\mathbb{E}\left[\mathbb{1}_{\{\Gamma_{st}\le x\}}\,\middle|\,\gamma_s\,,\gamma_t\,,\gamma_u\,,\gamma_v\right]\,\mathbb{E}\left[\mathbb{1}_{\{\Gamma_{uv}\le y\}}\,\middle|\,\gamma_s\,,\gamma_t\,,\gamma_u\,,\gamma_v\right]\right] \\ &= \mathbb{E}\left[N\left(x\,((1-\gamma_{st})\,(\gamma_{st}))^{-\frac{1}{2}}\right)\right]\,\mathbb{E}\left[N\left(y\,((1-\gamma_{uv})\,(\gamma_{uv}))^{-\frac{1}{2}}\right)\right], \end{aligned} \tag{37}$$

where in the final step we use (30) along with properties of the Brownian bridge. □

A straightforward calculation shows that if $0 \le s \le t \le u$ and $t > 0$ then

$$\Gamma_{su} = (\gamma_{tu})^{\frac{1}{2}}\;\Gamma_{st} + \gamma_{st}\,\Gamma_{tu}\,. \tag{38}$$

With this result at hand we obtain the following:

Theorem 2. *The processes $\{\Gamma_{tT}\}_{0\le t\le T}$ and $\{\gamma_{tT}\}_{0\le t\le T}$ are jointly Markov.*

Proof. To establish the Markov property it suffices to show that for any bounded measurable function $\phi : \mathbb{R}\times\mathbb{R}\to\mathbb{R}$, any $n\in\mathbb{N}$, and any $0 \le t_n \le t_{n-1} \le \ldots \le t_1 \le t \le T$, we have

$$\begin{aligned} &\mathbb{E}\left[\phi(\Gamma_{tT},\gamma_{tT})\,\middle|\,\Gamma_{t_1T},\,\gamma_{t_1T},\,\Gamma_{t_2T},\,\gamma_{t_2T},\,\ldots\,,\Gamma_{t_nT},\,\gamma_{t_nT}\right] \\ &\quad = \mathbb{E}\left[\phi(\Gamma_{tT},\gamma_{tT})\,\middle|\,\Gamma_{t_1T},\,\gamma_{t_1T}\right]. \end{aligned} \tag{39}$$

We present the proof for $n = 2$. Thus we need to show that

$$\begin{aligned}&\mathbb{E}\left[\phi(\Gamma_{tT}, \gamma_{tT}) \,\middle|\, \Gamma_{t_1T}, \gamma_{t_1T}, \Gamma_{t_2T}, \gamma_{t_2T}\right]\\ &\quad = \mathbb{E}\left[\phi(\Gamma_{tT}, \gamma_{tT}) \,\middle|\, \Gamma_{t_1T}, \gamma_{t_1T}\right]. \end{aligned} \tag{40}$$

As a consequence of (38) we have

$$\begin{aligned}&\mathbb{E}\left[\phi(\Gamma_{tT}, \gamma_{tT}) \,\middle|\, \Gamma_{t_1T}, \gamma_{t_1T}, \Gamma_{t_2T}, \gamma_{t_2T}\right]\\ &\quad = \mathbb{E}\left[\phi(\Gamma_{tT}, \gamma_{tT}) \,\middle|\, \Gamma_{t_1T}, \gamma_{t_1T}, \Gamma_{t_2t_1}, \gamma_{t_2t_1}\right]. \end{aligned} \tag{41}$$

Therefore, it suffices to show that

$$\begin{aligned}&\mathbb{E}\left[\phi(\Gamma_{tT}, \gamma_{tT}) \,\middle|\, \Gamma_{t_1T}, \gamma_{t_1T}, \Gamma_{t_2t_1}, \gamma_{t_2t_1}\right]\\ &\quad = \mathbb{E}\left[\phi(\Gamma_{tT}, \gamma_{tT}) \,\middle|\, \Gamma_{t_1T}, \gamma_{t_1T}\right]. \end{aligned} \tag{42}$$

Let us write

$$f_{\Gamma_{tT}, \gamma_{tT}, \Gamma_{t_1T}, \gamma_{t_1T}, \Gamma_{t_2t_1}, \gamma_{t_2t_1}}(x, y, a, b, c, d) \tag{43}$$

for the joint density of Γ_{tT}, γ_{tT}, Γ_{t_1T}, γ_{t_1T}, $\Gamma_{t_2t_1}$, $\gamma_{t_2t_1}$. Then for the conditional density of Γ_{tT} and γ_{tT} given $\Gamma_{t_1T} = a$, $\gamma_{t_1T} = b$, $\Gamma_{t_2t_1} = c$, $\gamma_{t_2t_1} = d$ we have

$$g_{\Gamma_{tT}, \gamma_{tT}}(x, y, a, b, c, d) = \frac{f_{\Gamma_{tT}, \gamma_{tT}, \Gamma_{t_1T}, \gamma_{t_1T}, \Gamma_{t_2t_1}, \gamma_{t_2t_1}}(x, y, a, b, c, d)}{f_{\Gamma_{t_1T}, \gamma_{t_1T}, \Gamma_{t_2t_1}, \gamma_{t_2t_1}}(a, b, c, d)}. \tag{44}$$

Thus,

$$\begin{aligned}&\mathbb{E}\left[\phi(\Gamma_{tT}, \gamma_{tT}) \,\middle|\, \Gamma_{t_1T}, \gamma_{t_1T}, \Gamma_{t_2t_1}, \gamma_{t_2t_1}\right]\\ &\quad = \int_{\mathbb{R}}\int_{\mathbb{R}} \phi(x, y)\, g_{\Gamma_{tT}, \gamma_{tT}}(x, y, \Gamma_{t_1T}, \gamma_{t_1T}, \Gamma_{t_2t_1}, \gamma_{t_2t_1})\, \mathrm{d}x\, \mathrm{d}y. \end{aligned} \tag{45}$$

Similarly,

$$\begin{aligned}&\mathbb{E}\left[\phi(\Gamma_{tT}, \gamma_{tT}) \,\middle|\, \Gamma_{t_1T}, \gamma_{t_1T}\right]\\ &\quad = \int_{\mathbb{R}}\int_{\mathbb{R}} \phi(x, y)\, g_{\Gamma_{tT}, \gamma_{tT}}(x, y, \Gamma_{t_1T}, \gamma_{t_1T})\, \mathrm{d}x\, \mathrm{d}y, \end{aligned} \tag{46}$$

where for the conditional density of Γ_{tT} and γ_{tT} given $\Gamma_{t_1T} = a$, $\gamma_{t_1T} = b$ we have

$$g_{\Gamma_{tT}, \gamma_{tT}}(x, y, a, b) = \frac{f_{\Gamma_{tT}, \gamma_{tT}, \Gamma_{t_1T}, \gamma_{t_1T}}(x, y, a, b)}{f_{\Gamma_{t_1T}, \gamma_{t_1T}}(a, b)}. \tag{47}$$

Note that the conditional probability densities that we introduce in formulae such as those above are "regular" conditional densities (Williams 1991, p. 91). We shall show that

$$g_{\Gamma_{tT}, \gamma_{tT}}(x, y, \Gamma_{t_1T}, \gamma_{t_1T}, \Gamma_{t_2t_1}, \gamma_{t_2t_1}) = g_{\Gamma_{tT}, \gamma_{tT}}(x, y, \Gamma_{t_1T}, \gamma_{t_1T}). \tag{48}$$

Writing

$$\begin{aligned}&F_{\Gamma_{tT}, \gamma_{tT}, \Gamma_{t_1T}, \gamma_{t_1T}, \Gamma_{t_2t_1}, \gamma_{t_2t_1}}(x, y, a, b, c, d)\\ &\quad = \mathbb{E}\left[\mathbb{1}_{\{\Gamma_{tT} < x\}} \mathbb{1}_{\{\gamma_{tT} < y\}}\, \mathbb{1}_{\{\Gamma_{t_1T} < a\}} \mathbb{1}_{\{\gamma_{t_1T} < b\}}\, \mathbb{1}_{\{\Gamma_{t_2t_1} < c\}} \mathbb{1}_{\{\gamma_{t_2t_1} < d\}}\right] \end{aligned} \tag{49}$$

for the joint distribution function, we see that

$$\begin{aligned}
&F_{\Gamma_{tT},\gamma_{tT},\Gamma_{t_1T},\gamma_{t_1T},\Gamma_{t_2t_1},\gamma_{t_2t_1}}(x,\,y,\,a,\,b,\,c,\,d)\\
&=\mathbb{E}\left[\mathbb{1}_{\{\Gamma_{tT}<x\}}\mathbb{1}_{\{\gamma_{tT}<y\}}\,\mathbb{1}_{\{\Gamma_{t_1T}<a\}}\mathbb{1}_{\{\gamma_{t_1T}<b\}}\,\mathbb{1}_{\{\Gamma_{t_2t_1}<c\}}\mathbb{1}_{\{\gamma_{t_2t_1}<d\}}\right]\\
&=\mathbb{E}\left[\mathbb{E}\left[\mathbb{1}_{\{\Gamma_{tT}<x\}}\,\mathbb{1}_{\{\gamma_{tT}<y\}}\,\mathbb{1}_{\{\Gamma_{t_1T}<a\}}\,\mathbb{1}_{\{\gamma_{t_1T}<b\}}\,\mathbb{1}_{\{\Gamma_{t_2t_1}<c\}}\mathbb{1}_{\{\gamma_{t_2t_1}<d\}}\,\middle|\,\gamma_{t_2},\,\gamma_{t_1},\,\gamma_t,\,\gamma_T\right]\right]\\
&=\mathbb{E}\left[\mathbb{1}_{\{\gamma_{tT}<y\}}\,\mathbb{1}_{\{\gamma_{t_1T}<b\}}\,\mathbb{1}_{\{\gamma_{t_2t_1}<d\}}\mathbb{E}\left[\mathbb{1}_{\{\Gamma_{tT}<x\}}\,\mathbb{1}_{\{\Gamma_{t_1T}<a\}}\,\mathbb{1}_{\{\Gamma_{t_2t_1}<c\}}\,\middle|\,\gamma_{t_2},\,\gamma_{t_1},\,\gamma_t,\,\gamma_T\right]\right]\\
&=\mathbb{E}\Bigg[\mathbb{E}\left[\mathbb{1}_{\{\Gamma_{tT}<x\}}\,\mathbb{1}_{\{\gamma_{tT}<y\}}\,\mathbb{1}_{\{\Gamma_{t_1T}<a\}}\,\mathbb{1}_{\{\gamma_{t_1T}<b\}}\,\middle|\,\gamma_{t_1},\,\gamma_t,\,\gamma_T\right]\\
&\qquad\qquad\times N\left(\frac{c}{\sqrt{(1-\gamma_{t_2t_1})\,(\gamma_{t_2t_1})}}\right)\mathbb{1}_{\{\gamma_{t_2t_1}<d\}}\Bigg],
\end{aligned}\tag{50}$$

where the last step follows as a consequence of Lemma 2. Thus we have

$$\begin{aligned}
&F_{\Gamma_{tT},\gamma_{tT},\Gamma_{t_1T},\gamma_{t_1T},\Gamma_{t_2t_1},\gamma_{t_2t_1}}(x,\,y,\,a,\,b,\,c,\,d)\\
&=\mathbb{E}\left[\mathbb{1}_{\{\Gamma_{tT}<x\}}\,\mathbb{1}_{\{\gamma_{tT}<y\}}\,\mathbb{1}_{\{\Gamma_{t_1T}<a\}}\,\mathbb{1}_{\{\gamma_{t_1T}<b\}}\,N\left(\frac{c}{\sqrt{(1-\gamma_{t_2t_1})\,(\gamma_{t_2t_1})}}\right)\mathbb{1}_{\{\gamma_{t_2t_1}<d\}}\right]\\
&=\mathbb{E}\left[\mathbb{1}_{\{\Gamma_{tT}<x\}}\,\mathbb{1}_{\{\gamma_{tT}<y\}}\,\mathbb{1}_{\{\Gamma_{t_1T}<a\}}\,\mathbb{1}_{\{\gamma_{t_1T}<b\}}\right]\mathbb{E}\left[N\left(\frac{c}{\sqrt{(1-\gamma_{t_2t_1})\,(\gamma_{t_2t_1})}}\right)\mathbb{1}_{\{\gamma_{t_2t_1}<d\}}\right]\\
&=F_{\Gamma_{tT},\gamma_{tT},\Gamma_{t_1T},\gamma_{t_1T}}(x,\,y,\,a,\,b)\times F_{\Gamma_{t_2t_1},\gamma_{t_2t_1}}(c,\,d)\,,
\end{aligned}\tag{51}$$

where the next to last step follows by virtue of the fact that Γ_{st} and γ_{uv} are independent for $0\le s\le t\le u\le v$ and $t>0$. Similarly,

$$\begin{aligned}
&F_{\Gamma_{t_1T},\gamma_{t_1T},\Gamma_{t_2t_1},\gamma_{t_2t_1}}(a,\,b,\,c,\,d)\\
&=\mathbb{E}\left[\mathbb{1}_{\{\Gamma_{t_1T}<a\}}\mathbb{1}_{\{\gamma_{t_1T}<b\}}\,\mathbb{1}_{\{\Gamma_{t_2t_1}<c\}}\mathbb{1}_{\{\gamma_{t_2t_1}<d\}}\right]\\
&=\mathbb{E}\left[\mathbb{E}\left[\mathbb{1}_{\{\Gamma_{t_1T}<a\}}\mathbb{1}_{\{\gamma_{t_1T}<b\}}\,\mathbb{1}_{\{\Gamma_{t_2t_1}<c\}}\mathbb{1}_{\{\gamma_{t_2t_1}<d\}}\,\middle|\,\gamma_{t_2},\,\gamma_{t_1},\,\gamma_T\right]\right]\\
&=\mathbb{E}\left[\mathbb{1}_{\{\gamma_{t_1T}<b\}}\,\mathbb{1}_{\{\gamma_{t_2t_1}<d\}}\mathbb{E}\left[\mathbb{1}_{\{\Gamma_{t_1T}<a\}}\,\mathbb{1}_{\{\Gamma_{t_2t_1}<c\}}\,\middle|\,\gamma_{t_2},\,\gamma_{t_1},\,\gamma_T\right]\right],
\end{aligned}\tag{52}$$

and hence

$$\begin{aligned}
&F_{\Gamma_{t_1T},\gamma_{t_1T},\Gamma_{t_2t_1},\gamma_{t_2t_1}}(a,\,b,\,c,\,d)\\
&=\mathbb{E}\left[N\left(\frac{a}{\sqrt{(1-\gamma_{t_1T})\,(\gamma_{t_1T})}}\right)\mathbb{1}_{\{\gamma_{t_1T}<b\}}\,N\left(\frac{c}{\sqrt{(1-\gamma_{t_2t_1})\,(\gamma_{t_2t_1})}}\right)\mathbb{1}_{\{\gamma_{t_2t_1}<d\}}\right]\\
&=\mathbb{E}\left[N\left(\frac{a}{\sqrt{(1-\gamma_{t_1T})\,(\gamma_{t_1T})}}\right)\mathbb{1}_{\{\gamma_{t_1T}<b\}}\right]\mathbb{E}\left[N\left(\frac{c}{\sqrt{(1-\gamma_{t_2t_1})\,(\gamma_{t_2t_1})}}\right)\mathbb{1}_{\{\gamma_{t_2t_1}<d\}}\right]\\
&=F_{\Gamma_{t_1T},\gamma_{t_1T}}(a,\,b)\times F_{\Gamma_{t_2t_1},\gamma_{t_2t_1}}(c,\,d)\,.
\end{aligned}\tag{53}$$

Thus we deduce that

$$f_{\Gamma_{tT},\gamma_{tT},\Gamma_{t_1T},\gamma_{t_1T},\Gamma_{t_2t_1},\gamma_{t_2t_1}}(x,\,y,\,a,\,b,\,c,\,d) \tag{54}$$

$$= f_{\Gamma_{tT},\gamma_{tT},\Gamma_{t_1T},\gamma_{t_1T}}(x,\,y,\,a,\,b) \times f_{\Gamma_{t_2t_1},\gamma_{t_2t_1}}(c,\,d)\,, \tag{55}$$

and

$$f_{\Gamma_{t_1T},\gamma_{t_1T},\Gamma_{t_2t_1},\gamma_{t_2t_1}}(a,\,b,\,c,\,d) = f_{\Gamma_{t_1T},\gamma_{t_1T}}(a,\,b) \times f_{\Gamma_{t_2t_1},\gamma_{t_2t_1}}(c,\,d)\,, \tag{56}$$

and the theorem follows. □

4. Variance Gamma Information

Fix $T > 0$ and let $\{\Gamma_{tT}\}$ be a normalized variance gamma bridge, as defined by (30). Let $\{\gamma_{tT}\}$ be the associated gamma bridge defined by (22). Let X_T be a random variable and assume that X_T, $\{\gamma_t\}_{t\geq 0}$ and $\{W_t\}_{t\geq 0}$ are independent. We are led to the following:

Definition 2. *By a variance-gamma information process carrying the market factor X_T we mean a process $\{\xi_t\}_{t\geq 0}$ that takes the form*

$$\xi_t = \Gamma_{tT} + \sigma\,\gamma_{tT}\,X_T \tag{57}$$

for $0 \leq t \leq T$ and $\xi_t = \sigma X_T$ for $t > T$, where σ is a positive constant.

The market filtration is assumed to be the standard augmented filtration generated jointly by $\{\xi_t\}$ and $\{\gamma_{tT}\}$. A calculation shows that if $0 \leq s \leq t \leq T$ and $t > 0$ then

$$\xi_s = \Gamma_{st}\,(\gamma_{tT})^{\frac{1}{2}} + \xi_t\,\gamma_{st}\,. \tag{58}$$

We are thus led to the following result required for the valuation of assets.

Theorem 3. *The processes $\{\xi_t\}_{0\leq t\leq T}$ and $\{\gamma_{tT}\}_{0\leq t\leq T}$ are jointly Markov.*

Proof. It suffices to show that for any $n \in \mathbb{N}$ and $0 < t_1 < t_2 < \cdots < t_n$ we have

$$\mathbb{E}\left[\phi(\xi_t,\gamma_{tT})\,\middle|\,\xi_{t_1},\,\xi_{t_2},\,\ldots,\xi_{t_n},\,\gamma_{t_1T},\,\gamma_{t_2T},\,\ldots,\gamma_{t_nT}\right] = \mathbb{E}\left[\phi(\xi_t,\gamma_{tT})\,\middle|\,\xi_{t_1},\,\gamma_{t_1T}\right]. \tag{59}$$

We present the proof for $n = 2$. Thus, we propose to show that

$$\mathbb{E}\left[\phi(\xi_t,\gamma_{tT})\,\middle|\,\xi_{t_1},\,\xi_{t_2},\,\gamma_{t_1T},\,\gamma_{t_2T}\right] = \mathbb{E}\left[\phi(\xi_t,\gamma_{tT})\,\middle|\,\xi_{t_1},\,\gamma_{t_1T}\right]. \tag{60}$$

By (58), we have

$$\begin{aligned}
&\mathbb{E}\left[\phi(\xi_t,\gamma_{tT})\,\middle|\,\xi_{t_1},\,\xi_{t_2},\,\gamma_{t_1T},\,\gamma_{t_2,T}\right]\\
&\quad= \mathbb{E}\left[\phi(\xi_t,\gamma_{tT})\,\middle|\,\xi_{t_1},\,\xi_{t_2},\,\gamma_{t_1T},\,\gamma_{t_2t_1}\right]\\
&\quad= \mathbb{E}\left[\phi(\xi_t,\gamma_{tT})\,\middle|\,\xi_{t_1},\,\Gamma_{t_2t_1},\,\gamma_{t_1T},\,\gamma_{t_2t_1}\right]\\
&\quad= \mathbb{E}\left[\phi(\Gamma_{tT}+\gamma_{tT}\,\sigma\,X_T,\gamma_{tT})\,\middle|\,\Gamma_{t_1T}+\gamma_{t_1T}\,\sigma\,X_T,\,\Gamma_{t_2t_1},\,\gamma_{t_1T},\,\gamma_{t_2t_1}\right].
\end{aligned} \tag{61}$$

Finally, we invoke Lemma 2, and Theorem 2 to conclude that

$$\begin{aligned}\mathbb{E}\left[\phi(\xi_t,\gamma_{tT})|\xi_{t_1},\,\xi_{t_2},\,\gamma_{t_1T},\,\gamma_{t_2,T}\right]\\ &= \mathbb{E}\left[\phi(\Gamma_{tT}+\gamma_{tT}\,\sigma\,X_T,\gamma_{tT})\,\middle|\,\Gamma_{t_1T}+\gamma_{t_1T}\,\sigma\,X_T,\,\gamma_{t_1T}\right]\\ &= \mathbb{E}\left[\phi(\xi_t,\gamma_{tT})|\xi_{t_1},\,\gamma_{t_1T}\right].\end{aligned} \tag{62}$$

The generalization to $n > 2$ is straightforward. □

5. Information Based Pricing

Now we are in a position to consider the valuation of a financial asset in the setting just discussed. One recalls that $\mathbb{P}$ is understood to be the risk-neutral measure and that the interest rate is constant. The payoff of the asset at time T is taken to be an integrable random variable of the form $h(X_T)$ for some Borel function h, where X_T is the information revealed at T. The filtration is generated jointly by the variance-gamma information process $\{\xi_t\}$ and the associated gamma bridge $\{\gamma_{tT}\}$. The value of the asset at time $t \in [0, T)$ is then given by the general expression (2), which on account of Theorem 3 reduces in the present context to

$$S_t = \mathrm{e}^{-r\,(T-t)}\,\mathbb{E}\left[h(X_T)\,|\,\xi_t,\,\gamma_{tT}\right], \tag{63}$$

and our goal is to work out this expectation explicitly.

Let us write F_{X_T} for the *a priori* distribution function of X_T. Thus $F_{X_T} : x \in \mathbb{R} \mapsto F_{X_T}(x) \in [0, 1]$ and we have

$$F_{X_T}(x) = \mathbb{P}\left(X_T \le x\right). \tag{64}$$

Occasionally, it will be typographically convenient to write $F^{(x)}_{X_T}$ in place of $F_{X_T}(x)$, and similarly for other distribution functions. To proceed, we require the following:

Lemma 3. *Let X be a random variable with distribution $\{F_X(x)\}_{x\in\mathbb{R}}$ and let Y be a continuous random variable with distribution $\{F_Y(y)\}_{y\in\mathbb{R}}$ and density $\{f_Y(y)\}_{y\in\mathbb{R}}$. Then for all $y \in \mathbb{R}$ for which $f_Y(y) \neq 0$ we have*

$$F^{(x)}_{X|Y=y} = \frac{\int_{u\in(-\infty,x]} f^{(y)}_{Y|X=u}\,\mathrm{d}F^{(u)}_X}{\int_{u\in(-\infty,\infty)} f^{(y)}_{Y|X=u}\,\mathrm{d}F^{(u)}_X}, \tag{65}$$

where $F^{(x)}_{X|Y=y}$ denotes the conditional distribution $\mathbb{P}\left(X \le x \mid Y = y\right)$, and where

$$f^{(y)}_{Y|X=u} = \frac{\mathrm{d}}{\mathrm{d}y}\mathbb{P}\left(Y \le y \mid X = u\right). \tag{66}$$

Proof. For *any* two random variables X and Y it holds that

$$\begin{aligned}\mathbb{P}\left(X \le x,\,Y \le y\right) &= \mathbb{E}\left[\mathbb{1}_{\{X\le x\}}\,\mathbb{1}_{\{Y\le y\}}\right]\\ &= \mathbb{E}\left[\mathbb{E}\left[\mathbb{1}_{\{X\le x\}}\middle|Y\right]\mathbb{1}_{\{Y\le y\}}\right]\\ &= \mathbb{E}\left[F^{(x)}_{X|Y}\,\mathbb{1}_{\{Y\le y\}}\right].\end{aligned} \tag{67}$$

Here we have used the fact that for each $x \in \mathbb{R}$ there exists a Borel measurable function $P_x : y \in \mathbb{R} \mapsto P_x(y) \in [0,1]$ such that $\mathbb{E}\left[\mathbb{1}_{\{X \le x\}} \middle| Y\right] = P_x(Y)$. Then for $y \in \mathbb{R}$ we define

$$F^{(x)}_{X|Y=y} = P_x(y)\,. \tag{68}$$

Hence

$$\mathbb{P}\left(X \le x,\, Y \le y\right) = \int_{v \in (-\infty, y]} F^{(x)}_{X|Y=v}\, \mathrm{d}F^{(v)}_Y\,. \tag{69}$$

By symmetry, we have

$$\mathbb{P}\left(X \le x,\, Y \le y\right) = \int_{u \in (-\infty, x]} F^{(y)}_{Y|X=u}\, \mathrm{d}F^{(u)}_X\,, \tag{70}$$

from which it follows that we have the relation

$$\int_{u \in (-\infty, x]} F^{(y)}_{Y|X=u}\, \mathrm{d}F^{(u)}_X = \int_{v \in (-\infty, y]} F^{(x)}_{X|Y=v}\, \mathrm{d}F^{(v)}_Y\,. \tag{71}$$

Moving ahead, let us consider the measure $F_{X|Y=y}(\mathrm{d}x)$ on $(\mathbb{R}, \mathcal{B})$ defined for each $y \in \mathbb{R}$ by setting

$$F_{X|Y=y}(A) = \mathbb{E}\left[\mathbb{1}_{\{X \in A\}} \middle| Y = y\right] \tag{72}$$

for any $A \in \mathcal{B}$. Then $F_{X|Y=y}(\mathrm{d}x)$ is absolutely continuous with respect to $F_X(\mathrm{d}x)$. Indeed, suppose that $F_X(B) = 0$ for some $B \in \mathcal{B}$. Now, $F_{X|Y=y}(B) = \mathbb{E}\left[\mathbb{1}_{\{X \in B\}} \middle| Y = y\right]$. But if $\mathbb{E}\left[\mathbb{1}_{\{X \in B\}}\right] = 0$, then $\mathbb{E}\left[\mathbb{E}\left[\mathbb{1}_{\{X \in B\}} \middle| Y\right]\right] = 0$, and hence $\mathbb{E}\left[\mathbb{1}_{\{X \in B\}} \middle| Y\right] = 0$, and therefore $\mathbb{E}\left[\mathbb{1}_{\{X \in B\}} \middle| Y = y\right] = 0$. Thus $F_{X|Y=y}(B)$ vanishes for any $B \in \mathcal{B}$ for which $F_X(B)$ vanishes. It follows by the Radon-Nikodym theorem that for each $y \in \mathbb{R}$ there exists a density $\{g_y(x)\}_{x \in \mathbb{R}}$ such that

$$F^{(x)}_{X|Y=y} = \int_{u \in (-\infty, x]} g_y(u)\, \mathrm{d}F^{(u)}_X\,. \tag{73}$$

Note that $\{g_y(x)\}$ is determined uniquely apart from its values on F_X-null sets. Inserting (73) into (71) we obtain

$$\int_{u \in (-\infty, x]} F^{(y)}_{Y|X=u}\, \mathrm{d}F^{(u)}_X = \int_{v \in (-\infty, y]} \int_{u \in (-\infty, x]} g_v(u)\, \mathrm{d}F^{(u)}_X\, \mathrm{d}F^{(v)}_Y\,, \tag{74}$$

and thus by Fubini's theorem we have

$$\int_{u \in (-\infty, x]} F^{(y)}_{Y|X=u}\, \mathrm{d}F^{(u)}_X = \int_{u \in (-\infty, x]} \int_{v \in (-\infty, y]} g_v(u)\, \mathrm{d}F^{(v)}_Y\, \mathrm{d}F^{(u)}_X\,. \tag{75}$$

It follows then that $\{F^{(y)}_{Y|X=x}\}_{x \in \mathbb{R}}$ is determined uniquely apart from its values on F_X-null sets, and we have

$$F^{(y)}_{Y|X=x} = \int_{v \in (-\infty, y]} g_v(x)\, \mathrm{d}F^{(v)}_Y\,. \tag{76}$$

This relation holds quite generally and is symmetrical between X and Y. Indeed, we have not so far assumed that Y is a continuous random variable. If Y is, in fact, a continuous random variable, then its distribution function is absolutely continuous and admits a density $\{f^{(y)}_Y\}_{y \in \mathbb{R}}$. In that case, (76) can be written in the form

$$F^{(y)}_{Y|X=x} = \int_{v\in(-\infty,y]} g_v(x)\, f^{(v)}_Y \,\mathrm{d}v\,, \tag{77}$$

from which it follows that for each value of x the conditional distribution function $\{F^{(y)}_{Y|X=x}\}_{y\in\mathbb{R}}$ is absolutely continuous and admits a density $\{f^{(y)}_{Y|X=x}\}_{y\in\mathbb{R}}$ such that

$$f^{(y)}_{Y|X=x} = g_y(x)\, f^{(y)}_Y\,. \tag{78}$$

The desired result (65) then follows from (73) and (78) if we observe that

$$f^{(y)}_Y = \int_{u\in(-\infty,\infty)} f^{(y)}_{Y|X=u}\,\mathrm{d}F^{(u)}_X\,, \tag{79}$$

and that concludes the proof. □

Armed with Lemma 3, we are in a position to work out the conditional expectation that leads to the asset price, and we obtain the following:

Theorem 4. *The variance-gamma information-based price of a financial asset with payoff $h(X_T)$ at time T is given for $t<T$ by*

$$S_t = \mathrm{e}^{-r\,(T-t)} \int_{x\in\mathbb{R}} h(x)\, \frac{\mathrm{e}^{\left(\sigma\,\xi_t\,x-\frac{1}{2}\,\sigma^2\,x^2\,\gamma_{tT}\right)\,(1-\gamma_{tT})^{-1}}}{\int_{y\in\mathbb{R}}\mathrm{e}^{\left(\sigma\,\xi_t\,y-\frac{1}{2}\,\sigma^2\,y^2\,\gamma_{tT}\right)\,(1-\gamma_{tT})^{-1}}\mathrm{d}F^{(y)}_{X_T}}\mathrm{d}F^{(x)}_{X_T}\,. \tag{80}$$

Proof. To calculate the conditional expectation of $h(X_T)$, we observe that

$$\mathbb{E}\left[h(X_T)\,|\,\xi_t,\,\gamma_{tT}\right] = \mathbb{E}\left[\mathbb{E}\left[h(X_T)\,|\,\xi_t,\,\gamma_{tT},\,\gamma_T\right]\,\middle|\,\xi_t,\,\gamma_{tT}\right], \tag{81}$$

by the tower property, where the inner expectation takes the form

$$\mathbb{E}\left[h(X_T)\,|\,\xi_t=\xi,\,\gamma_{tT}=b,\,\gamma_T=g\right] = \int_{x\in\mathbb{R}} h(x)\,\mathrm{d}F^{(x)}_{X_T|\xi_t=\xi,\,\gamma_{tT}=b,\,\gamma_T=g}\,. \tag{82}$$

Here by Lemma 3 the conditional distribution function is

$$\begin{aligned} F^{(x)}_{X_T|\xi_t=\xi,\,\gamma_{tT}=b,\,\gamma_T=g} &= \frac{\int_{u\in(-\infty,\,x\,]} f^{(\xi)}_{\xi_t\,|\,X_T=u,\,\gamma_{tT}=b,\,\gamma_T=g}\,\mathrm{d}F^{(u)}_{X_T\,|\,\gamma_{tT}=b,\,\gamma_T=g}}{\int_{u\in\mathbb{R}} f^{(\xi)}_{\xi_t\,|\,X_T=u,\,\gamma_{tT}=b,\,\gamma_T=g}\,\mathrm{d}F^{(u)}_{X_T\,|\,\gamma_{tT}=b,\,\gamma_T=g}} \\ &= \frac{\int_{u\in(-\infty,\,x\,]} f^{(\xi)}_{\xi_t\,|\,X_T=u,\,\gamma_{tT}=b,\,\gamma_T=g}\,\mathrm{d}F^{(u)}_{X_T}}{\int_{u\in\mathbb{R}} f^{(\xi)}_{\xi_t\,|\,X_T=u,\,\gamma_{tT}=b,\,\gamma_T=g}\,\mathrm{d}F^{(u)}_{X_T}} \\ &= \frac{\int_{u\in(-\infty,\,x\,]}\mathrm{e}^{\left(\sigma\,\xi\,u-\frac{1}{2}\,\sigma^2\,u^2\,b\right)\,(1-b)^{-1}}\mathrm{d}F^{(u)}_{X_T}}{\int_{\mathbb{R}}\mathrm{e}^{\left(\sigma\,\xi\,u-\frac{1}{2}\,\sigma^2\,u^2\,b\right)\,(1-b)^{-1}}\mathrm{d}F^{(u)}_{X_T}}\,. \end{aligned} \tag{83}$$

Therefore, the inner expectation in Equation (81) is given by

$$\mathbb{E}\left[h(X_T)\,|\,\xi_t,\,\gamma_{tT},\,\gamma_T\right]=\int_{x\in\mathbb{R}}h(x)\,\frac{\mathrm{e}^{\left(\sigma\,\xi_t\,x-\frac{1}{2}\,\sigma^2\,x^2\,\gamma_{tT}\right)\,(1-\gamma_{tT})^{-1}}}{\int_{y\in\mathbb{R}}\mathrm{e}^{\left(\sigma\,\xi_t\,y-\frac{1}{2}\,\sigma^2\,y^2\,\gamma_{tT}\right)\,(1-\gamma_{tT})^{-1}}\mathrm{d}F^{(y)}_{X_T}}\mathrm{d}F^{(x)}_{X_T}\,. \tag{84}$$

But the right hand side of (84) depends only on ξ_t and γ_{tT}. It follows immediately that

$$\mathbb{E}\left[h(X_T)\,|\,\xi_t,\,\gamma_{tT}\right]=\int_{x\in\mathbb{R}}h(x)\,\frac{\mathrm{e}^{\left(\sigma\,\xi_t\,x-\frac{1}{2}\,\sigma^2\,x^2\,\gamma_{tT}\right)\,(1-\gamma_{tT})^{-1}}}{\int_{y\in\mathbb{R}}\mathrm{e}^{\left(\sigma\,\xi_t\,y-\frac{1}{2}\,\sigma^2\,y^2\,\gamma_{tT}\right)\,(1-\gamma_{tT})^{-1}}\mathrm{d}F^{(y)}_{X_T}}\mathrm{d}F^{(x)}_{X_T}\,, \tag{85}$$

which translates into Equation (80), and that concludes the proof. □

6. Examples

Going forward, we present some examples of variance-gamma information pricing for specific choices of (a) the payoff function $h:\mathbb{R}\to\mathbb{R}^+$ and (b) the distribution of the market factor X_T. In the figures, we display sample paths for the information processes and the corresponding prices. These paths are generated as follows. First, we simulate outcomes for the market factor X_T. Second, we simulate paths for the gamma process $\{\gamma_t\}_{t\geq 0}$ over the interval $[0,T]$ and an independent Brownian motion $\{W_t\}_{t\geq 0}$. Third, we evaluate the variance gamma process $\{W_{\gamma_t}\}_{t\geq 0}$ over the interval $[0,T]$ by subordinating the Brownian motion with the gamma process, and we evaluate the resulting gamma bridge $\{\gamma_{tT}\}_{0\leq t\leq T}$. Fourth, we use these ingredients to construct sample paths of the information processes, where these processes are given as in Definition 2. Finally, we evaluate the pricing formula in Equation (80) for each of the simulated paths and for each time step.

Example 1: Credit risky bond. We begin with the simplest case, that of a unit-principal credit-risky bond without recovery. We set $h(x)=x$, with $\mathbb{P}(X_T=0)=p_0$ and $\mathbb{P}(X_T=1)=p_1$, where $p_0+p_1=1$. Thus, we have

$$F_{X_T}(x)=p_0\delta_0(x)+p_1\delta_1(x)\,, \tag{86}$$

where

$$\delta_a(x)=\int_{y\in(-\infty,x]}\delta_a(\mathrm{d}y)\,, \tag{87}$$

and $\delta_a(\mathrm{d}x)$ denotes the Dirac measure concentrated at the point a, and we are led to the following:

Proposition 1. *The variance-gamma information-based price of a unit-principal credit-risky discount bond with no recovery is given by*

$$S_t=\mathrm{e}^{-r\,(T-t)}\,\frac{p_1\,\mathrm{e}^{\left(\sigma\,\xi_t-\frac{1}{2}\,\sigma^2\,\gamma_{tT}\right)\,(1-\gamma_{tT})^{-1}}}{p_0+p_1\,\mathrm{e}^{\left(\sigma\,\xi_t-\frac{1}{2}\,\sigma^2\,\gamma_{tT}\right)\,(1-\gamma_{tT})^{-1}}}\,. \tag{88}$$

Now let $\omega\in\Omega$ denote the outcome of chance. By use of Equation (57) one can check rather directly that if $X_T(\omega)=1$, then $\lim_{t\to T}S_t=1$, whereas if $X_T(\omega)=0$, then $\lim_{t\to T}S_t=0$. More explicitly, we find that

$$S_t\Big|_{X_T(w)=0}=\mathrm{e}^{-r(T-t)}\,\frac{p_1\,\exp\left[\sigma\,\left(\gamma_T^{-1/2}\,(W_{\gamma_t}-\gamma_{tT}\,W_{\gamma_T})-\frac{1}{2}\,\sigma\,\gamma_{tT}\right)\,(1-\gamma_{tT})^{-1}\right]}{p_0+p_1\,\exp\left[\sigma\,\left(\gamma_T^{-1/2}\,(W_{\gamma_t}-\gamma_{tT}\,W_{\gamma_T})-\frac{1}{2}\,\sigma\,\gamma_{tT}\right)\,(1-\gamma_{tT})^{-1}\right]}\,, \tag{89}$$

whereas

$$S_t\Big|_{X_T(w)=1} = \mathrm{e}^{-r(T-t)}\,\frac{p_1\,\exp\left[\sigma\,\left(\gamma_T^{-1/2}\,(W_{\gamma_t}-\gamma_{tT}\,W_{\gamma_T})+\frac{1}{2}\,\sigma\,\gamma_{tT}\right)\,(1-\gamma_{tT})^{-1}\right]}{p_0+p_1\,\exp\left[\sigma\,\left(\gamma_T^{-1/2}\,(W_{\gamma_t}-\gamma_{tT}\,W_{\gamma_T})+\frac{1}{2}\,\sigma\,\gamma_{tT}\right)\,(1-\gamma_{tT})^{-1}\right]}\,, \tag{90}$$

and the claimed limiting behaviour of the asset price follows by inspection. In Figures 1 and 2 we plot sample paths for the information processes and price processes of credit risky bonds for various values of the information flow-rate parameter. One observes that for $\sigma = 1$ the information processes diverge, thus distinguishing those bonds that default from those that do not, only towards the end of the relevant time frame; whereas for higher values of σ the divergence occurs progressively earlier, and one sees a corresponding effect in the price processes. Thus, when the information flow rate is higher, the final outcome of the bond payment is anticipated earlier, and with greater certainty. Similar conclusions hold for the interpretation of Figures 3 and 4.

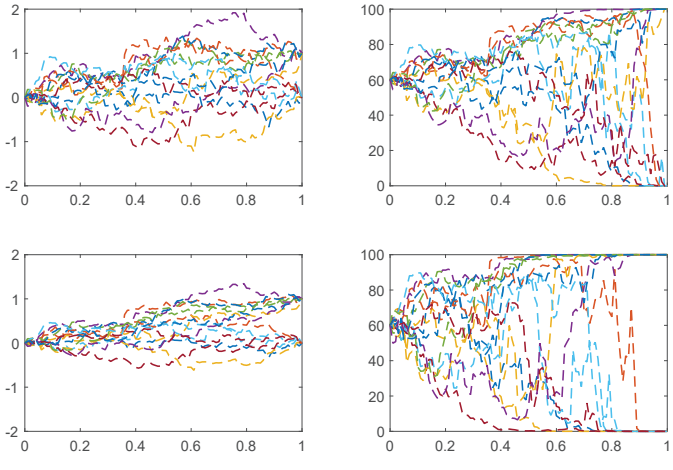

Figure 1. Credit-risky bonds with no recovery. The panels on the left show simulations of trajectories of the variance gamma information process, and the panels on the right show simulations of the corresponding price trajectories. Prices are quoted as percentages of the principal, and the interest rate is taken to be zero. From top to bottom, we show trajectories having $\sigma = 1$, 2, respectively. We take $p_0 = 0.4$ for the probability of default and $p_1 = 0.6$ for the probability of no default. The value of m is 100 in all cases. Fifteen simulated trajectories are shown in each panel.

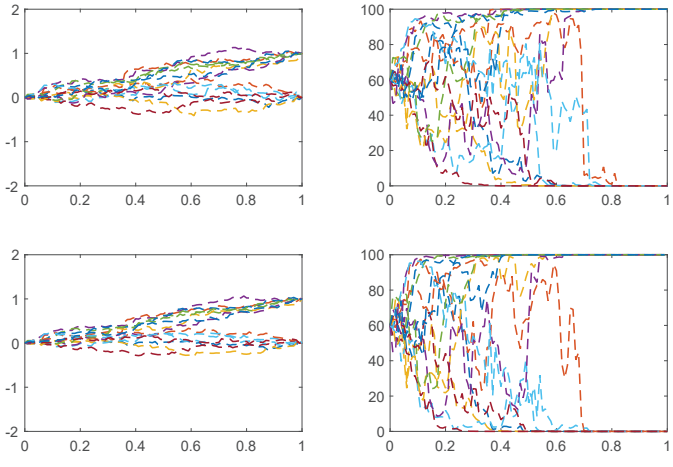

Figure 2. Credit-risky bonds with no recovery. From top to bottom we show trajectories having $\sigma = 3$, 4, respectively. The other parameters are the same as in Figure 1.

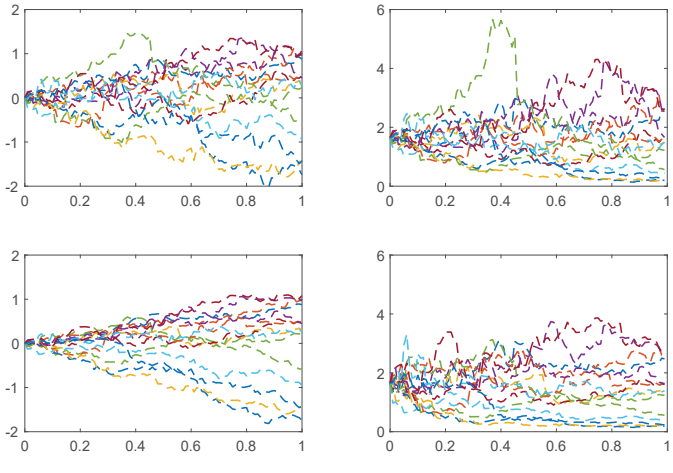

Figure 3. Log-normal payoff. The panels on the left show simulations of the trajectories of the information process, whereas the panels on the right show simulations of the corresponding price process trajectories. From the top to bottom, we show trajectories having $\sigma = 1$, 2, respectively. The value for m is 100. We take $\mu = 0$, $\nu = 1$, and show 15 simulated trajectories in each panel.

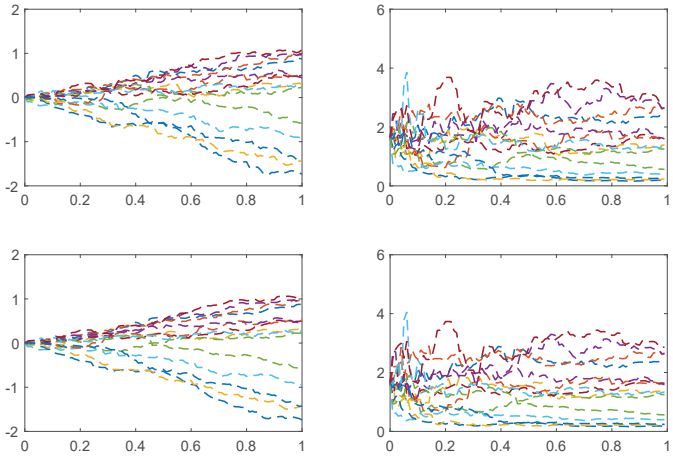

Figure 4. Log-normal payoff. From the top row to the bottom, we show trajectories having $\sigma = 3$, 4, respectively. The other parameters are the same as those in Figure 3.

Example 2: Random recovery. As a somewhat more sophisticated version of the previous example, we consider the case of a defaultable bond with random recovery. We shall work out the case where $h(x) = x$ and the market factor X_T takes the value c with probability p_1 and X_T is uniformly distributed over the interval $[a, b]$ with probability p_0, where $0 \leq a < b \leq c$. Thus, for the probability measure of X_T we have

$$F_{X_T}(\mathrm{d}x) = p_0 \, \mathbb{1}_{\{a \leq x < b\}} \, \mathrm{d}x + p_1 \, \delta_c(\mathrm{d}x) \,, \tag{91}$$

and for the distribution function we obtain

$$F_{X_T}(x) = p_0 \, x \, \mathbb{1}_{\{a \leq x < b\}} + \mathbb{1}_{\{x \geq c\}} \,. \tag{92}$$

The bond price at time t is then obtained by working out the expression

$$S_t = \mathrm{e}^{-r\,(T-t)} \, \frac{p_0 \int_a^b x \, \mathrm{e}^{\left(\sigma\,\xi_t\,x - \frac{1}{2}\,\sigma^2\,x^2\,\gamma_{tT}\right)\,(1-\gamma_{tT})^{-1}} \, \mathrm{d}x + p_1 \, c \, \mathrm{e}^{\left(\sigma\,\xi_t - \frac{1}{2}\,\sigma^2\,\gamma_{tT}\right)\,(1-\gamma_{tT})^{-1}}}{p_0 \int_a^b \mathrm{e}^{\left(\sigma\,\xi_t\,x - \frac{1}{2}\,\sigma^2\,x^2\,\gamma_{tT}\right)\,(1-\gamma_{tT})^{-1}} \, \mathrm{d}x + p_1 \, \mathrm{e}^{\left(\sigma\,\xi_t - \frac{1}{2}\,\sigma^2\,\gamma_{tT}\right)\,(1-\gamma_{tT})^{-1}}} \,, \tag{93}$$

and it should be evident that one can obtain a closed-form solution. To work this out in detail, it will be convenient to have an expression for the incomplete first moment of a normally-distributed random variable with mean μ and variance ν^2. Thus we set

$$N_1(x, \mu, \nu) = \frac{1}{\sqrt{2\,\pi\,\nu^2}} \int_{-\infty}^{x} y \, \exp\left(-\frac{1}{2}\,\frac{(y-\mu)^2}{\nu^2}\right) \mathrm{d}y \,, \tag{94}$$

and for convenience we set

$$N_0(x, \mu, \nu) = \frac{1}{\sqrt{2\,\pi\,\nu^2}} \int_{-\infty}^{x} \exp\left(-\frac{1}{2}\,\frac{(y-\mu)^2}{\nu^2}\right) \mathrm{d}y \,. \tag{95}$$

Then we have

$$N_1(x,\mu,\nu) = \mu\, N\left(\frac{x-\mu}{\nu}\right) - \frac{\nu}{\sqrt{2\,\pi}}\,\exp\left(-\frac{1}{2}\,\frac{(x-\mu)^2}{\nu^2}\right), \tag{96}$$

and of course

$$N_0(x,\mu,\nu) = N\left(\frac{x-\mu}{\nu}\right), \tag{97}$$

where $N(\,\cdot\,)$ is defined by (34). We also set

$$f(x,\mu,\nu) = \frac{1}{\sqrt{2\,\pi\,\nu^2}}\,\exp\left(-\frac{1}{2}\,\frac{(x-\mu)^2}{\nu^2}\right). \tag{98}$$

Finally, we obtain the following:

Proposition 2. *The variance-gamma information-based price of a defaultable discount bond with a uniformly-distributed fraction of the principal paid on recovery is given by*

$$S_t = \mathrm{e}^{-r\,(T-t)}\,\frac{p_0\,\big(N_1(b,\mu,\nu) - N_1(a,\mu,\nu)\big) + p_1\,c\,f(c,\mu,\nu)}{p_0\,\big(N_0(b,\mu,\nu) - N_0(a,\mu,\nu)\big) + p_1\,f(c,\mu,\nu)}, \tag{99}$$

where

$$\mu = \frac{1}{\sigma}\,\frac{\xi_t}{\gamma_{tT}}, \quad \nu = \frac{1}{\sigma}\,\sqrt{\frac{1-\gamma_{tT}}{\gamma_{tT}}}\,. \tag{100}$$

Example 3: Lognormal payoff. Next we consider the case when the payoff of an asset at time T is log-normally distributed. This will hold if $h(x) = \mathrm{e}^x$ and $X_T \sim \text{Normal}(\mu,\nu^2)$. It will be convenient to look at the slightly more general payoff obtained by setting $h(x) = \mathrm{e}^{q\,x}$ with $q \in \mathbb{R}$. If we recall the identity

$$\frac{1}{\sqrt{2\,\pi}}\int_{-\infty}^{\infty}\exp\left(-\frac{1}{2}Ax^2 + Bx\right)\mathrm{d}x = \frac{1}{\sqrt{A}}\,\exp\left(\frac{1}{2}\,\frac{B^2}{A}\right), \tag{101}$$

which holds for $A > 0$ and $B \in \mathbb{R}$, a calculation gives

$$\begin{aligned} I_t(q) &:= \int_{-\infty}^{\infty}\mathrm{e}^{q\,x}\,\frac{1}{\sqrt{2\,\pi}\,\nu}\,\exp\left[-\frac{1}{2}\,\frac{(x-\mu)^2}{\nu^2} + \frac{1}{1-\gamma_{tT}}\left(\sigma\,\xi_t\,x - \frac{1}{2}\,\sigma^2\,x^2\,\gamma_{tT}\right)\right]\mathrm{d}x \\ &= \frac{1}{\nu\sqrt{A_t}}\,\exp\left(\frac{1}{2}\,\frac{B_t^2}{A_t} - C\right), \end{aligned} \tag{102}$$

where

$$A_t = \frac{1-\gamma_{tT}+\nu^2\sigma^2\,\gamma_{tT}}{\nu^2(1-\gamma_{tT})}, \quad B_t = q + \frac{\mu}{\nu^2} + \frac{\sigma\,\xi_t}{1-\gamma_{tT}}, \quad C = \frac{1}{2}\,\frac{\mu^2}{\nu^2}\,. \tag{103}$$

For $q = 1$, the price is thus given in accordance with Theorem 4 by

$$S_t = \mathrm{e}^{-r(T-t)}\,\frac{I_t(1)}{I_t(0)}\,. \tag{104}$$

Then clearly we have

$$S_0 = \mathrm{e}^{-r\,T}\,\exp\left[\mu + \frac{1}{2}\,\nu^2\right], \tag{105}$$

and a calculation leads to the following:

Proposition 3. *The variance-gamma information-based price of a financial asset with a log-normally distributed payoff such that* $\log(S_{T^-}) \sim \text{Normal}(\mu, \nu^2)$ *is given for* $t \in (0, T)$ *by*

$$S_t = \mathrm{e}^{r\,t}\, S_0 \, \exp\left[\frac{\nu^2\,\sigma^2\,\gamma_{tT}\,(1-\gamma_{tT})^{-1}}{1+\nu^2\,\sigma^2\,\gamma_{tT}\,(1-\gamma_{tT})^{-1}}\left(\frac{1}{\sigma\,\gamma_{tT}}\,\xi_t - \mu - \frac{1}{2}\,\nu^2\right)\right]. \tag{106}$$

More generally, one can consider the case of a so-called power-payoff derivative for which

$$H_T = (S_{T^-})^q\,, \tag{107}$$

where $S_{T^-} = \lim_{t\to T} S_t$ is the payoff of the asset priced above in Proposition 3. See Bouzianis and Hughston (2019) for aspects of the theory of power-payoff derivatives. In the present case if we write

$$C_t = \mathrm{e}^{-r\,(T-t)}\,\mathbb{E}_t\left[(S_{T^-})^q\right] \tag{108}$$

for the value of the power-payoff derivative at time t, we find that

$$C_t = \mathrm{e}^{r\,t}\,C_0\,\exp\left[\frac{\nu^2\,\sigma^2\,\gamma_{tT}\,(1-\gamma_{tT})^{-1}}{1+\nu^2\,\sigma^2\,\gamma_{tT}\,(1-\gamma_{tT})^{-1}}\left(\frac{q}{\sigma\,\gamma_{tT}}\,\xi_t - q\,\mu - \frac{1}{2}\,q^2\,\nu^2\right)\right], \tag{109}$$

where

$$C_0 = \mathrm{e}^{-r\,T}\,\exp\left[q\,\mu + \frac{1}{2}\,q^2\,\nu^2\right]. \tag{110}$$

Example 4: Exponentially distributed payoff. Next we consider the case where the payoff is exponentially distributed. We let $X_T \sim \exp(\lambda)$, so $\mathbb{P}[X_T \in \mathrm{d}x] = \lambda\,\mathrm{e}^{-\lambda\,x}\,\mathrm{d}x$, and take $h(x) = x$. A calculation shows that

$$\int_0^\infty x\,\exp\left[-\lambda\,x + \left(\sigma\,\xi_t\,x - \frac{1}{2}\,\sigma^2\,x^2\,\gamma_{tT}\right)\,(1-\gamma_{tT})^{-1}\right]\mathrm{d}x = \frac{\mu - N_1(0,\mu,\nu)}{f(0,\mu,\nu)}\,, \tag{111}$$

where we set

$$\mu = \frac{1}{\sigma}\,\frac{\xi_t}{\gamma_{tT}} - \frac{\lambda}{\sigma^2}\,\frac{1-\gamma_{tT}}{\gamma_{tT}}\,, \quad \nu = \frac{1}{\sigma}\,\sqrt{\frac{1-\gamma_{tT}}{\gamma_{tT}}}\,, \tag{112}$$

and

$$\int_0^\infty \exp\left[-\lambda\,x + \left(\sigma\,\xi_t\,x - \frac{1}{2}\,\sigma^2\,x^2\,\gamma_{tT}\right)\,(1-\gamma_{tT})^{-1}\right]\mathrm{d}x = \frac{1 - N_0(0,\mu,\nu)}{f(0,\mu,\nu)}\,. \tag{113}$$

As a consequence we obtain:

Proposition 4. *The variance-gamma information-based price of a financial asset with an exponentially distributed payoff is given by*

$$S_t = \frac{\mu - N_1(0,\mu,\nu)}{1 - N_0(0,\mu,\nu)}\,, \tag{114}$$

where N_0 *and* N_1 *are defined as in Example 2.*

7. Conclusions

In the examples considered in the previous section, we have looked at the situation where there is a single market factor X_T, which is revealed at time T, and where the single cash flow occurring at T depends on the outcome for X_T. The value of a security S_t with that cash flow is determined by the information available at time t. Given the Markov property of the extended information process $\{\xi_t, \gamma_{tT}\}$ it follows that there exists a function of three variables $F : \mathbb{R} \times [0,1] \times \mathbb{R}^+ \to \mathbb{R}^+$ such that $S_t = F(\xi_t, \gamma_{tT}, t)$, and we have worked out this expression explicitly for a number of different cases, given in Examples 1–4. The general valuation formula is presented in Theorem 4.

It should be evident that once we have specified the functional dependence of the resulting asset prices on the extended information process, then we can back out values of the information process and the gamma bridge from the price data. So in that sense the process $\{\xi_t, \gamma_{tT}\}$ is "visible" in the market, and can be inferred directly, at any time, from a suitable collection of prices. This means, in particular, that given the prices of a certain minimal collection of assets in the market, we can then work out the values of other assets in the market, such as derivatives. In the special case we have just been discussing, there is only a single market factor; but one can see at once that the ideas involved readily extend to the situation where there are multiple market factors and multiple cash flows, as one expects for general securities analysis, following the principles laid out in Brody et al. (2007, 2008a), where the merits and limitations of modelling in an information-based framework are discussed in some detail.

The potential advantages of working with the variance-gamma information process, rather than the highly tractable but more limited Brownian information process should be evident—these include the additional parametric freedom in the model, with more flexibility in the distributions of returns, but equally important, the scope for jumps. It comes as a pleasant surprise that the resulting formulae are to a large extent analytically explicit, but this is on account of the remarkable properties of the normalized variance-gamma bridge process that we have exploited in our constructions. Keep in mind that in the limit as the parameter m goes to infinity our model reduces to that of the Brownian bridge information-based model considered in Brody et al. (2007, 2008a), which in turn contains the standard geometric Brownian motion model (and hence the Black-Scholes option pricing model) as a special case. In the case of a single market factor X_T, the distribution of the random variable X_T can be inferred by observing the current prices of derivatives for which the payoff is of the form

$$H_T = \mathrm{e}^{rT} \mathbb{1}_{X_T \leq K}, \tag{115}$$

for $K \in \mathbb{R}$. The information flow-rate parameter σ and the shape parameter m can then be inferred from option prices. When multiple factors are involved, similar calibration methodologies are applicable.

Author Contributions: The authors have made equal contributions to the work. Both have read and agreed to the published version of the manuscript.

Funding: This research has received no external funding.

Acknowledgments: The authors wish to thank G. Bouzianis and J. M. Pedraza-Ramírez for useful discussions. LSB acknowledges support from (a) Oriel College, Oxford, (b) the Mathematical Institute, Oxford, (c) Consejo Nacional de Ciencia y Tenconología (CONACyT), Ciudad de México, and (d) LMAX Exchange, London. We are grateful to the anonymous referees for a number of helpful comments and suggestions.

Conflicts of Interest: The authors declare no conflict of interest.

References

Abramowitz, Milton, and Irene A. Stegun, eds. 1972. *Handbook of Mathematical Functions with Formulas, Graphs, and Mathematical Tables*. United State Department of Commerce, National Bureau of Standards, Applied Mathematics Series 55. Washington: National Bureau of Standards.

Bouzianis, George, and Lane P. Hughston. 2019. Determination of the Lévy Exponent in Asset Pricing Models. *International Journal of Theoretical and Applied Finance* 22: 1950008. [CrossRef]

Brody, Dorje C., Lane P. Hughston, and Andrea Macrina. 2007. Beyond Hazard Rates: A New Framework for Credit-Risk Modelling. In *Advances in Mathematical Finance*. Edited by Michael C. Fu, Robert A. Jarrow, Ju-Yi J. Yen and Robert J. Elliot. Basel: Birkhäuser.

Brody, Dorje C., Lane P. Hughston, and Andrea Macrina. 2008a. Information-Based Asset Pricing. *International Journal of Theoretical and Applied Finance* 11: 107–42. [CrossRef]

Brody, Dorje C., Lane P. Hughston, and Andrea Macrina. 2008b. Dam Rain and Cumulative Gain. *Proceeding of the Royal Society A* 464: 1801–22. [CrossRef]

Brody, Dorje C., Mark H. A. Davis, Robyn L. Friedman, and Lane P. Hughston. 2009. Informed Traders. *Proceedings of the Royal Society A* 465: 1103–22. [CrossRef]

Brody, Dorje C., Lane P. Hughston, and Andrea Macrina. 2010. Credit Risk, Market Sentiment and Randomly-Timed Default. In *Stochastic Analysis in 2010*. Edited by Dan Crisan. Berlin: Springer-Verlag.

Brody, Dorje C., Lane P. Hughston, and Andrea Macrina. 2011. Modelling Information Flows in Financial Markets. In *Advanced Mathematical Methods for Finance*. Edited by Giulia Di Nunno and Bernt Øksendal. Berlin: Springer-Verlag.

Carr, Peter, Hélyette Geman, Dilip B. Madan, and Marc Yor. 2002. The Fine Structure of Asset Returns: An Empirical Investigation. *Journal of Business* 75: 305–32. [CrossRef]

Émery, Michel, and Marc Yor. 2004. A Parallel between Brownian Bridges and Gamma Bridges. *Publications of the Research Institute for Mathematical Sciences, Kyoto University* 40: 669–88. [CrossRef]

Filipović, Damir, Lane P. Hughston, and Andrea Macrina. 2012. Conditional Density Models for Asset Pricing. *International Journal of Theoretical and Applied Finance* 15: 1250002. [CrossRef]

Hoyle, Edward. 2010. Information-Based Models for Finance and Insurance. Ph.D. Thesis, Imperial College London, UK.

Hoyle, Edward, Lane P. Hughston, and Andrea Macrina. 2011. Lévy Random Bridges and the Modelling of Financial Information. *Stochastic Processes and their Applications* 121: 856–84. [CrossRef]

Hoyle, Edward, Lane P. Hughston, and Andrea Macrina. 2015. Stable-1/2 Bridges and Insurance. In *Advances in Mathematics of Finance*. Edited by Andrzej Palczewski and Lukasz Stettner. Warsaw: Polish Academy of Sciences.

Hoyle, Edward, Andrea Macrina, and Levent A. Mengütürk. 2020. Modulated Information Flows in Financial Markets. *International Journal of Theoretical and Applied Finance* 23: 2050026. [CrossRef]

Hughston, Lane P., and Andrea Macrina. 2012. Pricing Fixed-Income Securities in an Information-Based Framework. *Applied Mathematical Finance* 19: 361–79. [CrossRef]

Karatzas, Ioannis, and Steven E. Shreve. 1998. *Methods of Mathematical Finance*. New York: Springer-Verlag.

Kyprianou, Andreas E. 2014. *Fluctuations of Lévy Processes with Applications*, 2nd ed. Berlin: Springer-Verlag.

Macrina, Andrea. 2006. An Information-Based Framework for Asset Pricing: X-factor Theory and Its Applications. Ph.D. Thesis, King's College London, UK.

Macrina, Andrea, and Jun Sekine. 2019. Stochastic Modelling with Randomized Markov Bridges. *Stochastics* 19: 1–27. [CrossRef]

Madan, Dilip, and Eugene Seneta. 1990. The Variance Gamma (VG) Model for Share Market Returns. *Journal of Business* 63: 511–24. [CrossRef]

Madan, Dilip, and Frank Milne. 1991. Option Pricing with VG Martingale Components. *Mathematical Finance* 1: 39–55. [CrossRef]

Madan, Dilip, Peter Carr, and Eric C. Chang. 1998. The Variance Gamma Process and Option Pricing. *European Finance Review* 2: 79–105. [CrossRef]

Mengütürk, Levent A. 2013. Information-Based Jumps, Asymmetry and Dependence in Financial Modelling. Ph.D. Thesis, Imperial College London, UK.

Mengütürk, Levent A. 2018. Gaussian Random Bridges and a Geometric Model for Information Equilibrium. *Physica A* 494: 465–83. [CrossRef]

Rutkowski, Marek, and Nannan Yu. 2007. An Extension of the Brody-Hughston-Macrina Approach to Modeling of Defaultable Bonds. *International Journal of Theoretical and Applied Finance* 10: 557–89. [CrossRef]

Williams, David. 1991. *Probability with Martingales*. Cambridge, UK: Cambridge University Press.

Yor, Marc. 2007. Some Remarkable Properties of Gamma Processes. In *Advances in Mathematical Finance*. Edited by Michel C. Fu, Robert A. Jarrow, Ju-Yi J. Yen and Robert J. Elliot. Basel: Birkhäuser.

risks

MDPI

Communication

A Poisson Autoregressive Model to Understand COVID-19 Contagion Dynamics

Arianna Agosto and Paolo Giudici *

Department of Economics and Management, University of Pavia, 27100 Pavia, Italy; arianna.agosto@unipv.it
* paolo.giudici@unipv.it

Received: 9 June 2020; Accepted: 11 July 2020; Published: 16 July 2020

Abstract: We present a statistical model which can be employed to understand the contagion dynamics of the COVID-19, which can heavily impact health, economics and finance. The model is a Poisson autoregression of the daily new observed cases, and can reveal whether contagion has a trend, and where is each country on that trend. Model results are exemplified from some observed series.

Keywords: poisson autoregressive models; contagion; predictive monitoring

1. Motivation

The spread of the COVID-19 virus at the beginning of 2020 caught many countries and governments by surprise and unveiled a widespread lack of pandemic preparedness at the global and national level.

Currently, given the absence of a vaccine and the incomplete information about several aspects of contagion, such as the role of different risk factors, the dynamics of transmission and the role of asymptomatic transmission, governments operate under significant uncertainty. Against this background, data from countries where the virus has initially spread (notably China) are a precious source of information for the countries that are fighting against the virus. The more data becomes available, the more policies can be formulated with the backing of evidence as regards the "curve" and the "peak" of the contagion.

Early attempts to model the contagion curve of the COVID-19 include (Danon et al. 2020), which predicted that the outbreak would peak 126 to 147 days (around 4 months) after the start of person-to-person transmission in England and Wales, at a time in which the virus had been found in just 25 countries; and (Kucharski et al. 2020), which combines a stochastic transmission model with four datasets on cases of COVID-19 originated in Wuhan to estimate how transmission varied over time, and calculate the probability that newly introduced cases might generate outbreaks in other areas. In Imperial College COVID-19 Response Team (2020), researchers modified an individual-based simulation model developed to support pandemic influenza planning to explore scenarios for COVID-19 in Great Britain.

Particularly relevant studies for our work are Gu et al. (2020) and Giordano et al. (2020) which, while mathematically expressing the current practices in the modelling on the global spread of diseases, draw policy making suggestions. We follow the same line of research, combining mathematical rigour with attention to drawing results that can be useful for policy makers. Specifically, our contribution is a new statistical model for disease spread which, by taking dependence between daily contagion counts into account, can better capture the contagion curve dynamics and, thus, can draw further light on the understanding of its possible future path.

Our approach is connected to the exponential growth models employed in the SIR literature (Biggerstaff et al. 2014), to which we contribute by including an autoregressive component in the growth dynamics.

2. Methodology

We aim to build a monitoring model which can provide support to policy makers engaged in contrasting the spread of the COVID-19, and their economical consequences. To this aim, we propose a statistical model that can estimate when the peak of contagion is reached, so that preventive measures (such as mobility restrictions) can be applied and/or relaxed.

To be built the model requires, for each country (or region), the daily count of new infections. In the study of epidemics, it is usually assumed that infection counts follow an exponential growth, driven by the reproduction number R (see, e.g., Biggerstaff et al. 2014). The latter can be estimated by the ratio between the new cases arising in consecutive days: a short-term dependence. This procedure, however, may not be adequate: incubation time is quite variable among individuals and data occurrence and measurement is not uniform across different countries (and, sometimes, along time): these aspects induce a long-term dependence.

From the previous considerations, it follows that it would be ideal to model newly infected counts as a function of both a short-term and a long-term component. A model of this kind has been recently proposed by Agosto et al. (2016), in the context of financial contagion. We propose to adapt this model to the COVID-19 contagion.

Formally, resorting to the log-linear version of Poisson autoregression, introduced by Fokianos and Tjøstheim (2011), we assume that the statistical distribution of new cases at time (day) t, conditional on the information up to $t-1$, is Poisson, with a log-linear autoregressive intensity, as follows:

$$y_t|\mathcal{F}_{t-1} \sim Poisson(\lambda_t)$$

$$\log(\lambda_t) = \omega + \alpha \log(1 + y_{t-1}) + \beta \log(\lambda_{t-1}),$$

where $\mathcal{F}_{t-1}$ denotes the σ-field generated by $\{y_0, ..., y_t\}$, $y_t \in \mathbb{N}$, $\omega \in \mathbb{R}$, $\alpha \in \mathbb{R}$, $\beta \in \mathbb{R}$. Note that the inclusion of $\log(1 + y_{t-1})$, rather than $\log(y_{t-1})$, allows to deal with zero values.

In the model, ω is the intercept term, whereas α and β express the dependence of the expected number of new infections, λ_t, on the past counts of new infections. Specifically, the α component represents the short-term dependence on the previous time point. The β component represents a trend component, that is, the long-term dependence on all past values of the observed process. The inclusion of the β component is analogous to moving from an ARCH (Engle 1982) to a GARCH (Engle and Bollerslev 1986) model in Gaussian processes, and allows to capture long memory effects. The advantage of a log-linear intensity specification, rather than the linear one known as integer-valued GARCH (see, e.g., Ferland et al. 2006), is that it allows for negative dependence. From an inferential viewpoint, Fokianos and Tjøstheim (2011) show that the model can be estimated by a maximum likelihood method.

3. Results

The model can be applied to any country, region, and in different time periods. We exemplify its usage, without loss of generality, using data available until 31 March 2020. The data source is the daily World Health Organisation reports (see World Health Organisation 2020), from which we have extracted the "Total confirmed new cases". Figure 1 presents the observed evolution of the daily new cases of infection: for China (starting from 20 January), Iran, South Korea and Italy (starting from 21 February). We choose to consider data until the end of March (Figure 1) and make predictions for the beginning of April because at that time contagion counts in the analysed countries were still high and predictions challenging. Being the count response variable a Poisson, its variance depends on the number of observed counts, a number which has been declining in the considered countries, from April onwards, when not before.

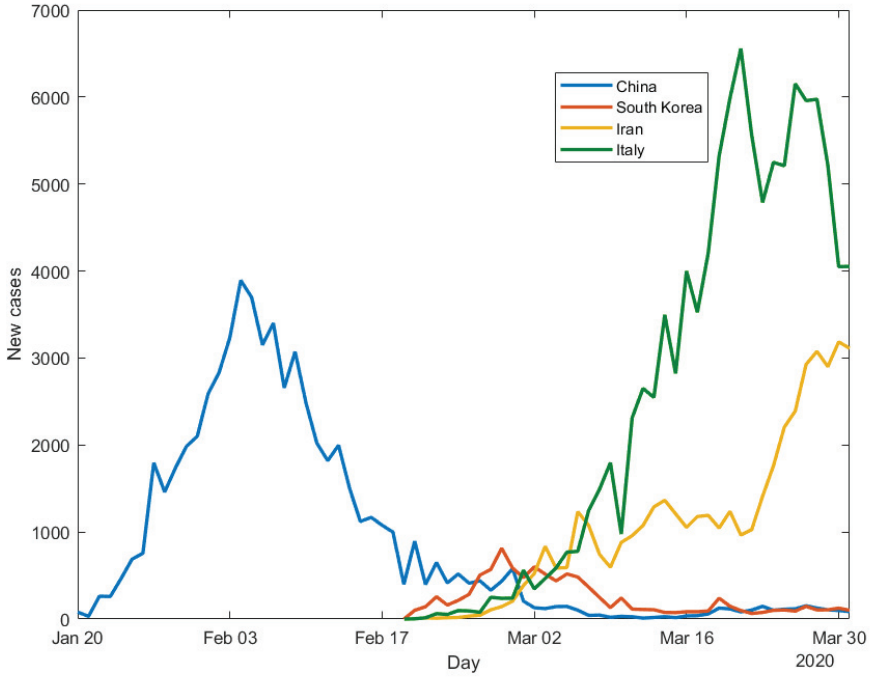

Figure 1. Observed infection counts.

Figure 1 shows that, as of 31 March 2020, COVID-19 contagion in China has completed a full cycle, with an upward trend, a peak, and a downward trend. South Korea seems to have had a similar situation, with a smaller intensity. Italy has followed a similar path, with a larger intensity. The contagion dynamics in Iran is more difficult to interpret, and is still quite erratic.

The application of our model can better qualify these conclusions. The estimated model parameters for China, using all data available until 31 March, are shown in Table 1.

Table 1. Model estimates for China, with standard errors and *p*-values.

Parameter	Estimate	Std Error (*p*-Value)
ω	0.337	0.247 (0.177)
α	0.823	0.069 (0.000)
β	0.133	0.062 (0.016)

Table 1 shows that all estimated autoregressive coefficients are significant, confirming the presence of both a short-term dependence and a long-term trend. From an interpretational viewpoint, the estimate of α shows that, if the expectation of new cases for yesterday was close to 0, 100 new cases observed yesterday generate about 40 new expected cases today. According to the value estimated for β, an expectation of 100 new cases for yesterday generates instead about 2 new expected cases today, if no cases were observed yesterday.

With the aim of better interpreting the time series of the other countries, which on 31 March seem not to have completed their contagion cycle yet, we repeatedly fit the model to the Chinese data, using increasing amounts of data, in a retrospective way. More precisely, we first fit the model on the

first 15 counts from China (a minimal requirement for statistical consistency of the results), then on the first 16, and so on. For each fit we plot the estimated α and β parameters in Figure 2.

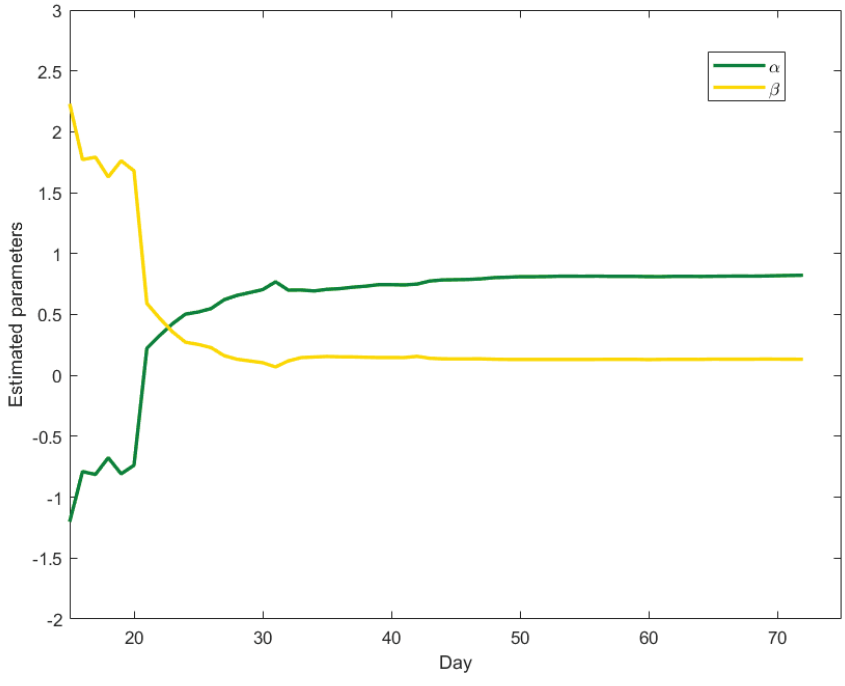

Figure 2. Evolution of the α and β parameters for Chinese daily infection counts.

Figure 2 shows that, until February 11th (the 23rd day reported) β is greater than α, indicating the presence of a still increasing trend (the β component) that absorbs the short-term component. After that time, downward trend data is accumulated, β starts decreasing and α increasing. The results approximate the values in Table 1 around 20 February: after this date the estimated parameters become stable, as the difference between subsequent estimates becomes lower than 0.01.

What obtained from the Chinese data suggests to use the PAR model to assess at which stage the contagion cycle is in the other countries. We thus estimate the model parameters for the other three countries, using the data available until 31 March. Our results show that, for Iran, on that date the α parameter prevails, with an estimated value equal to 0.96, indicating a process mainly driven by a short-term dependence on the previous time points. However, further analyses reveal that the parameters estimated for Iran are very unstable. The estimated β parameter for South Korea is not significant, indicating absence of a trend effect on the daily counts, consistently with what observed in Figure 1. For Italy, instead, α is about 0.51, higher than β 0.38, similarly to China but with a lower difference between the two parameters, indicating that, at the end of March, the trend component is weakening.

To conclude, we believe that our model can constitute a useful statistical tool for decision makers: in each country, once a minimal series of data is collected (we suggest 15 days) the values of α and β can be monitored along time, to reveal at which stage the contagion dynamics is: well beyond the peak (as in China and South Korea); close to or right after the peak (as Italy on 31 March); or in a situation that could indicate that the peak has been reached, but which needs more data to be understood (as Iran at the end of March).

The full reproducibility of our model can easily extend its application to more countries and time periods as data becomes available.

To better understand the advantages of our proposed specification and, at the same time, to show its possible improvement, we now compare it with two alternative models, one simpler and one more complex.

The first one is a classic exponential growth model, that is a regression of the number of daily new cases on the time, expressed as days since the outbreak:

$$\log(y_t) = \kappa_0 + \kappa_1 t. \tag{1}$$

The second alternative model we consider is a PARX model Agosto et al. (2016), that is a Poisson autoregressive model with a covariate. As a covariate we use time: the number of days since the outbreak, as in the classical exponential model. Thus, we extend the PAR model as follows:

$$\log(\lambda_t) = \omega + \alpha \log(1 + y_{t-1}) + \beta \log(\lambda_{t-1}) + \gamma t,$$

We now apply the three models-estimated using data until the end of March - to make 10-day ahead predictions of the daily new cases. The results obtained for South Korea, Iran and Italy are shown in Figures 3–5.

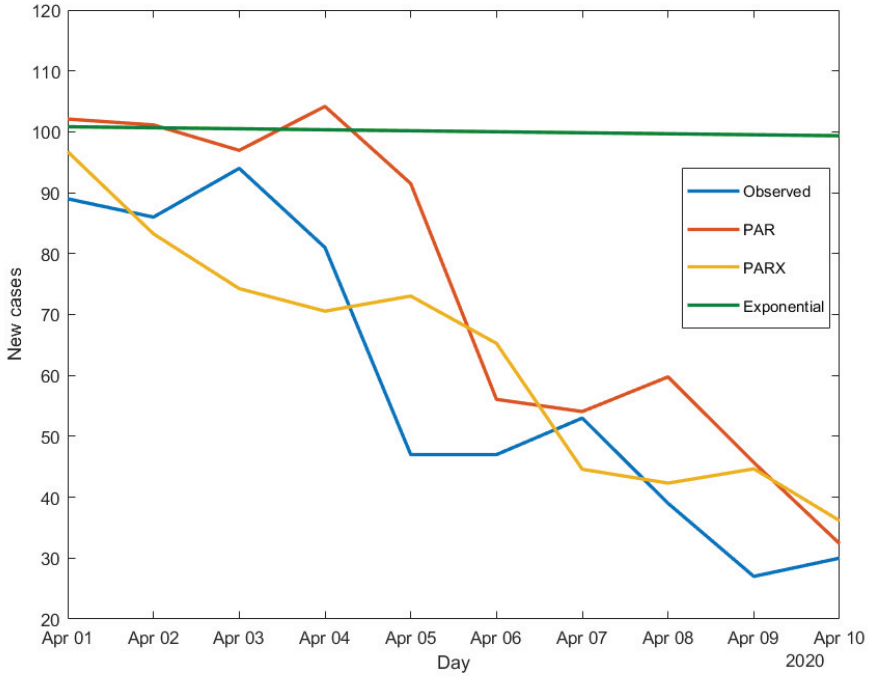

Figure 3. Daily infection counts in South Korea: observed and predicted values.

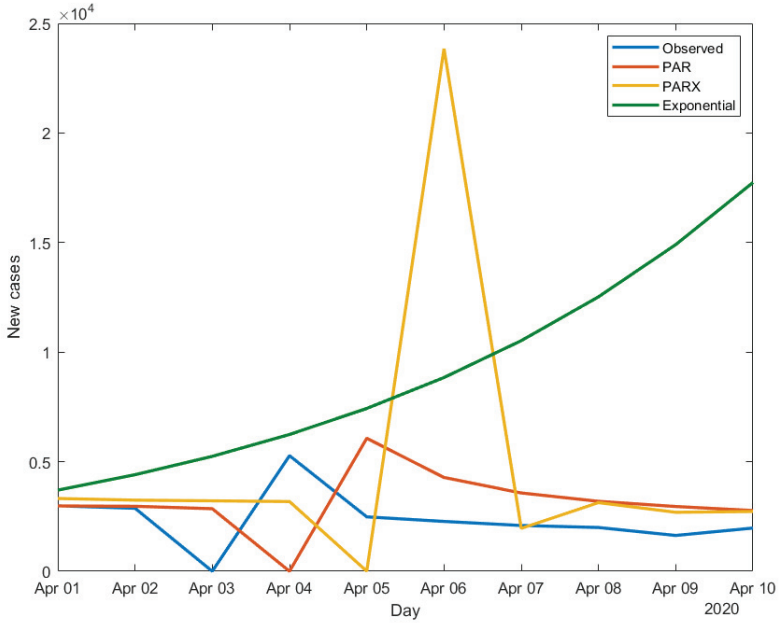

Figure 4. Daily infection counts in Iran: observed and predicted values.

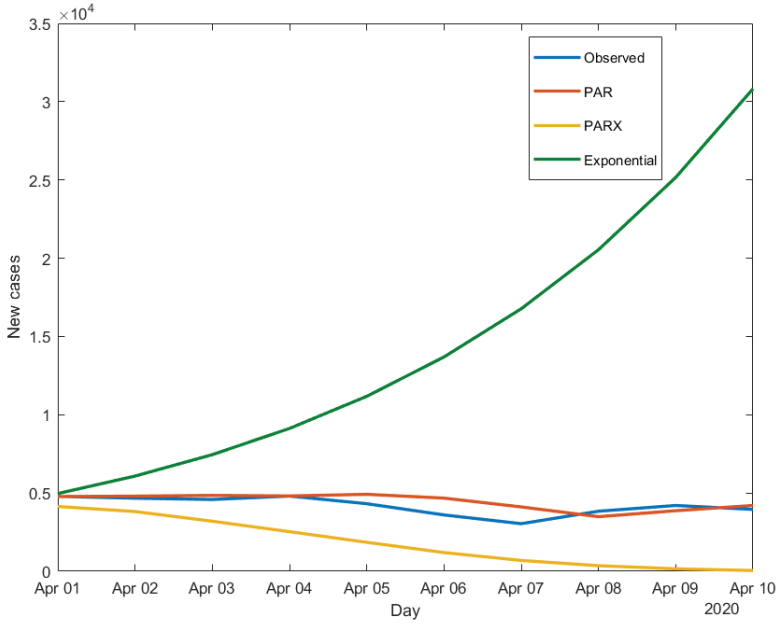

Figure 5. Daily infection counts in Italy: observed and predicted values.

Figures 3–5 all show the limits of the exponential model, which, being a "static" model, cannot capture time variations in the contagion dynamics, differently from both the PAR and the PARX. The latter, being dynamic models, can better adapt to disease count variations, without the need to often adjust the estimates and find a saturation point, as it would be the case for the exponential model.

To compare the models in terms of out-of-sample predictive performance, in Table 2 we report the value of Root Mean Squared Error (RMSE) and Mean Percentage error (MPE) for the three specifications.

Table 2. Out-of-sample error measures.

	South Korea		Iran		Italy	
Model	**RMSE**	**MPE**	**RMSE**	**MPE**	**RMSE**	**MPE**
PAR	19.48	−31.04%	2426.2	−0.29%	551.79	−7.69%
PARX	14.18	−14.44%	6996.1	−49.33%	2633.4	59.63%
Exponential	47.28	−103.1%	8399.5	−156.30%	13,441	−269.17%

The results in Table 2 show that the PAR model always outperforms the other two, except in the case of South Korea, for which the preferable specification turns out to be Poisson autoregression including the time since outbreak as a covariate. This finding is consistent with what observed in Figures 3–5 and confirms the superiority of Poisson autoregressive models over the exponential growth model. This advantage explains the potential impact of our proposal, which is successfully implemented and weekly updated in the infographic website of the Center for European Policy Studies[1].

Author Contributions: All authors have read and agreed to the published version of the manuscript.

Funding: This research received no external funding.

Acknowledgments: The work of the Authors is receiving support from the European Union's Horizon 2020 training and innovation programme "FIN-TECH", under the grant agreement No. 825215 (Topic ICT-35-2018, Type of actions: CSA). The paper is the result of the joint collaboration between the two authors.

Conflicts of Interest: The authors declare no conflicts of interest.

References

Agosto, Arianna, Giuseppe Cavaliere, Dennis Kristensen, and Anders Rahbek. 2016. Modeling Corporate Defaults: Poisson Autoregressions with Exogenous Covariates (PARX). *Journal of Empirical Finance* 38: 640–63. [CrossRef]

Biggerstaff, Matthew, Simon Cauchemez, Carrie Reed, Manoj Gambhir, and Lyn Finelli. 2014. Estimates of the reproduction number for seasonal, pandemic, and zoonotic influenza: A systematic review of the literature. *BMC Infectious Diseases* 14: 480. [CrossRef] [PubMed]

Danon, Leon, Ellen Brooks-Pollock, Mick Bailey, and Matt J. Keeling. 2020. A Spatial Model of CoVID-19 Transmission in England and Wales: Early Spread and Peak Timing. Available online: https://www.medrxiv.org/content/10.1101/2020.02.12.20022566v1 (accessed on 30 April 2020).

Engle, Robert F. 1982. Autoregressive Conditional Heteroscedasticity with Estimates of the Variance of U. K. Inflation. *Econometrica: Journal of the Econometric Society* 50: 987–1008. [CrossRef]

Engle, Robert F., and Tim Bollerslev. 1986. Modelling the persistence of conditional variances. *Econometric Reviews* 5: 1–50. [CrossRef]

Ferland, René, Alain Latour, and Driss Oraichi. 2006. Integer-valued GARCH processes. *Journal of Time Series Analysis* 27: 923–42. [CrossRef]

[1] https://infogram.com/covid-1hd12y0d0dpw6km?live.

Fokianos, Konstantinos, and Dag Tjøstheim. 2011. Log-linear Poisson autoregression. *Journal of Multivariate Analysis* 102: 563–78. [CrossRef]

Giordano, Giulia, Franco Blanchini, Raffaele Bruno, Patrizio Colaneri, Alessandro Di Filippo, Angela Di Matteo, and Marta Colaneri. 2020. Modelling the COVID-19 epidemic and implementation of population wide interventions in Italy. *Nature Medicine* 26: 855–60. [CrossRef] [PubMed]

Gu, Chenlin, Wei Jiang, Tianyuan Zhao, and Ban Zheng. 2020. Mathematical Recommendations to Fight against COVID-19. Available online: https://papers.ssrn.com/sol3/papers.cfm?abstract_id=3551006 (accessed on 30 April 2020).

Imperial College COVID-19 Response Team. 2020. Impact of Non-Pharmaceutical Interventions (NPIs) to Reduce COVID19 Mortality and Healthcare Demand. Available online: https://www.imperial.ac.uk/media/imperial-college/medicine/sph/ide/gida-fellowships/Imperial-College-COVID19-NPI-modelling-16-03-2020.pdf (accessed on 30 April 2020).

Kucharski, Adam J., Timothy W. Russell, Charlie Diamond, Yang Liu, John Edmunds, Sebastian Funk, Rosalind M. Eggo, Fiona Sun, Mark Jit, James D Munday, et al. 2020. Early Dynamics of Transmission and Control of COVID-19: A Mathematical Modelling Study. Centre for Mathematical Modelling of Infectious Diseases COVID-19 Working Group. Available online: http://docplayer.fr/11284694-Tables-de-probabilites-et-statistique.html (accessed on 30 April 2020).

World Health Organisation. 2020. Novel Coronavirus (2019-nCoV) Situation Reports. pp. 1–49. Available online: https://apps.who.int/iris/bitstream/handle/10665/330762/nCoVsitrep23Jan2020-eng.pdf (accessed on 30 April 2020).

risks

MDPI

Article

Price Discovery and Market Reflexivity in Agricultural Futures Contracts with Different Maturities

Steffen Volkenand *, Günther Filler and Martin Odening

Department of Agricultural Economics, Humboldt-Universität zu Berlin, 10099 Berlin, Germany; guenther.filler@agrar.hu-berlin.de (G.F.); m.odening@agrar.hu-berlin.de (M.O.)
* Correspondence: steffen.volkenand@agrar.hu-berlin.de

Received: 12 May 2020; Accepted: 8 July 2020; Published: 11 July 2020

Abstract: The purpose of this paper is to analyze market reflexivity in agricultural futures contracts with different maturities. To this end, we apply a four-dimensional Hawkes model to storable and non-storable agricultural commodities. We find market reflexivity for both storable and non-storable commodities. Reflexivity accounts for about 50 to 70% of the total trading activity. Differences between nearby and deferred contracts are less pronounced for non-storable than for storable commodities. We conclude that the co-existence of exogenous and endogenous price dynamics does not change qualitative characteristics of the price discovery process that have been observed earlier without the consideration of market reflexivity.

Keywords: agricultural commodity futures; price discovery; market reflexivity; Hawkes process

JEL Classification: G14; C49

1. Introduction

Prices of commodity futures contracts with different maturities are linked through the forward curve. Understanding of the shape and the characteristics of the term structure is of utmost importance for storage decisions, hedging and roll-over strategies as well as calendar spread trading. Several strands of literature address this topic. The theoretical underpinning of the forward curve goes back to Working's (1949) theory of storage that establishes an equilibrium relation between nearby and distant futures contracts and explains storage under backwardation by the concept of convenience yield (Brennan 1958). In contrast, Keynes' theory of normal backwardation decomposes a futures price into an expected future spot price and an expected risk premium that risk-averse hedgers grant to speculators (Fama and French 1987). The statistical modelling of the forward curve has benefitted from Nelson and Siegel's (1987) proposal to describe the term structure parsimoniously in terms of level, slope and curvature. A dynamic version of this model has been introduced by Diebold and Li (2006). Applications to commodity futures can be found in Karstanje et al. (2017). An alternative method uses a set of state variables (factors), particularly spot price, convenience yield, and interest rate, to derive the forward curve under no-arbitrage conditions (Gibson and Schwartz 1990; Schwartz 1997). Applications of this approach to agricultural futures include Geman and Nguyen (2005) and Sorensen (2002), among others.

With the rise of the modern market microstructure, interest has shifted from the estimation of equilibrium relations towards the understanding of price discovery, i.e., the question of how new information is absorbed in asset prices and how this information is transferred along the forward curve. Since there is no explicit market microstructure theory designed for commodity futures with different maturities, most studies in this area are non-structural and try to identify empirical patterns in

data. Mallory et al. (2015) use contemporaneous and time-lagged correlations of nearby and deferred futures contracts for corn to investigate the speed at which liquidity providers revise their beliefs in response to the occurrence of an information event. They find that the correlation of price revisions disappears even for short time lags and conclude that new information to the market is immediately transmitted across all contract maturities. Hu et al. (2017) pursue a similar objective, but instead of simple correlations, they apply co-integration techniques to explore price discovery among nearby and deferred futures contracts of corn and live cattle. They report a larger share of price discovery in nearer to maturity contracts. The dominance of nearer contracts, however, is less pronounced for live cattle than for corn, which is explained by differences in the storability of these commodities. Recently, Volkenand et al. (2019) investigate the duration dependence among agricultural futures with different maturities, exploiting the fact that the time between market events (transactions or price changes) carries information (Easley and O'Hara 1992). They apply an autoregressive conditional duration (ACD) model to price durations for corn, wheat, live cattle, and lean hog. The authors report linkages between nearby and deferred futures contracts. They conclude that information is quickly processed along the forward curve.

The aforementioned studies rest on a traditional view of the price discovery mechanism according to which price revisions are driven by the arrival of exogenous information. This view has been challenged by the concept of market reflexivity (Soros 1987) which assumes that trading activity is also endogenously driven by positive feedback mechanisms. Sources of potential endogeneity encompass informational cascades leading to herding, as well as speculation based on technical analysis (e.g., momentum trading) and algorithmic trading (Filimonov et al. 2014). Furthermore, hedging strategies combined with portfolio execution rules can lead to self-excitement of price moves (Kyle and Obizhaev 2019). While this co-existence of exogenous and endogenous price dynamics contradicts the efficient market hypothesis (Fama 1970), it can be helpful to understand puzzling phenomena on financial markets, such as "flash crashes" or excess volatility (Hardiman et al. 2013). The concept of market reflexivity has originally been introduced in a narrative, non-technical manner, but since then it experienced an underpinning by statistical methods that allow one to disentangle exogenous and endogenous sources of market activities and thus measure the degree of market reflexivity. More specifically, self-exiting Hawkes processes have been proposed as a device to quantify reflexivity (e.g., Filimonov and Sornette 2012). Bacry et al. (2016), for example, find that less than 5% of the price changes in the DAX (German stock index) and BUND (German Bond) futures markets are driven by external sources. In the context of commodity futures markets, Filimonov et al. (2014) find that reflexivity has increased since the mid-2000s to 70%. They trace this back to the increase in automated trading in the course of the transition to an electronic trading environment. In fact, automated trading generated about 40% of the total futures volume traded in the grain and oilseed markets between 2012 and 2014 (Haynes and Roberts 2015).

Despite the increasing interest in market reflexivity as an alternative to the prevalent tenet of market efficiency and rational expectations, there exists no empirical study applying this concept to the forward curve of commodities. Against this backdrop, our objective is to examine price discovery in nearby and deferred agricultural futures contracts while explicitly taking into account potential market reflexivity. We apply a four-dimensional Hawkes model to storable and non-storable agricultural commodities. The Hawkes model allows us to divide the intensity of the trading activity in a futures contract with a certain maturity into three parts: a reaction on external sources like new information, market reflexivity, and reactions on trading activity in contracts of different maturities. Using this approach, we review previous findings regarding price discovery in nearby and deferred futures contracts. In particular, we examine whether nearby contracts dominate deferred contracts in price discovery while accounting for potential market reflexivity (e.g., Gray and Rutledge 1971). We also explore whether price discovery and potential market reflexivity differ between storable and non-storable commodities. In line with Hu et al. (2017), we expect that dominance of nearby contracts in price discovery is more pronounced for storable commodities. Moreover, we conjecture

that commodities with a high share of automated trading, such as grains and oilseeds, show a higher level of endogeneity. Since market microstructure theory emphasizes the importance of the direction of the transactions in the price discovery process (cf. Glosten and Milgrom 1985), we differentiate between buyer- and seller-initiated transactions in our analyses.

The remainder of the paper is organized as follows: Section 2 explains the statistical methods used in the analyses. Section 3 presents the dataset and the results of the empirical application and Section 4 concludes.

2. Methodology

The price discovery process has been mainly examined using two measures: The Hasbrouck information share (Hasbrouck 1995) and the Harris–McInish–Wood component share (Harris et al. 2002). Both measures are derived from a reduced form vector error correction model that is estimated based on equidistant time intervals. However, Easley and O'Hara (1992) show that liquidity providers also consider the time between market events within the price setting process. Since the timing of transactions and the frequency in which they occur have information value of their own, fixed-interval aggregation schemes lead to a loss of information (cf. Bauwens and Hautsch 2007). Taking into account the irregular occurrence of transactions requires one to consider the data as a point process. The simplest type of point process is the homogeneous Poisson process. Since the homogeneous Poisson process assumes independently distributed events, it is not suited to describe well-known structures such as correlations and clustering of transactions. The ACD model (Engle and Russell 1998), in contrast, accounts for correlation structures in the data and can be used to model the time between transactions. However, in a multivariate framework, the asynchronous arrival of transactions renders the application of the ACD model difficult and dynamic intensity models are preferable. In autoregressive conditional intensity (ACI) models (Russell 1999), the intensity is directly modeled in terms of an autoregressive process. On the other hand, Hawkes processes (Hawkes 1971) describe the intensity in terms of an additive structure and can be regarded as clusters of Poisson processes. According to this view, all events belong to one of two classes—immigrants and descendants. The exogenous immigrants can trigger clusters of descendants, each of whom in turn can trigger own descendants. In this branching process, the so-called branching ratio is defined as the average number of daughter events per mother event. Hautsch (2004), Bowsher (2007), and Large (2007) confirm that Hawkes processes model the dynamics in financial point processes remarkably well. Since the linear structure of the Hawkes model allows one to separate external influences on the process from internal feedback mechanisms, it is well suited to examine price discovery and potential market reflexivity. Technically speaking, Hawkes processes refer to a class of models for stochastic self-exciting and mutually exciting point processes (Hawkes 1971). These can be regarded as non-homogeneous Poisson processes whose intensity depends on both time t and the history of the process. The intensity function $\lambda_i(t)$ of a Hawkes process is defined as:

$$\lambda_i(t) = \mu_i + \sum_{j=1}^{D} \sum_{t_k^j < t} \phi_{ij}\left(t - t_k^j\right), \forall i, j \in [1 \dots D] \tag{1}$$

where D is the number of dimensions in the process. The non-negative parameter μ is the baseline intensity and commonly assumed to be constant. The baseline intensity describes the arrival rate of events triggered by external sources. In our analysis, we use μ to examine how futures contracts of different maturities react to new information. The non-negative kernel function, ϕ, describes the arrival rate of events that are triggered by previous events within the process. Various kernel functions can be found in the literature. The most widely used are power-law and exponential parameterizations of the kernel function. In our analysis, we follow Bacry et al. (2017) and choose the following exponential parametrization of the kernel functions:

$$\|\phi\|_{ij}(t) = \alpha_{ij}\beta_{ij}exp\left(-\beta_{ij}t\right)1_{t>0} \tag{2}$$

where α and $\beta > 0$. In this parametrization, α describes the degree of influence of past points on the intensity process and β determines the time decay of the influence of past points on the intensity process. From the chosen parametrization, it follows

$$\int_0^\infty \phi(t)dt = \alpha = \|\phi\|_1 \tag{3}$$

where $\|\phi\|_1$ is a matrix of kernel norms. Each matrix element describes the total impact that events of the type defined by a column of the matrix has on events of the type defined by a row of the matrix. According to the population representation of a Hawkes process (Hawkes and Oakes 1974), the process is considered stable if $\|\phi\|_1 < 1$. For a stable Hawkes process, a kernel norm $\|\phi_{ii}\|_1$ stands for the average number of events of type i that is directly triggered by a past event of the same type i. In our analysis, we use $\|\phi_{ii}\|_1$ to measure market reflexivity in futures contracts with different maturities. On the other hand, a kernel norm $\|\phi_{ij}\|_1$ with $i \neq j$ stands for the average number of events of type i that is directly triggered by an event of a different type j. We use $\|\phi_{ij}\|_1$ to measure price discovery between futures contracts with different maturities. Furthermore, following Bacry et al. (2016), the ratio between the baseline intensity μ_i and the average intensity γ_i describes an exogeneity ratio, i.e., the ratio between the number of events that is triggered by external sources and the total number of events of type i:

$$R_i = \frac{\mu_i}{\gamma_i} \tag{4}$$

where the average intensities can be derived by

$$\gamma = (I - \|\phi\|_1)^{-1}\mu \tag{5}$$

with I as the identity matrix.

Various methods to estimate Hawkes processes have been proposed in the literature. Estimation procedures include maximum likelihood estimation (Ogata 1998) and the resolution of a Wiener–Hopf system (Bacry et al. 2016). In our analysis, we follow Bacry et al. (2017) and estimate the Hawkes process with least-squares. To assess the goodness-of-fit of the estimated Hawkes model, we carry out a residual analysis according to Ogata (1989). Ogata's residual analysis of point process data is based on the random time change theorem by Meyer (1971). The random time change theorem states that a point process is transformed into a homogeneous Poisson process by its compensator $\Lambda(t)$. The compensator is determined by the Doob–Meyer decomposition of a point process and is described by the following monotonically increasing function:

$$\Lambda(t) = \int_0^t \lambda(t)dt. \tag{6}$$

In accordance with Ogata (1989), we use the compensator with the conditional intensity $\hat{\lambda}$ of the estimated Hawkes model to transform the observed data and regard the resulting process as a residual process. In line with the random time change theorem, if the residual process behaves like a homogeneous Poisson process, then the conditional intensity $\hat{\lambda}$ of the estimated Hawkes model is a good approximation to the true intensity λ of the observed point process. To check whether the residual process behaves similar to a homogeneous Poisson process, we apply Kolmogorov–Smirnov and Ljung–Box tests. On the one hand, the Kolmogorov–Smirnov test examines the null hypothesis that the distribution of the residuals is a homogeneous Poisson distribution. On the other hand, the Ljung–Box test examines the null hypothesis that the residuals are independently distributed. If the null hypothesis of both the Kolmogorov–Smirnov test and the Ljung–Box test cannot be rejected at the 5% significance level, we conclude that the estimated Hawkes process is a good approximation of the observed point process.

3. Empirical Application

3.1. Data

Empirical analyses of market reflexivity can be conducted for different time horizons. Long term analyses are useful if the development of endogeneity and its determinants over time are of interest. Long-term reflexivity is expected to be caused mainly by herding. In this paper, however, we focus on the analysis of short-term reflexivity. Short-term reflexivity is expected to be caused by algorithmic trading (Filimonov et al. 2014) that is supposed to distort the price discovery process in electronic commodity futures markets (cf. Tang and Xiong 2012; Bicchetti and Maystre 2013). For our analysis we utilize the Chicago Mercantile Exchange (CME) Group's best-bid–best-offer (BBO) futures data. We focus on corn, wheat, live cattle and lean hog. These commodities represent the most actively traded storable and non-storable agricultural futures contracts, respectively. The analysis is based on futures contracts of the first two maturities, i.e., the nearest (front contract) and the next to nearest (back contract).[1] We confine our analysis to the daytime trading session because the trading activity is much higher compared to the evening trading session. At the beginning of the daytime trading session, orders that have accumulated in the previous night are processed (cf. Gurgul and Syrek 2017), which can lead to a distorted picture of the price discovery process. Therefore, we exclude the first hour of the daytime trading session. Furthermore, to ensure stationarity of the parameters of the estimated Hawkes process, we follow Filimonov et al. (2014) and base our estimations on intervals of 10 min. Intervals of 10 min are considered to contain a sufficient number of events for reliable estimation. It can be assumed that in short intervals of 10 min, market reflexivity is not caused by behavioral mechanisms, such as herding, but instead is mainly caused by automated trading. The observation period covers all trading days in March 2016, which corresponds to 528 intervals of 10 min. March has been chosen as the observation period, because we want to exclude a rollover of contracts and the effect of a new harvest. On the other hand, we are interested in the effect of a release of three public reports on the short-term reflexivity: a World Agricultural Supply and Demand Estimates (WASDE) report on world agricultural supply and demand estimations, the United States Department of Agriculture (USDA) report on prospective plantings, and a National Agricultural Statistics Service (NASS) report on grain stocks. BBO data contain top-of-book quotes, transactions, and corresponding time stamps with a resolution of one second. In line with the above-mentioned market microstructure models, we regard the trading activity as the starting point of the price formation process and base our analyses on transactions. However, many transactions share the same time stamp. Therefore, to take all transactions into account, we follow Wang et al. (2016) and simulate sub-second time stamps. In addition, BBO data do not include the direction of transactions. Therefore, to distinguish between buyer- and seller-initiated transactions, we apply the trade classification algorithm proposed by Lee and Ready (1991). To summarize, we analyze a four-dimensional point process whose dimensions are buyer- and seller-initiated transactions in a futures front and back contract for corn, wheat, live cattle and lean hog.

3.2. Descriptive Statistics

Table 1 contains descriptive statistics for the considered commodities. The total number of buyer- and seller-initiated transactions is considerably higher in the front contract than in the back contract for corn and wheat. In contrast, the total number of transactions is similar in the front and back contract for live cattle and lean hog. The number of seller-initiated transactions is higher than the number of buyer-initiated transactions in both the front and back contract for corn. In contrast, the number of seller-initiated transactions is lower than the number of buyer-initiated transactions in both the front

[1] An inclusion of further contracts with longer maturities would be desirable to obtain a clearer picture of price discovery along the entire term structure curve. However, this comes at the cost of increasing the dimension of the Hawkes model. Moreover, the number of transactions becomes rather small for futures contracts with longer maturity, which renders the estimation unreliable.

and back contract for live cattle. The coefficients of variation show that the number of transactions varies more widely over the intervals for storable than for non-storable commodities.

Table 1. Descriptive statistics.

Variable	Commodity	Corn				Wheat			
	Contract	Front		Back		Front		Back	
	Type	Buy	Sell	Buy	Sell	Buy	Sell	Buy	Sell
Number of Transactions	Total	102,778	105,822	30,607	31,762	80,038	77,586	22,873	23,273
	Min.	14	34	1	4	12	11	1	1
	Mean	194.655	200.420	58.078	60.155	145.524	141.065	41.815	42.469
	Max.	2127	2519	946	889	1237	1392	349	277
	Std Dev	177.603	191.665	67.799	66.629	129.876	127.539	37.675	36.888
	CV	1.096	1.046	0.857	0.903	1.120	1.106	1.110	1.151
Volume (number of contracts)	Min.	149	110	4	12	50	84	8	4
	Mean	1991	2083	402	434	781	763	180	175
	Max.	22,131	29,561	5926	7546	6771	6,206	2127	1468
	Std Dev	2009	2467	516	596	775	714	197	174
	CV	1.009	1.185	1.284	1.372	0.993	0.937	1.099	0.995
Mid-quotes (cents per bushel)	Min.	348		352		446		453	
	Mean	364		369		466		472	
	Max.	373		377		479		486	
	Std Dev	5.683		5.594		8.199		8.341	
	CV	0.016		0.015		0.018		0.018	
Variable	**Commodity**	**Live Cattle**				**Lean Hog**			
	Contract	**Front**		**Back**		**Front**		**Back**	
	Type	**Buy**	**Sell**	**Buy**	**Sell**	**Buy**	**Sell**	**Buy**	**Sell**
Number of Transactions	Total	35,801	35,474	36,426	35,025	25,077	26,892	25,160	23,845
	Min.	1	1	1	1	1	1	1	1
	Mean	70.061	69.285	71.424	68.811	49.364	52.833	49.237	46.755
	Max.	426	373	532	584	371	371	261	328
	Std Dev	52.744	50.727	52.819	54.116	44.705	43.991	36.408	34.376
	CV	1.328	1.366	1.352	1.272	1.104	1.201	1.352	1.360
Volume (number of contracts)	Min.	2	2	2	2	0	0	0	0
	Mean	248	249	237	232	171	179	152	142
	Max.	2532	1512	1962	2416	1586	1661	106	1343
	Std Dev	225	210	209	214	181	179	135	128
	CV	0.905	0.842	0.882	0.922	1.058	1.003	0.883	0.898
Mid-quotes (cents per pound)	Min.	131		123		68		80	
	Mean	137		127		70		82	
	Max.	142		131		73		84	
	Std Dev	2.553		2.131		0.937		1.040	
	CV	0.019		0.017		0.013		0.013	

The trading volume is much higher for storable than for non-storable commodities. Moreover, the trading volume is significantly higher in the front contract than in the back contract for corn and for wheat. In contrast, the trading volume is similar in both the front and back contract for live cattle and lean hog. Furthermore, the imbalance between the buy-and-sell volume is larger for corn and wheat than for live cattle and lean hog. A high coefficient of variation indicates that the trading volume varies considerably over the intervals. The coefficient of variation is highest for corn.

To avoid bid–ask bounce effects, our descriptive statistics are based on mid-quotes rather than transaction prices. The mid-quotes are higher in the back contract than in the front contract for corn, wheat, and lean hog. This points to a normal forward curve during the observation period. In contrast, mid-quotes are higher in the front contract than in the back contract for live cattle. This points to an inverted forward curve during the observation period. The standard deviation of the mid-quotes is higher for storable than for non-storable commodities. However, low coefficients of variation for all commodities indicate that prices exhibit little volatility during the observation period.

3.3. Results

Table 2 shows the estimated baseline intensities μ, the derived average intensities γ, and exogeneity ratios R. All figures for μ, γ, and R are mean values over 528 intervals of 10 min. As a robustness check, we conducted additional calculations with a different time interval length (30 min) for corn and lean hog (see Tables A1 and A2, Figure A1 in the Appendix A). The qualitative findings are similar and, thus, we focus on the discussion of the results of the 10-min intervals in what follows.

Table 2. Estimated baseline intensities, average intensities, and exogeneity ratios.

Contract	**Front**		**Back**		**Front**		**Back**	
Transaction	**Buy**	**Sell**	**Buy**	**Sell**	**Buy**	**Sell**	**Buy**	**Sell**
Commodity	Corn				Wheat			
Baseline intensity	0.194	0.193	0.061	0.062	0.15	0.149	0.046	0.048
Average intensity	0.327	0.337	0.097	0.101	0.25	0.241	0.071	0.072
Exogeneity ratio	0.636	0.629	0.663	0.67	0.654	0.657	0.704	0.726
Commodity	Live cattle				Lean Hog			
Baseline intensity	0.077	0.078	0.083	0.081	0.058	0.063	0.061	0.059
Average intensity	0.119	0.117	0.121	0.117	0.085	0.09	0.085	0.08
Exogeneity ratio	0.701	0.699	0.714	0.733	0.743	0.741	0.76	0.772
Commodity	Corn				Wheat			
Baseline intensity	0.194	0.193	0.061	0.062	0.150	0.149	0.046	0.048
Average intensity	0.327	0.337	0.097	0.101	0.250	0.241	0.071	0.072
Exogeneity ratio	0.636	0.629	0.663	0.670	0.654	0.657	0.704	0.726
Commodity	Live cattle				Lean Hog			
Baseline intensity	0.077	0.078	0.083	0.081	0.058	0.063	0.061	0.059
Average intensity	0.119	0.117	0.121	0.117	0.085	0.090	0.085	0.080
Exogeneity ratio	0.701	0.699	0.714	0.733	0.743	0.741	0.760	0.772

The baseline intensity μ is by far the highest for the front contract of corn. This means that in absolute terms, the number of transactions that is triggered by external sources is highest for the front contract of corn. In addition, μ is of similar size for buyer- and seller-initiated transactions in a contract of a certain maturity for all commodities. It is striking that μ is noticeably larger in the front contract than in the back contract for corn and wheat. In contrast, μ is of similar size in the front contract and back contract for live cattle and lean hog. This suggests that price discovery takes place in the front contract for storable commodities, but not for non-storable commodities. These estimation results for the baseline intensity μ are therefore in line with Working (1949) and Gray and Rutledge (1971). Compared to the baseline intensity, the derived average intensity γ is higher for all examined contracts. Similar to the baseline intensity, γ is considerably larger in the front contract than in the back contract for corn and wheat. In contrast, γ is of similar size in the front and back contract for live cattle and lean hog. The derived exogeneity ratio R is higher for non-storable than for storable commodities. About 75% (65%) of all observed transactions in the lean hog (corn) futures are triggered by external sources. The results also find that R is of similar size for buyer- and seller-initiated transactions in a commodity futures contract of a certain maturity. Moreover, R is slightly higher in the back contract than in the front contract for all commodities. Apparently, the derived exogeneity ratio is considerably higher for the examined agricultural futures contracts than for the DAX and BUND futures contracts examined by Bacry et al. (2016). Moreover, the derived exogeneity ratios are higher than the corresponding figures in Filimonov et al. (2014).

Figure 1 presents the estimated matrices of kernel norms $\|\phi\|_1$. Each kernel norm describes the total impact that transactions of a certain contract type have on transactions of the same or on other contracts. Figure 1 has to be interpreted column-wise. A darker background color of a kernel norm

illustrates a larger impact than a lighter color. A kernel norm $\|\phi_{ii}\|_1$ on the diagonals of the matrices describes the impact that transactions of a certain type have on transactions of the same type. A kernel norm $\|\phi_{ij}\|_1$ on the off-diagonals of the matrices describes the impact that transactions of a certain type have on transactions of a different type. In general, the kernel norm values are higher for storable than for non-storable commodities. According to the population representation of the Hawkes process, each buyer-initiated (seller-initiated) transaction directly triggers 0.3102 buyer-initiated transactions (0.3147 seller-initiated) on average in the front contract for corn. The respective values for other commodities are slightly smaller. Apparently, the kernel norm values on the diagonals of the matrix are considerably higher compared to those on the off-diagonals for all commodities. This indicates that a substantial part of the observed transactions is endogenously driven and points to the presence of market reflexivity for all commodities. In addition, the kernel norm values on the diagonals of the matrix are higher in the front contract than in the back contract for corn and wheat. In contrast, the kernel norm values on the diagonals are of similar size in the front and back contract for live cattle and lean hog. As expected, the estimation results for the matrices of kernel norms $\|\phi\|_1$ show that differences between front and back contracts are less pronounced for non-storable than for storable commodities.

Corn		Front		Back	
		Buy	Sell	Buy	Sell
Front	Buy	0.3102	0.0315	0.0128	0.0100
	Sell	0.0284	0.3147	0.0094	0.0138
Back	Buy	0.0531	0.0375	0.2434	0.0252
	Sell	0.0363	0.0596	0.0186	0.2301

Wheat		Front		Back	
		Buy	Sell	Buy	Sell
Front	Buy	0.2868	0.0288	0.0152	0.0106
	Sell	0.0344	0.2828	0.0091	0.0136
Back	Buy	0.0570	0.0389	0.1946	0.0206
	Sell	0.0421	0.0634	0.0228	0.1787

Live cattle		Front		Back	
		Buy	Sell	Buy	Sell
Front	Buy	0.2132	0.0170	0.0488	0.0184
	Sell	0.0197	0.2490	0.0136	0.0236
Back	Buy	0.0675	0.0181	0.2046	0.0169
	Sell	0.0186	0.0269	0.0165	0.2137

Lean hog		Front		Back	
		Buy	Sell	Buy	Sell
Front	Buy	0.1925	0.0179	0.0377	0.0172
	Sell	0.0163	0.2012	0.0191	0.0272
Back	Buy	0.0359	0.0188	0.1718	0.0199
	Sell	0.0161	0.0405	0.0156	0.1611

Figure 1. Estimated matrices of kernel norms.

The kernel norms on the off-diagonals show that in the cases of corn and wheat, the impact of front contracts on back contracts is larger than vice versa. This relationship, however, is not prevalent for live cattle and lean hog. Thus, our results are in line with Hu et al. (2017), who show that nearby futures contracts dominate deferred futures contracts in price discovery for storable commodities, but not for non-storable commodities. No differences can be identified between buyer- and seller-initiated transactions.

Table 3 contains the results of the residual analyses of the estimated Hawkes processes. For more than about 80% of the 10-min intervals, the Kolmogorov–Smirnov test does not reject the null hypothesis that the distribution of the residuals is homogeneous Poisson at the 5% significance level for the considered commodities. Except for the front contracts of corn and wheat, for more than approximately 90% of the 10-min intervals, the Ljung–Box test does not reject the null hypothesis that the residuals are independently distributed at the 5% significance level. We can therefore conclude that the estimated Hawkes process with the chosen parameterization of the kernel function is a good approximation of the observed point process.

Table 3. Residual analyses.

Contract	**Front**		**Back**		**Front**		**Back**	
Transaction	**Buy**	**Sell**	**Buy**	**Sell**	**Buy**	**Sell**	**Buy**	**Sell**
Commodity	Corn				Wheat			
Kolmogorov–Smirnov	0.84	0.84	0.88	0.89	0.87	0.83	0.89	0.89
Ljung–Box	0.64	0.67	0.94	0.92	0.78	0.80	0.94	0.94
Commodity	Live cattle				Lean Hog			
Kolmogorov–Smirnov	0.91	0.87	0.91	0.88	0.93	0.93	0.91	0.90
Ljung–Box	0.92	0.91	0.91	0.91	0.94	0.93	0.93	0.93

Figure 2 displays the evolution of the average intensity γ over the whole observation period. The figure is based on daily mean values of the average intensity. In general, the evolution of γ for the front contract is similar to the evolution of γ for the back contract for all commodities. In particular, γ is higher for the front contract than for the back contract throughout the whole observation period for corn and wheat. In contrast, for live cattle and lean hog, γ is higher for the front contract than for the back contract in the first half of the observation period only. In addition, the evolution of the average intensity of buyer-initiated transactions is similar to the evolution of the average intensity of seller-initiated transactions in a contract of a certain maturity for all commodities.

In general, the average intensity shows a relatively constant progression for all commodities; however, γ increases around certain days where public information became available. For instance, the average intensity increases for all commodities on 9 March 2016 when the USDA released its monthly WASDE report (USDA 2016b). Furthermore, γ increases for live cattle on 22 March 2016 following a USDA cattle on feed report (USDA 2016c). Most notably, γ increases considerably towards the end of the observation period for corn and wheat on 31 March 2016. On this day (11:00 a.m.), the USDA reported an unexpected increase in the corn acreage (USDA 2016a). On the same day, the USDA published its quarterly grain stocks reports (USDA 2016d). This may explain why the increase in average intensities is rather pronounced at that time. Overall, Figure 2 documents that the publication of USDA reports affects not only volatility and trading volume, but also the intensity of trading activity.

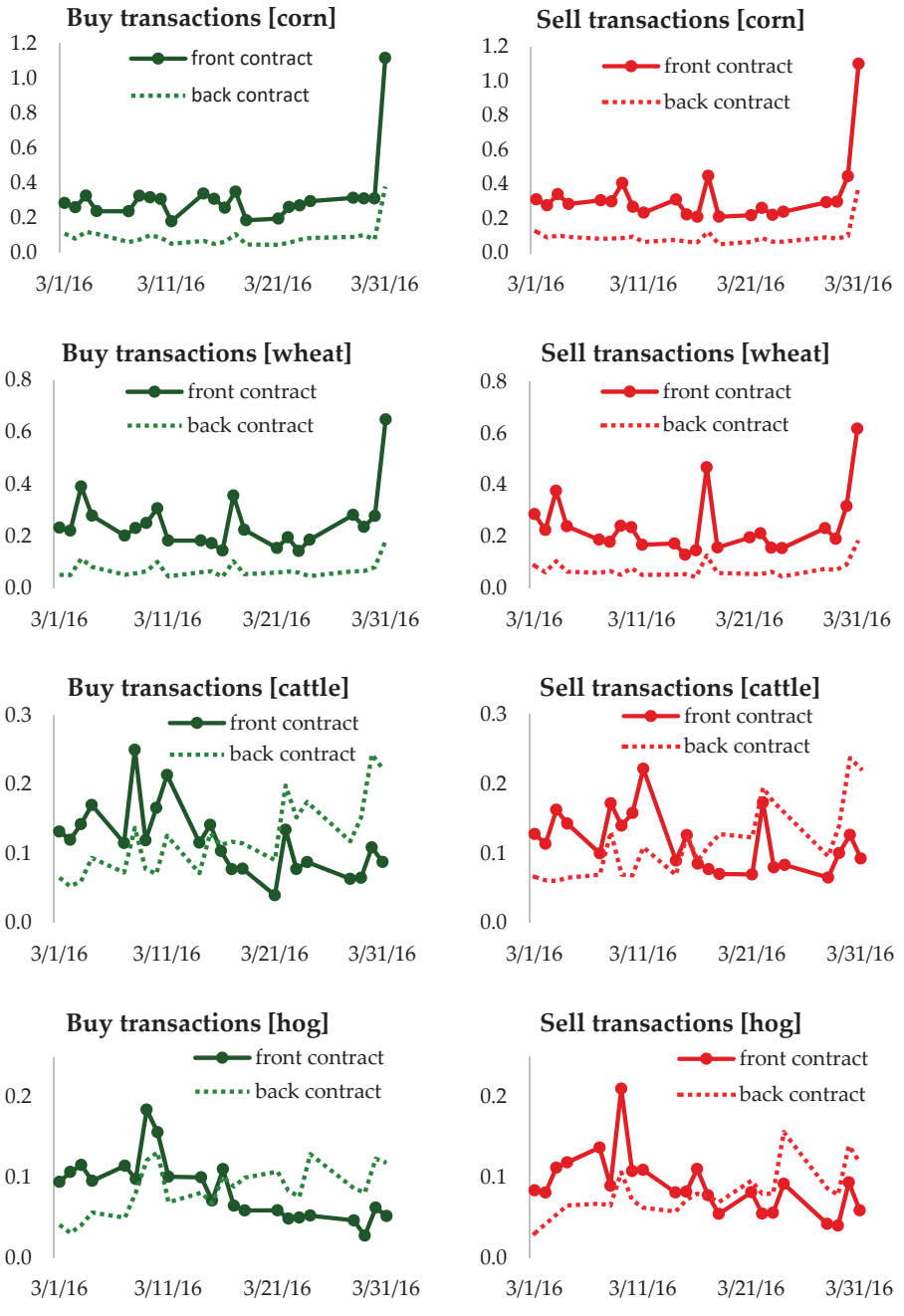

Figure 2. Evolution of average intensities (y-axis) in both buy and sell transactions for corn, wheat, live cattle, and lean hog in March 2016.

Figure 3 depicts the evolution of the baseline intensity μ on 31 March 2016 for corn. The figure is based on 24 intervals of 10 min. The baseline intensity μ increases considerably at the time of

the publication of the USDA report for transactions in both the front and back contract. Moreover, the evolution of μ for seller-initiated transactions is similar to the evolution of μ for buyer-initiated transactions at the time of the publication of the USDA report for the front contract. In contrast, for the back contract, the evolution of μ for seller-initiated transactions differs from the evolution of μ for buyer-initiated transactions at the time of the publication of the USDA report.

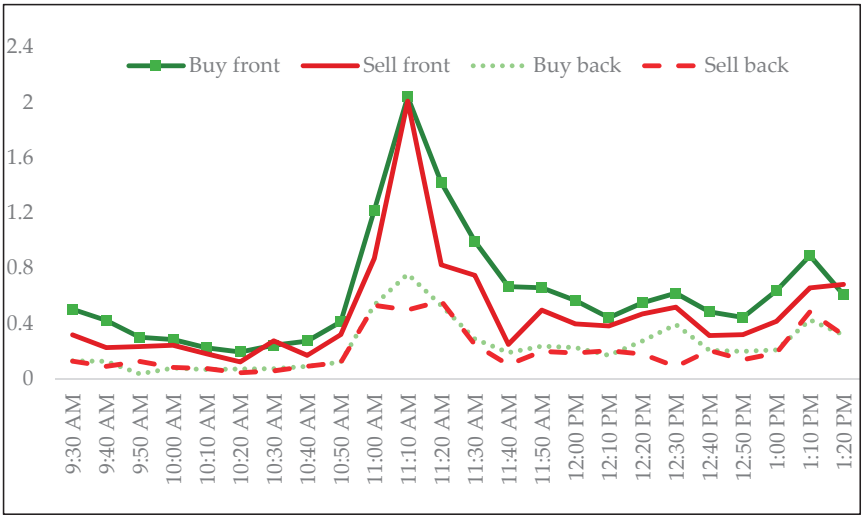

Figure 3. Evolution of the baseline intensity (y-axis) for corn on 31 March 2016.

The evolution of the baseline intensity for corn on 31 March 2016 suggests that new information is quickly incorporated into market prices through trading activity. Moreover, it is becoming clearer that new information does not only affect nearby futures contracts, but also affects deferred futures contracts.

Figure 4 presents the estimated matrix of kernel norms $\|\phi\|_1$ for corn on 31 March 2016. The figures are mean values over 24 intervals of 10 min.

Corn (March 31, 2016)		Front		Back	
		Buy	Sell	Buy	Sell
Front	Buy	0.3770	0.0290	0.0170	0.0130
	Sell	0.0360	0.4380	0.0120	0.0290
Back	Buy	0.0370	0.0420	0.2660	0.0260
	Sell	0.0120	0.1090	0.0200	0.2990

Figure 4. Estimated matrix of kernel norms for corn on 31 March 2016.

Compared to the whole observation period, the kernel norm values $\|\phi_{ii}\|_1$ on the diagonal of the matrix are considerably higher for corn on 31 March 2016. This indicates an increase in market

reflexivity on the publication day of the USDA report. Moreover, compared to the whole observation period, the kernel norm values $\|\phi_{ij}\|_1$ on the off-diagonal of the matrix are higher for the back contract for corn on 31 March 2016. This indicates an increase in the impact that transactions in the back contract have on transactions in both the front and back contract on the publication day of the USDA report.

To gain an overall picture of the price formation process in agricultural futures contracts with different maturities, Figure 5 illustrates the composition of the estimated intensity of the trading activity in both the front and back contract exemplarily for corn and live cattle. The figure is based on mean values of 528 intervals of 10 min. It shows the relative contribution of the estimated baseline intensity μ_i and the kernel norms $\|\phi_{ii}\|_1$ and $\|\phi_{ij}\|_1$ to the total intensity $\hat{\lambda}_i$.

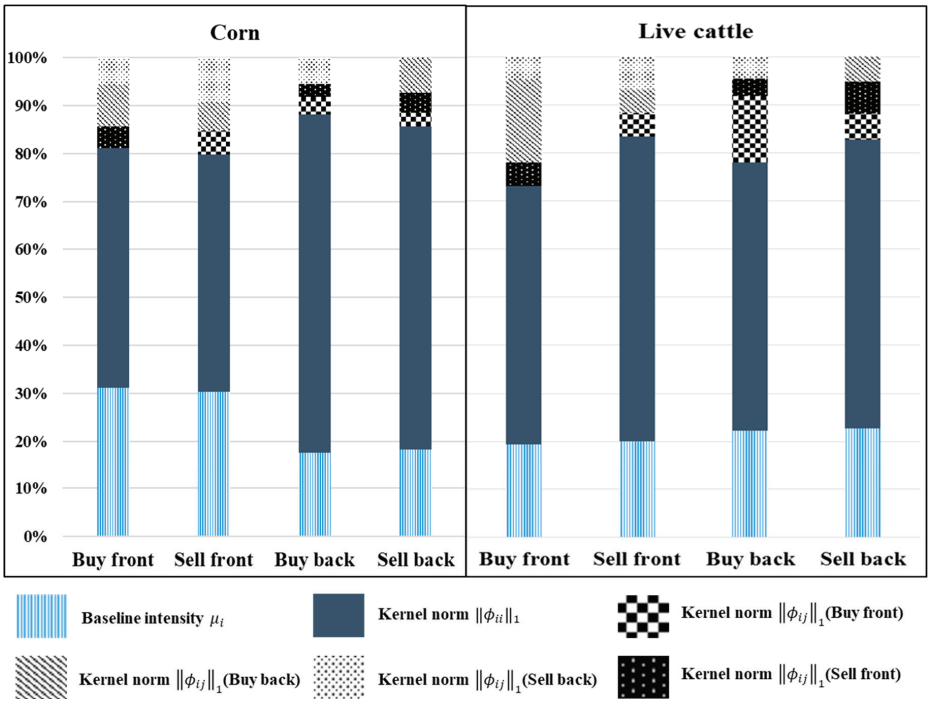

Figure 5. Composition of the estimated intensity for corn and live cattle.

The relative contribution of the baseline intensity μ_i to the total intensity $\hat{\lambda}_i$ is largest for the front contract of corn. It amounts to approximately 30%. This means that external sources, such as new information, account for approximately 30% of the total intensity of both buyer-initiated and seller-initiated transactions for the front contract of corn. Moreover, the relative contribution of μ_i is noticeably larger in the front contract than in the back contract for corn. In contrast, the relative contribution of μ_i is of similar size in the front and back contract for live cattle. Therefore, in line with Working Working (1949) and Gray and Rutledge (1971), the composition of the estimated intensity suggests that nearby futures contracts dominate deferred futures contracts in price discovery for storable commodities, but not for non-storable commodities.

Compared to the relative contribution of μ_i, the relative contribution of the kernel norms $\|\phi_{ii}\|_1$ to the total intensity is considerably larger. More specifically, the relative contribution of $\|\phi_{ii}\|_1$ to the total intensity is largest for the back contract of corn. It amounts to roughly 70%, which means that market reflexivity accounts for about 70% of the total intensity of both buyer-initiated and seller-initiated transactions for the back contract of corn. Moreover, the relative contribution of $\|\phi_{ii}\|_1$ is clearly larger

in the back contract than in the front contract for corn. In contrast, the relative contribution of $\|\phi_{ii}\|_1$ is of similar size in the front and back contract for live cattle.

As expected, the composition of the estimated intensity shows that differences between front and back contracts in the degree of market reflexivity are less pronounced for live cattle than for corn. Compared to the relative contribution of $\|\phi_{ii}\|_1$, the relative contribution of the kernel norms $\|\phi_{ij}\|_1$ to the total intensity is considerably smaller. More specifically, the relative contribution of $\|\phi_{ij}\|_1$ to the total intensity is higher for live cattle than for corn. It is shown that buyer-initiated transactions in the back contract account for almost 20% of the total intensity of buyer-initiated transactions in the front contract for live cattle. On the other hand, buyer-initiated transactions in the back contract account for approximately 10% of the total intensity of buyer-initiated transactions in the front contract for corn. Therefore, in line with Kendall (1982), the composition of the estimated intensity suggests that interdependencies of current and subsequent supply might link futures contracts of different maturities to non-storable commodities.

4. Conclusions

This paper is the first to examine price discovery in nearby and deferred agricultural commodities futures contracts while explicitly considering potential market reflexivity. For this purpose, we apply a four-dimensional Hawkes model with an exponential parametrization of the kernel functions to storable and non-storable agricultural commodities. We find market reflexivity for both storable and non-storable commodities. Reflexivity accounts for about 50 to 70% of the total trading activity, irrespective of whether transactions have been buyer- or seller-initiated. Storable commodities show a higher level of reflexivity than non-storable commodities and differences between nearby and deferred contracts are less pronounced for non-storable commodities than for storable ones. We conjecture that the degree of reflexivity is related to the trading intensity and the amount of automated trading. Endogeneity results from backward-looking trading strategies, which exploit information from previous trading activities. Most likely, this source of endogeneity is more prevalent in liquid markets than in thin markets. Storable commodities are more frequently traded compared with non-storable commodities, but this holds only for the front contract (c.f. Table 1). Moreover, grains show a higher share of automated trading than livestock contracts (e.g., Haynes and Roberts 2015; Couleau et al. 2019). It appears that these differences are reflected in the endogeneity of the price formation process.

What are the implications of these findings for the price discovery process in agricultural commodity futures? The presence of market reflexivity seems to contradict the efficient market hypothesis, and Filimonov et al. (2014) argue that reflexivity is likely to result in a less efficient price discovery process. Though our analysis does not allow an evaluation of the presence of reflexivity, we can at least compare our results with previous empirical findings on price discovery in agricultural commodity futures markets and screen them for irregularities. Regarding the relation between nearby and deferred futures contracts, our results are in line with Mallory et al. (2015), who find that new information to the market is immediately transmitted across all contract maturities. Moreover, we can replicate the finding of Hu et al. (2017) that nearby contracts are dominant in price discovery for storable commodities, but not for non-storable commodities. Finally, we observe an increased baseline intensity at the time of a USDA publication, suggesting that external information is quickly incorporated into market prices through trading activity despite the presence of market reflexivity. From these findings, we conclude that the co-existence of exogenous and endogenous price dynamics does not change qualitative characteristics of the price discovery process that have been observed earlier without the consideration of market reflexivity.

Some aspects could be incorporated in further empirical analyses to obtain a clearer picture about price discovery in agricultural commodity futures in the presence of market reflexivity. The empirical basis could be broadened by including additional commodities. Moreover, price discovery and market reflexivity should be examined over a longer observation period covering, for example, markets in normal backwardation and in contango. From a methodological point of view, the Hawkes model

can be extended and amended in several ways. Covariates such as order imbalances between buyer- and seller-initiated transactions can be included into the intensity function. Other parameterizations of the kernel function such as power-law parameterizations or other estimation methods such as non-parametric estimation techniques can be applied to check the robustness of the results. Finally, methods allowing the assessment of the direct impact of market reflexivity on the price formation process need to be explored.

Author Contributions: Conceptualization, S.V., G.F. and M.O.; data curation, S.V. and G.F.; formal analysis, S.V.; methodology, S.V. and G.F.; software, S.V.; supervision, M.O.; validation, S.V. and G.F.; visualization, S.V. and G.F.; writing—original draft, S.V., G.F. and M.O.; writing—review and editing, S.V., G.F. and M.O. All authors have read and agreed to the published version of the manuscript.

Funding: This research received no external funding.

Acknowledgments: We thank three anonymous reviewers for helpful comments and suggestions.

Conflicts of Interest: The authors declare no conflict of interest.

Appendix A

Table A1. Estimated baseline intensities, average intensities, and exogeneity ratios (corn, lean hog) for a 30-min interval.

Contract	**Front**		**Back**		**Front**		**Back**	
Transaction	**Buy**	**Sell**	**Buy**	**Sell**	**Buy**	**Sell**	**Buy**	**Sell**
Commodity	Corn (30-min interval)				Lean Hog (30-min interval)			
Baseline intensity	0.164	0.163	0.054	0.056	0.052	0.058	0.054	0.052
Average intensity	0.303	0.312	0.089	0.093	0.087	0.091	0.087	0.082
Exogeneity ratio	0.567	0.565	0.643	0.638	0.669	0.681	0.683	0.697

Table A2. Residual analyses (corn, lean hog) for a 30-min interval.

Contract	**Front**		**Back**		**Front**		**Back**	
Transaction	**Buy**	**Sell**	**Buy**	**Sell**	**Buy**	**Sell**	**Buy**	**Sell**
Commodity	Corn (30-min interval)				Lean Hog (30-min interval)			
Kolmogorov–Smirnov	0.460	0.465	0.758	0.757	0.830	0.800	0.794	0.790
Ljung–Box	0.373	0.374	0.791	0.770	0.807	0.785	0.829	0.860

Corn 30 min		Front		Back	
		Buy	Sell	Buy	Sell
Front	Buy	0.3696	0.0403	0.0103	0.0079
	Sell	0.0369	0.3727	0.0082	0.0126
Back	Buy	0.0585	0.0434	0.2766	0.0275
	Sell	0.0315	0.0570	0.0152	0.2747

Lean Hog 30 min		Front		Back	
		Buy	Sell	Buy	Sell
Front	Buy	0.2294	0.0210	0.0520	0.0274
	Sell	0.0188	0.2331	0.0241	0.0486
Back	Buy	0.0552	0.0287	0.2183	0.0216
	Sell	0.0252	0.0488	0.0247	0.1951

Figure A1. Estimated matrices of kernel norms (corn, lean hogs) for a 30-min interval.

References

Bacry, Emmanuel, Martin Bompaire, Stéphane Gaıffas, and Soren Poulsen. 2017. Tick: A Python library for statistical learning, with a particular emphasis on time-dependent modeling. *arXiv*, 1707.03003.

Bacry, Emmanuel, Thibault Jaisson, and Jean–François Muzy. 2016. Estimation of slowly decreasing Hawkes kernels: Aplication to high-frequency order book dynamics. *Quantitative Finance* 16: 1179–201. [CrossRef]

Bauwens, Luc, and Nikolaus Hautsch. 2007. Modelling Financial High Frequency Data Using Point Processes. SFB 649 Discussion Paper 2007-066. Available online: http://sfb649.wiwi.hu-berlin.de/papers/pdf/SFB649DP2007-066.pdf (accessed on 29 October 2018).

Bicchetti, David, and Nicolas Maystre. 2013. The synchronized and long-lasting structural change on commodity markets: Evidence from high frequency data. *Algorithmic Finance* 2: 233–39. [CrossRef]

Bowsher, Clive G. 2007. Modelling Security Markets in Continuous Time: Intensity-based, Multivariate Point Process Models. *Journal of Econometrics* 141: 876–912. [CrossRef]

Couleau, Anabelle, Teresa Serra, and Philip Garcia. 2019. Microstructure noise and realized variance in the live cattle futures market. *American Journal of Agricultural Economics* 101: 563–78. [CrossRef]

Brennan, M. J. 1958. The supply of storage. *American Economic Review* 48: 50–72.

Diebold, Francis X., and Canlin Li. 2006. Forecasting the term structure of government bond yields. *Journal of Econometrics* 130: 337–64. [CrossRef]

Easley, David, and Maureen O'Hara. 1992. Time and the process of security price adjustment. *Journal of Finance* 47: 577–604. [CrossRef]

Engle, Robert F., and Jeffrey R. Russell. 1998. Autoregressive conditional duration: A new model for irregularly spaced transaction data. *Econometrica* 66: 1127–62. [CrossRef]

Fama, Eugene F. 1970. Efficient capital markets: A review of theory and empirical work. *The Journal of Finance* 25: 383–417. [CrossRef]

Fama, Eugene F., and Kenneth R. French. 1987. Commodity Futures Prices: Some Evidence on Forecast Power, Premiums, and the Theory of Storage. *The Journal of Business* 60: 55–73. [CrossRef]

Filimonov, Vladimir, and Didier Sornette. 2012. Quantifying reflexivity in financial markets: Toward a prediction of flash crashes. *Physical Review E* 85: 056108. [CrossRef]

Filimonov, Vladimir, David Bicchetti, Nicolas Maystre, and Didier Sornette. 2014. Quantification of the high level of endogeneity and of structural regime shifts in commodity markets. *Journal of International Money and Finance* 42: 174–92. [CrossRef]

Geman, Helyette, and Vu-Nhat Nguyen. 2005. Soybean Inventory and Forward Curve Dynamics. *Management Science* 51: 1076–91. [CrossRef]

Gibson, Rajna, and Eduardo S. Schwartz. 1990. Stochastic Convenience Yield and the Pricing of Oil Contingent Claims. *Journal of Finance* 45: 959–76. [CrossRef]

Glosten, Lawrence R., and Paul R. Milgrom. 1985. Bid, Ask, and Transaction Prices in a Specialist Market with Heterogeneously Informed Agents. *Journal of Financial Economics* 14: 71–100. [CrossRef]

Gray, Roger W., and David J. S. Rutledge. 1971. The economics of commodity futures markets: A survey. *Review of Marketing and Agricultural Economics* 39: 57–108.

Gurgul, Henryk, and Robert Syrek. 2017. Trading volume and volatility patterns across selected Central European stock markets from microstructural perspective. *Managerial Economics* 18: 87. [CrossRef]

Hardiman, Stephen J., Nicolas Bercot, and Jean-Philippe Bouchard. 2013. Critical reflexivity in financial markets: A Hawkes process analysis. *The European Physical Journal B* 86: 442. [CrossRef]

Harris, Frederick H. deB., Thomas H. McInish, and Robert A. Wood. 2002. Security price adjustment across exchanges: An investigation of common factor components for Dow stocks. *Journal of Financial Markets* 5: 277–308. [CrossRef]

Hasbrouck, Joel. 1995. One Security, Many Markets: Determining the Contributions to Price Discovery. *The Journal of Finance* 50: 1175–95. [CrossRef]

Hautsch, Nikolaus. 2004. *Modelling Irregularly Spaced Financial Data*. Berlin: Springer.

Hawkes, Alan G. 1971. Point spectra of some mutually-exciting point processes. *Journal of the Royal Statistical Society* 33: 438–43. [CrossRef]

Hawkes, Alan G., and David Oakes. 1974. A cluster process representation of a self-exciting process. *Journal of Applied Probability* 11: 493–503. [CrossRef]

Haynes, Richard, and John S. Roberts. 2015. Automated Trading in Futures Markets. CFTC White Paper. Available online: https://www.cftc.gov/sites/default/files/idc/groups/public/@economicanalysis/documents/file/oce_automatedtrading.pdf (accessed on 25 October 2019).

Hu, Zhepeng, Mindy Mallory, Teresa Serra, and Philip Garcia. 2017. Measuring Price Discovery between Nearby and Deferred Contracts in Storable and Non-Storable Commodity Futures Markets. *arXiv*, 1711.03506.

Karstanje, Dennis, Michel van der Wel, and Dick J. C. van Dijk. 2017. Common Factors in Commodity Futures Curves. *SSRN Working Paper*. [CrossRef]

Kendall, David Laurence. 1982. Intertemporal Price Relationships in Noninventory Futures Markets. Ph.D. thesis, North Carolina State University, Raleigh, NC, USA.

Kyle, Albert S., and Anna Obizhaev. 2019. Large Bets and Stock Market Crashes. Working Paper. Available online: https://ssrn.com/abstract=2023776 (accessed on 25 October 2019).

Large, Jeremy. 2007. Measuring the Resiliency of an Electronic Limit Order Book. *Journal of Financial Markets* 10: 1–25. [CrossRef]

Lee, Charles M. C., and Mark J. Ready. 1991. Inferring trade direction from intraday data. *The Journal of Finance* 46: 733–46. [CrossRef]

Mallory, Mindy, Philip Garcia, and Teresa Serra. 2015. Nearby and Deferred Quotes: What They Tell Us about Linkages and Adjustments to Information. Proceedings of the NCCC-134 Conference on Applied Commodity Price Analysis, Forecasting, and Market Risk Management. Available online: http://www.farmdoc.illinois.edu/nccc134/conf_2015/pdf/Mallory_Garcia_Serra_NCCC_134_2015.pdf (accessed on 25 October 2019).

Meyer, Paul-André. 1971. Démonstration simplifiée d'un théorème Knight. *Lecture Notes in Mathematics* 191: 191–95.

Nelson, Charles R., and Andrew F. Siegel. 1987. Parsimonious modeling of yield curve. *Journal of Business* 60: 473–89. [CrossRef]

Ogata, Yosihiko. 1989. Statistical Models for Earthquake Occurrences and Residual Analysis for Point Processes. *Journal of the American Statistical Association* 83: 9–27. [CrossRef]

Ogata, Yosihiko. 1998. Space-time point-process models for earthquake occurrences. *Annals of the Institute of Statistical Mathematics* 50: 379–402. [CrossRef]

Russell, Jeffrey R. 1999. Econometric Modeling of Multivariate Irregularly-Spaced High-Frequency Data. Working Paper, University of Chicago. Available online: http://citeseerx.ist.psu.edu/viewdoc/download?doi=10.1.1.202.486&rep=rep1&type=pdf (accessed on 5 November 2018).

Schwartz, Eduardo S. 1997. The Stochastic Behavior of Commodity Prices: Implications for Valuation and Hedging. *The Journal of Finance* 52: 923–73. [CrossRef]

Sorensen, Carsten. 2002. Modeling seasonality in agricultural commodity futures. *The Journal of Futures Markets* 22: 393–426. [CrossRef]

Soros, George. 1987. *The Alchemy of Finance: Reading the Mind of the Market*. New York: John Wiley & Sons.

Tang, Ke, and Wei Xiong. 2012. Index investment and the financialization of commodities. *Financial Analysts Journal* 68: 54–74. [CrossRef]

USDA. 2016a. Prospective Plantings (March 2016). United States Department of Agriculture, National Agricultural Statistics Service. Available online: https://downloads.usda.library.cornell.edu/usda-esmis/files/x633f100h/9c67wq58w/rx913s37m/ProsPlan-03-31-2016.pdf (accessed on 25 October 2019).

USDA. 2016b. United States Department of Agriculture, National Agricultural Statistics Service. Available online: https://downloads.usda.library.cornell.edu/usda-esmis/files/3t945q76s/zs25x8827/d504rk71k/wasde-03-09-2016.pdf (accessed on 25 October 2019).

USDA. 2016c. United States Department of Agriculture, National Agricultural Statistics Service. Available online: https://downloads.usda.library.cornell.edu/usda-esmis/files/m326m174z/8623j006q/q524jq148/CattOnFe-03-18-2016.pdf (accessed on 25 October 2019).

USDA. 2016d. United States Department of Agriculture, National Agricultural Statistics Service. Available online: https://downloads.usda.library.cornell.edu/usda-esmis/files/xg94hp534/08612q46m/fj236409h/GraiStoc-03-31-2016.pdf (accessed on 25 October 2019).

Volkenand, Steffen, Günther Filler, Marlene Kionka, and Martin Odening. 2019. Duration dependence among agricultural futures with different maturities. *Applied Economics Letters*. [CrossRef]

Wang, Xiaoyang, Philip Garcia, and Scott H. Irwin. 2016. Are agricultural futures getting noisier? The impact of high frequency quoting in the corn market. Working paper, University of Illinois, Urbana-Champaign. Available online: https://legacy.farmdoc.illinois.edu/irwin/research/Wang_Garcia_Irwin_Oct%202016.pdf (accessed on 25 October 2019).

Working, Hoolbrock. 1949. The theory of price of storage. *The American Economic Review* 39: 1254–62.

risks

MDPI

Article

Risk and Policy Uncertainty on Stock–Bond Return Correlations: Evidence from the US Markets

Thomas C. Chiang

Department of Finance, LeBow College of Business, Drexel University, Philadelphia, PA 19104, USA; chiangtc@drexel.edu

Received: 4 May 2020; Accepted: 27 May 2020; Published: 1 June 2020

Abstract: This paper investigates dynamic correlations of stock–bond returns for different stock indices and bond maturities. Evidence in the US shows that stock–bond relations are time-varying and display a negative trend. The stock–bond correlations are negatively correlated with implied volatilities in stock and bond markets. Tests show that stock–bond relations are positively correlated with economic policy uncertainty, however, are negatively correlated with the monetary policy and fiscal policy uncertainties. Correlation coefficients between stock and bond returns are positively related to total policy uncertainty for returns of the Dow-Jones Industrial Average (DJIA) and the S&P 500 Value stock index (VALUE), but negatively correlated with returns of S&P500 (Total market), the NASDAQ Composite Index (NASDAQ), and the RUSSELL 2000 (RUSSELL).

Keywords: stock–bond correlation; VIX; economic policy uncertainty; monetary policy uncertainty; fiscal policy uncertainty

JEL Classification: C12; C13; G10; G11

1. Introduction

The investigation on correlations of stock and bond returns has long been a key concern of portfolio managers and financial market strategists (Connolly et al. 2005; Panchenko and Wu 2009; Baur and Lucey 2009; Li et al. 2019, among others). This is because the derived parametric relations could provide useful guidance in portfolio selection, dynamic asset allocation, and risk management. For most of this time, two questions have dominated the literature. First, are stock returns and bond returns positively or negatively correlated? Second, what are the factors that cause correlations to vary over time? The theoretical claim of the first issue contends that both required rates of return for stock and bond yields are viewed as part of a discount factor to calculate the future cash flows of investments. This argument is based on the valuation model that has been adopted and used in the "Fed model" (Kwan 1996; Yardeni 1997). It is observed that any economic shocks, such as income, inflation rate, policy innovation, or external shock that disturb an existing equilibrium, will cause investors to reallocate their funds between assets with lower returns to ones with higher returns. An efficient arbitrage will eliminate the return differentials and establish return parity conditions after executing full adjustment (Tobin 1969). This view focuses on economic fundamentals analyzed over a long-run perspective.

However, evidence of the decoupling phenomenon observed by Gulko (2002) finds a negative sign for the correlation that obviously occurred in the crisis period; this finding reflects a short run "flight-to-quality" process (Baur and Lucey 2009). To advance the study, Connolly et al. (2005) examine the US market and discover that the implied stock volatility (VIX) spikes during periods of market turmoil leads to decline in stock prices (Whaley 2009). It is argued that the VIX variable has a power in predicting stock returns (Connolly et al. 2005) and find that VIX displays a negative effect on the

stock–bond correlation. Further study by Chiang et al. (2015) documents that both implied volatility of stock and conditional volatility of bond returns have significantly negative effects on variations in stock–bond returns.

To distinguish their work from previous models, some researchers identify economic policy uncertainty (EPU) as a key factor that dictates the time-varying correlations between stock and bond returns (Antonakakis et al. 2013; Jones and Olson 2013; Li et al. 2015). Antonakakis et al. (2013) show that the dynamic correlation between EPU and S&P500 returns is consistently negative over time, with exception of a financial crisis period. Li et al. (2015) report that innovations in EPU have a negative and asymmetrical impact on subsequent stock–bond correlations, since a rise in EPU will likely prompt risk averse investors to sell off risky stocks and purchase lower risk bonds, leading to a negative correlation.[1]

Considering the above evidence of risk/uncertainty on stock returns, this paper attempts to contribute to the study of the effects of policy uncertainty on stock–bond relations. This study differs from existing models in the following ways. First, this study focus on broad information in developing measures of financial risks such as VIX, Merrill Lynch Option Volatility Estimate (MOVE) and uncertainty (EMU) to explain the time-varying correlations between stock and bond returns. Second, in addition to EPU, this study investigates the impact of categorical policy uncertainties, including both fiscal policy uncertainty (FPU) and monetary policy uncertainty (MPU). The testing result suggests that the FPU and MPU give rise to different effects vis-à-vis that of EPU. Third, instead of testing a correlation coefficient derived from a single measure of aggregate stock returns that covaries with a specific bond yield, this study conducts tests on the return correlations involving different measures of aggregate stock returns and a spectrum of bond yields for different maturities. Thus, the estimated results will provide broad coverage of dynamic correlation behavior. Fourth, the net effect of various policy uncertainty is summarized in total policy uncertainty (TPU). Evidence demonstrates that the results are mixed due to the different impact, which the income and substitution effects have on stock–bond return correlations.

The remainder of the paper is structured as follows. Section 2 describes a dynamic correlation model and derives the time-varying correlations. Section 3 provides rationales for using risk and uncertainty variables to explain the time-varying behavior of stock–bond return correlation. Section 4 describes the sample data. Section 5 reports the estimates developed from the use of policy uncertainty to explain the dynamic stock–bond correlations. Section 6 provides robustness tests. Section 7 concludes the paper.

2. The Relationship between Stock Returns and Bond Returns

As mentioned earlier, stock and bond returns are positively correlated since both stock and bond markets commonly react to economic news, such as changes in inflation rate, economic growth, the real interest rate, and business cycle, in similar ways. When investors perceive that economic prospects are good, demand for bonds increase, as does demand for stocks, leading to a positive correlation. Experience from the late 1990s suggests that an upward shift in the wealth effect encourages investors to hold both types of assets simultaneously. Campbell and Ammer (1993), Kwan (1996), and d'Addona and Kind (2006) document this phenomenon.

Historical experience also reveals a negative correlation between stock–bond returns, which is especially noticeably in the stock market during a downturn period or a financial crisis. When the stock market plummets, risk averse investors may move funds from the stock market to safer assets and increase the demand for bond market, forming a "flight-to-quality" phenomenon (Baur and Lucey 2009; Hakkio and Keeton 2009). On the contrary, when the economy recovers and stock prices start to rally, investors become less risk averse and opt to switch back to stock market, leading to a "flight-from-quality"

[1] Li et al. (2015) argue that when EPU declines, a flight from quality could also occur, resulting in a reduction in the correlations. However, the reduction in EPU can signify an improvement in the market environment, which would raise investors' demand for both stocks and bonds, thereby pushing up their correlations. This could produce an asymmetric effect.

phenomenon. Thus, the correlation between stock and bond returns displays a negative relation. Evidence by Gulko (2002), Connolly et al. (2005), Baur and Lucey (2009), and Chiang et al. (2015) support this hypothesis.

Despite their contributions, which use VIX as a measure to explain the time-varying correlation of stock–bond returns, their work appears to inadequately capture all the necessary information associated with uncertainty. For instance, President Trump revealed in the first week of October that high-level trade negotiations between the US and China had concluded in a "very substantial phase one deal" and that phase two would start almost immediately after phase one was signed. This statement, a sure sign of reduced uncertainty, would be expected to improve investors' sentiment, and indeed, Wall Street stocks closed higher on 11 October 2019 as the S&P 500 gained 32.14 points (or 1.09%), DJIA moved ahead 319.92 points (or 1.21%) and Nasdaq 106.26 advanced points (1.34%). This episode motivates this study to investigate the role of economic policy uncertainty on asset prices. In addition, the impacts of monetary policy uncertainty (MPU) and fiscal policy uncertainty (FPU) are also included to the test equation as a way of differentiating the impact of dynamic correlation behavior of stock–bond returns.

It is generally recognized that a sudden rise in EPU is likely to impede the smoothness of operations in economic activities and hence cause income uncertainty, which tamps down liquidity (Brunnermeier and Pedersen 2009) and leads to a decline in demand for assets (Bloom 2009, 2014; Chiang 2019). This phenomenon may be called the income uncertainty effect. Conversely, as EPU lessens, investors feel less uncertain about the future and more encouraged to increase their demand for assets, driving a positive correlation between stock and bond returns (Hong et al. 2014).

On the other hand, the substitution effect describes a phenomenon in which stock and bond returns move in opposite directions as uncertainty about economic activity changes in the market. This occurs as uncertainty heightens; investors then sell off their riskier assets (stock) and move their funds into safer assets (bond). This shift results in a negative relation between stock and bond returns. Further, as uncertainty declines, investors then switch from lower return assets (bond) to higher return assets (stocks), causing a negative relation between stock and bond returns (Li et al. 2015). Thus, the substitution effect tends to produce a negative relation between stock and bond returns. In fact, the concept of income effect is essentially derived from Tobin (1969) and then applied by Barsky (1989), Hong et al. (2014), and Li et al. (2015) to analyze the impact of economic uncertainty, triggered by economic policy uncertainty, on asset returns. The analysis can be extended to examine the impacts of monetary policy uncertainty (MPU) and fiscal policy uncertainty (FPU). As stated above, the impacts of MPU and FPU on stock return and bond return could also be attributed to the income effect and substitution effect; the ultimate impact on the returns of these two asset classes depends on the relative influence of these two forces.

3. A Dynamic Conditional Correlation Model

To derive the dynamic correlation series, the literature follows a seminal study by Engle (2002) who proposes a dynamic conditional correlation model, which is designed to estimate asset market returns (de Goeij and Marquering 2004; Chiang et al. 2007; Yu et al. 2010; Antonakakis et al. 2013; Jones and Olson 2013; Li et al. 2015; Ehtesham and Siddiqui 2019; Allard et al. 2019). This model is frequently used because of its ability to capture a vector of return correlations and describe the volatility clustering phenomenon. Moreover, it could alleviate the heteroscedasticity problem (Forbes and Rigobon 2002). In this study, $\{\boldsymbol{R_t}\}$ represents a bivariate return series, expressed as

$$\boldsymbol{R}_t = \mu_t + \boldsymbol{u_t} \tag{1}$$

where $\boldsymbol{R}_t = [R_{1,t} \;\; R_{2,t}]'$ is a 2×1 vector for stock market returns, μ_t is the mean value of asset 1 or 2, which has the conditional expectation of multivariate time series properties[2], $\boldsymbol{u_t}|F_{t-1} = [u_{1,t}u_{2,t}]' \sim$

[2] Some researchers use domestic macroeconomic factors, such as inflation rate, business cycle patterns, and policy stance, on the stock–bond correlation (Ilmanen 2003; Yang et al. 2009; Dimic et al. 2016; Pericoli 2018).

$N(0, H_t), F_{t-1}$ is the information set up for (and including) time $t-1$. In the context of this study, it is convenient to treat $R_{1,t}$ as the return on stocks and $R_{2,t}$ as the bond return for one of the bond instruments. In the multivariate DCC-GARCH structure, the conditional variance-covariance matrix H_t is assumed to be

$$H_t = D_t P_t D_t \tag{2}$$

where $D_t = diag\{H_t\}^{-1/2}$ is the 2×2 diagonal matrix of time-varying standard deviations from univariate models, and P_t is the time-varying conditional correlation matrix, which satisfies the following conditions:

$$P_t = diag\{Q_t\}^{-1/2} Q_t diag\{Q_t\}^{-1/2} \tag{3}$$

Now P_t in Equation (3) is a correlation matrix with ones on the diagonal and off-diagonal elements that have an absolute value less than one. Use of an asymmetric DCC model recognizes a shock dynamic adjustment of correlation for negative shock may be different than it is for a positive outcome (Cappiello et al. 2006; Engle 2009).[3] In this expression, it can be written as:

$$Q_t = \Omega + a\ \varepsilon_{t-1}\varepsilon'_{t-1} + \gamma \eta_{t-1}\eta'_{t-1} + \beta Q_{t-1} \tag{4}$$

where the Q_t is positive definite and $\eta_{t-1} = \min[\varepsilon_t, 0]$.

The product of $\eta_{i,t}\eta_{j,t}$ will be nonzero; only these two variables are negative. Thus, a positive value of γ indicates that correlations increase more in response to market falls than they do to market rises. The equation is written as

$$\hat{\Omega} = (1 - \alpha - \beta)\overline{Q} - \gamma \overline{N} \tag{5}$$

where $Q_t = \left(Q_{ij,t}\right)$ is the 2×2 time-varying covariance matrix of ε_t, $\overline{Q} = E[\varepsilon_t \varepsilon'_t]$ is the 2×2 unconditional variance matrix of ε_t (where $\varepsilon_{i,t} = u_{i,t} / \sqrt{h_{ii,t}}$, $i = 1$ and 2), $\overline{N} = E\left[\gamma \eta_t \eta'_t\right]$ is the 2×2 unconditional variance matrix of η_t; a, β, and γ are non-negative scalar parameters satisfying $(1 - \alpha - \beta - \gamma) > 0$. The substitution of Equation (5) for four yields

$$\rho_{ij,t} = \frac{Q_{ij,t}}{\sqrt{Q_{ii,t}}\sqrt{Q_{jj,t}}} \tag{6}$$

which can be used to calculate the correlations for the two assets. As proposed by Engle (2002, 2009) and Cappiello et al. (2006), the asymmetric dynamic correlation (ADCC) model can be estimated by using a two-stage approach to maximize the log-likelihood function.

4. Data

The data in this study cover the US aggregate stock market index (TTMK-US$*RI*) for the monthly observations spanning from January 1990 through June 2019. To measure the risks in the stock and bond markets, I use the implied stock market volatility (VIX_t) obtained from the S&P 500 index options and $MOVE_t$, the one-month Merrill Lynch Option Volatility Estimate of bond volatility. To conduct robustness tests, the US aggregate stock market indices also include the Dow-Jones Industrial Average (DJIA), the NASDAQ Composite Index (NASDAQ), the RUSSELL 2000 (RUSSELL), and the S&P 500 Value stock index (VALUE). For bond markets, the data cover the bond price indices of maturities for 30 years, 10 years, seven years, five years, and two years. The data for the total stock market, VIX, MOVE, and bond markets indices are obtained from Thomson Reuters' Datastream. Returns are constructed by taking the log-difference of the price indices times 100.

The data for the categorical uncertainty indices are equivalent to the economic policy uncertainty (EPU) data used by Baker et al. (2016). The construction of the EPU index is based on the following components: newspaper coverage of policy-related economic uncertainty, which is based on 10 large

[3] This section follows closely to Engle (2009, pp. 45–49).

newspapers; the number of federal tax code provisions set to expire in future years; and disagreements among economic forecasters, which are used as a proxy for uncertainty. Based on a similar procedure, Baker, Bloom, and Davis (BBD) construct categorical indices, including the MPU and FPU indices. Of these indices, the MPU and FPU are based on several dimensions of information: (i) the Access World News database of over 2000 newspapers; (ii) a balanced panel of 10 major national and regional US papers, including a broader set of terms designed to capture domestic and foreign sources of monetary policy and fiscal policy uncertainties; and (iii) data scaled by the total number of articles. The term sets for economic policy, monetary policy, and fiscal policy uncertainty indices are given in the Appendix A. These data can be downloaded from the link given below: http://www.policyuncertainty.com/categorical_terms.html.

Note that the choice of the US data is based on the rationale that these data can be used to construct a dynamic correlation between stocks and bonds with combinations of different stock indices and maturities of bonds. More importantly, our goal is to use policy uncertainty, including economic policy uncertainty, fiscal policy uncertainty and monetary policy uncertainty to explain the dynamic correlations. These data are more consistently available in the US market and not as accessible in other markets. The data constraint limits our research scope.

5. Empirical Estimations

5.1. Estimated Stock–Bond Dynamic Correlations

Table 1 provides different correlation matrices of stock returns, bond returns, risk and uncertainty. Panel A. reports the correlations of total stock market (TTMK) return and bond returns with different maturities. The statistics show negative correlation coefficients ranging from −0.12 to −0.15. The corresponding t-ratios are statistically significant, the only exception is the coefficient of a two-year bond. The other elements in this table are the correlations of bond returns, which range between 0.59 and 0.98. Panel B presents the correlations among different measures of stock returns and range from 0.74 to 0.95 (VALUE and DJIA). Due to the high correlation in both types of assets, most researchers tend to use only one type of stock measure, i.e., total market return, and one type of bond return, i.e., 10-year bond, to engage empirical analysis. Panel C provides a correlation matrix that illustrates the correlation of VIX and different categorical policy uncertainties. It shows that FPU and MPU are highly correlated with EPU, and VIX has the highest correlation with MOVE. To visually demonstrate, Figure 1 presents time varying correlations for VIX, MOVE, EPU, FPU, and MPU in the US market. Panel D reports the summary of statistics for VIX and uncertainty variables. Among them, the FPU surprisingly has the highest standard deviation, while the VIX has the lowest. The information is not usually observable by the public.

Table 1. Correlation matrices of stock returns, bond returns, risk, and uncertainty.

Correlation (t-Statistic)	Rm_TTMK	Rb_30Y	Rb_10Y	Rb_7Y	Rb_5Y	Rb_2Y
Rm_TTMK	1					
	—					
Rb_30Y	−0.1209	1				
	−2.28	—				
Rb_10Y	−0.1191	0.9215	1			
	−2.24	44.39	—			
Rb_7Y	−0.1191	0.8638	0.9809	1		
	−2.24	32.08	94.42	—		
Rb_5Y	−0.1456	0.7798	0.9407	0.9701	1	
	−2.75	23.31	51.87	74.76	—	
Rb_2Y	−0.1544	0.5934	0.7764	0.8278	0.9073	1
	−0.15	13.79	23.05	27.60	40.37	—

Panel A. Correlations of bond index returns.

Table 1. *Cont.*

Correlation (t-Statistic)	Rm_TTMK	R_DJIA	R_Nasdaq	R_Russell	R_Value
Rm_TTMK	1				
	——				
R_DJIA	0.9333	1			
	48.70	——			
R_Nasdaq	0.8752	0.7391	1		
	33.90	20.56	——		
R_Russell	0.8466	0.7543	0.8552	1	
	29.80	21.52	30.92	——	
R_Value	0.9447	0.9451	0.7350	0.8101	1
	53.96	54.19	20.31	25.89	——

Panel B. Correlations of stock index returns.

Correlation (t-Statistic)	VIX	MOVE	EPU	FPU	MPU
VIX	1				
	——				
MOVE	0.5969	1			
	13.84	——			
EPU	0.4099	0.2997	1		
	8.36	5.84	——		
FPU	0.2945	0.1490	0.8974	1	
	5.73	2.80	37.84	——	
MPU	0.3803	0.3020	0.7659	0.5515	1
	7.65	5.89	22.16	12.30	——

Panel C. Correlations of financial risk and categorical uncertainty.

Statistics	VIX	MOVE	EPU	FPU	MPU
Mean	19.32	93.84	96.74	101.71	87.58
Median	17.40	91.30	85.92	81.96	71.37
Maximum	59.89	213.90	271.83	374.31	407.94
Minimum	9.51	46.20	37.27	23.05	16.57
Std. Dev.	7.44	27.16	41.05	63.54	56.14
Skewness	1.72	0.95	1.18	1.59	1.80
Kurtosis	7.60	5.24	4.26	5.68	8.06
Observations	348.00	348.00	348.00	348.00	348.00

Panel D. Summary of statistics of risk and uncertainty.

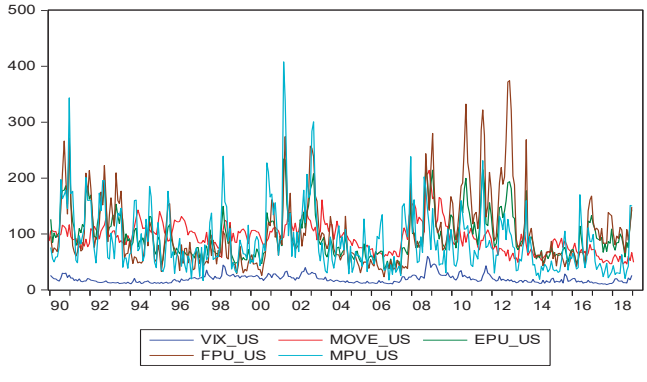

Figure 1. Time-varying VIX, MOVE, EPU, FPU, and MPU in the US market.

5.2. Estimated Stock–Bond Correlation Coefficients

Table 2 contains parametric estimates of the covariance between stock and various bond returns using the ADCC-GARCH model as represented by the system of Equations (1)–(5). Estimates in Table 2 are pairwise covariances between TTMK stock returns and one of the bond returns from 30 year to two year bonds, $h_{ij}(R_m R_b^{30y})$, $h_{ij}(R_m R_b^{10y})$, $h_{ij}(R_m R_b^{7y})$, $h_{ij}(R_m R_b^{5y})$, and $h_{ij}(R_m R_b^{2y})$. The reported statistics for conditional variances indicate that the lagged conditional variance, β_{ij}, and the lagged shock squared, α_{ij}, are largely statistically significant except for α_{11}. This result indicates that the GARCH-type model is relevant. Turning to the asymmetric impact of shocks on conditional variance, we find that most of the estimated coefficients in the stock and bond markets $\left(\gamma_{ij}\right)$ are highly significant. The exception is $\gamma_{11,}$ which is not consistent with the expected sign. Judging from the estimated coefficient and the associated t-statistics, the variance equation is apparently dominated by the predictive power from the lagged variance term.[4] Having estimated $h_{ij}(R_m, R_b)$, it can derive: $\hat{\rho}_{ij,t} = \frac{h_{ij,t}}{\sqrt{h_{ii,t}}\sqrt{h_{jj,t}}}$.

Table 2. Estimates of the asymmetric dynamic correlation (ADCC) models parameters for stock–bond return correlations.

Parameters	$h_{ij}(R_m R_b^{30y})$		$h_{ij}(R_m R_b^{10y})$		$h_{ij}(R_m R_b^{7y})$		$h_{ij}(R_m R_b^{5y})$		$h_{ij}(R_m R_b^{2y})$	
ω_{11}	0.708	2.21	1.281	2.70	1.357	2.62	1.169	2.35	1.280	2.68
ω_{12}	0.030	0.80	0.002	0.02	−0.066	−1.05	−0.088	−2.09	0.002	0.02
ω_{22}	0.865	2.44	0.325	1.81	0.121	1.41	0.050	1.30	0.325	1.79
α_{11}	0.082	1.57	0.094	1.42	0.099	1.29	0.120	1.54	0.094	1.39
α_{12}	0.022	4.03	0.138	4.83	0.094	2.79	0.067	2.46	0.138	4.21
α_{22}	0.136	3.03	0.096	2.79	0.106	2.41	0.103	2.29	0.096	2.70
γ_{11}	0.070	1.40	0.175	2.33	0.192	2.31	0.133	1.67	0.175	2.30
γ_{12}	−0.052	−3.71	−0.057	−1.50	0.033	0.52	0.073	1.36	−0.058	−0.92
γ_{22}	−0.206	−3.71	−0.149	−3.55	−0.150	−2.88	−0.118	−2.40	−0.149	−3.39
β_{11}	0.844	19.49	0.743	12.38	0.728	11.35	0.746	11.49	0.743	12.38
β_{12}	0.998	17.63	0.823	23.69	0.843	21.83	0.859	24.09	0.823	23.68
β_{22}	0.898	21.75	0.897	17.83	0.918	19.57	0.914	18.19	0.897	17.62
LLF		−1844		−1672		−1594		−1488		−1673

Note: This table estimate the parameters for conditional variance and covariance between total stock returns and various bond returns. For an $ADCC(R_m R_b^{10y})$ model, the model is given by:

$$\begin{bmatrix} h_{11,t} \\ h_{12,t} \\ h_{22,t} \end{bmatrix} = \begin{bmatrix} \omega_{11} \\ \omega_{12} \\ \omega_{22} \end{bmatrix} + \begin{bmatrix} \alpha_{11} & 0 & 0 \\ 0 & \alpha_{12} & 0 \\ 0 & 0 & \alpha_{22} \end{bmatrix} \begin{bmatrix} \varepsilon^2_{1,t-1} \\ \varepsilon_{1,t-1}\varepsilon_{2,t-1} \\ \varepsilon^2_{2,t-1} \end{bmatrix} + \begin{bmatrix} \gamma_{11} & 0 & 0 \\ 0 & \gamma_{12} & 0 \\ 0 & 0 & \gamma_{22} \end{bmatrix} \begin{bmatrix} \eta^2_{1,t-1} \\ \eta_{1,t-1}\eta_{2,t-1} \\ \eta^2_{2,t-1} \end{bmatrix} \text{for } (\eta_{1,t-1} < 0, \eta_{2,t-1} < 0)$$
$$+ \begin{bmatrix} \beta_{11} & 0 & 0 \\ 0 & \beta_{12} & 0 \\ 0 & 0 & \beta_{22} \end{bmatrix} \begin{bmatrix} h_{11,t-1} \\ h_{12,t-1} \\ h_{22,t-1} \end{bmatrix}.$$

The estimated result for $ADCC(R_m R_b^{10y})$ model is given by:

$$\begin{bmatrix} h_{11,t} \\ h_{12,t} \\ h_{22,t} \end{bmatrix} = \begin{bmatrix} 1.280 \\ 0.002 \\ 0.325 \end{bmatrix} + \begin{bmatrix} 0.094 & 0 & 0 \\ 0 & 0.138 & 0 \\ 0 & 0 & 0.096 \end{bmatrix} \begin{bmatrix} \varepsilon^2_{1,t-1} \\ \varepsilon_{1,t-1}\varepsilon_{2,t-1} \\ \varepsilon^2_{2,t-1} \end{bmatrix} + \begin{bmatrix} 0.175 & 0 & 0 \\ 0 & -0.057 & 0 \\ 0 & 0 & -0.149 \end{bmatrix} \begin{bmatrix} \eta^2_{1,t-1} \\ \eta_{1,t-1}\eta_{2,t-1} \\ \eta^2_{2,t-1} \end{bmatrix}$$
$$+ \begin{bmatrix} 0.743 & 0 & 0 \\ 0 & 0.823 & 0 \\ 0 & 0 & 0.897 \end{bmatrix} \begin{bmatrix} h_{11,t-1} \\ h_{12,t-1} \\ h_{22,t-1} \end{bmatrix}$$

[4] To illustrate the model, in the footnote of Table 2, one can plug the estimated parameters into the model using $h_{ij}(R_m R_b^{10y})$.

The parameter $h_{ij,t}$ is the variance and covariance of asset i and j in the estimated equation (subscripts $i = (R_m)$ and $j = (R_b)$, which stand for stock and bond returns, respectively); ω, α, and β are the parameters for the conditional variance equation; and γ is an asymmetric parameter. The first column is the estimated parameters and the second column is the t-statistics. The critical values at the 1%, 5%, and 10% are 2.60, 1.97, and 1.65, respectively. LLF denotes the log-likelihood function.

Figure 2 shows time series plots of dynamic conditional correlations for the monthly data between TTMK return and bond returns with different maturities based on Equation (6). Correlations between the returns of the two assets display noticeable variations throughout the sample period. In general, the plots clearly show a downward slope up to the time of 2004. During the beginning of the 2000s when the US market suffered from the dotcom collapse, the stock market dropped dramatically, and there was less of a decline in bond returns, causing the correlation to move downward as shown in the Figure 2 in this period. These results are consistent with the findings of Connolly et al. (2005), Chiang et al. (2015), and Li et al. (2015). However, during the global financial crisis period in 2008–2010, the stock market plummeted again, and the correlation coefficient also deepened in this period. After this crisis time the relationships become stationary and fluctuate around a very mild negative regime. A special feature derived from this study is that despite of their common movement around turning points, the dynamic paths show that the stock–bond return correlations vary with different bond maturities, which reflect different market conditions and preferences for bond maturities with different bondholders. These results suggest that the path of $\rho_{SB,t}$ is based on only one stock return and one bond return, as is the case in conventional studies, which could produce a misleading and biased estimator.

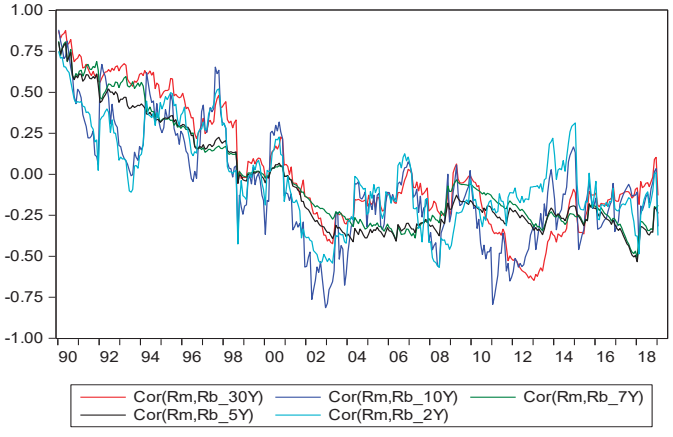

Figure 2. Dynamic correlations between stock (TTMK) and various bond returns in the US.

5.3. The Role of Uncertainty

Early studies by Connolly et al. (2005), Andersson et al. (2008), and Chiang et al. (2015) stress the notion of using volatility measure as a proxy for uncertainty. Connolly et al. (2005) find that the correlation between stock and bond returns declines during periods with substantial increases in VIX. Andersson et al. (2008), Chiang et al. (2015), and Dimic et al. (2016) report that periods of elevated stock market uncertainty cause a decoupling between the relation of stock and bond returns, which is consistent with the "flight-to-quality" phenomenon. Antonakakis et al. (2013) and Li et al. (2015) employ the economic policy uncertainty in modeling the dynamic correlations. The current study extends this approach by adding monetary policy uncertainty and fiscal policy uncertainty in the test equation to explain the dynamic correlations between stock and bond returns. This notion is summarized in the regression model as follows:

$$\hat{\rho}^{*}_{Sb,t} = \varphi_0 + \varphi_1 VIX_{t-1} + \varphi_2 MOVE_{t-1} + \varphi_3 EPU_{t-1} + \varphi_4 MPU_{t-1} + \varphi_5 FPU_{t-1} + \varphi_6 Trend + \varepsilon_t \quad (7)$$

where $\hat{\rho}^{*}_{Sb,t}$ is a Fisher transformation of stock–bond correlation coefficient, $\hat{\rho}_{SB,t}$, that is, $\hat{\rho}^{*}_{Sb,t} = \frac{1}{2} ln[\frac{1+\hat{\rho}_{SB,t}}{1-\hat{\rho}_{SB,t}}]$ and is bound to interval [−1,+1]. VIX_{t-1} and $MOVE_{t-1}$ are the 1-month implied volatility in stock and bond markets, respectively. The EPU_{t-1} is the economic policy uncertainty at time $t-1$, while MPU_{t-1} and FPU_{t-1} are the monetary policy and fiscal policy uncertainties at time $t-1$. Two special features are included in Equation (7). First, the financial risk and uncertainty are treated as independent factors to explain the stock–bond return correlations; second, in addition to the EPU_{t-1}, the categorical policy impacts, such as the MPU_{t-1} and FPU_{t-1}, are included to highlight their distinctive effects. In the last term, the trend factor is added to capture of the presence of non-stationarity.

Table 3 presents consistent estimates (Newey and West 1987) of Equation (7) without including EPU_{t-1}, MPU_{t-1} and FPU_{t-1}, while Table 4 shows results for this equation where the restriction of $\varphi_3 = \varphi_4 = \varphi_5 = 0$ has been relaxed. Both models perform very well, the adjusted *R*-squares for the unrestricted model, which range from 0.48 to 0.81, are notably higher than those of the restricted model, indicating that the inclusion of the uncertainty variables helps to increase their explanatory power. Since the results in Table 3 are nested in Table 4, our interpretations focus on Table 4. Several points are noteworthy.

Table 3. Estimates of aggregate and categorical EPU, FPU, and MPU and on stock (TTMK)–bond return correlations.

PI = TTMK	$\hat{\rho}^{*}_{t}(R_m R^{30y}_b)$		$\hat{\rho}^{*}_{t}(R_m R^{10y}_b)$		$\hat{\rho}^{*}_{t}(R_m R^{7y}_b)$		$\hat{\rho}^{*}_{t}(R_m R^{5y}_b)$		$\hat{\rho}^{*}_{t}(R_m R^{2y}_b)$	
C	0.945	14.34	0.668	8.80	0.642	5.26	0.673	13.27	0.781	12.79
VIX_{t-1}	−0.006	−2.52	−0.005	−1.73	0.001	0.25	0.001	0.56	−0.005	−2.33
$MOVE_{t-1}$	−0.002	−2.15	−0.003	−3.10	−0.001	−1.33	−0.002	−3.74	−0.003	−5.30
Trend	−0.004	−24.65	−0.003	−14.28	−0.003	−10.93	−0.003	−27.75	−0.002	−15.42
$\overline{R}^2$	0.68		0.41		0.71		0.72		0.48	

Note: This table presents evidence of VIX and MOVE on $\hat{\rho}^{*}_{t}$, the Fisher transformation of $\hat{\rho}_{t,}$ which is the dynamic correlations between value stock–bond returns. That is, $\hat{\rho}^{*}_{Sb,t}(\cdots) = \frac{1}{2}\ln[\frac{1+\hat{\rho}_t}{1-\hat{\rho}_t}])$. The subscript "sb" is suppressed to save space in table. For each model, the first column reports the estimated coefficients, the second column contains the estimated t-statistics. The critical values of t-distribution at the 1%, 5%, and 10% levels of significance are 2.60, 1.98, and 1.66, respectively. The numbers in the brackets are the *p*-values. $\overline{R}^2$ is the adjusted R-squared.

Table 4. Estimates of aggregate and categorical EPU, FPU, and MPU, and on stock (TTMK)–bond return correlations.

PI = TTMK	$\hat{\rho}^{*}_{t}(R_m R^{30y}_b)$		$\hat{\rho}^{*}_{t}(R_m R^{10y}_b)$		$\hat{\rho}^{*}_{t}(R_m R^{7y}_b)$		$\hat{\rho}^{*}_{t}(R_m R^{5y}_b)$		$\hat{\rho}^{*}_{t}(R_m R^{2y}_b)$	
C	0.000	0.00	0.370	1.91	−0.680	−5.91	−0.444	−3.66	0.513	3.13
VIX_{t-1}	−0.007	−2.00	−0.003	−1.00	−0.002	−1.73	−0.001	−0.99	−0.005	−2.12
$MOVE_{t-1}$	−0.001	−1.40	−0.002	−2.97	−0.001	−3.82	−0.002	−5.27	−0.003	−5.54
EPU_{t-1}	0.857	6.15	0.674	5.43	0.766	10.79	0.715	9.34	0.406	3.96
FPU_{t-1}	−0.409	−4.59	−0.415	−6.11	−0.231	−5.67	−0.250	−5.79	−0.203	−3.57
MPU_{t-1}	−0.254	−4.55	−0.222	−5.01	−0.236	−9.25	−0.217	−8.18	−0.157	−4.60
Trend	−0.004	−11.98	−0.002	−11.93	−0.003	−28.00	−0.003	−27.70	−0.002	−14.60
$\chi^2(3)$	38.12	[0.00]	18.30	[0.00]	197.92	[0.00]	127.64	[0.00]	21.86	[0.00]
$\chi^2(2)$	29.81	[0.00]	17.60	[0.00]	91.81	[0.00]	74.36	[0.00]	21.85	[0.00]
$\overline{R}^2$	0.73		0.48		0.81		0.79		0.51	

Note: This table presents evidence of financial risk and policy uncertainty on $\hat{\rho}^{*}_{Sb,t'}$ the Fisher transformation of $\hat{\rho}_{t,}$ which is the dynamic correlations between TTMK stock–bond returns. That is, $\hat{\rho}^{*}_{Sb,t}(\cdots) = \frac{1}{2}\ln[\frac{1+\hat{\rho}_t}{1-\hat{\rho}_t}]$. The subscript "sb" is suppressed to save space in the table. For each model, the first column reports the estimated coefficients, the second column contains the estimated t-statistics. The critical values of t-distribution at the 1%, 5%, and 10% levels of significance are 2.60, 1.98, and 1.66, respectively. The numbers in the brackets are the *p*-values. $\overline{R}^2$ is the adjusted R-squared.

First, the coefficients of the trend factor are negative, indicating that in general the correlations between stock and bond returns slope downward, although feathering in the stochastic process is present. This result is consistent with the findings reported by Connolly et al. (2005) and Chiang et al. (2015).

Second, the risk variables of VIX_{t-1} and $MOVE_{t-1}$ are negative, revealing that investors are actively switching between stock and bond depending on the level of risk in the market. This movement resembles a flight-to-quality as risk increases and flight-from-quality as risk declines. This finding is consistent with the results in the literature (Gulko 2002; Connolly et al. 2005; Andersson et al. 2008; Chiang et al. 2015).

Third, the estimated coefficients of EPU_{t-1} are positive and highly significant. This conforms with a market phenomenon in which a sudden rise in uncertainty impedes prospects for economic activities, thereby dampening output production and future cash flows. Facing weakening liquidity, investors tend to sell off stocks and bonds. The dominance of this income effect will lead to a positive movement between stock and bond prices, a reaction that is consistent with a study by Hong et al. (2014), which emphasizes the response to market volatile.

Fourth, the estimated coefficients for FPU_{t-1} and MPU_{t-1} are negative and significant at the one percent level. This should not be surprising, since a rise in MPU tends to increase uncertainty in interest rate, which is more likely to create a strong substitution effect that causes a shift from high uncertainty asset-stocks to relatively low uncertainty asset-bonds and leads to a decoupling of stock and bond returns. A similar shift also holds true for an upward shift in FPU, especially in the case of bond financing of government deficits. It is recognized that an increase in FPU_{t-1} and MPU_{t-1} could create an income effect; however, the negative coefficients imply that the substitution effect dominates the income effect.

Fifth, the estimated results favor the inclusion of uncertainty variables as incremental variables. This can be seen in the reported $\chi^2(3)$ statitic, which tests the joint significance of the coefficients with $\varphi_3 = \varphi_4 = \varphi_5 = 0$. The *p*-values of the Chi-squared test, which are in brackets, indicate the rejection of the null, suggesting that the inclusion of the uncertainty variables helps to improve the explanation of the dynamic correlations between stock and bond returns. Evidence thus indicates that the exclusion of uncertainty variables in the literature (Connolly et al. 2005; Andersson et al. 2008; Chiang et al. 2015) is subject to an omitted variable problem. In addition, the $\chi^2(2)$ statistic for testing equality of coefficients for $\varphi_4 = \varphi_5 = 0$ against alternatives is also significant in all of cases, this test indicates the exclusion of categorical uncertainty even in the case of *EPU* (Antonakakis et al. 2013; Li et al. 2015) suffers from a missing variable problem.

In summary, this study contributes to the literature in two ways. First, the effect of risk is separated from the uncertainty effect, showing both types of variables contribute to the variations of stock–bond correlations. Second, unlike the EPU, evidence shows the coefficients of FPU and MPT are negative, which provides an incremental contribution in the ability to predict time-varying correlations of stock and bond returns, $\hat{\rho}^*_{Sb,t}$. These categorical uncertainty variables have not been explored in the literature.

6. Robustness Tests

6.1. Difference of Stock Indices

Despite of successful outcomes of the time-varying behavior of $\hat{\rho}^*_{Sb,t}$ in relation to the risk/uncertainty, it is important to examine the robustness of the parametric relations, which can be done by using alternative measures of stock indices. In this section, the test equations apply to stock indices including the DJIA, NASDAQ, RUSSELL, and VALUE. Pairings of stock returns with bond returns of maturities of 30 years, 10 years, seven years, five years, and two years are used to derive $\hat{\rho}^*_{Sb,t}(\cdot)$. The estimated equations are reported in Tables 5–8, and the test results are summarized as follows.

Table 5. Estimates of aggregate and categorical EPU, FPU, and MPU and on stock (DJIA)–bond return correlations.

PI = DJIA	$\hat{\rho}_t^*(R_m R_b^{30y})$		$\hat{\rho}_t^*(R_m R_b^{10y})$		$\hat{\rho}_t^*(R_m(R_m R_b^{7y})$		$\hat{\rho}_t^*(R_m R_b^{5y})$		$\hat{\rho}_t^*(R_m R_b^{2y})$	
C	−1.148	−4.66	−1.116	−9.04	−1.019	−9.09	−0.834	−7.19	0.100	0.93
VIX_{t-1}	−0.016	−4.62	0.000	−0.04	−0.004	−3.08	0.003	2.59	0.000	0.11
$MOVE_{t-1}$	−0.001	−0.69	−0.002	−3.62	−0.000	−0.63	−0.002	−4.87	−0.002	−3.90
EPU_{t-1}	1.003	7.35	0.874	9.94	0.725	9.04	0.706	8.43	0.279	3.56
FPU_{t-1}	−0.252	−3.20	−0.229	−4.79	−0.172	−3.96	−0.203	−4.56	−0.127	−3.09
MPU_{t-1}	−0.308	−5.16	−0.274	−8.63	−0.215	−7.30	−0.233	−7.86	−0.104	−3.83
Trend	−0.004	−10.01	−0.004	−23.49	−0.003	−24.63	−0.003	−21.82	−0.002	−16.65
$\chi^2(3)$	76.80	[0.00]	216.77	[0.00]	232.68	[0.00]	130.12	[0.00]	15.60	[0.00]
$\chi^2(2)$	28.91	[0.00]	74.98	[0.00]	53.30	[0.00]	62.22	[0.00]	15.52	[0.00]
$\overline{R}^2$	0.73		0.82		0.84		0.77		0.61	

Note: This table presents evidence of financial risk and policy uncertainty on $\hat{\rho}^*_{Sb,t}$, the Fisher transformation of $\hat{\rho}_t$, which is the dynamic correlations between DJIA stock–bond returns. That is, $\hat{\rho}^*_{Sb,t}(\cdots) = \frac{1}{2}\ln[\frac{1+\hat{\rho}_t}{1-\hat{\rho}_t}]$. The subscript "sb" is suppressed to save space in the table. For each model, the first column reports the estimated coefficients, the second column contains the estimated t-statistics. The critical values of t-distribution at the 1%, 5%, and 10% levels of significance are 2.60, 1.98, and 1.66, respectively. The numbers in the brackets are the p-values. $\overline{R}^2$ is the adjusted R-squared.

Table 6. Estimates of aggregate and categorical EPU, FPU and MPU and on stock (NASDAQ)–bond return correlations.

PI = NASD	$\hat{\rho}_t^*(R_m R_b^{30y})$		$\hat{\rho}_t^*(R_m R_b^{10y})$		$\hat{\rho}_t^*(R_m R_b^{7y})$		$\hat{\rho}_t^*(R_m R_b^{5y})$		$\hat{\rho}_t^*(R_m R_b^{2y})$	
C	−0.641	−4.21	0.100	0.76	0.056	0.46	0.182	1.51	0.307	2.76
VIX_{t-1}	0.003	1.29	0.003	1.27	0.003	1.71	0.002	1.20	0.001	0.76
$MOVE_{t-1}$	−0.002	−1.89	−0.002	−4.50	−0.003	−5.20	−0.003	−6.12	−0.003	−6.07
EPU_{t-1}	0.670	4.08	0.467	5.31	0.438	5.17	0.357	4.20	0.285	3.52
FPU_{t-1}	−0.258	−3.33	−0.293	−6.18	−0.265	−5.87	−0.211	−4.63	−0.188	−4.34
MPU_{t-1}	−0.186	−2.83	−0.145	−4.76	−0.139	−4.76	−0.124	−4.28	−0.093	−3.37
Trend	−0.003	−7.14	−0.002	−11.36	−0.001	−9.84	−0.001	−11.66	−0.002	−13.7
$\chi^2(3)$	20.07	[0.00]	50.21	[0.00]	44.47	[0.00]	30.44	[0.00]	29.01	[0.00]
$\chi^2(2)$	11.36	[0.00]	40.53	[0.00]	36.68	[0.00]	24.90	[0.00]	19.78	[0.00]
$\overline{R}^2$	0.67		0.48		0.41		0.46		0.52	

Note: This table presents evidence of financial risk and policy uncertainty on $\hat{\rho}^*_{Sb,t}$, the Fisher transformation of $\hat{\rho}_t$, which is the dynamic correlations between NASDAQ stock–bond returns. That is, $\hat{\rho}^*_{Sb,t}(\cdots) = \frac{1}{2}\ln[\frac{1+\hat{\rho}_t}{1-\hat{\rho}_t}]$). The subscript "sb" is suppressed to save space in the table. For each model, the first column reports the estimated coefficients, the second column contains the estimated t-statistics. The critical values of t-distribution at the 1%, 5%, and 10% levels of significance are 2.60, 1.98, and 1.66, respectively. The numbers in the brackets are the p-values. $\overline{R}^2$ is the adjusted R-squared.

First, the evidence clearly indicates that the coefficients of stock–bond return correlations slope downward as indicated by the negative sign and are statistically significant. However, the coefficients of VIX_{t-1} have mixed signs. Although most of them are negative, yet, the coefficients of VIX_{t-1} in the NASDAQ and RUSSELL stock returns are positive, reflecting the possibility that investors with different stocks holding have different degrees of sensitivity to financial shock and react differently. From an econometric point of view, this may also result from a spurious correlation. Another financial risk variable, $MOVE_{t-1}$, however, presents consistent results. Except $\hat{\rho}_t^*(R_m R_b^{7y})$ (in Tables 7 and 8), the coefficients show negative signs and are statistically significant.

Table 7. Estimates of aggregate and categorical EPU, FPU, and MPU and on stock (RUSSELL)–bond return correlations.

PI = RUSS	$\hat{\rho}_t^*(R_m R_b^{30y})$		$\hat{\rho}_t^*(R_m R_b^{10y})$		$\hat{\rho}_t^*(R_m R_b^{7y})$		$\hat{\rho}_t^*(R_m R_b^{5y})$		$\hat{\rho}_t^*(R_m R_b^{2y})$	
C	−0.258	−1.37	−0.160	−1.46	−1.440	−5.56	−0.037	−0.38	0.231	2.35
VIX_{t-1}	0.005	1.84	0.004	2.76	−0.023	−7.96	0.003	2.41	0.003	1.84
$MOVE_{t-1}$	−0.001	−0.92	−0.002	−4.31	0.001	0.94	−0.002	−4.70	−0.002	−4.16
EPU_{t-1}	0.555	3.26	0.465	4.83	1.063	7.83	0.269	3.49	0.181	2.53
FPU_{t-1}	−0.321	−3.47	−0.273	−5.81	−0.215	−2.77	−0.157	−4.05	−0.143	−3.76
MPU_{t-1}	−0.152	−2.17	−0.138	−3.62	−0.400	−9.01	−0.094	−3.16	−0.065	−2.40
Trend	−0.002	−5.23	−0.001	−8.38	−0.002	−11.31	−0.001	−9.62	−0.001	−12.26
$\chi^2(3)$	14.87	[0.00]	37.73	[0.00]	190.74	[0.00]	19.85	[0.00]	29.16	[0.00]
$\chi^2(2)$	12.08	[0.00]	34.93	[0.00]	81.31	[0.00]	16.67	[0.00]	14.17	[0.00]
$\overline{R}^2$	0.49		0.39		0.47		0.37		0.45	

Note: This table presents evidence of financial risk and policy uncertainty on $\hat{\rho}^*_{Sb,t}$, the Fisher transformation of $\hat{\rho}_{t,}$ which is the dynamic correlations between Russell stock–bond returns. That is, $\hat{\rho}^*_{Sb,t}(\cdots) = \frac{1}{2}\ln[\frac{1+\hat{\rho}_t}{1-\hat{\rho}_t}])$. The subscript "sb" is suppressed to save space in the table. For each model, the first column reports the estimated coefficients, the second column contains the estimated t-statistics. The critical values of t-distribution at the 1%, 5%, and 10% levels of significance are 2.60, 1.98, and 1.66, respectively. The numbers in the brackets are the p-values. $\overline{R}^2$ is the adjusted R-squared.

Table 8. Estimates of aggregate and categorical EPU, FPU, and MPU and on stock (VALUE)–bond return correlations.

PI = VALUE	$\hat{\rho}_t^*(R_m R_b^{30y})$		$\hat{\rho}_t^*(R_m R_b^{10y})$		$\hat{\rho}_t^*(R_m R_b^{7y})$		$\hat{\rho}_t^*(R_m R_b^{5y})$		$\hat{\rho}_t^*(R_m R_b^{2y})$	
C	−1.259	−3.62	−1.241	−9.10	−1.910	−8.44	−0.871	−7.28	0.249	1.95
VIX_{t-1}	−0.022	−4.90	−0.003	−2.07	−0.027	−8.63	0.003	2.06	−0.002	−1.23
$MOVE_{t-1}$	−0.000	−0.38	−0.001	−1.78	0.002	3.11	−0.002	−3.71	−0.002	−3.33
EPU_{t-1}	1.209	7.61	0.947	9.32	1.235	8.24	0.763	9.04	0.326	3.82
FPU_{t-1}	−0.315	−3.03	−0.227	−4.29	−0.263	−3.08	−0.225	−4.98	−0.150	−3.23
MPU_{t-1}	−0.381	−5.43	−0.294	−7.55	−0.399	−7.79	−0.246	−8.05	−0.136	−4.60
Trend	−0.004	−9.37	−0.004	−23.90	−0.003	−15.83	−0.003	−23.56	−0.002	−17.94
$\chi^2(3)$	70.86	[0.00]	233.42	[0.00]	219.45	[0.00]	140.30	[0.00]	21.86	[0.00]
$\chi^2(2)$	33.35	[0.00]	57.04	[0.00]	61.84	[0.00]	66.15	[0.00]	21.85	[0.00]
$\overline{R}^2$	0.67		0.83		0.65		0.80		0.60	

Note: This table presents evidence of financial risk and policy uncertainty on $\hat{\rho}^*_t$, the Fisher transformation of $\hat{\rho}_{t,}$ which is the dynamic correlations between Value stock–bond returns. That is, $\hat{\rho}^*_t(\cdots) = \frac{1}{2}\ln[\frac{1+\hat{\rho}_t}{1-\hat{\rho}_t}])$. The subscript "sb" is suppressed to save space in the table. For each model, the first column reports the estimated coefficients, the second column contains the estimated t-statistics. The critical values of t-distribution at the 1%, 5%, and 10% levels of significance are 2.60, 1.98, and 1.66, respectively. The numbers in the brackets are the p-values. $\overline{R}^2$ is the adjusted R-squared.

Turning to the performance of the coefficients of EPU_{t-1}, FPU_{t-1}, and MPU_{t-1}, the signs are consistent with the results in Table 4. That is, the coefficients of EPU_{t-1} continue to present positive signs, showing the impact of a positive income effect on the stock–bond return correlation, while the coefficients of FPU_{t-1} and MPU_{t-1} display negative signs, revealing that stock and bond returns are dominated by a substitution effect and move in diverse directions. The testing results suggest that a portfolio combination of stocks and bonds are a better hedge against uncertainty if it originates from monetary policy or fiscal policy uncertainty. However, the benefits of stock and bond diversification are less apparent if the uncertainty is the result of a general economic policy uncertainty, since its impact on economic activity is pervasive.[5]

[5] Instead of stressing the sources of policy uncertainty, Baele et al. (2010) analyze monetary policy impact on the direction of equity-bond correlation by focusing on the effects of inflation. In periods with a contractionary monetary policy, which is usually associated with low inflation rate, the correlation displays a positive relation; nonetheless, during periods of high inflation, the stock–bond correlation presents a negative relation. Thus, it is hard to justify whether inflation plays a role in uncertainty or a real income effect. However, Pericoli (2018) shows that inflation rate is a significant factor. Further, instead

6.2. Total Policy Uncertainty

The above tests suggest that the EPU_{t-1} has a positive effect, while FPU_{t-1} and MPU_{t-1}have a negative effect on the $\hat{\rho}^{*}_{Sb,t}(\cdot)$. It is natural to pool all the uncertainty information together regardless of the sources of uncertainty. To this end, I define $TPU_t = EPU_t + FPU_t + MPU_t$ as total policy uncertainty (TPU_t). Table 9 reports the estimates of the test equation, which uses TPU_t as a measure of uncertainty. Consistent with previous findings, the coefficients of VIX_{t-1} have mixed signs. However, the signs for $MOVE_{t-1}$ consistently present negative signs and most of them are statistically significant.

Table 9. Estimates of correlations of total stock market returns and 10-year bond returns in response to financial risk and total policy uncertainty.

Indpt. Variable	TTMK		DJIA		NASDAQ		RUSSELL		VALUE	
	$\hat{\rho}^{*}_{t}(R_m R_b^{10y})$		$\hat{\rho}^{*}_{t}(R_m R_b^{10y})$		$\hat{\rho}^{*}_{t}(R_m R_b^{10y})$		$\hat{\rho}^{*}_{t}(R_m R_b^{10y})$		$\hat{\rho}^{*}_{t}(R_m R_b^{10y})$	
C	1.239	7.59	−0.207	−1.77	0.704	6.87	0.427	3.96	−0.270	−2.06
VIX_{t-1}	−0.001	−0.47	0.000	0.04	0.004	1.78	0.005	3.34	−0.003	−1.68
$MOVE_{t-1}$	−0.002	−2.80	−0.002	−2.89	−0.002	−4.23	−0.002	−4.10	−0.001	−1.37
TPU_{t-1}	−0.048	−4.23	0.060	7.28	−0.032	−4.49	−0.023	−3.18	0.074	8.18
Trend	−0.003	−13.08	−0.003	−19.94	−0.002	−12.61	−0.001	−9.15	−0.004	−20.60
$\overline{R}^2$	0.43		0.73		0.42		0.33		0.75	

Notes: This table presents evidence of financial risk and policy uncertainty on $\hat{\rho}^{*}_{Sb,t}$, the Fisher transformation of $\hat{\rho}_{t,}$ which is the dynamic correlations between Value stock–bond returns. That is, $\hat{\rho}^{*}_{Sb,t}(\cdots) = \frac{1}{2}\ln[\frac{1+\hat{\rho}_t}{1-\hat{\rho}_t}]$). The subscript "sb" is suppressed to save space in the table. For each model, the first column reports the estimated coefficients, the second column contains the estimated t-statistics. The critical values of t-distribution at the 1%, 5%, and 10% levels of significance are 2.60, 1.98, and 1.66, respectively. $\overline{R}^2$ is the adjusted R-squared.

With respect to the sign of TPU_{t-1}, evidence shows that the coefficients on TTMK, NASDAQ, and RUSSELL exhibit negative signs and are statistically significant. This result is consistent with market behavior of investors who during a rise in TPU_{t-1} tend to sell off more uncertain stock and move their funds to bonds, effectively exhibiting the substitution effect. However, the coefficients of TPU_{t-1} for the DJIA and VALUE stocks are positive and statistically significant, indicating a dominance of the income effect. A review of the S&P 500 Value index, which has a style-concentrated index designed to track the performance of stocks that exhibit the strongest value, shows that the value of these stocks is very much in line with that of the DJIA. In sum, estimates of correlations between total stock market returns and 10-year bond returns show different signs in response to total policy uncertainty is essentially executed under different degrees of force from income effect and substitution effect.

7. Conclusions

This paper examines the impact of financial market risk and policy uncertainties on the correlation between stock and bond returns. Analyzing the financial data of US markets for the period January 1990–June 2019, I derive several important empirical conclusions. First, empirical estimations based on the asymmetric dynamic correlation model (ADCC) suggest that stock–bond correlations are time-varying and display a negative relation overtime, especially for the period before 2002.

Second, evidence confirms that the stock–bond relationship is negatively correlated with the implied volatility in stock market (VIX), suggesting a higher market risk would cause a "flight-to-safety." This phenomenon appears in stock markets of TTMK and VALUE. However, for indices such as the DJIA (with two-year and five-year bonds), the NASDAQ and RUSSELL, the sign turns out to be positive. The mixed results reflect differing attitudes toward risks of investors who hold different stock portfolios. This finding suggests that the use of a single stock index to measure stock returns and one specific

of using government bonds, one might use junk bonds to trace the dynamic correlations (Glassman 2018), which will be the subject of future research.

form of bond maturity (10-year bond) as was done in the previous research (Connolly et al. 2005) could produce a biased estimator and hence a misleading statistical inference.

Third, with respect to the performance of implied bond volatility ($MOVE_{t-1}$), this study arrives at more consistent results. In this case, the coefficients tend to have negative signs with a couple of exceptions. For this reason, we can reach a more concrete conclusion that a rise in $MOVE_{t-1}$ leads to a decoupling of stock and bond returns. Thus, $MOVE_{t-1}$ to some extent reflects different market information and complementarily contributes to explaining movements in stock and bond return correlations.

Fourth, this study find evidence that estimated coefficient of the EPU_{t-1} has a positive and significant effect on the stock–bond return correlation. This result is consistent with a dominant income effect resulting from a rise in economic policy uncertainty that impedes economic activities and leads to a decline in income. This decline brings about a decrease in liquidity and in turn weakens demand for both stocks and bonds. Therefore, both stock and bond prices move in the same direction.

Fifth, testing results conclude that the estimated coefficients for both FPU_{t-1} and MPU_{t-1} are negative and highly significant. The negative sign of this policy uncertainty is mainly due to the dominance of the substitution effect, which prompts investors to replace higher uncertainty assets with lower uncertainty assets due to an upward shift in policy uncertainty. This occurs because of a policy stance that causes a sudden rise in MPU_{t-1} (or FPU_{t-1} in bond financing) and increases uncertainty in interest rates, prompting a selloff in stocks and a flight-to-quality phenomenon. Note that this market action essentially stems from a heightened fear from policy uncertainty rather than something of inherent in the asset's return. It is possible that a rise in MPU_{t-1} (or FPU_{t-1}) could threaten the future cash flow and reduce the demand for both stocks and bonds. However, the evidence of a negative coefficient indicates the dominant force of the substitution effect. An implication of a negative coefficient suggests that a portfolio can benefit from a combination of stocks and bonds as a way of diversification and hedging against monetary policy or fiscal policy uncertainty.

Sixth, by testing the total policy uncertainty on the dynamic correlations between stock–bond returns, the evidence turns out to display mixed signs. For DJIA and VALUE stocks, the correlation coefficients present positive signs, indicating the dominance of an income effect attributable to general economic policy uncertainty; however, correlations of the TTMK, NASDAQ, and RUSSELL stocks with bond returns display negative signs, suggesting the dominance of a substitution effect, resulting from the reallocation of assets from ones with higher uncertainty to those with lower uncertainty in response to a rise in total policy uncertainty.

In sum, this paper provides significant empirical evidence to support the impact of MPU_{t-1} and FPU_{t-1} on stock–bond correlations. In addition to the VIX_{t-1}, $MOVE_{t-1}$ and EPU_{t-1}, our Chi-squared statistics consistently suggest the rejection of the null, $MPU_{t-1} = FPU_{t-1} = 0$, and support the incremental significance of MPU_{t-1} and FPU_{t-1} in the test equation. This evidence has not previously been shown in the literature to explain the stock–bond return correlation.

Further, this study has practical implications for investment firms by tracing the time-varying correlations and is distinct from more commonly taken approaches by calculating the individual, constant correlations (Forbes and Rigobon 2002) within a given period of time. This study identifies categorical policy uncertainties as factors to explain the change in stock–bond correlations over time. Given the model parameters, firms can access information via newspapers to make projections related to stock–bond dynamics.

Funding: This research received no external funding.

Conflicts of Interest: The author declares no conflict of interest.

Appendix A

Table A1. Some major term sets for policy category uncertainty indices.

Variable	Description	Source
EPU_t	Economic policy uncertainty index involves: "economic" or "economy"; "uncertain" or "uncertainty"; and one or more of "Congress," "deficit," "Federal Reserve," "legislation," "regulation," or "White House" in 10 major newspapers.	Baker et al. (2016) *
FPU_t	Fiscal policy uncertainty index involves terms of "government budget" or discretionary fiscal policy", "government revenue", "tax" or "Taxation", "government deficit", "government spending" or "government expenditure", "social security expenditures", "defense spending", "Legislation", "public debt" or "government debt", "National bonds", among others.	Davis (2016) **
MPU_t	Monetary policy uncertainty index involves terms of "monetary policy", monetary easing", quantitative easing", "negative interest rate", "official discount rate", "monetary operation(s)", "inflation target", among others.	Davis (2016) **

* Baker et al. (2016). http://www.policyuncertainty.com. ** Source: 'Measuring Economic Policy Uncertainty' by Scott Baker, Nicholas Bloom and Davis, S.J. at www.PolicyUncertainty.com.

References

Allard, Anne-Florence, Leonardo Iania, and Kristien Smedts. 2019. Stock–Bond Return Correlations: Moving away from 'One-Frequency-Fits-All' by Extending the DCC-MIDAS Approach. Available online: https://ssrn.com/abstract=3190071 (accessed on 29 May 2020).

Andersson, Magnus, Elizaveta Krylova, and Sami Vähämaa. 2008. Why does the correlation between stock and bond returns vary over time? *Applied Financial Economics* 18: 139–51. [CrossRef]

Antonakakis, Nikolaos, Ioannis Chatziantoniou, and George Filis. 2013. Dynamic co-movements of stock market returns, implied volatility and policy uncertainty. *Economics Letters* 120: 87–92. [CrossRef]

Baele, Lieven, Geert Bekaert, and Inghelbrecht Koen. 2010. The determinants of stock and bond return comovements. *Review of Financial Studies* 23: 2374–428. [CrossRef]

Baker, Scott R., Nicholas Bloom, and Steven J. Davis. 2016. Measuring economic policy uncertainty. *Quarterly Journal of Economics* 131: 1593–636. [CrossRef]

Barsky, R. 1989. Why don't the prices of stocks and bonds movetogether? *American Economic Review* 79: 1132–45.

Baur, Dirk, and Brian Lucey. 2009. Flight and contagion—An empirical analysis of stock–bond correlations. *Journal of Financial Stability* 5: 339–52. [CrossRef]

Bloom, Nicholas. 2009. The impact of uncertainty shocks. *Econometrica* 77: 623–85.

Bloom, Nicholas. 2014. Fluctuations in Uncertainty. *Journal of Economic Perspectives* 28: 153–76. [CrossRef]

Brunnermeier, Markus, and Lasse H. Pedersen. 2009. Market liquidity and funding liquidity. *Review of Financial Studies* 22: 2201–38. [CrossRef]

Campbell, John Y., and John Ammer. 1993. What moves the stock and bond markets? A variance decomposition for long-term asset returns. *Journal of Finance* 48: 3–37. [CrossRef]

Cappiello, Lorenzo, Robert F. Engle, and Kevin Sheppard. 2006. Asymmetric dynamics in the correlations of global equity and bond returns. *Journal of Financial Econometrics* 4: 537–72. [CrossRef]

Chiang, Thomas Chinan. 2019. Economic policy uncertainty, risk and stock returns: Evidence from G7 stock markets. *Finance Research Letters* 29: 41–49. [CrossRef]

Chiang, Thomas Chinan, Bang Nam Jeon, and Huimin Li. 2007. Dynamic correlation analysis of financial contagion: Evidence from Asian markets. *Journal of International Money and Finance* 26: 1206–28. [CrossRef]

Chiang, Thomas Chinan, Jiandong Li, and Sheng-Yung Yang. 2015. Dynamic stock–bond return correlations and financial market uncertainty. *Review of Quantitative Finance and Accounting* 45: 59–88. [CrossRef]

Connolly, Robert A., Chris T. Stivers, and Licheng Sun. 2005. Stock market uncertainty and the stock–bond return relation. *Journal of Financial and Quantitative Analysis* 40: 161–94. [CrossRef]

d'Addona, Stefano, and Axel H. Kind. 2006. International stock–bond correlations in a simple affine asset pricing model. *Journal of Banking and Finance* 30: 2747–65. [CrossRef]

de Goeij, Peter, and Wessel Marquering. 2004. Modeling the conditional covariance between stock and bond returns: A multivariate GARCH approach. *Journal of Financial Econometrics* 2: 531–64. [CrossRef]

Dimic, Nabojsa, Jarmo Kivisha, Vanja Piljak, and Janne Äijö. 2016. Impact of financial market uncertainty and macroeconomic factors on stock–bond correlation in emerging markets. *Research in International Business and Finance* 36: 41–51. [CrossRef]

Ehtesham, Qurat, and Danish Siddiqui. 2019. Analyzing Stock–bond Correlation in Emerging Markets. Research in Applied Economics. Available online: https://www.researchgate.net/publication/336283757_Analyzing_Stock--bond_Correlation_in_Emerging_Markets (accessed on 29 May 2020).

Engle, Robert F. 2002. Dynamic conditional correlation: A simple class of multivariate generalized autoregressive conditional heteroskedasticity models. *Journal of Business and Economic Statistics* 20: 339–50. [CrossRef]

Engle, Robert F. 2009. *Anticipating Correlations: A New Paradigm for Risk Management*. Princeton: Princeton University Press.

Forbes, Kristin, and Roberto Rigobon. 2002. No contagion, only interdependence: measuring stock market comovements. *Journal of Finance* 57: 2223–61. [CrossRef]

Glassman, Barry. 2018. The Most Confused Identity in Your Portfolio: High Yield Bonds. Available online: https://www.forbes.com/sites/advisor/2018/03/13/the-most-confused-identity-in-your-portfolio-high-yield-bonds/#cccd5ea2b8b6 (accessed on 30 May 2020).

Gulko, Les. 2002. Decoupling. *Journal of Portfolio Management* 28: 59–66. [CrossRef]

Hakkio, Craig S., and William R. Keeton. 2009. Financial stress: What is it, how can it be measured, and why does it matter? *Federal Reserve Bank of Kansas City Economic Review* 2: 5–50.

Hong, GWangheou, Youngsoo Kim, and Bong-Soo Lee. 2014. Correlations between stock returns and bond returns: income and substitution effects. *Quantitative Finance* 14: 1999–2018. [CrossRef]

Ilmanen, Antti. 2003. Stock–bond correlations. *Journal of Fixed Income* 13: 55–66. [CrossRef]

Jones, Paul M., and Eric Olson. 2013. The time-varying correlation between uncertainty, output, and inflation: Evidence from a DCC-GARCH model. *Economic Letters* 118: 33–37. [CrossRef]

Kwan, Simon H. 1996. Firm-specific information and the correlation between individual stocks and bonds. *Journal of Financial Economics* 40: 63–80. [CrossRef]

Li, Xiao-Ming, Bing Zhang, and Ruzhao Gao. 2015. Economic policy uncertainty shocks and stock–bond correlations: Evidence from the US market. *Economics Letters* 132: 191–96. [CrossRef]

Li, Erica X.N., Tao Zha, Ji Zhang, and Hao Zhou. 2019. Active Monetary or Fiscal Policy and Stock–bond Correlation. Available online: http://abfer.org/media/abfer-events-2019/annualconference/cebra/AC19P1019_Active_Monetary_or_Fiscal_Policy_and_Stock--bond_Correlation.pdf (accessed on 29 May 2020).

Newey, Whitney K., and Kenneth D. West. 1987. A simple, positive semi-definite, heteroskedasticity and autocorrelation consistent covariance matrix. *Econometrica* 55: 703–8. [CrossRef]

Panchenko, Valentyn, and Eliza Wu. 2009. Time-varying market integration and stock and bond return concordance in emerging markets. *Journal of Banking and Finance* 33: 1014–21. [CrossRef]

Pericoli, Marcello. 2018. Macroeconomics Determinants of the Correlation between Stocks and Bonds. Bank of Italy Working Paper No. 1198. Available online: https://ssrn.com/abstract=3429148 (accessed on 31 May 2020).

Tobin, James. 1969. A general equilibrium approach to monetary theory. *Journal of Money Credit and Banking* 1: 15–29. [CrossRef]

Whaley, Robert E. 2009. Understanding the VIX. *Journal of Portfolio Management* 35: 98–105. [CrossRef]

Yang, Jian, Yinggang Zhou, and Zijun Wang. 2009. The stock–bond correlation and macroeconomic conditions: One and a half centuries of evidence. *Journal of Banking and Finance* 33: 670–80. [CrossRef]

Yardeni, Edward. 1997. Fed's Stock Market Model Finds Overvaluation. US Equity Research, Deutsche Morgan Grenfell. Available online: http://www.yardeni.com/premiumdata/t_970825.pdf (accessed on 29 May 2020).

Yu, IP-Win, Kang-Por Fung, and Chi-Sang Tam. 2010. Assessing financial market integration in Asia—Equity markets. *Journal of Banking and Finance* 34: 2874–85. [CrossRef]

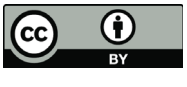

risks

MDPI

Article

How Do Health, Care Services Consumption and Lifestyle Factors Affect the Choice of Health Insurance Plans in Switzerland?

Veronika Kalouguina [1] and Joël Wagner [1,2,*]

[1] Department of Actuarial Science, University of Lausanne, Faculty HEC, Extranef, 1015 Lausanne, Switzerland; veronika.kalouguina@unil.ch
[2] Swiss Finance Institute, University of Lausanne, 1015 Lausanne, Switzerland
* Correspondence: joel.wagner@unil.ch

Received: 10 March 2020; Accepted: 25 April 2020; Published: 27 April 2020

Abstract: In compulsory health insurance in Switzerland, policyholders can choose two main features, the level of deductible and the type of plan. Deductibles can be chosen among six levels, which range from CHF 300 to 2500. While the coverage and benefits are identical, insurers offer several plans where policyholders must first call a medical hotline, consult their family doctor, or visit a doctor from a defined network. The main benefit of higher deductibles and insurance plans with limitations is lower premiums. The insureds' decisions to opt for a specific cover depend on observed and unobserved characteristics. The aim of this research is to understand the correlation between insurance plan choices and lifestyle through the state of health and medical care consumption in the setting of Swiss mandatory health insurance. To do so, we account for individual health and medical health care consumption as unobserved variables employing structural equation modeling. Our empirical analysis is based on data from the Swiss Health Survey wherein lifestyle factors like the body mass index, diet, physical activity, and commuting mode are available. From the 9301 recorded observations, we find a positive relationship between having a "healthy" lifestyle, a low consumption of doctors' services, and choosing a high deductible, as well as an insurance plan with restrictions. Conversely, higher health care services' usage triggers the choice of lower deductibles and standard insurance plans.

Keywords: medical services' consumption; lifestyle factors; insurance plan; structural equation model

1. Introduction

Health insurers try to foster healthy lifestyles among their insureds by promoting exercise, supporting fitness center memberships, and more recently, the use of wearable connected devices. The data collected from the latter permit insurance companies to track the individual's physical activity, diet, or sleep patterns for instance. Subsequently, insureds carrying on a healthy lifestyle benefit from premium discounts or other kinds of monetary rewards. Why health insurers promote a healthy lifestyle is not unfounded. There is a strand of medical literature assessing the effect of the lifestyle on health documenting that a healthier lifestyle leads to better health, relating to lower medical costs (Johansson and Sundquist 1999; Andersen et al. 2000; Lee and Skerrett 2001; Joshipura et al. 2001; Penedo and Dahn 2005; Dauchet et al. 2006; Inyang and Okey-Orji 2015; Miller et al. 2017). However, the relationship between health and health insurance decisions has been sparsely investigated. While there is a clearly demonstrated link between lifestyle and health in the medical literature, this relation has not been used in actuarial science, leaving the field with little or no evidence of the effect of lifestyle on health insurance decisions.

In our study, using data from the Swiss Health Survey (SHS), we aim to seize the indirect effect of lifestyle—encompassed by the body mass index (BMI), diet, physical activity and commuting mode—on health insurance decisions, i.e., the choice of the plan and the level of deductible. We consider that the decisions are mediated through latent variables linked to health and health care consumption. We set up a structural equation modeling (SEM) framework that allows capturing such indirect effects. We define health as a latent variable embodied by the self-assessed health, as well as chronic and limiting daily activities health conditions. Thereby, the latter offer an objective measure. Further, health directly impacts health care consumption, our second latent variable captured by the number of doctor visits and hospital stays. Additionally, the model is able to account for the bidirectional relationship between health care consumption and the choice of the insurance plan and the deductible level.

The results from our model provide empirical support for the correlation between health insurance choice and lifestyle via health and health care consumption. Using 9301 observations obtained from the SHS dataset, we control the choice of deductible and insurance plan for socio-economic characteristics (gender, nationality, education, income, number of children in the household, importance of freedom of choice of the specialist doctor, linguistic region, and urbanization) and allow for the two endogenous variables to correlate. We show that an increase in age and BMI correlates with a decrease in health, whereas an increase in the number of portions of fruits and vegetables eaten per day, the number of physical activities performed in a week, and the usage of a bike to commute correlates with an increase in health. Further results display a negative correlation between health and health care consumption, where the latter variable is positively associated with the choice of a standard, i.e., non-restricting, health insurance plan. Similarly, an increase in health care consumption correlates positively with a low level of deductible. Linking our results, we obtain the indirect effect of lifestyle on insurance decisions. Thereby, an increase in age and BMI is associated with having a low deductible and opting for a standard insurance plan whereas, having a "healthy" lifestyle (good diet and physical activity) correlates with having a high deductible and preferring a more restrictive insurance plan at lower cost.

The remainder of this paper is organized as follows: In Section 2, we briefly review the Swiss health insurance system, as well as the literature related to the development of our research hypotheses. In Section 3, we pursue the setup of the model. Results are displayed along with a discussion in Section 4. Finally, we conclude in Section 5.

2. Background Information and Research Hypotheses

2.1. Insurance Plans and Deductibles in the Swiss Health System

Before developing our research, we expose some basic features of the Swiss health insurance system that are relevant for the matter of this study. Basic health insurance in Switzerland is mandatory and regulated by Federal law, which sets up the reimbursement policies. Under Federal law, basic health insurance coverage is compulsory for all residents and organized through private insurance companies. All insurance companies proposing basic health insurance are obliged to accept any individual independently of the health status. Premiums are calculated by the insurers, are determined by regions along cantons and urbanicity, and are validated by the Swiss government. Note that prices are the same for all individuals within the three age classes: up to 18 years, 19 to 25 years, and 26 years or more. Thus, insurers are not allowed to take into account other variables like gender, exact age, or health status. Beyond the basic plan, individuals can subscribe to private complementary health insurance. Regarding the catalog of reimbursements, on the one hand, the basic plan covers basic health risks, but does not extend to dental treatments, to alternative medicine techniques, nor to glasses or lens purchases, with exceptions made for some specific medical conditions. On the other hand, complementary health policies cover the costs that go beyond the basic insurance scheme. In this study, we focus on the decisions on basic health insurance by individuals aged 18 years and older. These individuals face several choices for their insurance plan and deductible level.

2.1.1. Insurance Plans

The insurance policies currently offered in Switzerland can be grouped into four families. The first plan is the "standard" plan, and it is chosen by most individuals. This policy offers the freedom of choice to visit any doctor or specialist and presents no specific restriction. This plan has the highest premium. The second most popular plan is the so-called "family doctor" model. Its peculiarity lies in the importance of the general practitioner (GP) that acts as a gatekeeper and centralizes information of the individual. Indeed, holders of this type of policy commit to always consulting the same GP in case of any health issues. They have to chose their doctor in advance from a list of recognized GPs provided by their health insurer. As a gatekeeper, the GP transfers the patient to a specialist if necessary. This plan typically displays premiums that are 15 to 20% lower than those of standard plans. The third most common plan is known as "CallMed". As its name suggests, this model brings the constraint of calling a medical hotline prior to physically seeking advice from a doctor. Depending on the specific policy rules, there may be an unrestricted choice of the doctor after the phone consultation. Policyholders from this scheme profit from premium reductions of up to 20%. Finally, there is the "HMO" model where the acronym stands for health maintenance organization. Under this model, the insureds commit to always pass through a doctor affiliated with the selected HMO group for a first consultation. Like in the CallMed model, if necessary, the following consultation may take place outside of the HMO medical team, depending on the health insurer. This last type of plan can come with premiums up to 25% below the standard plan.

2.1.2. Deductible Levels

In all insurance plans and on a yearly basis, policyholders chose a deductible. Here, the decision environment is less complex. With amounts regulated by the health insurance law, there exist six levels of deductibles, namely CHF 300, 500, 1000, 1500, 2000, and 2500. Once medical costs up to the chosen level are paid out-of-pocket, there only remains a co-payment of 10% up to CHF 700 on the additional costs, whereafter the health insurer entirely reimburses the spending.

2.2. Literature Review and Development of the Hypothesis

While partial insights into our research can be gained by studying descriptive statistics, we propose to structure our analyses around selected conjectures and embed the latter in the body of existing literature. A recent study conducted by Li et al. (2018) identified five health risk-reducing lifestyle factors. Among them, three characteristics are of particular interest for our study. Indeed, three lifestyle indicators are found to play a role in mortality. More specifically, life expectancy increases with a BMI ranging between 18.5 and 24.9, 30 min or more per day of exercising, and a healthy diet. In addition to these measures, we considered in our research another factor: the commuting mode. This variable has been found to be a relevant factor for health conditions in the literature (Oja et al. 1991; Pucher et al. 2010 and Riiser et al. 2018). Since these factors are relatively easily trackable and modifiable, as opposed to, for example, alcohol or tobacco consumption, we used them as determinants for lifestyle.

2.2.1. BMI

The effect of BMI on health outcomes has been extensively studied, and the results are unambiguous. In reports published as early as 1959, the Society of Actuaries has assessed this link by studying the relationship between mortality rates and weight (Society of Actuaries 1959; Courtland C. and Edward A. 1979). It was found that as weight increases, so does the mortality rate. Following studies have confirmed and extended the negative effect of a high BMI on health. Indeed, a higher BMI is associated with a higher risk for coronary heart disease (CHD), cardiovascular disease (CVD), and for congestive health failure (Hubert et al. 1983; Jousilahti et al. 1996). An increase in BMI also increases the vulnerability to endometrial, sigmoidal, colorectal, and hormone-related cancer and type II diabetes (non-insulin dependent diabetes mellitus; see Pi-Sunyer 1991; Le Marchand et al. 1992; World Health Organization 2000; Stommel and

Schoenborn 2010). Overall, a higher BMI is associated with higher incidence rates of diseases (see also, e.g., Felson et al. 1992; Stommel and Schoenborn 2010).

2.2.2. Diet

The old adage "You are what you eat" has been proven right in multiple stances. Two literature reviews (Block et al. 1992; Steinmetz and Potter 1996) assessed the incidence of fruit and vegetable intake on several cancers, reporting their protective effect. A healthier diet composed of a greater number of fruits and vegetables decreases the likelihood of cancers like esophagus, pancreas, and breast cancer. Other studies focused on the beneficial impact of an increase of fruit and vegetable consumption on CHD or CVD and reported a lower incidence, as well as lower mortality related to heart deficiencies (Joshipura et al. 2001; Bazzano et al. 2002; Dauchet et al. 2006; Oyebode et al. 2014; Miller et al. 2017).

2.2.3. Physical Activity

Similar to the effect of the diet on health, the positive effect of physical activity on health is well established. A literature review conducted by Warburton et al. (2006) assessed 152 studies and highlighted that increased levels of physical activity were found to reduce relative risks of death by 20 to 35%; inversely, individuals in the lowest quantiles of physical activity had an increased risk of death from any cause compared to those in the top quantiles. They also accounted for a reduced incidence of type II diabetes in those individuals who reported weekly physical activity. Other studies also investigated this relationship and backed up the review of Warburton et al. (2006). Johansson and Sundquist (1999), Lee and Skerrett (2001), and Matthews et al. (2007) associated a higher frequency of physical activity to a reduced mortality rate and better overall health, while Gerhardsson et al. (1988), Thune et al. (1997), Thune and Furberg (2001), and Penedo and Dahn (2005) related a less active lifestyle to increased risks of colon, breast, prostate, and colorectal cancers.

2.2.4. Commuting Mode

The mode of commuting most frequently used to go to work, to school, for grocery shopping, or other activities is an integral part of the lifestyle definition. The medical literature has especially aimed its attention at walking and cycling as a means of transportation. Most papers pool together individuals who walk or cycle to commute; when a distinction was made, the results may present slight differences, but overall, they pointed to similar effects. For instance, Oja et al. (1991) and Riiser et al. (2018) both found a positive effect of walking or cycling on health measures such as having a high level of good cholesterol (HDL) or a decreased heart rate and systolic tension. The authors also identified an inverse relationship between walking or cycling to work and the risk of having diabetes, results that were equally found by Pucher et al. (2010). Aside from these pooled analyses, the literature review by Oja et al. (1991) focused on the effect of cycling on health. Of the 16 cycling-specific studies considered therein, all but two showed that cycling provided a health benefit and particularly for CVD and CHD risks.

Conjecture 1. An increase in BMI negatively influences health, while an increase in fruit and vegetable intake and an increase in physical activity frequency positively relate to health. Walking and cycling for commuting also enhance health.

2.2.5. Health Care Utilization

The usage of health care services is most often approximated by the number of doctor visits (GP and specialist), outpatient and inpatient hospitalization, or drug use. In the literature from the medical and economics fields, health care seeking has been studied under several perspectives, theoretically and empirically (to cite a few, Grossman 1972; Pohlmeier and Ulrich 1995; Ang 2010). Many of them addressed the demand for health care from a socio-economic, including from an insurance, point of view. However, health, as a determinant, has seldom been investigated, as the relationship may seem

trivial. Fylkesnes (1993) found that self-rated health was the most important driver of health care utilization.

Another factor that could lead to the increase in health care consumption is the enrollment in health insurance. This incentive effect has been extensively studied, and the conclusion was shared among the literature reviews of Schmitz (2012) and Prinja et al. (2017): insurance take up leads to an increase in health care services' utilization. Schmitz (2012) specified that insurance plans with a deductible had lower consumption compared to plans without such a feature. Gardiol et al. (2005) performed this analysis in Switzerland and outlined that 25% of health care expenditures could be attributable to the incentive effect linked to deductibles. Further, alternative plans have been introduced in Switzerland to contain health costs by limiting doctors' visits through the primary usage of telephone hotlines and directing patients to the most efficient doctors' networks. Thus, we expected health care utilization to be negatively linked to alternative insurance plans.

Conjecture 2. Health is the most important driver of health care consumption. As health improves, health care consumption declines. Further, a low deductible and standard insurance plan should incentivize health care consumption.

2.2.6. Insurance Demand

The empirical literature on health insurance demand is relatively limited. Firstly, health as a component of the decision-making process has been less exploited, probably due to the endogeneity it may present and the difficulty to deal with it. Secondly, papers rather address the demand for complementary (private) health insurance through expected health care expenditures. In our context, we focused on the choices made in a compulsory health insurance environment. Finally, we note that other socio-economic variables have nonetheless been used as drivers of health insurance demand: e.g., gender, age, marital status, country of origin, education, occupation, or income (Van de Ven and Van Praag 1981; Cameron et al. 1988). Among these covariates, it is the effect of income that has been the most extensively estimated (see Schneider 2004 for a literature review). It is needless to emphasize the lack of empirical evidence linking health and health insurance demand, let alone the effect of lifestyle. Our research aims at providing an instance of the relationship between lifestyle and health insurance demand via the health and health care consumption channels.

Conjecture 3. The effect of socio-economic covariates, namely gender, education, and income, on decisions for the insurance plan and the deductible is significant.

Linking the arguments on health, health care utilization, and insurance demand, we further propose the following conjecture:

Conjecture 4. The effect of health through health care consumption is believed to be significant for the health insurance decisions. Higher health care usage is associated with a low deductible and a standard insurance plan.

Finally, it is interesting to consider Conjectures 2 and 4 together. When reconsidering Conjecture 2, we can state that riskier individuals, i.e., unhealthy individuals, come along with higher health care consumption, which, in line with Conjecture 4, is associated with choosing a standard insurance contract with a low insurance deductible. This is aligned with the common contributions in the insurance economics literature (Zweifel and Eisen 2012). In our model framework, we will consider the bidirectional relationship between health care consumption and insurance decisions. Indeed, while our main interest is on how one's own health and health care consumption trigger insurance decisions (deductible, insurance plan). We know from the economics literature that a given insurance coverage will also have an impact on the consumption (cf. the presence of moral hazard; see the above discussion in the section "Health Care Utilization").

3. Model Framework and Available Data

3.1. Structural Equation Model

To study the above questions and conjectures, the choice of SEM was guided by the several advantages that this technique presents. Health is a difficult concept to quantify and is oftentimes estimated by its outcomes, namely chronic disease occurrence or mortality rates. This method, however, does not provide a complete, nor a sufficient picture of the individual's state of physical and mental well-being. In view of these elements, in our SEM model, we let health be a latent variable, influenced by the lifestyle. Doing so, we avoided at the same time any reporting bias and measurement errors of health-related variables (on which Crossley and Kennedy (2002) shed light). Indeed, some authors used the self-assessed health of the individual as a proxy for the unobserved health, especially in the labor market field (see Haan and Myck 2009; Strully 2009; Böckerman and Ilmakunnas 2009, for a few examples). The issue in this procedure lies in the unobserved characteristics such as risk aversion, which may, for instance, affect both one's own health perception and health insurance demand. Solely relying on the self-reported health at face value is also prone to severe measurement biases highlighted in the literature (mostly attributed to social desirability, discussed in Huang et al. 1998 and Van de Mortel et al. 2008). In an SEM setting, on the contrary, health can be captured by several more objective measures called manifest variables and, by this means, minimize the bias. The same rationale applies to the latent variable of health care seeking. Like health, the unobservable variable of the demand of health care services is a difficult notion to grasp by a single variable or even a set (as for instance in Bourne et al. 2009) and may be subject to omitted variables' bias. Again, SEM is well suited for using several variables at once to define the concept.

Additionally, in dealing with the above issues, SEM can indicate simultaneous direct relationships called paths. These paths can be specified as well between exogenous as between endogenous variables, thus allowing for a more thorough and exhaustive analysis. Because of this convenient ability of the model to assess the simultaneous relationship between multiple unobserved variables and observed outcomes, SEM frameworks have been widely used in the sociology- and psychology-related literature (Sobel 1987; Cuttance and Ecob 2009; MacCallum and Austin 2000; Martens 2005). Moreover, we note that usual econometric methodologies like fixed effects regressions cannot be applied in our context due to the cross-sectional nature of data from surveys. In an SEM, the estimation of the parameters comes from a maximization of likelihood between the actual covariance matrices of the relationships between variables and the estimated covariance matrices of the model (for more information, see Bollen 1989).

Our research aims to assess the relationship between lifestyle and health insurance decisions. Figure 1 gives a graphical representation of the model that we employed. We measured lifestyle from four behaviors, namely BMI (BMI), diet (DIT), sports (SPT), and commuting modes (CMW, CMB, CMP, CMV), while we controlled for age (AGE). In our model, however, lifestyle was not assumed to have a direct effect on insurance decisions (insurance plan PLN and deductible DED), but rather an indirect one mediated via health (HLT) and health care consumption (HCC). Health was hypothesized to play a role in health care usage, which in turn was conjectured to drive health insurance decisions, thus creating a bridge to lifestyle. Finally, the health insurance choice was controlled by socio-demographic characteristics (gender SEX, nationality NAT, education EDU and income INC levels, number of children in the household KID, freedom of choice for specialist doctors SPE, language region LNR, and urbanicity RUR). Further, health was measured using information on self-reported health SRH, chronic health conditions CHR, and limiting health conditions LIM, while health care consumption was evaluated from GP visits (GPV), specialist and gynecologist visits (SPV), and hospital stays (HOS). In Table 1, we summarize and describe the variables that we used.

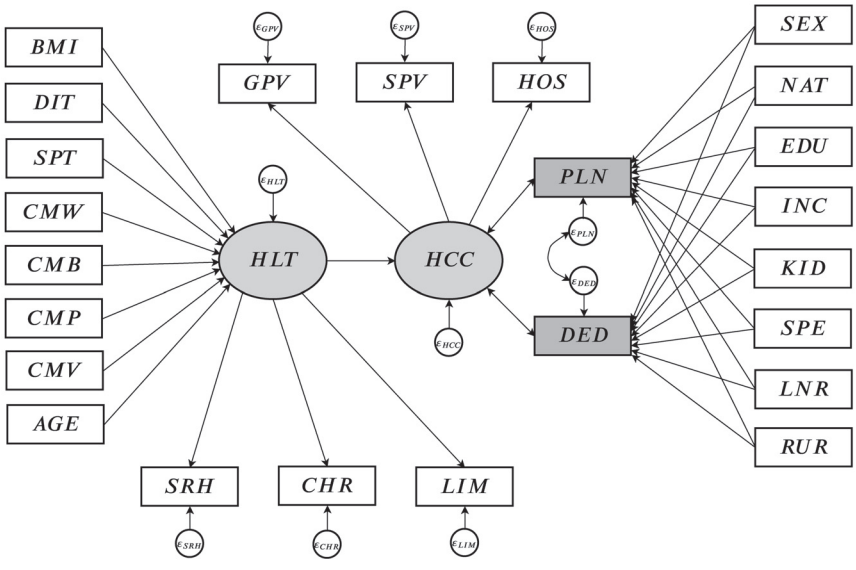

Figure 1. Illustration of the path diagram of the structural equation model.

Table 1. Description of the variables used in the model.

Variables	Type	Description	Values
AGE	Exogenous	Age	integer (19+)
BMI	Exogenous	BMI according to the WHO scale	categories: 0–18.4, 18.5–24.9, 25–29.9, 30+
DIT	Exogenous	Diet, portions of fruits and vegetables consumed on average per day	categories: 0–2, 3–4, 5+
SPT	Exogenous	Sports sessions with perspiration, per week	categories: 0, 1–2, 3+
CMW	Exogenous	Commuting mode: walking	no, yes
CMB	Exogenous	Commuting mode: biking	no, yes
CMP	Exogenous	Commuting mode: public transportation	no, yes
CMV	Exogenous	Commuting mode: motorized vehicle	no, yes
HLT	Latent	Health	–
SRH	Manifest	Self-reported health, (Likert scale)	0 (very bad), 0.25 (bad), 0.5 (average), 0.75 (good), 1 (very good)
CHR	Manifest	Chronic health conditions lasting at least 6 months	no, yes
LIM	Manifest	Limiting health conditions in everyday activities	no, yes
HCC	Latent	Health care consumption	–
GPV	Manifest	Number of general practitioner and family doctor visits in the past 12 months	integer
SPV	Manifest	Specialist and gynecologist visits in the past 12 months	integer
HOS	Manifest	Any hospital stays of at least one night	no, yes
SEX	Exogenous	Gender	male, female
NAT	Exogenous	Nationality	Swiss, other
EDU	Exogenous	Level of education	primary, secondary (professional and general), tertiary (professional and general)
INC	Exogenous	Level of income in CHF	categories: 0–3000, 3001–4500, 4501–6000, 6001+
KID	Exogenous	Number of children in household < 18 y.o.	categories: 0, 1, 2, 3, 4+
SPE	Exogenous	Freedom of choice of specialist important	no, yes
LNR	Exogenous	Language region	German, French, Italian
RUR	Exogenous	Rural region	no, yes
PLN	Endogenous	Insurance plan	standard, other (HMO, family doctor, telmed, other)
DED	Endogenous	Deductible in CHF	high (2500), low (300)

3.1.1. Measurement of Health

To run the analysis, we designed our model with health (HLT) as a latent variable. This latent variable was measured by three observed variables: the self-rated health (SRH), having or having had a chronic health condition lasting at least six months (CHR), and having health conditions limiting daily activities during the past six months (LIM). These three indicators were assumed to correlate perfectly with the unobserved health variable. We considered the following set of equations:

$$\begin{aligned} SRH_i &= \kappa_{SRH} HLT_i + \varepsilon_{SRH,i} \\ CHR_i &= \kappa_{CHR} HLT_i + \varepsilon_{CHR,i} \\ LIM_i &= \kappa_{LIM} HLT_i + \varepsilon_{LIM,i} \end{aligned} \tag{1}$$

In the system of Equation (1), κ_{SRH}, κ_{CHR}, and κ_{LIM} are the loading factors. $\varepsilon_{\cdot,i}$ are the error terms for the individual i linked to each of the indicator variables. For our modeling, we assumed the error terms to be uncorrelated with each other and with the latent variable HLT, as well as having an expectation value of zero.

3.1.2. Regression Model for Health

The following Equation (2) describes the regression of health on the lifestyle variables including a control for age as depicted in the left-hand part of the graph in Figure 1.

$$\begin{aligned} HLT_i = \beta_0 + \beta_{AGE} AGE_i + \beta_{BMI} BMI_i + \beta_{DIT} DIT_i + \beta_{SPT} SPT_i + \beta_{CMW} CMW_i \\ + \beta_{CMB} CMB_i + \beta_{CMP} CMP_i + \beta_{CMV} CMV_i + \varepsilon_{HLT,i} \end{aligned} \tag{2}$$

The respective β_0 and $\beta_\cdot$ coefficients correspond to the baseline, respectively the regression coefficients linked to the variables. The error term $\varepsilon_{HLT,i}$ was assumed to have a zero expected value and to be uncorrelated with the error terms in the other submodels.

3.1.3. Measurement of Health Care Consumption

Our second latent variable was the individual's inherent health care consumption (HCC). Three variables were used to approximate this behavior: the number of GP or family doctor visits (GPV), the number of specialists visits (SPV), and whether the respondent had an inpatient hospitalization (HOS). All three variables were accounted for during the past 12 months and were assumed to correlate perfectly with our unobserved health variable.

$$\begin{aligned} GPV_i &= \lambda_{GPV} HCC_i + \varepsilon_{GPV,i}, \\ SPV_i &= \lambda_{SPV} HCC_i + \varepsilon_{SPV,i}, \\ HOS_i &= \lambda_{HOS} HCC_i + \varepsilon_{HOS,i} \end{aligned} \tag{3}$$

In the system of Equation (3), λ_{GPV}, λ_{SPV}, and λ_{HOS} are the loading factors. $\varepsilon_{\cdot,i}$ denote the error terms for the individual i in each indicator variable. The errors were assumed to be uncorrelated with each other and with the latent variable HCC. Errors were supposed to have an expected value of zero.

3.1.4. Regression Model for Health Care Consumption

The following Equation (4) is the regression of health care consumption on health (HLT) and the insurance characteristics (plan PLN and deductible DED):

$$HCC_i = \delta_0 + \delta_{HLT} HLT_i + \delta_{PLN} PLN_i + \delta_{DED} DED_i + \varepsilon_{HCC,i} \tag{4}$$

The respective δ_0 and $\delta_\cdot$ coefficients correspond to the baseline, respectively the variables' regression coefficients. The error term $\varepsilon_{HCC,i}$ was assumed to have a zero expected value and to be uncorrelated with other error terms.

3.1.5. Regression Models for Health Insurance Decisions

The two following regressions express the choice of the insurance plan (PLN) and deductible level (DED) according to health care consumption and socio-demographic characteristics. The variable PLN takes the value of one if the respondent chooses an alternative plan (HMO, family doctor, telmed, other) and zero for the standard plan. Concerning the deductible levels DED, if the individual has opted for a yearly deductible of CHF 300, the variable takes the value of zero. The value is one if the chosen deductible is CHF 2500. Here, we built a simple model by selecting only the two extreme values because we considered that they unveiled a clear choice towards the highest versus the lowest coverage. We disregarded all individuals with other choices. The resulting respective probit models (choices 0 and 1) were modeled through latent variables. Indeed, for our SEM, we supposed there existed auxiliary random variables PLN^* and DED^* such that:

$$\begin{aligned} PLN_i^* = \gamma_0^{PLN} + \gamma_{HCC}^{PLN} \cdot HCC_i + \gamma_{SEX}^{PLN} \cdot SEX_i + \gamma_{NAT}^{PLN} \cdot NAT_i + \gamma_{EDU}^{PLN} \cdot EDU_i + \gamma_{INC}^{PLN} \cdot INC_i \\ + \gamma_{KID}^{PLN} \cdot KID_i + \gamma_{SPE}^{PLN} \cdot SPE_i + \gamma_{LNR}^{PLN} \cdot LNR_i + \gamma_{RUR}^{PLN} \cdot RUR_i + \varepsilon_{PLN,i} \end{aligned} \tag{5}$$

and:

$$\begin{aligned} DED_i^* = \gamma_0^{DED} + \gamma_{HCC}^{DED} \cdot HCC_i + \gamma_{SEX}^{DED} \cdot SEX_i + \gamma_{NAT}^{DED} \cdot NAT_i + \gamma_{EDU}^{DED} \cdot EDU_i + \gamma_{INC}^{DED} \cdot INC_i \\ + \gamma_{KID}^{DED} \cdot KID_i + \gamma_{SPE}^{DED} \cdot SPE_i + \gamma_{LNR}^{DED} \cdot LNR_i + \gamma_{RUR}^{DED} \cdot RUR_i + \varepsilon_{DED,i} \end{aligned} \tag{6}$$

for which we had PLN and DED variables acting as indicators:

$$PLN_i = \begin{cases} 1 & \text{if } PLN_i^* > 0 \\ 0 & \text{otherwise} \end{cases} \tag{7}$$

and:

$$DED_i = \begin{cases} 1 & \text{if } DED_i^* > 0 \\ 0 & \text{otherwise} \end{cases} \tag{8}$$

The values γ_0^{PLN} and $\gamma_\cdot^{PLN}$, respectively γ_0^{DED} and $\gamma_\cdot^{DED}$, follow the standard notations for regression coefficients. Further, the error terms $\varepsilon_{PLN,i}$ and $\varepsilon_{DED,i}$ were assumed to come from a standard normal distribution and were allowed to correlate with each other.

3.2. Swiss Health Survey Data

We based our study on data obtained from the Swiss Health Survey, a cross-sectional nation-wide survey (Swiss Federal Statistical Office 2019; Swiss Federal Statistical Office 2018).[1] The survey was carried out by the Swiss Federal Statistical Office on behalf of the Federal Council every five years since 1992. In the following, we used the wave of 2017, which was the sixth and most recent one. The survey responses were firstly collected via computer-assisted telephone interviews and followed up by an additional written questionnaire available in the three official Swiss languages (German, French, and Italian). The included population was aged 15 years or over and lived in Switzerland in a private household. The total sample of 2017 included 22,134 telephone interviews and 18,832 subsequently completed and returned questionnaires. The information collected concerned the state of health of each individual (e.g., physical and mental well-being, health conditions, health limitations),

[1] For more information, see https://www.bfs.admin.ch/bfs/fr/home/statistiques/sante/enquetes/sgb.html.

the use of health care (e.g., doctor consultations, hospitalization, use of drugs), the health insurance status (e.g., insurance plan, deductible, purchase of complementary insurance), behaviors susceptible to have an influence on health (e.g., alcohol intake, drug consumption), and socio-demographic characteristics (e.g., employment status, income, nationality).

To conduct our empirical analysis, we extracted a sample of "complete" answers comprising 9301 observations. The completeness of an observation was defined by the absence of entries that were not available (NA). We could consider that the NAs were distributed randomly across the original data since our extracted sample was not markedly different from the original one. Regrading the lifestyle indicators, our final sample had a slightly higher median age, i.e., 52 versus 49 years. As concerned the BMI, the diet (number of portions of fruits and vegetables eaten per day) or the frequency of physical activity[2], and commuting, the average values and shares were very close. Regarding the other exogenous variables, the original sample displayed the same level of self-rated health (good), and a smaller percentage had health conditions limiting daily activities, which was most probably due to a lower proportion of individuals aged over 50 years; our final sample contained a higher number of individuals with chronic health conditions. Overall, we considered that our extracted sample did not present any selection bias thanks to the sampling performed beforehand by the Swiss Federal Statistical Office and the relatively large sample size when compared to other surveys (where the number of observations is often considerably smaller).

3.3. Descriptive Statistics

3.3.1. Exogenous Characteristics Affecting Health

In Table 2, we present some descriptive statistics based on our data along with the variables appearing in our hypotheses. The lifestyle was conjectured to have an effect on health, which was defined in our model by the self-rated health (SRH), the past or ongoing existence of a chronic disease lasting for six months or more (CHR), and a health condition coming with a limitation in daily activities (LIM). Subsequently, through health, they impacted health care consumption, gauged in our model by the number of GP visits (GPV), the number of specialists visits (SPV, gynecologists excluded, to avoid pregnancy-related bias), and the individual's hospital stays of one night or over (HOS). The first column in Table 2 counts the number of observations N per category in each variable, while the second represents the corresponding share from the whole sample of 9301 observations (total N). The other six columns display the mean for each manifest variable. Over the total sample (cf. the last row of the table), the mean self-rated health was at 0.81, that is good health on average; 35% of the sample's population reported chronic, and 21% health conditions limiting daily activities. Alongside this, the average number of GP visits was 2.27, and the number of visits to specialists was 1.99. Finally, 18% of the sampled individuals stayed in a hospital for more than one night during the 12 months preceding the survey.

Concerning the lifestyle variables, when grouping individuals by BMI categories, we deciphered the pattern that was documented in the literature, i.e., respondents with a BMI comprised between 18.5 and 24.9 declared the highest self-rated health (0.84) and the lowest propensity of having a chronic or a limiting health condition (0.31 and 0.18). Additionally, as the BMI increased, the SRH decreased (from 0.84 to 0.72 for the category with highest BMI), and the proportion of individuals having chronic or limiting health conditions increased (moving from 0.31 and 0.18 to 0.50 and 0.30 for CHR, respectively LIM, in the group with the highest BMI), thus matching observations from the literature (cf. Section 2.2). An increase in BMI was also positively associated with health care services' utilization. According to our descriptive statistics, the effect of the diet on the health and health care usage proxies was mitigated. Two associations could be made: an increase in the number of fruits and vegetables

[2] Note that we excluded individuals not being able to walk at least 200 m by themselves.

eaten on average per day came with an increase in self-rated health (0.80 to 0.83), but also with an increase of visits to specialists (1.33 to 1.66). Further analysis, including the study of significance, was performed in our SEM. When it came to physical activity, however, the relationship seemed indisputable. As the frequency of sports activities increased, the data presented a clear increase in the self-rated health variable (0.74 to 0.85), coupled with a decrease in the occurrence of health conditions (0.42 to 0.30 for CHR and 0.26 to 0.18 for LIM). This beneficial association continued on health care seeking through all indicators where we observed declining consumption. Concerning the effect on the commuting mode, we observed that it largely depended on the type. Biking as a means of transportation exhibited the most notable link to our indicators: individuals who bike reported a higher self-rated health (0.85 against 0.80) and a lower in-group propensity to have a chronic or limiting health condition (0.33 versus 0.36 for CHR and 0.19 versus 0.21 for LIM). By the same token, the number of GP visits dropped from 2.42 to 1.82 on average, the number of visits to specialists from 1.48 to 1.32, and the inpatient stays going down by three percentage points. Finally, age displayed the expected effect, that is as age increased, the self-rated health decreased, and the propensity in each category of having a chronic or a limiting health condition increased, along with the frequency of all medical visits. Finally, to supplement our descriptive statistics, we document in Table 3 the correlation coefficients between our proxy variables, as well as their standard deviations.

Table 2. Descriptive statistics of the exogenous characteristics affecting health.

	N	(%)	*SRH*	*CHR*	*LIM*	*GPV*	*SPV*	*HOS*
BMI								
0–18.4	260	(2.8)	0.82	0.35	0.20	2.10	1.72	0.12
18.5–24.9	5075	(54.6)	0.84	0.31	0.18	1.99	1.37	0.10
25.0–29.9	2973	(32.0)	0.79	0.37	0.22	2.36	1.42	0.12
30.0+	993	(10.7)	0.72	0.50	0.30	3.42	1.76	0.17
Diet								
0–2 portions per day	4309	(46.3)	0.80	0.35	0.21	2.33	1.30	0.12
3–4 portions per day	3043	(32.7)	0.82	0.35	0.20	2.15	1.49	0.11
5+ portions per day	1949	(21.0)	0.83	0.35	0.21	2.30	1.66	0.11
Sports								
No activity	2947	(31.7)	0.74	0.42	0.26	2.91	1.72	0.14
1–2 times per week	3641	(39.1)	0.84	0.33	0.18	1.92	1.24	0.10
3+ times per week	2713	(29.2)	0.85	0.30	0.18	2.02	1.39	0.11
Commuting: walking								
No	4732	(50.9)	0.81	0.34	0.20	2.28	1.46	0.11
Yes	4569	(49.1)	0.81	0.36	0.21	2.25	1.42	0.11
Commuting: biking								
No	6892	(74.1)	0.80	0.36	0.21	2.42	1.48	0.12
Yes	2409	(25.9)	0.85	0.33	0.19	1.82	1.32	0.09
Commuting: public transport								
No	6000	(64.5)	0.81	0.34	0.20	2.30	1.38	0.12
Yes	3301	(35.5)	0.81	0.36	0.22	2.21	1.54	0.11
Commuting: motorized vehicle								
No	3092	(33.2)	0.81	0.35	0.21	2.23	1.50	0.11
Yes	6209	(66.8)	0.81	0.35	0.21	2.28	1.41	0.11
Age								
19–26	568	(6.1)	0.87	0.21	0.14	1.95	1.20	0.08
25–40	2117	(22.8)	0.87	0.23	0.13	1.80	1.38	0.11
41–50	1732	(18.6)	0.83	0.29	0.17	1.86	1.15	0.09
51–60	1840	(19.8)	0.79	0.38	0.21	2.28	1.71	0.10
61–70	1552	(16.7)	0.77	0.46	0.26	2.58	1.55	0.13
71–80	1173	(12.6)	0.75	0.48	0.31	3.06	1.61	0.17
81+	319	(3.4)	0.72	0.45	0.36	3.55	1.06	0.15
Total	9301	(100.0)	0.81	0.35	0.21	2.27	1.99	0.18

Table 3. Correlation coefficients and standard deviation of the indicator variables.

	SRH	***CHR***	***LIM***	***GPV***	***SPV***	***HOS***
SRH	1.00	−0.58	−0.50	−0.53	−0.46	−0.31
CHR	−0.58	1.00	0.49	0.35	0.27	0.14
LIM	−0.50	0.49	1.00	0.27	0.18	0.15
GPV	−0.53	0.35	0.27	1.00	0.51	0.39
SPV	−0.46	0.27	0.18	0.51	1.00	0.33
HOS	−0.31	0.14	0.15	0.39	0.33	1.00
Std. dev.	0.19	0.48	0.40	3.85	3.86	0.32

3.3.2. Exogenous Characteristics Affecting Health Insurance Decisions

In the following Table 4, we provide an overview of the distribution of the observations along the second set of exogenous variables, i.e., the socio-demographic characteristics, linked to insurance decisions. We provide the shares of individuals along the insurance plan and deductible choices. In addition to the control variables, we present the distribution along the health and health care utilization indicator variables.

Firstly, when comparing the statistics of health insurance decisions based on socio-demographic variables, we observed several trends. Between both genders, we noted one important difference with women being more likely to choose a lower deductible when compared to men (65.9% of the women, 52.2% of the men). Regarding the nationality, Swiss nationals tended to opt more often for an alternative plan, whereas non-Swiss individuals rather went for the standard one. Education, income, and the number of children in the household seemed to demonstrate differences. As the level of education, income, or the number of children increased, the majority switched from the low to the high level of deductible. Moreover, increasing education levels came along with a favor for alternative insurance plans. Along the two other variables, the majority already favored alternative plans with a slight increase in the share as income and number of children became higher. Finally, the last markedly different result with respect to the socio-demographic variables was the specificity of German-speaking respondents regarding the choice of the insurance plan: most individuals from the German-speaking language area tended towards alternative models, which was not the case in the French- and Italian-speaking regions.

Secondly, when focusing on health-related variables, we observed that higher levels of self-rated health went along with individuals that had chosen the high level deductible, as well as an alternative insurance plan. This observation was not at odds with economic logic as an individual with a lower self-rated health may expect to have higher yearly expenses and hence would prefer to pick a model with a higher coverage. The same observation could be drawn for individuals disclosing chronic or other limiting health conditions. The distribution of individuals who did not report having or having had any chronic health conditions was fairly even among both models (43.3% standard) and deductible levels (49.7% low). For individuals with a limiting health condition, the figures were still very similar. When focusing on people reporting any chronic or limiting health conditions, the shares regarding the model choices remained in fact relatively stable, but presented a strong increase in the share opting for the low deductible, i.e., 77.8% for *CHR* and 78.5% for *LIM*.

Finally, concerning our manifest variables accounting for health care consumption, the observations met the economic intuition. Regarding the models, the relationship was constant: as the number of visits, disregarding the type of doctor, increased, health care consumption did as well. Respondents typically favor an alternative insurance plan. Strong differences appeared with regard to the deductible. As an example, individuals not reporting any visits to a GP were 36.6% in the low deductible category; this percentage rose to 84.4% for those reporting four visits or more during the past 12 months. The same pattern could be observed throughout all three variables.

Table 4. Descriptive statistics of the exogenous characteristics affecting insurance decisions.

			Insurance Plan		Deductible	
	N	**(%)**	**Std. (%)**	**Oth. (%)**	**Low (%)**	**High (%)**
Gender						
Male	4343	(46.7)	43.9	56.1	52.2	47.8
Female	4958	(53.3)	43.1	56.9	65.9	34.1
Nationality (baseline: Swiss)						
Swiss	7633	(82.1)	40.7	59.3	60.3	39.7
Other	1668	(17.9)	55.8	44.2	55.6	44.4
Education						
Primary	1152	(12.4)	55.2	44.8	83.4	16.6
Secondary: professional	3384	(36.4)	44.6	55.4	68.0	32.0
Secondary: general	1213	(13.0)	43.9	56.1	57.0	43.0
Tertiary: professional	1280	(13.8)	33.8	66.2	50.9	49.1
Tertiary: general	2261	(24.3)	40.6	59.4	40.7	59.3
Income						
0–3000	3502	(37.7)	45.8	54.2	70.1	29.9
3001–4500	1949	(21.0)	45.9	54.1	64.5	35.5
4501–6000	1738	(18.7)	39.8	60.2	54.0	46.0
6001+	2112	(22.7)	40.2	59.8	41.7	58.3
Children in household						
0	6720	(72.3)	45.6	54.4	65.9	34.1
1	354	(3.8)	42.1	57.9	56.8	43.2
2	774	(8.3)	42.4	57.6	45.1	54.9
3	220	(2.4)	43.6	56.4	47.3	52.7
4+	1233	(13.3)	32.5	67.5	36.4	63.6
Freedom of choice of specialist important						
No	2436	(26.2)	33.9	66.1	52.4	47.6
Yes	6865	(73.8)	46.8	53.2	62.0	38.0
Language region						
German	6273	(67.4)	39.0	61.0	60.1	39.9
French	2295	(24.7)	52.6	47.4	58.8	41.2
Italian	733	(7.9)	53.1	46.9	56.3	43.7
Rural region						
No	6412	(68.9)	44.6	55.4	59.5	40.5
Yes	2889	(31.1)	40.9	59.1	59.4	40.6
Self-rated health						
Very bad	32	(0.3)	46.9	53.1	87.5	12.5
Bad	212	(2.3)	57.5	42.5	93.4	6.6
Average	1020	(11.0)	51.9	48.1	90.3	9.7
Good	4218	(45.3)	43.2	56.8	66.6	33.4
Very good	3819	(41.1)	40.6	59.4	41.2	58.8
Chronic health conditions						
No	6062	(65.2)	43.3	56.7	49.7	50.3
Yes	3239	(34.8)	43.7	56.3	77.8	22.2
Limiting health conditions						
No	7385	(79.4)	43.2	56.8	54.5	45.5
Yes	1916	(20.6)	44.5	55.5	78.5	21.5
Visits to general practitioner						
0	2623	(28.2)	43.0	57.0	36.6	63.4
1	2459	(26.4)	41.7	58.3	54.0	46.0
2–3	2503	(26.9)	43.9	56.1	71.5	28.5
4+	1716	(18.4)	45.9	54.1	84.8	15.2
Visits to specialist						
0	5111	(55.0)	42.7	57.3	50.0	50.0
1	1977	(21.3)	42.1	57.9	64.9	35.1
2–3	1265	(13.6)	44.6	55.4	74.6	25.4
4+	948	(10.2)	48.6	51.4	78.7	21.3
Hospital inpatient stay						
No	8243	(88.6)	43.3	56.7	57.3	42.7
Yes	1058	(11.4)	44.3	55.7	76.5	23.5
Total	9301	(100.0)	59.5	40.5	43.4	56.6

4. Model Results and Discussion

In this section, we document the SEM results for our health measurement for the model defined through Equation (1), followed by the regression model for health, i.e., the coefficients of the lifestyle effects on health (see Equation (2)), the health care consumption measurement as modeled through Equation (3), succeeded by the health care consumption regression (Equation (4)). Finally, we present the results for the regression models on health insurance demand for both insurance plan (Equation (5)) and deductible (Equation (6)).

We estimated the SEM using diagonally weighted least squares, which best fits binary observed variables as it does not make any distributional assumptions, nor consider continuity contrary to the maximum likelihood method (for more information, see Muthén 1984 or Li 2016). To run our empirical analysis, we made use of the lavaan package in R (Rosseel 2012). Before presenting the model results and coefficients, we lay out the goodness-of-fit measures. The measures and indicators calculated for the overall model were the following. We obtained a comparative fit index (CFI) of 0.959 and a Tucker–Lewis index (TLI) of 0.995 for the incremental fit measures and a root mean squared error of the approximation (RMSEA) of 0.028 and a standardized root mean squared residual (SRMR) of 0.043 for the absolute fit indices. According to the cut-off values of Hooper et al. (2008), our model presented a good fit, and an RMSEA lower than 0.03, as in our case, was indicative of an excellent fit. In the following paragraphs and Tables 5–9, we display our results.

4.1. Measurement of Health

Our first results were on the establishment of the health latent variable. We set the loading factor κ_{SRH} to one as it set the scale of the HLT variable. The model results in Table 5 lay out that, expectedly, as individuals reported chronic or limiting health conditions, their health significantly decreased. Indeed, both variables CHR and LIM were highly significant at the 0.001 p-level, and the related κ coefficients were negative.

Table 5. Results for the measurement of health (Equation (1)).

	Health Measurement	
	κ	**Sig.**
$SRH_i \sim \kappa_{SRH} HLT_i$	1.000	
$CHR_i \sim \kappa_{CHR} HLT_i$	−1.760	***
$LIM_i \sim \kappa_{LIM} HLT_i$	−1.047	***

Note: *** $p < 0.001$.

4.2. Regression Model for Health

In Table 6, we report the coefficients stemming from the regression Equation (2), i.e., the results for the effect of lifestyle-defining behavior on the latent health variables. The first variable of interest was the BMI, and the displayed results were in line with the existing literature. The baseline category was a BMI ranging from 18.5 and 24.9 and showing no statistical difference with the lower category of BMI. However, when moving to higher categories, the obtained regression coefficients suggested that the negative effect on health became more salient: the value of the coefficient was multiplied by a factor of three between the third and last group, both coefficients being highly significant at the 0.001 level. Regarding the diet variable, which was characterized by the number of fruits and vegetables eaten on average per day, there was no strong effect in our sample. The only change in health may occur from an increase from 0–2 portions per day to 3–4 resulting in an increase with a 0.1 significance level. This result was somehow expected from our descriptive statistics where no striking differences between the several categories were observed. Sports activities when compared to the baseline of no activity were significantly linked to better health. When comparing individuals performing 1–2 sessions or 3+ sessions per week with the baseline, we observed very similar coefficient values. That is, an increase in

the number of sessions enhanced health rather similarly between both categories with a coefficient of 0.053 (1–2 sessions), respectively 0.057 (3+ sessions). We note that our findings concerning diet and sports were found to follow the same pattern as in Blanchard et al. (2004). Indeed, they found that among cancer survivors, individuals following the five fruits and vegetables per day recommendation did not witness an increase in their health-related quality of life contrary to individuals who performed physical activities. If we classified the commuting modes according to their impact on health, biking would be the most interesting way of transportation in this regard, and walking would come second. The stronger effect of biking rather than walking was also documented by Matthews et al. (2007). Using a motorized vehicle was still linked to better health, but with a lower significance (p-value of 0.1); using public transport was linked to worse health (significance level of 0.1). Finally, with increasing age, individuals had worse health levels. Overall, having a BMI lower than 25, eating three to four portions of fruits and vegetables per day on average, exercising with perspiration at least once per week, and biking or walking as a way to commute represented a lifestyle relating to better health. In the opposite manner, having a high BMI, a greens-deprived diet, as well as a sedentary lifestyle were linked to worse health levels. These results supported and specified our first conjecture.

Table 6. Results for the regression model for health (Equation (2)).

	Health	
	β	**Sig.**
BMI category (baseline: 18.5–24.9)		
0–18.4	−0.016	
25.0–29.9	−0.032	***
30.0+	−0.090	***
Diet (baseline: 0–2 portions per day)		
3–4 portions per day	0.007	.
5+ portions per day	0.002	
Sports (baseline: No activity)		
1–2 times per week	0.053	***
3+ times per week	0.057	***
Commuting mode: walking (baseline: No)		
Yes	0.010	*
Commuting mode: biking (baseline: No)		
Yes	0.016	***
Commuting mode: public transport (baseline: No)		
Yes	−0.008	.
Commuting mode: motorized vehicle (baseline: No)		
Yes	0.008	.
Age (baseline: 25–40)		
19–24	−0.001	
41–50	−0.029	***
51–60	−0.061	***
61–70	−0.080	***
71–80	−0.103	***
81+	−0.107	***

Note: . $p < 0.1$, * $p < 0.05$, *** $p < 0.001$.

4.3. Measurement of Health Care Consumption

Moving to the second latent variable construction defined in Equation (3), we set the loading factor λ_{GPV} to one defining the scale of the health care consumption variable HCC. From the results in Table 7, one can observe a positive relationship between the number of visits to specialist doctors or inpatient stays and health care consumption (both with a p-level of 0.001).

Table 7. Results for the measurement of health care consumption (Equation (3)).

Health Care Consumption Measurement		
	λ	**Sig.**
$GPV_i \sim \lambda_{GPV} HCC_i$	1.000	
$SPV_i \sim \lambda_{SPV} HCC_i$	0.828	***
$HOS_i \sim \lambda_{HOS} HCC_i$	0.042	***

Note: *** $p < 0.001$.

Regression Model for Health Care Consumption

In Table 8, we display the results of the variables conjectured to affect health care consumption. Undoubtedly, health had the strongest impact on health care consumption. Indeed, the health variable was highly significant at the 0.001 p-value level and showed a negative sign, i.e., better health came with lower care consumption. This confirmed the first part of the second conjecture.

Table 8. Results for the regression model for health care consumption (Equation (4)).

	Health Care Consumption	
	δ	**Sig.**
Health		
	−14.109	***
Insurance plan (baseline: standard)		
Other	0.096	.
Deductible (baseline: Low)		
High	0.284	*

Note: . $p < 0.1$, * $p < 0.05$, *** $p < 0.001$.

Further, we found that the type of plan, as well as the level of deductible played some role in the amount of health care services used. Our results suggested that an alternative insurance plan and a high level of deductible were related to higher health care consumption. These results were counterintuitive since higher deductibles and alternative insurance plans were thought to diminish care service utilization (see our Conjecture 2 and Gardiol et al. 2005; Schmitz 2012; Prinja et al. 2017). First, care must be taken when concluding since significance levels for both variables were much less strong then the one for the health variable. Second, the results contradicted our findings from the "reverse" regression models in Equations (5) and (6) where health care consumption was a predictor for insurance decisions (see below). Finally, the observed relationship linking the high deductible to higher consumption might be that individuals who already experienced expenses reaching the deductible may want "to make the most out of it" and use more services that they have been postponing beforehand. Thus, individuals with a low deductible may have less incentives to "overuse" health care services. More research, beyond the data available to us, is needed to resolve this issue.

At this stage, we remained with the one conclusion that health status was probably the single primary driver for health care consumption.

4.4. Regression Models for Health Insurance Decisions

Finally, we now turn to the probit regression models defined in Equations (5) and (6) linking the previously discussed variables and results to health insurance decisions. The results are presented in Table 9. We considered two insurance decisions. The first column of the table reports the coefficients of the model related to the decision of choosing an alternative or "other" insurance plan (versus the baseline of the standard plan). The second part of the table relates to choosing the high deductible (versus the baseline of the low deductible). The first and foremost result concerned health care consumption. For both the alternative insurance plan and the high level of deductible choices,

HCC displayed a negative sign with statistical significance above 0.001. This meant that higher care utilization went along with the choice of the standard insurance plan and the low deductible. This confirmed our fourth conjecture. It is noteworthy that both coefficients were statistically very strong (as was for example the case of health on health care consumption in Table 8). Assembling the results from the entire model, we could put forward the following reasoning: when we defined a healthy lifestyle as having a low BMI, a diet of 3+ portions of fruits and vegetables per day, practicing sports or commuting by bike or walking, such a lifestyle enhanced health; higher levels of health were associated with lower health care consumption, which in turn correlated with the choice of an alternative insurance model and a high deductible.

Table 9. Results for regression models for health insurance demand (Equations (5) and (6)).

	"Other" Insurance Plan		"High" Deductible	
	γ	Sig.	γ	Sig.
Health care consumption				
	−0.030	***	−0.308	***
Gender (baseline: Male)				
Female	0.059	.	−0.405	***
Nationality (baseline: Swiss)				
Other	−0.362	***	−0.060	
Education (baseline: primary)				
Secondary: professional	0.198	***	0.462	***
Secondary: general	0.105	*	0.271	***
Tertiary: professional	0.314	***	0.486	***
Tertiary: general	0.191	***	0.627	***
Income (baseline: 0–3000)				
3001–4500	0.003		−0.001	
4501–6000	0.064		0.052	
6001+	−0.004		0.229	***
Children in household (baseline: 0)				
1	0.067		-0.108	
2	0.058		0.021	
3	−0.005		0.039	
4+	0.201	***	0.115	*
Freedom of choice of specialist important (baseline: No)				
Yes	−0.317	***	−0.268	***
Language region (baseline: German)				
French	−0.284	***	0.064	.
Italian	−0.235	***	0.258	***
Rural region (baseline: No)				
Yes	0.059	.	0.099	**

Note: . $p < 0.1$, * $p < 0.05$, ** $p < 0.01$, *** $p < 0.001$.

Regarding the further control variables, we found several significant relationships that supported Conjecture 3. For example, we observed that women rather tended to prefer a low level of deductible when compared to men. Another notable difference lied in the choice of the insurance plan regarding the nationality: non-Swiss individuals rather selected a standard insurance plan while Swiss individuals, who might be more knowledgeable about the system and have a family doctor, rather went for other plans (p-value of 0.001). Next, an increase in the level of education correlated with the choice of an alternative insurance plan and a higher level of deductible. This might correlate with better system understanding or potentially an interaction with better health. Similarly, individuals from very high income classes rather selected a higher deductible. This somewhat unexpected observation about wealthier families opting for the higher level of deductible may be explained by two factors. Firstly, in Switzerland, health insurance subsidies are commonplace, and they may incentivize the uptake of a lower deductible. The second element could be the diminishing level of risk aversion with

wealth. As highlighted by, e.g., Schneider (2004), less wealthy households may be more risk averse than wealthier ones as unexpected medical expenses could push them into financial distress. Concerning the number of children in the household, only the last category was markedly different with larger households going for the less expensive alternative plan and the high deductible. Further, we found that respondents for whom the freedom of choice for the specialist doctor was important preferred the standard insurance plan and a low level of deductible. This was intuitive. Finally, our model included geographical control variables, as well as a variable controlling for urbanicity. We observed regional differences between German-speaking respondents and French- or Italian-speaking ones. The latter rather chose a standard insurance plan, but a high deductible (as seen already from the descriptive statistics). Regarding rural regions, individuals were more prone to choose an alternative insurance plan coupled with a high deductible.

5. Concluding Remarks

Using data from the Swiss Health Survey, we successfully established the relationship between lifestyle-defining behavior and decisions in a compulsory health insurance environment. Employing a structural equation model with health and health care consumption characterized by latent variables, we gave proof for the following conjectures. Firstly, we empirically demonstrated that an increase in BMI was negatively correlated with health, whereas an increase in fruit and vegetable intake, as well as an increase in the number of sports sessions with perspiration were linked to better health. Additionally, we found that biking and walking for commuting were also related to better health. Secondly, our results indicated health as being the most significant driver of health care consumption. In a third step, we confirmed that socio-economic, as well as geographic covariates played a role in health insurance decisions. Finally, we were able to document the positive relationship between the choice of an alternative health insurance plan coupled with a high deductible in the case where health care consumption was lower. Bridging the different findings, we understood that health-enhancing behavior correlated with decreased health care services' consumption, the choice of an alternative health insurance plan, and a high level of deductible.

Our research bound medical and actuarial aspects to provide a better understanding of health insurance. Most of the results were intuitive, but have not been researched so far for significance in a regression framework. Our results, although, were very specific to the Swiss health insurance scheme, and conclusions have to be drawn carefully. For further comprehension of the decision process, it may be interesting to perform analyses under other insurance environments, as well as make use of panel data, where available, for the implementation of other econometric techniques.

Author Contributions: Conceptualization, V.K. and J.W.; methodology, V.K. and J.W.; formal analysis, V.K.; writing–original draft preparation, V.K.; writing–review and editing, J.W.; supervision, J.W.; funding acquisition, J.W. All authors have read and agreed to the published version of the manuscript.

Funding: Financial support from the Swiss National Science Foundation (SNSF, Grant No. CRSII5_180350).

Conflicts of Interest: The authors declare no conflict of interest.

References

Andersen, Lars Bo, Peter Schnohr, Marianne Schroll, and Hans Ole Hein. 2000. All-cause mortality associated with physical activity during leisure time, work, sports, and cycling to work. *Archives of Internal Medicine* 160: 1621–28. [CrossRef] [PubMed]

Ang, James B. 2010. The determinants of health care expenditure in Australia. *Applied Economics Letters* 17: 639–44. [CrossRef]

Bazzano, Lydia A., Jiang He, Lorraine G. Ogden, Catherine M. Loria, Suma Vupputuri, Leann Myers, and Paul K. Whelton. 2002. Fruit and vegetable intake and risk of cardiovascular disease in US adults: The first National Health and Nutrition Examination Survey Epidemiologic Follow-up Study. *The American Journal of Clinical Nutrition* 76: 93–99. [CrossRef] [PubMed]

Blanchard, Chris M., Kevin D. Stein, Frank Baker, Mary F. Dent, Maxine M. Denniston, Kerry S. Courneya, and Eric Nehl. 2004. Association between current lifestyle behaviors and health-related quality of life in breast, colorectal, and prostate cancer survivors. *Psychology & Health* 19: 1–13.

Block, Gladys, Blossom Patterson, and Amy Subar. 1992. Fruit, vegetables, and cancer prevention: A review of the epidemiological evidence. *Nutrition and Cancer* 18: 1–29. [CrossRef]

Böckerman, Petri, and Pekka Ilmakunnas. 2009. Unemployment and self-assessed health: Evidence from panel data. *Health Economics* 18: 161–79. [CrossRef]

Bollen, Kenneth A. 1989. *Structural Equations with Latent Variables*. New York: Wiley.

Bourne, Paul Andrew. 2009. Socio-demographic determinants of health care-seeking behaviour, self-reported illness and self-evaluated health status in Jamaica. *International Journal of Collaborative Research on Internal Medicine & Public Health* 1: 101–30.

Cameron, A. Colin, Pravin K. Trivedi, Frank Milne, and John Piggott. 1988. A microeconometric model of the demand for health care and health insurance in Australia. *The Review of Economic Studies* 55: 85–106. [CrossRef]

Courtland C., Smith, and Lew Edward A. 1979. New investigation of build and blood pressure. *The Actuary* 13: 7–8.

Crossley, Thomas F., and Steven Kennedy. 2002. The reliability of self-assessed health status. *Journal of Health Economics* 21: 643–58. [CrossRef]

Cuttance, Peter, and Russell Ecob. 2009. *Structural Modeling by Example: Applications in Educational, Sociological, and Behavioral Research*. Cambridge: Cambridge University Press.

Dauchet, Luc, Philippe Amouyel, Serge Hercberg, and Jean Dallongeville. 2006. Fruit and vegetable consumption and risk of coronary heart disease: A meta-analysis of cohort studies. *The Journal of Nutrition* 136: 2588–93. [CrossRef]

Felson, David T., Yuqing Zhang, John M. Anthony, Allan Naimark, and Jennifer J. Anderson. 1992. Weight loss reduces the risk for symptomatic knee osteoarthritis in women: The Framingham Study. *Annals of Internal Medicine* 116: 535–39. [CrossRef] [PubMed]

Fylkesnes, Knut. 1993. Determinants of health care utilization—Visits and referrals. *Scandinavian Journal of Social Medicine* 21: 40–50. [CrossRef] [PubMed]

Gardiol, Lucien, Pierre-Yves Geoffard, and Chantal Grandchamp. 2005. *Separating Selection and Incentive Effects in Health Insurance*. Working Paper No. 2005-5380. London: Centre for Economic Policy Research.

Gerhardsson, Maria, Birgitta Floderus, and Staffan E. Norell. 1988. Physical activity and colon cancer risk. *International Journal of Epidemiology* 17: 743–46. [CrossRef]

Grossman, Michael. 1972. On the concept of health capital and the demand for health. *Journal of Political Economy* 80: 223–55. [CrossRef]

Haan, Peter, and Michal Myck. 2009. Dynamics of health and labor market risks. *Journal of Health Economics* 28: 1116–25. [CrossRef]

Hooper, Daire, Joseph Coughlan, and Michael R. Mullen. 2008. Structural equation modelling: Guidelines for determining model fit. *Electronic Journal of Business Research Methods* 6: 53–60.

Huang, Chiou-Yan, Hsin-Ya Liao, and Sue-Hwang Chang. 1998. Social desirability and the Clinical Self-Report Inventory: Methodological reconsideration. *Journal of Clinical Psychology* 54: 517–28. [CrossRef]

Hubert, Helen B., Manning Feinleib, Patricia M. McNamara, and William P. Castelli. 1983. Obesity as an independent risk factor for cardiovascular disease: A 26-year follow-up of participants in the Framingham Heart Study. *Circulation* 67: 968–77. [CrossRef]

Inyang, Mfrekemfon P., and Stella Okey-Orji. 2015. Sedentary Lifestyle: Health Implications. *IOSR Journal of Nursing and Health Science Ver. I* 4: 20–25. [CrossRef]

Johansson, Sven-Erik, and Jan Sundquist. 1999. Change in lifestyle factors and their influence on health status and all-cause mortality. *International Journal of Epidemiology* 28: 1073–80. [CrossRef] [PubMed]

Joshipura, Kaumudi J., Frank B. Hu, JoAnn E. Manson, Meir J. Stampfer, Eric B. Rimm, Frank E. Speizer, Graham Colditz, Alberto Ascherio, Bernard Rosner, Donna Spiegelman, and et al. 2001. The effect of fruit and vegetable intake on risk for coronary heart disease. *Annals of Internal Medicine* 134: 1106–14. [CrossRef] [PubMed]

Jousilahti, Pekka, Jaakko Tuomilehto, Erkki Vartiainen, Juha Pekkanen, and Pekka Puska. 1996. Body weight, cardiovascular risk factors, and coronary mortality: 15-year follow-up of middle-aged men and women in eastern Finland. *Circulation* 93: 1372–79. [CrossRef] [PubMed]

Le Marchand, Loïc, Lynne R. Wilkens, and Ming-Pi Mi. 1992. Obesity in youth and middle age and risk of colorectal cancer in men. *Cancer Causes & Control* 3: 349–54.

Lee, I-Min, and Patrick J. Skerrett. 2001. Physical activity and all-cause mortality: What is the dose-response relation? *Medicine and Science in Sports and Exercise* 33 (Suppl. 6): S459–71.

Li, Cheng-Hsien. 2016. Confirmatory factor analysis with ordinal data: Comparing robust maximum likelihood and diagonally weighted least squares. *Behavior Research Methods* 48: 936–49. [CrossRef] [PubMed]

Li, Yanping, An Pan, Dong D. Wang, Xiaoran Liu, Klodian Dhana, Oscar H. Franco, Stephen Kaptoge, Emanuele Di Angelantonio, Meir Stampfer, Walter C. Willett, and et al. 2018. Impact of healthy lifestyle factors on life expectancies in the US population. *Circulation* 138: 345–55. [CrossRef]

MacCallum, Robert C., and James T. Austin. 2000. Applications of structural equation modeling in psychological research. *Annual Review of Psychology* 51: 201–26. [CrossRef]

Martens, Matthew P. 2005. The use of structural equation modeling in counseling psychology research. *The Counseling Psychologist* 33: 269–98. [CrossRef]

Matthews, Charles E., Adriana L. Jurj, Xiao-ou Shu, Hong-Lan Li, Gong Yang, Qi Li, Yu-Tang Gao, and Wei Zheng. 2007. Influence of exercise, walking, cycling, and overall nonexercise physical activity on mortality in Chinese women. *American Journal of Epidemiology* 165: 1343–50. [CrossRef]

Miller, Victoria, Andrew Mente, Mahshid Dehghan, Sumathy Rangarajan, Xiaohe Zhang, Sumathi Swaminathan, Gilles Dagenais, Rajeev Gupta, Viswanathan Mohan, Scott Lear, and et al. 2017. Fruit, vegetable, and legume intake, and cardiovascular disease and deaths in 18 countries (pure): A prospective cohort study. *The Lancet* 390: 2037–49. [CrossRef]

Muthén, Bengt. 1984. A general structural equation model with dichotomous, ordered categorical, and continuous latent variable indicators. *Psychometrika* 49: 115–32. [CrossRef]

Oja, Pekka, Ari Tapio Mänttäri, Ari Heinonen, K. Kukkonen-Harjula, Raija Laukkanen, M. Pasanen, and Ilkka Vuori. 1991. Physiological effects of walking and cycling to work. *Scandinavian Journal of Medicine & Science in Sports* 1: 151–57.

Oyebode, Oyinlola, Vanessa Gordon-Dseagu, Alice Walker, and Jennifer S. Mindell. 2014. Fruit and vegetable consumption and all-cause, cancer and CVD mortality: Analysis of Health Survey for England data. *Journal Epidemiology Community Health* 68: 856–62. [CrossRef] [PubMed]

Penedo, Frank J., and Jason R. Dahn. 2005. Exercise and well-being: A review of mental and physical health benefits associated with physical activity. *Current Opinion in Psychiatry* 18: 189–93. [CrossRef]

Pi-Sunyer, F. Xavier. 1991. Health implications of obesity. *The American Journal of Clinical Nutrition* 53: 1595S–603S. [CrossRef]

Pohlmeier, Winfried, and Volker Ulrich. 1995. An econometric model of the two-part decisionmaking process in the demand for health care. *Journal of Human Resources* 30: 339–61. [CrossRef]

Prinja, Shankar, Akashdeep Singh Chauhan, Anup Karan, Gunjeet Kaur, and Rajesh Kumar. 2017. Impact of publicly financed health insurance schemes on healthcare utilization and financial risk protection in India: A systematic review. *PLoS ONE* 12: e0170996. [CrossRef]

Pucher, John, Ralph Buehler, David R. Bassett, and Andrew L. Dannenberg. 2010. Walking and cycling to health: A comparative analysis of city, state, and international data. *American Journal of Public Health* 100: 1986–92. [CrossRef]

Riiser, Amund, Ane Solbraa, Anne Karen Jenum, Kåre I. Birkeland, and Lars Bo Andersen. 2018. Cycling and walking for transport and their associations with diabetes and risk factors for cardiovascular disease. *Journal of Transport & Health* 11: 193–201.

Rosseel, Yves. 2012. Lavaan: An R package for structural equation modeling and more. Version 0.5–12 (BETA). *Journal of Statistical Software* 48: 1–36. [CrossRef]

Schmitz, Hendrik. 2012. More health care utilization with more insurance coverage? Evidence from a latent class model with german data. *Applied Economics* 44: 4455–68. [CrossRef]

Schneider, Pia. 2004. Why should the poor insure? Theories of decision-making in the context of health insurance. *Health Policy and Planning* 19: 349–55. [CrossRef]

Sobel, Michael E. 1987. Direct and indirect effects in linear structural equation models. *Sociological Methods & Research* 16: 155–76.
Society of Actuaries. 1959. *Build and Blood Pressure Study*. Schaumburg: Society of Actuaries, vol. 1.
Steinmetz, Kristi A., and John D. Potter. 1996. Vegetables, fruit, and cancer prevention: A review. *Journal of the American Dietetic Association* 96: 1027–39. [CrossRef]
Stommel, Manfred, and Charlotte A. Schoenborn. 2010. Variations in BMI and prevalence of health risks in diverse racial and ethnic populations. *Obesity* 18: 1821–26. [CrossRef]
Strully, Kate W. 2009. Job loss and health in the US labor market. *Demography* 46: 221–46. [CrossRef]
Swiss Federal Statistical Office. 2018. *Enquête Suisse sur la Santé 2017. Vue d'ensemble*. Neuchâtel: Swiss Federal Statistical Office.
Swiss Federal Statistical Office. 2019. *L'enquête Suisse sur la Santé 2017 en Bref. Conception, Méthode, Réalisation*. Neuchâtel: Swiss Federal Statistical Office.
Thune, Inger, Tormod Brenn, Eiliv Lund, and Maria Gaard. 1997. Physical activity and the risk of breast cancer. *New England Journal of Medicine* 336: 1269–75. [CrossRef]
Thune, Inger, and Anne-Sofie Furberg. 2001. Physical activity and cancer risk: Dose-response and cancer, all sites and site-specific. *Medicine and Science in Sports and Exercise* 33 (Suppl. 6): S530–50.
Van de Mortel, Thea F. 2008. Faking it: Social desirability response bias in self-report research. *The Australian Journal of Advanced Nursing* 25: 40.
Van de Ven, Wynand P. M. M., and Bernard M. S. Van Praag. 1981. The demand for deductibles in private health insurance: A probit model with sample selection. *Journal of Econometrics* 17: 229–52. [CrossRef]
Warburton, Darren E. R., Crystal Whitney Nicol, and Shannon S. D. Bredin. 2006. Health benefits of physical activity: The evidence. *CMAJ* 174: 801–9. [CrossRef]
World Health Organization. 2000. *Obesity: Preventing and Managing the Global Epidemic*. Number 894. Geneva: World Health Organization.
Zweifel, Peter, and Roland Eisen. 2012. *Insurance Economics*. Springer Texts in Business and Economics. Berlin/Heidelberg: Springer. [CrossRef]

MDPI
St. Alban-Anlage 66
4052 Basel
Switzerland
Tel. +41 61 683 77 34
Fax +41 61 302 89 18
www.mdpi.com

Risks Editorial Office
E-mail: risks@mdpi.com
www.mdpi.com/journal/risks

MDPI
St. Alban-Anlage 66
4052 Basel
Switzerland

Tel: +41 61 683 77 34
Fax: +41 61 302 89 18

www.mdpi.com

ISBN 978-3-0365-0713-2